

Mechanical Characterisation of New and Existing Timber Foundation Piles

For the assessment of historical timber foundations and their contemporary applications in structural design

Pagella, G.

DOI

[10.4233/uuid:0453f51b-e50a-4ec8-9924-3e5b53e85dfc](https://doi.org/10.4233/uuid:0453f51b-e50a-4ec8-9924-3e5b53e85dfc)

Publication date

2025

Document Version

Final published version

Citation (APA)

Pagella, G. (2025). *Mechanical Characterisation of New and Existing Timber Foundation Piles: For the assessment of historical timber foundations and their contemporary applications in structural design*. [Dissertation (TU Delft), Delft University of Technology]. <https://doi.org/10.4233/uuid:0453f51b-e50a-4ec8-9924-3e5b53e85dfc>

Important note

To cite this publication, please use the final published version (if applicable).
Please check the document version above.

Copyright

Other than for strictly personal use, it is not permitted to download, forward or distribute the text or part of it, without the consent of the author(s) and/or copyright holder(s), unless the work is under an open content license such as Creative Commons.

Takedown policy

Please contact us and provide details if you believe this document breaches copyrights.
We will remove access to the work immediately and investigate your claim.

Mechanical Characterisation of New and Existing Timber Foundation Piles

Mechanical Characterisation of New and Existing Timber Foundation Piles

For the assessment of historical timber foundations and their contemporary applications in structural design.

Dissertation

for the purpose of obtaining the degree of doctor

at Delft University of Technology

by the authority of the Rector Magnificus, Prof. dr. ir. T.H.J.J. van der Hagen,

Chair of the Board for Doctorates,

To be defended publicly on

Tuesday 25 March 2025 at 10:00 o'clock

By

Giorgio PAGELLA

Master of Science in Civil Engineering

University of Padova, Italy,

born in Padova, Italy.

This dissertation has been approved by the promotor.

Composition of the doctoral committee:

Rector Magnificus	Chairperson
Prof. dr. ir. J. W. G. van de Kuilen	Delft University of Technology, promotor
Dr. ir. G. J. P. Ravenshorst	Delft University of Technology, copromotor

Independent Members:

Prof. dr. H. M. Jonkers	Delft University of Technology
Prof. dr. K. G. Gavin	Delft University of Technology
Dr. ir. R. Scotta	University of Padova, IT
Dr. G. van den Ham	Gemeente Amsterdam, NL
Prof. dr. M. Veljkovic	Delft University of Technology, reserve member



The Delft University of Technology has conducted this research with the valuable support of the Municipality of Amsterdam.

Keywords: Timber, foundation piles, strength grading, mechanical properties, durability, bacterial decay, micro-drilling.

Printed by: Ipskamp printing, Enschede

Cover design: Giorgio Pagella

Copyright © 2025 by Giorgio Pagella

ISBN 978-94-6473-748-6

An electronic version of this dissertation is available at <http://repository.tudelft.nl/>

*"If we knew what it was we were doing,
it would not be called research, would it?"*

Albert Einstein

Summary

Timber pile foundations were historically adopted to improve the stability of buildings, bridges, and quay walls in delta cities in Europe such as Amsterdam (NL), typically characterized by soft soils with poor load-bearing capacity. Many historic buildings still rely on wooden piles, even though in current structures mostly concrete foundation piles are used. Presently, there is a growing interest in using timber foundation piles to support buildings, promoting a new circular construction ecosystem. However, the continued use of timber piles—whether in new constructions or maintaining older buildings—requires a thorough and accurate assessment of their current condition. Ensuring the structural reliability and safety of timber piles is essential, as their degradation over time could compromise the stability of the buildings they support.

The design and assessment of timber foundation piles are still open research topics, hindered by several knowledge gaps in understanding their material and mechanical properties. Timber piles have not been extensively studied in the literature, and the design standards offer minimal to no guidance on their utilization. To enable engineers to adequately design timber foundation piles, verification rules, reliable material properties, and grading specifications are required.

These aspects have to be considered alongside the fact that timber foundation piles remain submerged under the water table for their whole service life, enduring high moisture levels. This makes them susceptible to biological decay, which can strongly reduce their load-bearing capacity, leading to safety issues in the supported buildings. However, the current assessment techniques based on the extraction of drill cores from the pile are often cumbersome and do not provide a comprehensive overview of the effects of biological decay on the mechanical properties of the piles.

In this context, the goal of this dissertation is to characterize the material and mechanical properties of saturated timber piles to support their contemporary applications in structural design and their assessment in relation to biological decay. The main research question addressing these objectives is formulated as follows:

How can the mechanical properties along wooden foundation piles be methodically characterized through mechanical testing, in relation to biodegradation and quality variables that could possibly influence their compressive strength?

The research question is answered by conducting a large experimental campaign, aimed at characterizing 70 full-size “new” spruce (*Picea abies*) and pine (*Pinus sylvestris*) piles and 60 historical spruce (*Picea abies*) and fir (*Abies*) piles. The latter were retrieved from two bridges in the city of Amsterdam, after being in service for approximately 100, 135, and 295 years.

The first part involves the characterization of “new” piles throughout the execution of large-scale axial compression tests on 253 fully-saturated pile segments, with the goal of investigating the saturated compressive strength and stiffness along the piles.

The relationships between the saturated compressive strength and the experimentally- and visually-determined parameters were investigated. The results from the

characterization of “new” piles show that the saturated compressive strength of both spruce and pine decreases from head to tip, linked to variations in growth characteristics such as knot ratio (KR), number of annual rings (Age), and rate of growth (RoG). This downward trend was also attributed to the increasing proportion of juvenile wood toward the tip. The pile tip exhibited the lowest saturated compressive strength of the pile, associated with a higher proportion of less dense juvenile wood, the highest KR values and RoG, along with the lowest Age. Consequently, the mechanical properties of spruce and pine piles were primarily governed by their tips. The strong correlation of the piles with their visually-graded parameters highlighted the opportunity to create multiple strength classes based on visual grades, separately for spruce and pine, as well as for both species combined. The resulting strength classes can be applied to the entire pile or to its segments: the head, the middle section, or the tip. This has particular significance in the design of timber piles, as the tips represent the critical cross-section of the pile during service, especially given the high stresses associated with their smaller cross-section, which can vary depending on soil conditions and applied load.

The second part focuses on the characterization of historical timber piles, involving the investigation of the effects of biological decay from both the material and the mechanical point of view. As a first step, large-scale compression tests were carried out on a total of 201 segments extracted from head, middle-part and tip of historical spruce and fir foundation piles, allowing to characterize their mechanical properties along the length.

Micro-drilling measurements were used to evaluate decay in historical piles, providing a non-destructive alternative to the conventional method of extracting and analysing drill cores for timber pile assessment. The correlation between the material and mechanical properties of the piles and the micro-drilling signals was explored. Micro-drilling measurements were well correlated with such properties, providing both qualitative and quantitative information on the degradation of the piles, even underwater and regardless of moisture content. A TU-Delft developed algorithm was used (See Appendix E) for the analysis of more than 500 micro-drilling measurements, allowing to precisely quantify the *soft shell* depth – the extent of decay in the outer cross-section of the piles.

Different decay levels were found, where piles from 1922 and 1886 showed minimal degradation, while a larger soft shell depth up to 50 mm was observed in piles from 1727, leading to a reduction in remaining short-term compressive strength up to 50-60% compared to new piles. This significant strength loss was primarily due to decay, particularly in piles from 1727, which had a service life of approximately 300 years. However, even the more recent piles from 1922 and 1886 exhibited a 10–20% reduction in short-term compressive strength despite their lower levels of decay. The equivalent sound compressive strength of piles from 1727 was lower than those from 1922 and 1886, due to a larger decayed portion of sapwood, resulting in a remaining sound core with poorer mechanical properties, associated with the intrinsic lower compressive strength of juvenile wood. However, this might also be partly attributed to the mechanical degradation due to higher stress levels during the service life of piles from 1727, associated with their larger presence of decay and thus a smaller sound load-bearing cross section.

Summary

Small-scale testing, computed tomography scans, and light microscopy observations allowed to identify bacterial decay as the primary degradation type, suggesting that the tested piles in Amsterdam remained submerged in anoxic conditions throughout their service life. However, the presence of soft rot fungi in isolated spots or other piles cannot be ruled out. Decay (soft shell) was uniform along the pile length, allowing reliable assessments based on pile head measurements. However, due to the tapered geometry of the pile, the remaining sound core was smallest at the pile tip, affecting the distribution of the load-bearing capacity. Finally, it was established that decay within the cross-section of the piles was limited to the non-durable sapwood. These findings align with existing literature, highlighting the good durability of heartwood in spruce and fir piles up to 300 years old.

In conclusion, two regression models were developed to predict the short-term compressive strength of “new” saturated timber foundation piles, applicable to both spruce and pine, based on machine grading. These models complement the characteristic strength classes established through visual grading.

A direct prediction equation was formulated for the remaining saturated short-term compressive strength along in-situ historical timber piles, based on the remaining sound cross-sectional area assessed with micro-drilling. These allow underwater assessments of pile heads to predict the remaining short-term strength along the entire pile, particularly at the critical pile tip, which often experiences higher stresses.

The saturated compressive strength values and grading boundaries presented in this dissertation support the engineering design of timber foundation piles, aligning with the standards outlined in the new Eurocode 5 2023. The research conducted on the remaining mechanical properties of historical piles and the assessment of biological decay with micro-drilling can aid the city of Amsterdam in arranging timely maintenance interventions, and contribute to the research framework supporting the development of deterministic models and reliability-based design for assessing the remaining service life of timber pile foundations.

Samenvatting

Houten heipalen werden historisch gebruikt om de stabiliteit van gebouwen, bruggen en kademuren in deltasteden in Europa te verbeteren, zoals Amsterdam (NL), gekenmerkt door zachte bodems met een lage draagkracht. Hoewel moderne constructies doorgaans betonnen funderingspalen gebruiken, staan veel historische gebouwen nog steeds op houten heipalen. Met de groeiende interesse in een circulair constructie-ecosysteem, is er tegenwoordig een hernieuwde belangstelling voor het gebruik van houten funderingspalen onder gebouwen. Tegelijkertijd is het belangrijk om bestaande houten heipalen nauwkeurig te beoordelen om de betrouwbaarheid en veiligheid van de ondersteunde gebouwen te garanderen.

Het gebruik van houten funderingspalen in het ontwerpen en beoordelen van constructies is nog weinig onderzocht, vooral vanwege de kennisleemten in het begrijpen van hun materiaal- en mechanische eigenschappen. Houten palen zijn niet uitgebreid bestudeerd in de literatuur, en de ontwerpnormen bieden weinig tot geen richtlijnen voor hun gebruik. Om ingenieurs in staat te stellen houten funderingspalen adequaat te ontwerpen, zijn verificatieregels, betrouwbare materiaaleigenschappen en specificaties ter sortering vereist. Deze aspecten moeten worden overwogen evenals het feit dat houten funderingspalen hun hele levensduur onder de grondwaterspiegel blijven, blootgesteld aan hoge vochtigheidsniveaus. Hierdoor zijn ze vatbaar voor biologische aantasting, wat hun draagvermogen sterk kan verminderen en kan leiden tot veiligheidsproblemen in de ondersteunde gebouwen. De huidige beoordelingsmethoden, gebaseerd op het extraheren van houtmonsters uit een paal, zijn echter vaak omslachtig en bieden geen volledig overzicht van de effecten van biologische aantasting op de mechanische eigenschappen van de palen.

In dit verband is het doel van dit proefschrift om de materiaal- en mechanische eigenschappen van verzadigde houten heipalen te karakteriseren om hun hedendaagse toepassingen in structureel ontwerp te ondersteunen en hun beoordeling in relatie tot biologische aantasting te onderzoeken. De hoofdonderzoeksvraag die deze doelstellingen adresseert, is als volgt geformuleerd:

Hoe kunnen de mechanische eigenschappen langs houten funderingspalen methodisch worden gekarakteriseerd door middel van mechanische tests, in relatie tot biologische aantasting en kwaliteitsvariabelen die mogelijk hun druksterkte kunnen beïnvloeden?

De onderzoeksvraag wordt beantwoord door een grootschalige experimentele testcampagne uit te voeren, gericht op het karakteriseren van 70 volledige "nieuwe" vuren (*Picea abies*) en grenen (*Pinus sylvestris*) palen en 60 historische vuren (*Picea abies*) en dennen (*Abies*) palen. De laatstgenoemde werden geëxtraheerd uit twee bruggen in Amsterdam, na ongeveer 100, 135 en 295 jaar in gebruik te zijn geweest.

Het eerste deel betreft de karakterisering van "nieuwe" palen door middel van grootschalige axiale compressietests op 253 volledig verzadigde paalsegmenten, met als doel de verzadigde druksterkte en stijfheid langs de palen te onderzoeken. De relaties

tussen de verzadigde druksterkte en parameters gekarakteriseerd door visuele en machinale sortering werden onderzocht.

De resultaten van de karakterisering van “nieuwe” palen tonen aan dat de verzadigde druksterkte van zowel spar als pijnboom afneemt van de kop naar de voet, in verband met variaties in groeikenmerken zoals de hoeveelheid kwasten ten opzichte van de omtrek (KR, Knot Ratio), het aantal jaarringen (Age), en de groeisnelheid aan de hand van de dikte van de groeiringen (RoG, Rate of Growth). Deze neerwaartse trend werd ook toegeschreven aan het toenemende aandeel jong hout richting de voet.

De paalvoet vertoonde de laagste verzadigde druksterkte van de paal, geassocieerd met de hoogste KR-waarden en RoG, samen met de laagste leeftijd. Dientengevolge bleken de mechanische eigenschappen van vuren en grenen voornamelijk te worden bepaald door hun voet. De sterke correlatie van de palen met hun visueel gegradeerde parameters bood de mogelijkheid om meerdere sterkteklassen te creëren op basis van visuele sortering, afzonderlijk voor vuren en grenen, evenals voor beide soorten gecombineerd. De resulterende sterkteklassen kunnen worden toegepast op de gehele paal zoals ook op de segmenten kop, middenstuk of voet. Dit is van specifieke toepassing op het ontwerp van houten palen, aangezien de voet het kritieke dwarsprofiel vormt tijdens het gebruik. Dit is vooral belangrijk vanwege de hoge spanningen die optreden bij de kleinere doorsnede van de paal, welke kan variëren afhankelijk van de bodemomstandigheden en de aangebrachte belasting.

Het tweede deel richt zich op de karakterisering van historische houten funderingspalen, waarbij de effecten van biologische aantasting zowel vanuit materiaal- als mechanisch perspectief worden onderzocht.

Als eerste stap werden grootschalige compressietests uitgevoerd op een totaal van 201 segmenten, gehaald uit de kop, het middenstuk en de voet van historische vuren en dennen funderingspalen, waardoor hun mechanische eigenschappen langs de lengte konden worden gekarakteriseerd.

Micro-drilling metingen (microboormetingen) werden gebruikt om de biologische aantasting in historische palen te beoordelen, als niet-destructief alternatief voor de conventionele methode van het houtmonsteranalyse. De correlatie tussen de materiaaleigenschappen van de palen en de micro-drilling signalen werd onderzocht. Micro-drilling metingen bleken te correleren met deze eigenschappen, waardoor zowel kwalitatieve als kwantitatieve informatie over de aantasting van de palen werd verstrekt, zelfs onder water en ongeacht het vochtgehalte. Een door TU Delft ontwikkeld algoritme werd gebruikt (zie Bijlage E) voor de analyse van meer dan 500 microboormetingen, waardoor de zachte schil diepte – de mate van aantasting in de buitenste dwarsdoorsnede van de palen – nauwkeurig kon worden gekwantificeerd.

Er werden verschillende afmetingen van de diepte van de zachte schil gevonden, waarbij palen uit 1922 en 1886 minimale aantasting vertoonden, terwijl een grotere diepte van de zachte schil werd waargenomen bij palen uit 1727, die de buitenste 20-50 mm van hun doorsnede aantasten en leidden tot een vermindering van de resterende korteduursterkte tot 50-60% in vergelijking met nieuwe palen.

Dit significante verlies in sterkte was voornamelijk te wijten aan aantasting, met name in de palen uit 1727, die een levensduur van ongeveer 300 jaar hadden. Echter, zelfs de recentere palen uit 1922 en 1886 vertoonden een vermindering van 10–20% in de kortetermijn druksterkte, ondanks hun lagere niveaus van aantasting. De effectieve druksterkte van de palen uit 1727 was lager dan die van de palen uit 1922 en 1886, vanwege een groter aantasting gedeelte van het spinthout, wat resulteerde in een resterende geluidskern met slechtere mechanische eigenschappen, die samenhangen met de intrinsieke lagere druksterkte van jeugdhout. Dit kan echter ook gedeeltelijk worden toegeschreven aan de mechanische degradatie door hogere spanningsniveaus tijdens de levensduur van de palen uit 1727, die verband houden met hun grotere aantasting en dus een kleinere draagkrachtige dwarsdoorsnede.

Klein-schaaltesten, computertomografie-scans en lichtmicroscopische waarnemingen maakten het mogelijk bacteriële aantasting als het belangrijkste degradatietype te identificeren, wat suggereert dat de geteste palen in Amsterdam gedurende hun levensduur onder zuurstofarme omstandigheden bleven ondergedompeld

De aantasting (zachte schil) was uniform langs de lengte van de paal, waardoor betrouwbare beoordelingen op basis van de paalkopmetingen mogelijk waren. Vanwege de gedetailleerde geometrie van de paal was de resterende geluidskern echter het kleinst bij de punt van de paal, wat invloed had op de verdeling van de draagcapaciteit. Tot slot werd vastgesteld dat de verrotting in de dwarsdoorsnede van de palen beperkt was tot het niet-duurzame spinthout. Deze bevindingen komen overeen met de bestaande literatuur, die de goede duurzaamheid van het hart- hout in spar- en dennenhouten palen tot 300 jaar benadrukt.

Als conclusie werden twee regressiemodellen ontwikkeld om de kortetermijn druksterkte van “nieuwe” verzadigde houten funderingspalen te voorspellen, toepasbaar op zowel spar als pijnboom, gebaseerd op machinale sortering. Deze modellen vullen de gekarakteriseerde sterkteklassen aan die zijn vastgesteld door visuele sortering

Een voorspellingsformule werd opgesteld voor de resterende verzadigde kortetermijn druksterkte langs in-situ historische houten funderingspalen, gebaseerd op het resterende niet aangetaste doorsnee oppervlak beoordeeld door micro-drilling. Deze stellen onderwaterbeoordelingen van de paalkoppen in staat om de resterende kortetermijn druksterkte langs de gehele paal te voorspellen, met name bij de kritieke punt van de paal, die vaak hogere spanningen ervaart

De verzadigde korteduursterkte en graderinggrenzen gepresenteerd in dit proefschrift ondersteunen het constructieve ontwerp van houten funderingspalen, in overeenstemming met de normen zoals uiteengezet in de nieuwe Eurocode 5 2023. Het onderzoek naar de resterende mechanische eigenschappen van historische palen en de beoordeling van biologische aantasting met micro-drilling kan de stad Amsterdam helpen om tijdig onderhoudsinterventies te plannen, en bijdragen aan het onderzoeksraamwerk ter ondersteuning van de ontwikkeling van deterministische modellen en op betrouwbaarheid gebaseerde ontwerpevaluatie, inclusief voorspellingen voor de resterende levensduur van houten heifundamenten.

Contents

Summary	7
Samenvatting	11
Contents	15
Introduction	21
1.1 Background.....	21
1.2 Problem statement	23
1.2.1 Design of timber foundation piles.....	23
1.2.2 Assessment of historical timber foundation piles	24
1.3 Aim of the research.....	26
1.4 Research question	28
1.5 Outline of the dissertation	29
Wooden foundation piles: state of the art	33
2.1 Introduction.....	33
2.2 Wooden foundation piles through history	34
2.3 From the tree in the forest to the pile in the foundation	37
2.4 Structure of softwoods	40
2.4.1 Cellular structure.....	40
2.4.2 Macro structure.....	42
2.4.3 Physical properties	44
2.4.4 Wood defects.....	47
2.5 Mechanical properties of timber piles.....	53
2.5.1 Overview of the literature review on saturated compressive strength of timber piles	53
2.5.2 Saturated compressive strength	56
2.5.3 Variability of the saturated strength properties along timber piles.....	57
2.5.4 Influence of moisture content on the compressive strength	65
2.5.5 Design codes	66
2.5.6 Conclusions	68
2.6 Biological degradation in timber foundation piles.....	71

2.6.1	Introduction.....	71
2.6.2	Research studies on biological degradation.....	73
2.6.3	Assessment of wooden piles in Amsterdam	76
2.6.4	Conclusions	81
Materials and Methods.....		83
3.1	Introduction	83
3.2	Materials	85
3.2.1	“New” wooden piles felled in 2019	85
3.2.2	Historical timber piles from bridges in Amsterdam	87
3.3	Preliminary in-situ testing on full-length piles.....	89
3.4	Subdivision of the piles into segments	91
3.5	Characterization of the material properties	92
3.5.1	Experimentally-determined properties	92
3.5.2	Visually-determined growth characteristics	95
3.6	Full-scale compression tests.....	96
3.7	Visual grading of “new” wooden foundation piles.....	98
3.8	Determination of characteristic values	99
3.9	Assessment of decay with micro-drilling measurements.....	100
3.9.1	Determination of the soft shell with micro-drilling	101
3.9.2	Validation of the zones associated with the soft shell based on the results of mechanical testing.....	104
3.10	Influence of moisture content variation on micro-drilling signals.....	104
3.11	Determination of material and mechanical properties of small-scale prismatic samples.....	106
3.12	Computed Tomography (CT) scanning.....	109
3.12.1	Determination of the proportion of sapwood and heartwood of spruce piles	111
3.13	Light microscopy observation	112
Experimental results of “new” wooden foundation piles.....		115
4.1	Introduction	115
4.2	Results from material and mechanical characterization of saturated spruce and pine piles.....	116

4.2.1	Preliminary results on full-length piles	116
4.2.2	Results of the compression tests on pile segments.....	117
4.2.3	Results from the characterization of the material properties of pile segments	122
4.3	Correlations between strength and visually- and experimentally-determined parameters	125
4.3.1	Relationships among strength, stiffness and density	129
4.3.2	Influencing parameters on the compressive strength of the piles	131
4.4	Effect of pile driving and in-situ loading on the strength properties.....	132
4.5	Characteristics values for visual grading.....	135
4.5.1	Derivation of characteristic values based on combined visually-graded properties	136
4.5.2	Derivation of characteristic values based on individual visual grades	141
4.5.3	Derivation of characteristic values for visual grade of pile tips.....	145
4.5.4	Case study: application of visual grading on wooden pile.....	148
4.6	Proposal for compressive strength design values according to draft EC5 2023	150
4.7	Summary of the test results	152
Experimental results of historical wooden foundation piles		155
5.1	Introduction.....	155
5.2	Results of material and mechanical characterization of historic spruce and fir piles	156
5.2.1	Preliminary results on full-length piles	156
5.2.2	Compression test results of pile segments from different historical periods	157
5.2.3	Results from the characterization of the material properties of the historical piles.....	160
5.2.4	Relationship among the mechanical properties	163
5.2.5	Correlation analysis between the remaining short-term compressive strength and material properties	164
5.3	Decay assessment with micro-drilling approach.....	166
5.3.1	Determination of the soft shell and relative zero-strength zones	166

5.3.2	Equivalent sound compressive strength values	168
5.3.3	Validation of the soft shell for all piles based on the equivalent sound compressive strength.....	169
5.4	Influence of moisture content on decay assessment with micro-drilling	170
5.5	Effect of decay and physical properties on the remaining short-term compressive strength.....	175
5.6	Effect of decay on the material properties within the cross section.....	178
5.6.1	Material and mechanical properties within the cross section of the pile	178
5.6.2	Correlations between micro-drilling and material properties of the prisms	179
5.6.3	CT scans and light microscopy observations	181
5.6.4	Reconstruction of the density profile of the cross section from micro-drilling signals	184
5.7	Extent of decay within the cross section and along the piles	186
5.7.1	Extent of decay in spruce and fir sapwood	186
5.7.2	Decay distribution along the piles.....	188
5.7.3	Overview of the decay distribution in the foundation plan of bridge 30 and 41	189
5.8	Summary of the test results.....	193
Prediction equations for the short-term compressive strength		197
6.1	Introduction	197
6.2	Regression models for “new” spruce and pine foundation piles	198
6.2.1	Regression model for spruce piles.....	198
6.2.2	Regression model for pine piles.....	199
6.2.3	Regression model for “new” spruce and pine piles.....	200
6.3	Experimental equations for predicting the remaining short-term strength of historical piles	202
6.3.1	Micro-drilling assessment.....	202
6.3.2	Prediction of the remaining short-term strength along the pile	204
Conclusions and outlook.....		207

7.1	Main outcomes of the dissertation and concluding remarks	207
7.2	Recommendations for further research.....	211
References		213
Appendix A		225
A1	Introduction to regression analysis.....	225
A2	Indicating Properties (IPs)	226
A3	Determination of characteristic values based on IP limits.....	226
A4	Regression analysis statistics	228
Appendix B		231
B1	Results from the compression tests.....	231
B2	Test for normality of all categories of “new” spruce and pine piles	238
B3	t-Test for significant difference in mean $f_{c,0,wet}$	239
Appendix C		241
C1	Results from the compression tests.....	241
C2	Test for normality of the pile categories.....	253
C3	t-Test for significant difference in mean $f_{c,0,wet}$	253
C4	Results of small-scale compression tests on prismatic samples across the cross-section.....	254
Appendix D		257
D1	Results from validation of sapwood with CT scanning	257
Appendix E		260
E1	TU-Delft developed algorithm for micro-drilling signal analysis	260
E2	Steps outlining the functioning of the TU-Delft developed algorithm.	261
E3	Python script of TU-Delft developed algorithm programmed by dr. A. Roy.....	263
E4	Recommendations for execution of micro-drilling and signal analysis.....	273
List of Publications		279
Curriculum vitae		281
Acknowledgments		283

1

Introduction

1.1 Background

Timber foundation piles have always played an important role in supporting buildings on soft soils, such as clay and silt with high water content and poor load-bearing capacity [1]-[6]. By inserting a large number of tree logs vertically through the first silty-soil layers, a stable support for the foundation can be made, with timber piles reaching the stiffer and deeper sand layer (Figure 1.1) [3],[11].

In Europe, timber foundation piles were extensively used in the past to support many historic buildings, bridges, and quay walls [3]. In particular, the application of wooden foundation piles was widespread in The Netherlands, in delta cities such as Amsterdam (NL) and Rotterdam (NL), as shown in Figure 1.2, but also in cities like Venice (IT) and Hamburg (DE), where timber foundations can be found [1],[2],[3]. In this context, the city of Amsterdam (NL) constitutes one of the reference examples for such timber foundations, since it is estimated that more than eleven million timber piles are present [3]. One of the most famous buildings, still standing on 13659 spruce piles, is the Royal Palace on the Amsterdam Dam square built in the period from 1648 to 1655.

The assessment of the state of conservation and remaining load-bearing capacity of timber foundation piles is important for ensuring their long-term durability and performance [4]. When timber piles are in the ground below the water table, they can be subjected to biological decay, which may significantly reduce their load-bearing capacity, potentially leading to safety issues in the supported buildings [1],[3],[5],[6]. Biological decay in waterlogged soils can be caused by either soft rot fungi (in low-oxygen conditions), or bacteria (even in anoxic conditions) [10],[11],[1],[25]. Bacterial biodegradation progresses more slowly over time compared to fungal decay, which cannot survive underwater in the absence of oxygen [11],[14],[25]. This allows the piles to perform their function for centuries before showing a substantial reduction of the load-bearing capacity [145]. However, decayed timber piles can appear unaffected in the field, maintaining their shape and colour despite the degradation occurring [1]. This poses a challenge in the engineering

assessment of timber piles, exacerbated by the difficulty in inspecting the foundations hidden beneath the soil.

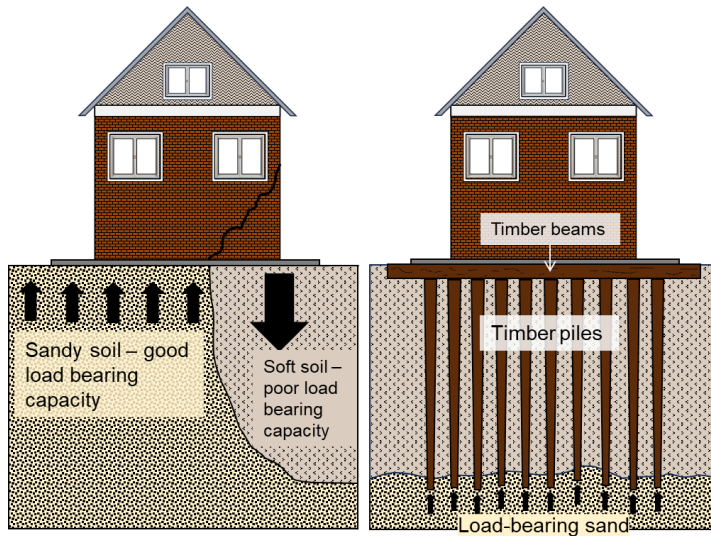


Figure 1.1: (a) Sandy soil with good load-bearing capacity to support the weight of the building and soft soil with poor load bearing capacity causing stability issues and possible settlements of the foundations; (b) timber foundation piles inserted through silty soils until reaching the load-bearing sand layer providing stable support to the building.

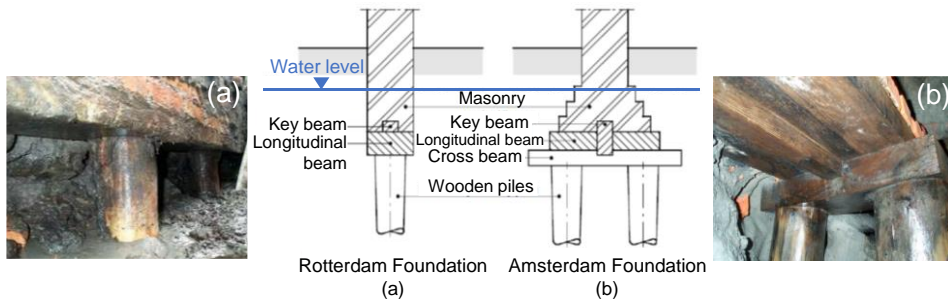


Figure 1.2: Wooden foundation types in Rotterdam (NL) and Amsterdam (NL): (a) Rotterdam foundation with a system of stand-alone wooden piles and only longitudinal beams; (b) Amsterdam foundation with cross beams and pair of piles (Adaptation from [17]).

Even in cases where the wooden foundations are in satisfactory condition, a structural assessment is often needed when modification, maintenance, or renovation works of existing structures are planned. In this context, the material properties of saturated timber piles have not been widely studied in the literature, and presently, little or no design guidance can be found in the design standards [18]-[23]. Timber piles have historically been designed with a load-bearing capacity ranging from 8 to 15 tons, with a maximum capacity of 20 tons. Also in the present design [17],[24], a reliable value of 10 tons (100 kN) has been used for design purposes, reflecting both historical practice and advancements in engineering understanding. However, the knowledge gaps with respect to the material

and mechanical properties of saturated timber piles and the effects of biological decay on wood degradation processes over time, prevent engineers from adequately assessing timber foundation piles. This could have considerable implications on the safety of buildings supported by timber foundations, further impacting the safety of the citizens and economic activities.



Figure 1.3: (a) Cutaway drawing of historical timber piles under bridge 41 (Johanna Borskibrug) in Amsterdam (NL); (b) a timber foundation pile retrieved from bridge 30 (De Isa van Eeghenbrug) in Amsterdam (NL).

1.2 Problem statement

1.2.1 Design of timber foundation piles

Historically, timber foundation piles were designed on experience and trial-and-error techniques to determine their optimal length and load-bearing capacity [145], as formal methods for soil analysis and geotechnical engineering had not yet been established. Despite current advancements in geotechnical and structural engineering, standards and guidelines for the design of timber piles remain limited. In the current Eurocode 5 (EC5) [18], which provides regulations for the design of timber structures, timber piles are not mentioned. In the Netherlands, where timber piles were extensively utilized across the country, the present Dutch National Annex to EC5 [19] and NEN 5491 [20] provide a single “dry” compressive strength design value (at 12% moisture content) based on historical data [32],[33], and grading rules for saturated timber piles and their application in soil. The design of saturated timber piles in the ground, enduring high moisture contents, starts from the “dry” strength value in [19], factoring in climate conditions and load durations using codified modification factors (k_{mod}) in the calculation, according to the design practice in the EC5. This is because the mechanical properties of timber are dependent on moisture content [37], where climate conditions with high moisture levels (such as saturated piles in the ground) result in lower strength and stiffness [106],[96],[101]. However, the modification factors in the standards were determined on the basis of edgewise bending tests conducted on timber boards [41], which may have different behaviour than round wood such as timber piles, as indicated in previous studies [36],[37]. In addition, the load duration is typically accounted for 50 years in the modification factors. However, the service life of timber pile foundations can be much longer than modern design, up to 300 years or more [1],[16]. These aspects highlight that the current

procedure outlined in the standards [18],[19] may not be adequate for the design of timber piles in wet conditions, suggesting the need for conducting research on the material properties of saturated timber piles.

In the existing literature [32],[33],[36], large uncertainties are present with regard to the material properties of saturated timber piles. The provided compressive strength and stiffness properties are not fully comprehensive for a correct design or assessment of timber piles, since they are based on a limited dataset, without providing grading boundaries and strength parameters spanning from the head to the tip of the pile. Since the piles are typically sourced from softwood trees [5],[19],[22], their material properties inherently vary from the lower section of the tree trunk (butt-log) to the tip [59]. Their tapered shape implies larger diameters at the butt-log (head) and smaller at the tip diameters [79]-[82]. The tip is especially critical as it features the poorest mechanical properties [59]. Moreover, depending on soil conditions, it corresponds to the critical cross section of the pile during service, primarily due to the high stresses associated with its smaller cross section.

In order to adequately design timber foundation piles, the following main issues have to be overcome:

- The calculation from dry to wet design values in the standards [19] highlighted several uncertainties regarding its application to saturated timber piles that remain in the ground under the water table for their whole service life. Therefore, the design procedure in the standards has to start from saturated design values, as suggested in the new draft of EC5 (2023) [21]. Moreover, the given k_{mod} values in the Draft EC5 (2023) are only to be used for load duration effects in a newly defined service class 4, for fully saturated conditions.
- The saturated mechanical and material properties of the piles in literature are based on a limited database, without providing grading boundaries and strength parameters covering the entire length of the pile, from the head to the tip. In order to enable engineers to adequately design timber foundation piles, reliable material properties along the timber piles have to be determined, in relation to their tapered shape and natural growth characteristics.

1.2.2 Assessment of historical timber foundation piles

Given the essential function of timber pile foundations and their widespread presence in delta-cities across Europe, such as Amsterdam, estimating the remaining mechanical properties of the piles is crucial for arranging timely maintenance interventions. As timber foundation piles were primarily designed on historical experience, the current material status can only be estimated through the assessment of the present structure. This includes the analysis of biological decay on timber piles, carried out with in-situ inspection techniques [16].

The inspection techniques adopted in Amsterdam adhered to the F3O guidelines [22] and the Dutch Standard NEN 8707 [23], involving the extraction of drill cores (with a length of roughly half the pile diameter) from the head of the wooden piles, roughly 50 cm below the pile head (Figure 1.4). The drill cores were taken underwater by divers with a hand-driven increment borer ($\varnothing 10$ mm), and collected in plastic tubes filled with water, to

preserve their physical properties. Subsequently, the drill cores were segmented into sub-sections and visually examined: the wood species, the type, and the degree of deterioration were determined under the microscope [5],[143]. The classification was conducted according to Varossieau (1949) [5], where 4 decay classes were used: sound, weak, moderate, and severe. The wood species mainly involved spruce, pine, and fir, with a smaller proportion of alder and oak.

From the analysis of the decay of the drill cores, it was concluded that bacterial decay was present in a significant number of piles. Subsequently, the remaining compression strength of the piles was estimated by using the maximum moisture content that a sub-section of the drill core could absorb, according to the model for pine piles in [5]. Using this model, the city of Amsterdam considered every sub-section of the drill core with predicted compression strength lower than 8 MPa (correspondent to disrupted wood structure, moisture content of 230 %), as being part of a so-called “soft shell”: the degraded part of the cross section to which no strength is assigned. In order to calculate the remaining load-bearing capacity of the piles, the compression strength for “new” piles provided in the Dutch National Annex to EC 5 [19] and NEN 8707 [23] was assigned to the remaining assumed sound part, deriving the design compression force according to the modification factors (k_{mod}) used in the EC 5 [18]. However, the derived compressive strength values of the piles could not be validated with the compressive forces acting on the piles that have been in service, since only very limited data was available.

In Amsterdam, the aforementioned inspection technique, which relies on the analysis of drill cores, facilitated the sampling of numerous piles within the city. However, several uncertainties were related to the assessment of decay with drill-core analysis, due to the following issues:

- Drill-core analysis was based on local measurements conducted at a specific localized spot, limited to the pile head and dependent on the diver’s expertise. Thus, a continuous representation over the cross section of the pile was not given.
- The analysis of the possible decay of the drill cores required specific expertise and extensive investigations, since after the extraction, microscopic analyses and application of experimental models needed to be conducted.
- The derived remaining compressive strength values of the piles were calculated based on the design values and the modification factors (k_{mod}) in EC5 [19]. However, these were found to be inadequate for timber piles (see Paragraph 1.2.1).

The aforementioned issues highlight the importance of conducting research on the material and mechanical properties of saturated timber piles and on the effects of decay on the material properties of historical timber piles after centuries of service life. Furthermore, since the drill-core analysis revealed knowledge gaps and uncertainties associated with the assessment of decay in timber piles, micro-drilling measurements are investigated as alternative non-destructive technique. Micro drilling allows to inspect the material status throughout the whole cross section of the pile, involving the utilization of a drilling tool, where a drilling needle is pushed into the material with a chosen drill and feed speed, resulting in a graphical representation of the resistance encountered during

the drilling process [26]-[29],[152],[153]. Among the available non-destructive techniques for assessing the state of conservation of wooden piles, micro-drilling stands out as a promising method. With micro-drilling, an assessment of the material can be conducted in different positions and directions, resulting in more available measurements, increased accuracy and faster in-situ testing.

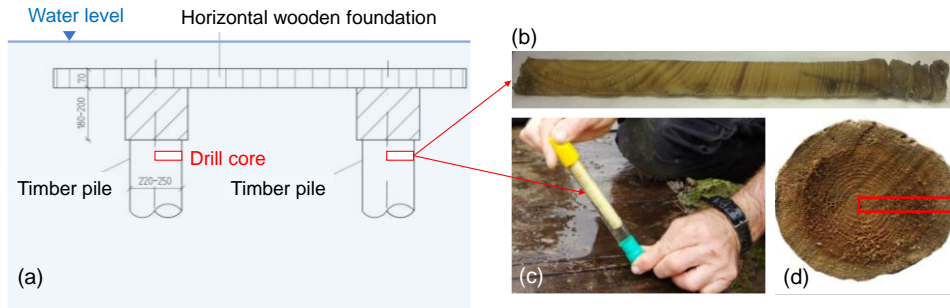


Figure 1.4: (a) Extraction of a drill core (in red) from the head of a timber foundation pile; (b) drill core; (c) drill core collected in a plastic tube filled with water; (d) cross-sectional view of the wooden pile and extraction depth of the drill core (in red).

1.3 Aim of the research

The knowledge gaps on timber foundation piles have given the opportunity to conduct specific research for improving the understanding of the mechanical properties of saturated timber piles, and the assessment of historical timber piles in relation to biological decay.

The aim of this research is to characterize the material and mechanical properties of 130 softwood saturated piles throughout a large experimental campaign. This includes 70 newly harvested, full-size saturated spruce (*Picea abies*) and pine (*Pinus sylvestris*) piles, sourced from forests in Holterberg (NL) and Nuremberg (DE), respectively. Additionally, 60 historic, full-size saturated spruce (*Picea abies*) and fir (*Abies alba*) piles, aged between 100 and 300 years and exhibiting varying decay levels, retrieved from two bridges in Amsterdam. The following methodology is adopted for achieving the main goals:

1. The mechanical properties along the full-size “new” piles are investigated throughout the execution of large-scale axial compression tests on pile segments, extracted from the piles’ head, middle-part, and tip. Pile segments with different diameters are studied (ranging from 130 mm to 280 mm), with the goal of investigating the variability of saturated compressive strength and stiffness along the pile. Moreover, all the piles segments are characterized with experimental and visual tests, to identify the most influencing parameters on their saturated compressive strength. On this basis, possible strength classes for the characteristic compressive strength based on visually graded parameters are determined for spruce and pine piles. The results of this study aims at improving the engineering design of European softwood foundation piles, supporting the integration of reliable design values into future versions of the Eurocode 5 [21].

2. The second objective of this work is the detailed characterization, in terms of material and mechanical properties, of the 60 historic saturated piles, with specific reference to the influence of bacterial decay on their remaining saturated compressive strength. The historical piles have been exposed in the soil for approximately 100, 135, and 295 years. Thus, the goal is to assess the remaining compressive strength of the piles in relation to bacterial decay after three distinct periods of service time. Several techniques are adopted for characterizing the extent of bacterial decay: micro-drilling measurements, computer tomography (CT) scans, and light microscopy observations. Furthermore, large-scale compression tests are performed on full-size segments extracted from the head, middle section, and tip of the piles to examine the impact of bacterial decay on the remaining compressive strength along the pile's length. In addition, small-scale compression tests are conducted on samples retrieved from the pile's cross-section to assess the influence of decay on the mechanical properties across the radial profile of the cross-section.
3. The applicability of micro-drilling measurements is studied to assess the amount of decay in the historic piles, as an alternative to the current extraction of drill cores. The primary objective is to investigate the correlations between the material and mechanical properties of the piles and the micro-drilling signals, in order to assess the reliability of micro-drilling for identifying decay from both qualitative and quantitative perspectives. Additionally, the research aims to adopt and validate a TU-Delft developed algorithm (Appendix E) to accurately determine the extent of decay at the specific location of the micro-drilling measurement.
4. Prediction models are developed for the saturated compressive strength of "new" spruce and pine piles, based on the machine graded dynamic modulus of elasticity, which can be measured in practice using frequency response measurements [161]. For existing piles, the aim is to develop a model that directly predicts the remaining saturated compressive strength along in-situ historic timber piles, based on micro-drilling measurements.

The novelty of this dissertation lies in the comprehensive characterization of the mechanical properties along the length of saturated spruce and pine piles, providing reliable saturated compressive strength values and grading specifications that enable engineers to effectively design and assess timber foundation piles. This research can contribute to the incorporation of accurate design values for saturated timber piles in future versions of Eurocode 5. Promoting the use and reuse of timber pile foundations offers a sustainable alternative, potentially minimizing the environmental impact of conventional concrete foundations and advancing the realization of fully biobased buildings.

This research introduces and validates an innovative methodology based on underwater micro-drilling measurements (Figure 1.5) for the in-situ assessment of historic timber foundation piles and the estimation of their remaining short-term compressive strength. This approach enables the reliable evaluation of bacterial decay and the remaining short-term strength of the piles. The TU-Delft developed algorithm (Appendix E) for analysing micro-drilling signals provides a quantitative estimation of the soft shell depth, derived

1.4 Research question

from statistical analysis of over 500 micro-drilling signals performed on 201 historic pile segments with varying decay levels. Experimental prediction equations can estimate the remaining short-term compressive strength along the pile, with potential integration into soil and load analyses to assess stress levels, considering load distribution and soil stratigraphy.

This methodology forms the basis for engineering retrofitting strategies for timber foundations currently supporting historic buildings and key infrastructure such as bridges and quay walls in Amsterdam. It contributes to the ongoing research framework in the city, aiding testing and modelling methods to estimate decay, residual load-bearing capacity, and service life of timber pile foundations. The knowledge generated from this research has broader applicability and can be extended to other delta cities across Europe, such as Stockholm (SE), Hamburg (DE), and Venice (IT), as well as overseas locations including Boston (US).

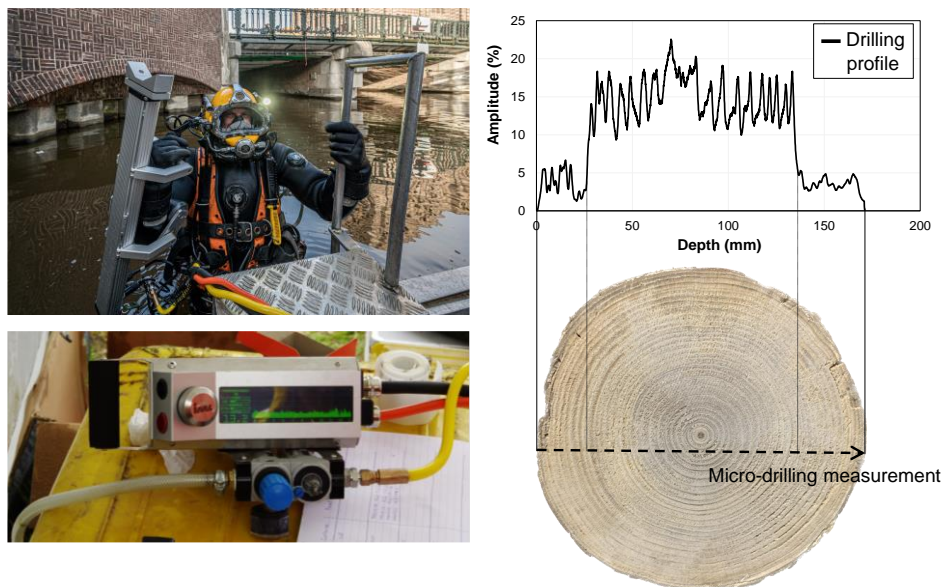


Figure 1.5: Micro-drilling measurements performed underwater by a diver in Amsterdam, and drilling profile throughout the cross section of a spruce pile.

1.4 Research question

The design and assessment of timber foundation piles are still open research topics, hindered by several knowledge gaps in understanding their material and mechanical properties. On the basis of the solutions and strategies described in the methodology, the overarching question can be formulated as follows:

How can the mechanical properties along wooden foundation piles be methodically characterized through mechanical testing, in relation to biodegradation and quality variables that could possibly influence their compressive strength?

The main research question is addressed through the following key questions:

1. How can an experimental program be designed to characterize the material and mechanical properties along the length of new and existing timber foundation piles? (Paragraph 3.4-3.6)
2. What is the correlation between the saturated compressive strength and experimentally- and visually-determined parameters of “new” timber piles? (Paragraph 3.7-3.8)
3. How can the extent of decay in historical timber piles be determined with micro-drilling measurements? (Paragraph 3.9-3.10)
4. How can the effects of biological decay on the mechanical properties of historical timber piles be characterized depending on its extent longitudinally and radially within the pile? (Paragraph 3.11-3.13)

1.5 Outline of the dissertation

The literature review in Chapter 2 provides an overview of the state of the art of timber foundation piles. The role of timber piles throughout history is initially presented. This is followed by the description of how timber piles are sourced from softwood trees, and how this influences their geometry and physical properties. The structure of softwoods is addressed to understand the material characteristics of timber piles. The mechanical properties of timber piles in saturated conditions are explained, limited to the few studies present in literature, along with their current utilization in the engineering standards. Finally, the effect of biological decay on the mechanical properties of timber piles is presented, and the current assessment of timber piles in Amsterdam is explained. Starting from this literature review, the knowledge gaps are addressed together with the elements of novelty in this dissertation.

Chapter 3 is primarily dedicated to the methodology adopted for the characterization of a substantial dataset comprising 70 “new” full-length timber piles, and 60 full-length historical timber piles spanning different ages (100, 135, and 295 years) with different levels of decay. Several techniques at full-scale and small-scale levels were adopted for this characterisation: large-scale compression tests on segments extracted along the piles’ length, small-scale compression tests on samples retrieved from their cross sections, experimentally- and visually-determined properties in saturated conditions, micro-drilling measurements, computed tomography (CT) scans, and light microscopy observations.

The results of the mechanical properties along 38 “new” spruce (*Picea abies*) and 32 “new” pine (*Pinus sylvestris*) saturated piles are reported and analysed in Chapter 4. The correlations between their saturated compressive strength and visually- and experimentally-determined properties are presented, to identify the key parameters that influence the saturated compressive strength. On this basis, possible strength classes for the characteristic compressive strength based on visually-graded parameters are proposed for both spruce and pine piles, in accordance with the provisions given in the new Eurocode 5 2023 [20].

Chapter 5 reports the results of the mechanical and material characterization of historical 55 spruce (*Picea abies*) and 5 fir (*Abies*) saturated piles, retrieved from the city of Amsterdam. The first section presents the results of the mechanical properties of the piles and their correlations with the material and physical properties. Subsequently, the micro-drilling approach is presented for assessing the amount of decay within the piles. The TU-Delft developed algorithm (appendix E) to investigate micro-drilling signals is calibrated and validated based on the large database collected from every historical pile segment. The effects of decay on the mechanical properties along the length of the piles are discussed. Moreover, the results of the small-scale mechanical testing and material analysis through the piles' cross section is reported and correlations are found with micro-drilling measurements. Finally, the extent of decay along the piles and radially within sapwood and heartwood is presented: this represents an important step towards predicting the remaining saturated compressive strength of historical piles with micro-drilling measurements.

Chapter 6 presents the development of two regression models for the prediction of the short-term compressive strength of "new" saturated timber foundation piles, one for spruce and one for pine piles, based on machine grading. These models add to the characteristic strength classes defined with visual grading in Chapter 4, providing another tool for the determination of the saturated compressive strength of the piles. Furthermore, a direct predictive equation is introduced for estimating the remaining short-term compressive strength of historical timber foundation piles, on the basis of micro-drilling measurements conducted in situ on the pile head. By analysing the remaining sound cross-sectional area of the pile head, the remaining short-term compressive strength can be predicted along the pile, both at the head, middle, and the tip, based on the experimental analyses of historic piles detailed in Chapter 5.

Chapter 7 concludes summarising the major findings of this thesis, accompanied by recommendations for inclusion of strength valued of new timber piles in the new engineering standards, Eurocode 5 2023, and strategies for the prediction of the remaining short-term strength of existing in-situ timber foundation piles. The chapter reviews the process of achieving the goals of the dissertation, highlights the key steps, and addresses the main research questions. Finally, suggestions and recommendations for further research are provided.

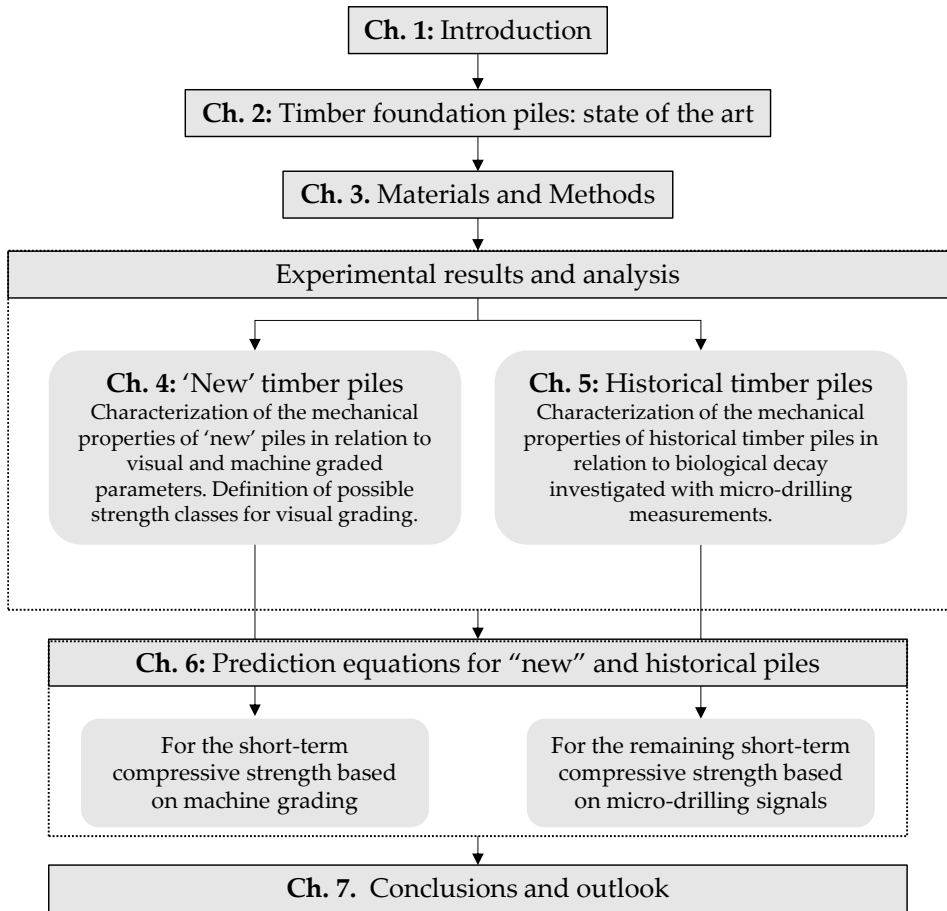


Figure 1.6: Outline of the dissertation

2

Wooden foundation piles: state of the art

2.1 Introduction

This chapter presents the literature review of the state of the art of wooden foundation piles in the Netherlands and within the European context, where wooden piles have been extensively employed as foundation systems in delta cities such as Amsterdam, for historic buildings. Section 2.2 explores the historical use of various types of wooden piles as foundational elements, tracing the evolution of techniques in the Netherlands from the Middle Ages to the present day. Section 2.3 discusses the process of selecting and harvesting timber foundation piles from softwood tree trunks, focusing on the natural growth conditions that influence the pile, and selection criteria based on trunk quality, diameter, and length. Section 2.4 explains the structure of softwoods along with their physical and material properties, to understand their interactions concerning mechanical behaviour under compression. The strength properties available in the literature for both saturated and dry piles are reported in Section 2.5, highlighting their distribution along the pile and the influence of moisture content. It also discusses how these strength properties are utilized in design codes, highlighting insights gained from the research and identifying knowledge gaps that require further investigation. In Section 2.6, the durability of the wooden piles are examined, focusing on bacterial degradation encountered in waterlogged anaerobic soils to understand how biodegradation influences the material and mechanical properties of timber over time. On this basis, the general framework of assessment techniques adopted in the Netherlands, particularly in the city of Amsterdam, is explained. This section highlights the inaccuracies of presently used assessment methods and the need for detailed knowledge of the mechanical properties of saturated wooden piles for their adequate assessment. The extensive literature review presented in this Chapter, allows to discuss about the lack of knowledge and elements of novelty that this dissertation covers.

2.2 Wooden foundation piles through history

Wooden foundation piles can be found especially in the western areas of The Netherlands, where the weakness of the soil (Figure 2.2) presents a limitation for engineering constructions [49]. During Roman times, short oak, ash, or alder piles were employed in Dutch foundations, acting as friction piles (the load is supported by the friction between the surface of the pile and the surrounding soil), supporting very simple lightweight constructions. As the Middle Ages unfolded, Dutch homes were primarily built with wood, involving foundations with many short friction piles next to each other, densely arranged to create a supportive base (Figure 2.1a-b). Around 1300-1400, longer piles (7-8 m) started to be used, still working as friction piles. Although their length was longer, the piles did not reach the load-bearing sandy layer, but they provided higher bearing capacity (Figure 2.1c) [145]. Until the end of the 16th century, timber piles remained predominantly adopted as friction piles, primarily due to the limited extent of pile-driving activities during that period [51].

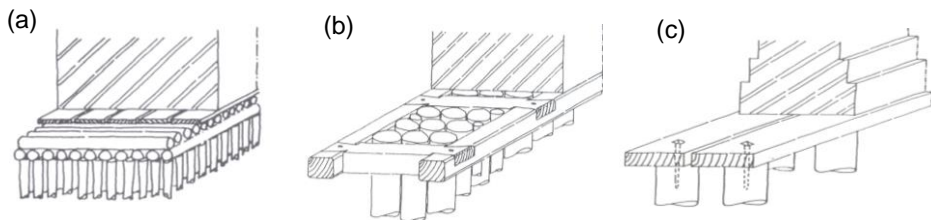


Figure 2.1: Examples of friction pile foundations (Adapted from [145]), made by: (a) many 3-4 m piles under a crosswise layer of small wooden trunks, working as a combination of friction piles to compact the soil; (b) improved system with a framework to prevent the horizontal displacements of the piles; (c) longer piles (7-8 m) with higher bearing capacity, still working as friction piles although their longer length, without reaching the load bearing sandy layer.

Before the late 16th century, housing structures started to evolve to larger sizes, incorporating stone and bricks as building material. The constructions became heavier and necessitated more stable foundations with a higher load-bearing capacity. Thus, timber foundation techniques in the Netherlands started to include the driving of long piles through the weak soil layers in order to reach the stable bearing sand layers [3]. A new foundation system made of horizontal timber beams and long vertical piles for deeper foundations emerged (Figure 2.3) [3],[145]. The horizontal foundational system with cross- and longitudinal beams gave very stable support, while long piles were reaching the dense sand layers (called “end bearing piles”) providing higher bearing capacity than friction piles.

Given the variable depth of the stable sand layer across different regions of The Netherlands, Dutch cities required piles of varying lengths and types for their foundations. In Amsterdam (NL), piles typically ranged at 10-12 m in length, typically spanning from 180 to 200 mm at the top and 120 to 140 mm at the bottom [55], with cross beams and pairs of piles (Figure 2.3b), known as “the Amsterdam foundation” (in Dutch: *Amsterdamse fundering*).

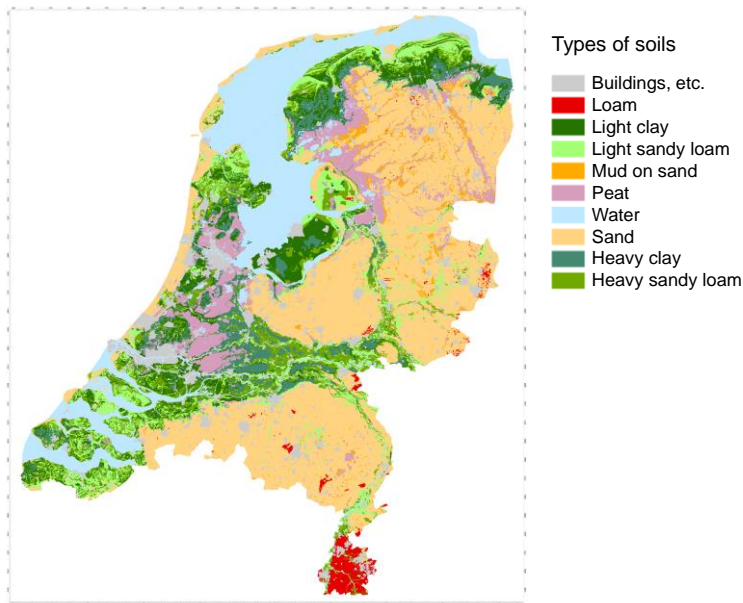


Figure 2.2: Type of soils in The Netherlands from TU Delft Library.

In Rotterdam (NL), the stable sandy soil was deeper than in Amsterdam, necessitating even longer piles up to 18 meters, with a foundation system of stand-alone piles and only longitudinal beams (Figure 2.3c), known as “the Rotterdam foundation” (in Dutch: *Rotterdamse fundering*) [145]. On the other hand, in Haarlem (NL) and The Hague (NL), shorter piles were used, spanning 2-6 m [3]. As the length of foundation piles varied through the years, this also influenced the selection of the wood species and their sourcing locations. Shorter piles were commonly crafted from pine, whereas longer piles were sourced from spruce or fir trees. The availability of spruce and fir piles was facilitated by the increasing timber importation from the 16th century onward, from Scandinavia, Poland, Germany, and Belgium [3].

The utilization of timber piles in The Netherlands firmly established itself in the 18th century, when the use of wooden foundation piles became a prevalent and customary practice. The rapid expansion of cities, beginning around 1875 with the advent of industrialization, led to the widespread use of wooden piles in construction [145]. Figure 2.4 shows the expansion of the city of Amsterdam (NL) between 1810 and 1889, and the land reclamation in its surrounding areas, involving mainly wooden foundations for supporting houses and buildings, but also bridges and quay walls built around the intricate system of canals. Between 1875 and 1960, engineers primarily relied on judgment and trial-and-error methods to determine the length and bearing capacity of these piles, as formal soil analysis and geotechnical engineering had yet to be developed [145].

Foundation construction techniques saw minimal evolution from the 18th through the 20th century, until the widespread adoption of concrete foundation piles following World War II. Over the past five decades, wooden foundation piles have seen continued use in smaller

2.2 Wooden foundation piles through history

structures such as greenhouses and sheds, with various wood types including larch, spruce, fir, and Douglas fir [22].



Figure 2.3: Adapted from [145]: (a) foundation system with horizontal cross- and longitudinal beams and long-end bearing piles used up to the first part of the 20th century; (b) example of timber foundation in Amsterdam (NL) with cross beams and pairs of piles; (c) example of a timber foundation in Rotterdam (NL), with system of stand-alone piles and only longitudinal beams.

Nowadays, the city of Amsterdam (NL) preserves its earliest surviving piled foundations, which can be traced back to the 17th century [52]. Examples are the (still standing) Royal Palace on the Amsterdam Dam square, opened in 1655 (364 years old) and based on 13659 spruce piles (approximately 11 m long), and the Amsterdam Maritime Museum, built in 1656, based on spruce and pine piles, and the tower of the Rotterdam St. Laurens church from 1655, built with 500 pine piles (ca. 14-m long) [3],[78],[145]. All these constitute an example of very good durability of wooden piles over the years, under the right circumstances! (further discussed in Section 2.6).

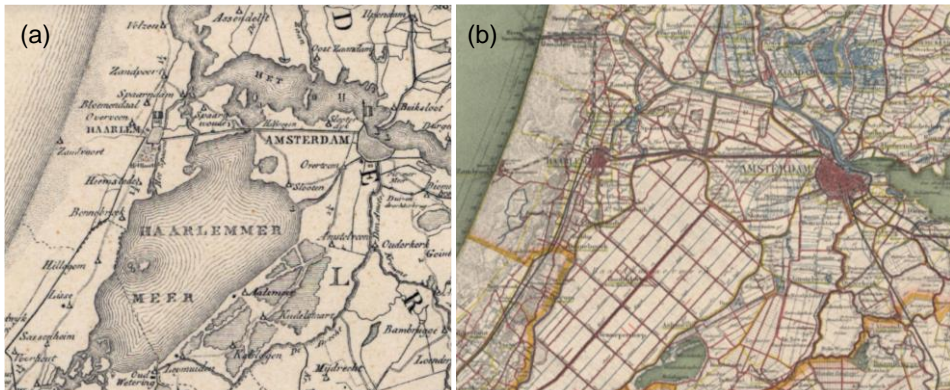


Figure 2.4: Map of Amsterdam (NL) and surroundings: water and soil through the years. Land reclamation around Amsterdam in two different periods: a) 1810; b) 1889. Sourced from *topotijdreis.nl*

2.3 From the tree in the forest to the pile in the foundation

When a tree is selected for harvesting and felled, the trunk is usually debranched and it can be used for different purposes in engineering constructions. Timber foundation piles are typically sourced from the lower section of a tree trunk, close to the base of the tree, commonly referred to as the "butt log" [79]. This specific portion is favoured due to its characteristics of being broader, straighter, and having a more consistent diameter compared to the upper segments of the tree [79], [88], also ensuring the optimal utilization of the material during harvesting, minimizing material waste. More specifically, the trees are cut approximately 25 cm from the ground, as close as possible to the soil level (G. van den Berg, Director of *RHS Rondhout*, Hierden (NL); personal communication, November 28, 2023). The first 2 meters of the trunk are usually considered as low-quality material, due to the natural growing deviation of the trunk at the base (Figure 2.5) often used for interior furniture and décor.

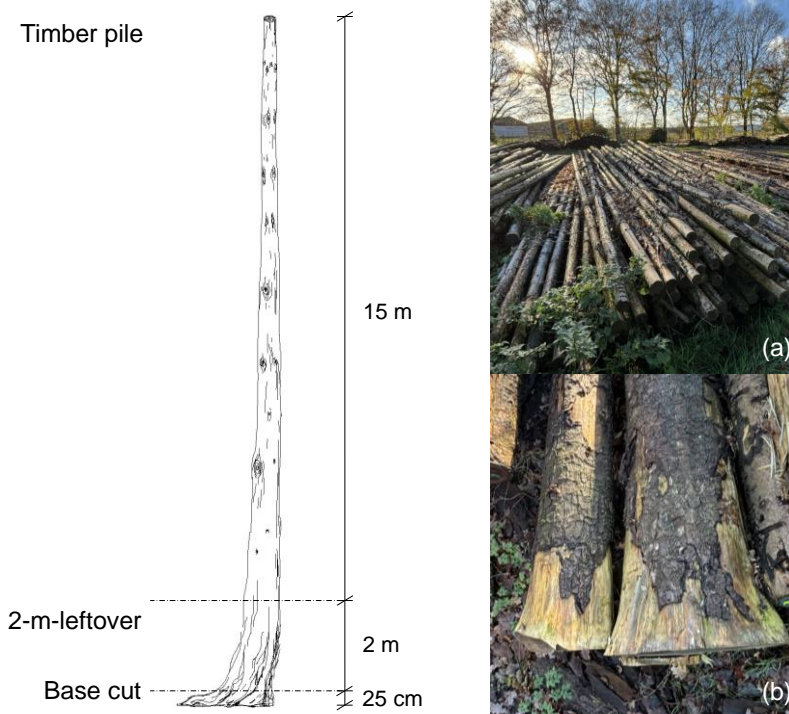


Figure 2.5: Cutting positions of a ca. 15-m-timber pile from a debranched tree trunk. (a) timber piles after cutting; (b) typical deviation of the bottom part of a tree trunk.

When timber piles are employed in foundations, there are two parameters used for the selection of the piles in the forest: the tip diameter and length. These parameters are chosen in relation to the foundation design project and soil stratigraphy. The loads acting on the individual pile influence the dimension of the diameter. The depth of the stable load-bearing sand layer determines the length needed for the pile. On this basis, the selection of the trees in the forest is carried out in 2 steps (Figure 2.6):

- *Step 1:* Identification of straight trees with the requested length, excluding the first 2 m of the trunk at the base.
- *Step 2:* Selection of the tree based on the requested diameter of the tip.
- *Step 3:* Cutting off the tree and debranching.

The wood species used for foundation piles in The Netherlands, mainly involve softwoods such as Scots pine (*Pinus sylvestris*) and European spruce (*Picea abies*) [59],[145]. Spruce is the only softwood species naturally growing and cultivated in the Netherlands. In contrast, pine has to be imported from Germany, Poland, or the Scandinavian countries [76]. Two factors are related to the sourcing areas of the piles, influencing the growth of the trees in the forest: climate and forest management [76],[78],[89]-[91].



Figure 2.6: Selection of a (pine) tree in the forest from which the pile is sourced depending on the tip diameter and pile length.

Warmer climates accelerate tree growth, contributing to increased scatter between head and tip diameters over the length (tapering). For example, Spruce growing in The Netherlands or France features tapering in general around 10-12 mm/m over the pile length [89],[91]. Colder temperatures imply that trees grow slower, resulting in lower

tapering, as in Scandinavian countries, where the tapering of spruce and pine trees is generally equal to 7-8 mm/m [83].

Also, forest management practices play a crucial role in commercial forestry including but not limited to timber piles. Optimal spacing among trees ensures that trees growing in proximity tend to grow straight and tall, while inadequate spacing can result in wider and less straight growth [84],[85]. These also comprise thinning activities, contributing to the optimal growth of the tree, where removing portions of standing trees in the forest results in extra growing space for the remaining ones [86].

In The Netherlands, the political focus on nature conservation and recreation has led to close-to-nature forestry, known as Integrated Forest Management (IFM, in Dutch: *geïntegreerd bosbeheer*) [89]. In IFM, multiple forest functions are pursued in an integrated manner, with a balance between timber production and nature conservation. This favours the utilization of natural processes, emphasizing natural regeneration, mixed timber species, uneven-aged trees, large and small stems, and the avoidance of biocides. However, IFM limits the production of proper timber, as foundation piles. This occurs because trees inherently exhibit diverse heights and irregular spacing in the forest, often leading to the development of less uniformly straight stems.

Contrarily, in countries such as Germany [90], and France [91], IFM is less widespread, and traditional forest management is established as monoculture plantations, where all trees are planted simultaneously at the initial stage. This planting strategy results in a uniform and synchronized growth pattern, typically with the aim of maximizing timber production and quality. The forests are then allowed to mature over a designated period, typically around 100 years, before being completely harvested. This is because, approaching 100 years, the growth rate of the trees decreases, leading to a consequent deceleration in timber production [92]. This clear-cutting practice, where the entire forest is harvested at once after reaching a specific age, offers certain advantages in terms of efficient resource utilization and management. However, it also comes with drawbacks, such as reduced biodiversity, potential soil degradation, and a less resilient ecosystem.

Next to IFM and traditional forest management, a third forestry technique is upcoming in European countries. This technique, called "Forest Development Type" (FDT), features mixed species of trees and a wider variety within the same species of stand structures. Mixed forests imply several positive ecological and economic effects, such as improved soil fertility, increased resistance against pests and warmer temperatures due to global warming [94]. For example, in Germany, mixtures of Scots pine and European beech have already shown positive effects on nutrient availability and humus type [90], [93].

2.4 Structure of softwoods

In this work, the main purpose is to investigate the compressive strength of saturated wooden piles at the level of gross features (macrostructure), on the basis of mechanical testing. The macroscopic analysis of timber piles can be useful to understand and predict the influence of macroscopical characteristics. Microscopical wood features are also taken into account in this research, especially regarding the influence of biodegradation on the material and mechanical properties of historical timber piles. The microscopic analysis allows to examine the wood structure and identify the possible presence of decay.

2.4.1 Cellular structure

The wooden piles used for foundations mainly consist of softwoods. Softwoods originate from conifers (gymnosperms). The species of conifers comprise Norway spruce (*Picea abies*), fir (*Abies*), and pine (*Pinus sylvestris*). These three types comprise the most used wooden pile species in The Netherlands, investigated in this research [3],[33],[36]. All softwoods are characterized by an anisotropic structure, consisting of mainly axial tracheids and ray cells (Figure 2.7). The tracheids are elongated tubular cells (with 3-10 μm thick walls), with variable length between 1-10 mm depending on the species, running in the longitudinal direction of the tree trunk [37],[96]. The tracheids compose almost 90% of the volume of the wood, and they provide mechanical support and water transport along the tree. Spruce and pine also consist of small amounts of parenchyma and epithelial cells, which have both storage and conduction functions [37].

The water transport between adjacent tracheids consists of cavities in the cell walls known as pits, allowing water to flow from cell to cell (Figure 2.7). The ray cells are aligned along the radial direction, and their primary function is the synthesis, storage, and lateral conduction of biochemical substances [37],[96].

The adhesion between the wood cells (tracheids) is provided by their external layer, the middle lamella (ML). Attached to the middle lamella is the primary wall (P) in Figure 2.8. The primary wall of the wood cell is thin and flexible (ca. 0.1 μm) and together with the lamella forms the compound middle lamella. Next to the primary wall is the secondary wall, which consists of 3 layers (S1, S2, and S3) [37],[40] (Figure 2.8). S1 is located between the primary wall and the other two secondary layers. It consists of 5-10% of the total thickness of the cell wall, being the thinnest layer of the secondary wall (0.1–0.35 μm thick). The S2 layer is the thickest in the secondary wall, and it has a crucial role in the mechanical properties of wood. S2 ranges at 1–10 μm and accounts for 75–85% of the total thickness of the cell wall. The last and innermost layer of the secondary wall is S3, ca. 0.5–1.1 μm thick. Finally, in the middle of the wood cell is located a void, called lumen, usually filled with water or air [37],[40].

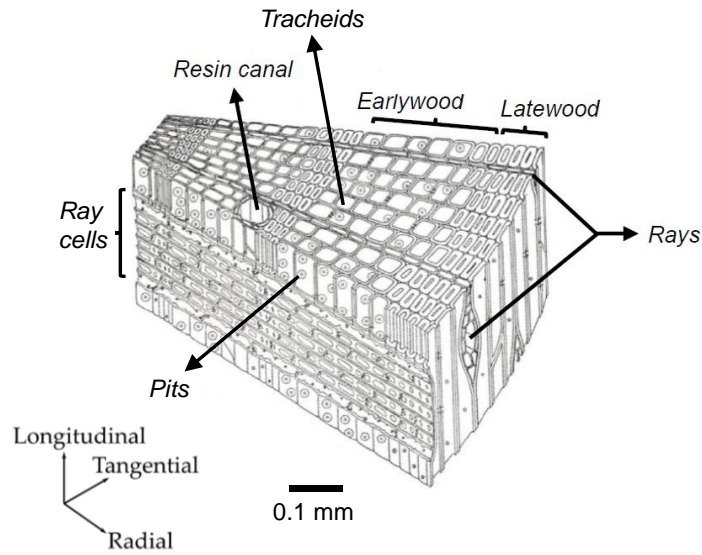


Figure 2.7: Softwood cellular structure (adapted from [38]).

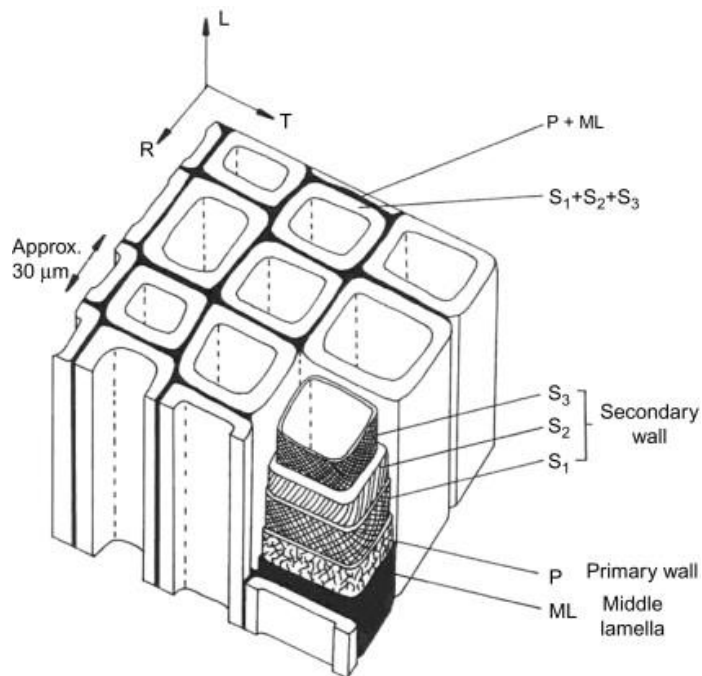


Figure 2.8: Adapted from [40]: Structure of softwood tracheids showing primary and secondary cell walls and orientation of cellulose microfibrils (black lines)

2.4.2 Macro structure

Growth rings

At a cross-sectional level, softwoods present growth increments, associated with a growth transition from the *earlywood* to the *latewood* (Figure 2.9 and Figure 2.10). Each annual ring comprises a combination of both early- and latewood, which can have an abrupt or gradual transition (or even a combination of both) [101]. During the spring, when growth is most rapid, trees produce "earlywood". Earlywood is less dense and consists of large cells with thinner walls (Figure 2.7). This period is succeeded by slower growth, leading to the formation of "latewood", which is characterized by more dense and smaller cells (Figure 2.7). Next to the pith, the gap between growth increments is wider, getting narrower when approaching the external part of the tree's cross section. This is because in the first 10-20 years the young tree grows at a faster speed, gradually decreasing in when getting mature. Growth increments formed annually by softwood species can vary depending on climate conditions and forest environments, as aforementioned in Section 2.3.

The boundaries of the growth increments are called *annual rings* (Figure 2.9b). They can give information regarding: the age of a tree, i.e. total number of annual rings in the cross section; the rate of growth, i.e. the average width of the growth rings over outer 0.75 R, where R is the radius of the pile's cross section (see Figure 2.9a) [37]. The first 0.25 R next to the pith is not considered for measuring the rate of growth, since it represents juvenile wood (Figure 2.10), where the width between growth rings is typically wider.

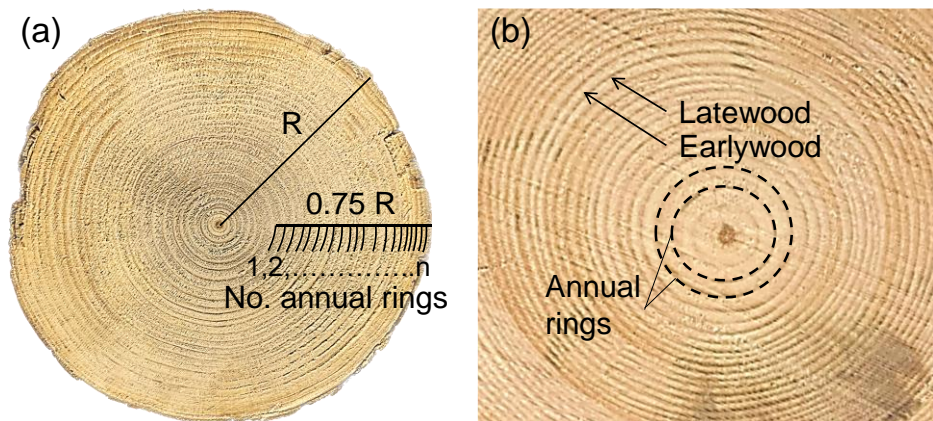


Figure 2.9: Cross-sectional distribution of incremental growth rings (annual rings) in a spruce (*Picea abies*) tree: (a) growth rate calculated over 75% of the radius; (b) latewood and earlywood transition.

Sapwood and heartwood

An important macrostructural feature visible in the cross section of softwoods is the *sapwood-heartwood* distinction (Figure 2.10) [37]. The outer, younger section of a tree stem carries sap upward from the roots to the crown. This part of the trunk is known as sapwood. As the cells in sapwood grow old, they study functioning physiologically generating heartwood, the inner part of the trunk.

Most softwoods present a dark-coloured heartwood and a light-coloured sapwood. However, this is not true for all the softwood species. In pine trunks, a distinct visual transition in the cross-section between heartwood and sapwood can be seen (Figure 2.10a). Meanwhile in spruce and fir, no distinction is visible [75] (Figure 2.10b). As a tree matures and expands in size, there is a notable increase in the proportion of heartwood in the central region of the trunk. This transformation occurs as living sapwood cells gradually transition into an absence of living cells within heartwood, leading to a shift in their functional role.

In both species, heartwood and sapwood can be considered two different materials, where weight, density, hygroscopicity, and permeability of heartwood and sapwood have been reported to differ [101]. In particular, sapwood presents an open wood structure, penetrable to moisture, solvents and air, and vulnerable to biological degradation. This is because sapwood is the living part of the tree, responsible for the transport of water, minerals, extractives and nutrients from the roots to the leaves of the tree [37]-[40]. In contrast, heartwood (the non-living part of the trunk) serves primarily as a structural support for the tree. It is characterized by a lower permeability than sapwood, and therefore less disposed to moisture fluctuations. This makes it more dense and durable than sapwood [96].

However, the resistance of sapwood to moisture and degradation can vary based on the wood species. For example, fir sapwood exhibits better durability to high moisture content compared to spruce and pine, due to a higher amount of natural resin, that creates a natural barrier against water penetration in the wood fibers [97]-[100]. Moreover, the grain distribution of fir is more uniform and tight, minimizing gaps among wood fibers and allowing fir wood to have higher density [97]-[100].

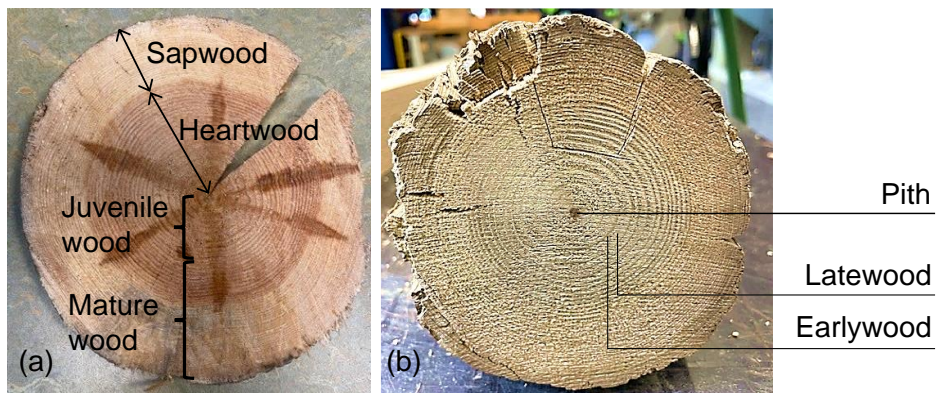


Figure 2.10: Cross-sectional structure of (a) pine (*Pinus sylvestris*) with lighter-coloured sapwood and darker-coloured heartwood; (b) spruce (*Picea abies*) with no apparent heartwood/sapwood boundary.

Juvenile and mature wood

Juvenile wood is the first-formed wood of the young tree, associated with the first 10-15 annual rings starting from the pith (Figure 2.10 and Figure 2.13). It is often characterized by up to 40 % lower stiffness (modulus of elasticity) than mature wood [37],[96], due to

the morphology of its cells, which instead of being long and straight (as mature wood), are often shorter and angled, twisted, or bent [96].

2.4.3 Physical properties

Density

Density is the most important physical property of timber. Most mechanical properties of timber piles are positively correlated to density as is the compressive strength parallel to the fiber [108]. Density is defined as the ratio between the mass (m) and the volume (V) of timber (Equation 2.1) [37].

$$\rho = m / V \quad (2.1)$$

Density is moisture dependent, since water permeates wood cells, adding to the mass and often causing the volume to shrink [37],[96]. Shrinkage occurs when water is penetrating the cell wall layers. When the cell wall is completely saturated, it reaches the point of fibre saturation (u_f). The density of wood at a moisture content u (%) is expressed in Equation 2.2 as:

$$\rho_u = \frac{m_u}{V_u} = \frac{m_{dry}(1+0.01u)}{V_{dry}(1+0.01\beta_v u)} = \rho_0 \frac{1+0.01u}{1+0.01\beta_v u} \quad (2.2)$$

Where m_{dry} , V_{dry} and ρ_{dry} are the mass, volume and density at zero moisture content. ρ_{dry} is defined as oven-dry density of dry density. β_v is the coefficient of volumetric shrinkage and it depends on the wood species. For spruce, fir and pine studied in this research, β_v can be assumed equal to 12% according to [96].

Wood and moisture

The moisture content (MC) is defined as the ratio of the mass of removable water m_{wet} to the dry mass of the wood (m_{dry}) (Equation 2.3). MC is expressed in percentage terms.

$$MC = \frac{m_{wet}}{m_{dry}} * 100 = \frac{m_{wet}-m_{dry}}{m_{dry}} * 100 \quad (2.3)$$

Many studies in literature cover the relationship between mechanical properties of wood with moisture content (MC) ranging from oven-dry material (MC = 0 %) to high degrees of moisture content at and above fiber saturation (30 % to 80 %), summarized in [96]. The term “fiber saturation”, is defined as the water content within wood in the absence of any free water in the cell lumina, the cell walls are saturated with chemically and physically bound water [37]. However, the fiber saturation is not a precise point, but it is defined in [96] as a moisture range that may vary depending on species, portion of sapwood and heartwood, age, type of soil, and moisture conditions.

Although the variability of the fiber saturation range, in textbooks such as [96] and in the European design code Eurocode 5 [18], the transition from the dry to water-saturated status of softwoods (such as spruce, pine, and fir), is assumed in a threshold of MC \approx 25%, after which the strength and stiffness properties of timber do not change anymore (Figure 2.11). In the case of timber foundation piles, mainly comprising softwoods, it was

demonstrated in Kollmann [37] from tests of spruce and fir, that the fiber saturation point ranges at 30-34%.

The findings in [37] suggested that reduction factors related to fiber saturation extend beyond the chosen fiber saturation limit of 22-25%. In addition, it was highlighted in [36] from fits literature data (Figure 2.12), that the moisture modification factor (k_{moist}) of 0.82, provided by the NEN-EN 1995-1-1/NB:2011 might not be appropriate for considering the reduction for the compression strength parallel to the fiber of softwoods in wet conditions. This issue is especially relevant for the design of saturated timber foundation piles that endure high moisture contents throughout their service life.

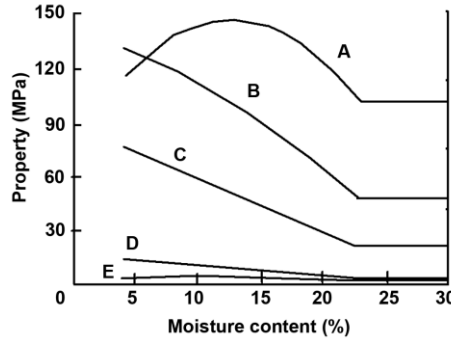


Figure 2.11: Adaptation from [96]: effect of moisture content on the strength properties of defect-free wood. (A) tension parallel to grain; (B) bending; (C) compression parallel to grain; (D) compression perpendicular to grain; (E) tension perpendicular to grain.

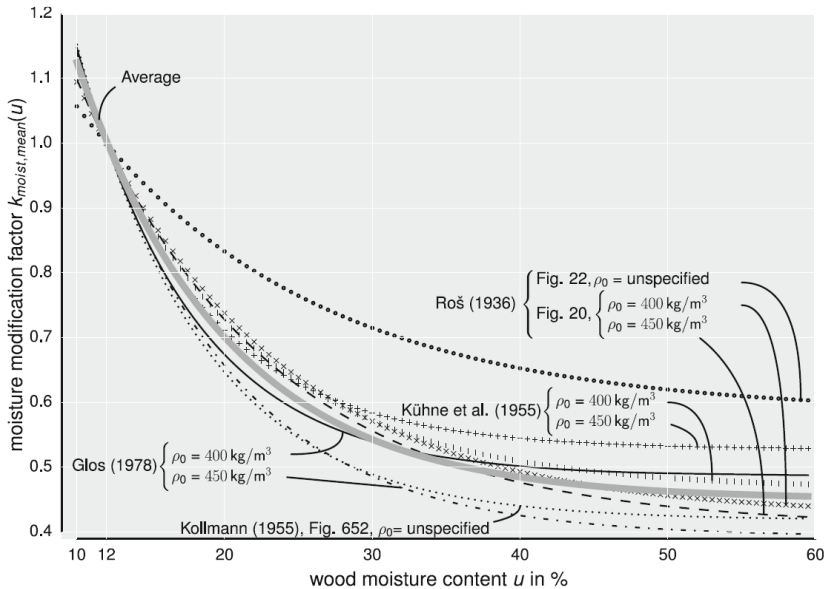


Figure 2.12: Curves for moisture modification factor (k_{moist}) for compression strength parallel to the grain of European spruce (*Picea abies*) and fir (*Abies alba*) derived in [36] from fits to literature data and equations in Kollmann [37], Roš [44], Kühne et al. [45], and Glos [46]. Adaptation from [36].

Variability of properties in timber piles

The varying proportions of heartwood and sapwood along the radial direction of a tree trunk result in distinct density distributions within the trunk's cross-section [106]. However, longitudinal density variations also occur along the trunk [106]-[108]. The longitudinal variation is not only caused by the changing heartwood-to-sapwood distribution from the tree's base to its crown, but also by the variation in the ratio between juvenile wood and mature wood (Figure 2.14). Also, the basic density (the ratio between the oven-dry mass of a wood sample and its wet volume), decreases up to 20-25% from the pith to the outer part of the cross section (from juvenile to mature wood), as studied for radiata pine in [108],[109]. Heartwood often contains all the juvenile wood, particularly at the tip of timber piles, which has lower density and lower strength and stiffness properties compared to the rest of the pile.

The basic density results to be higher in the lower part of the tree and lower in its upper part (Figure 2.14), showing similar basic density in the top parts of the tree, for ages ranging from 10 to 40 years. The basic density increases with the age in the rest of the trunk, due to larger mature wood in the butt log of older trees.

This is a piece of important information for wooden foundation piles, where the density can be different from the head to the tip, resulting in potentially different mechanical behaviour along the length. Notably, the study in [108] has highlighted that the density can be a good parameter for wood compressive strength, and it can vary in relation to larger mature wood content, higher age (related to smaller annual ring width), and lower position in the stem (Figure 2.13). Another important aspect to consider about the investigation of the compressive strength along wooden foundation piles.

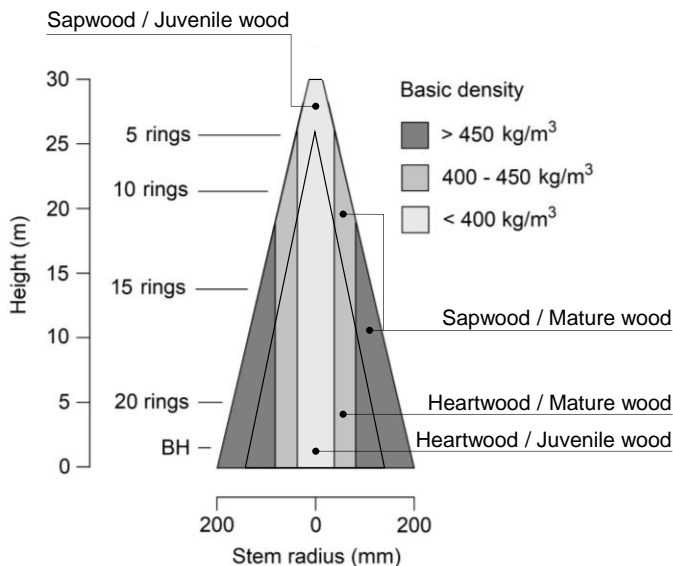


Figure 2.13: Adaptation from [108]. Distribution of sapwood-heartwood and juvenile-mature wood in a tree trunk and variations in extracted basic density within the stem of radiata pine from New Zealand [108]. BH: breast height defined as 1.35m up from the highest point of ground at the tree's base.

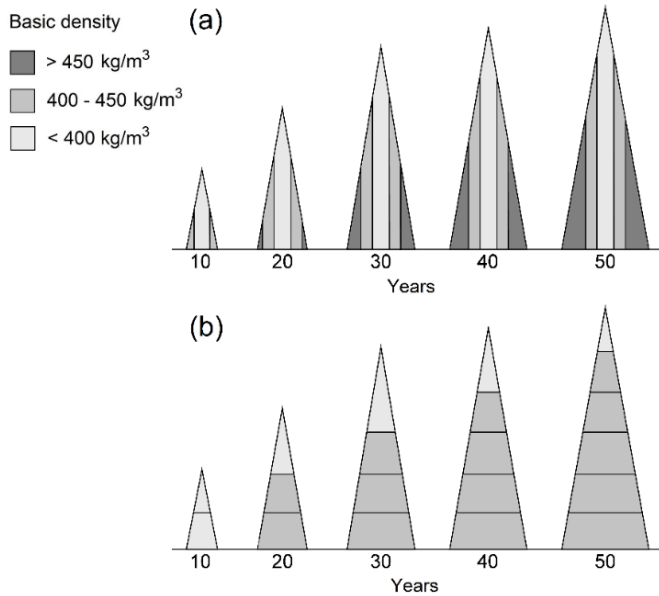


Figure 2.14: Within-tree variations in density for New Zealand radiata pine (Adaptation from [108]). (a) Basic density distribution from 10 to 50 years-old trees. (b) Basic density increases with age since the butt log of an old tree has proportionately more mature wood and higher basic density.

2.4.4 Wood defects

Timber piles are characterized by high variability and heterogeneity of the material, due to specific natural growth characteristics of trees. This results in the presence of defects that can influence the piles' mechanical behaviour, such as knots, compression wood, and slope of the grain (spiral grain), (Figure 2.15).

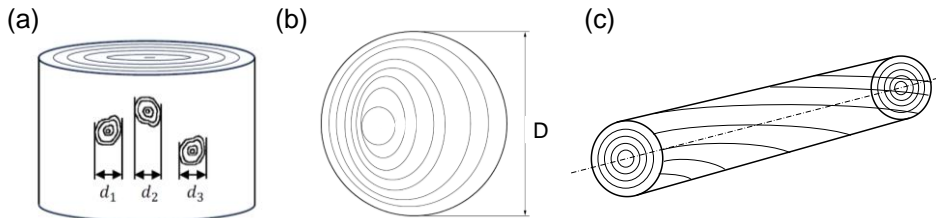


Figure 2.15: Most common wood defects: a) knots; b) compression wood (eccentric pith); c) slope of the grain (spiral grain). Adaptation from NEN-EN 1309-3:2018.

Wood knots

The most common natural defect is knots. A knot is the part of a branch embedded in the log. All knots have their origin in the pith and then progress outwards radially with a slight upward angle to the normal line of the log [101]. Knots can be categorized into two primary types: encased knots and intergrown knots (Figure 2.16), which describe the continuity, or lack, of the trunk wood with the wood of the branch [96]. In cases where the branch remained alive during the formation of the growth rings in the board, there is continuity between the trunk wood and the branch wood, forming an 'encased' knot. If

the branch has died during the growth of the tree, the growth rings continue uninterrupted out along the branch, creating an 'intergrown' knot.

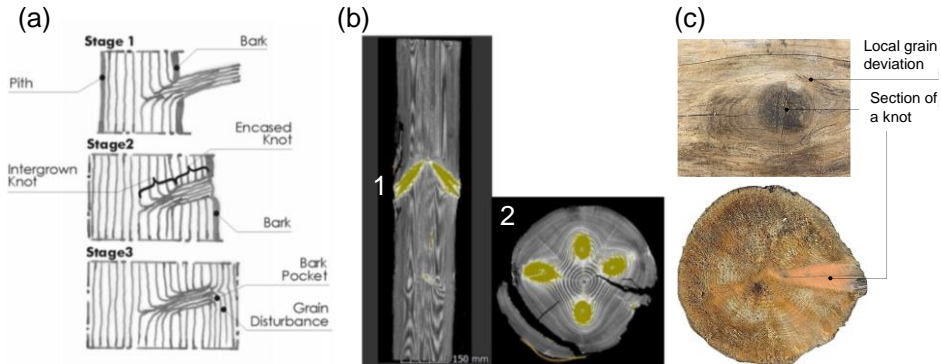


Figure 2.16: a) Overview of the stages of a growing knot (Adaptation from [107]); (b-1) X-ray scan of wood knots occurring in a section of the log, (b-2) an its cross sectional view; (c) Local grain deviation around a wood knot in the direction parallel to the trunk and cross-sectional view of a section of the knot.

In softwoods, such as spruce and pine (Figure 2.18), the branches grow at regular intervals in various directions, approximately at the same height in the log. The zone of the stem where several branches or knots occur at around the same cross section is named 'branch whorls' [112]. Branch whorls interrupt almost knot-free areas along trees [114]. This is illustrated in Figure 2.17, where several branch whorls occur at different intervals along a tip segment of a softwood pile.

The distribution of knots along the tree varies depending on the species. Knot-free areas are usually more common in the lower part of pine trees (Figure 2.18), since fewer and smaller branches are present in this zone, due to the natural development of the crown on the upper part of the tree.



Figure 2.17: Example of knots occurring at intervals along the length (4 meters) of a tip segment of a softwood pile.

However, spruce and fir trees present knots along their whole length, since the tree crown is evenly distributed along the tree (See Figure 2.18). Knots can occur in different sizes and numbers depending on the environmental conditions in which the tree grows, such as soil, climate, location, altitude, etc. [76],[77]. Notably, pine and spruce trees tend to have larger knots, when growing in warmer conditions [76],[77]. Larger spacing among the trees can also contribute to larger knots, since the trees are more prone to grow wider rather than taller, with consequent thicker and more frequent branches [116].

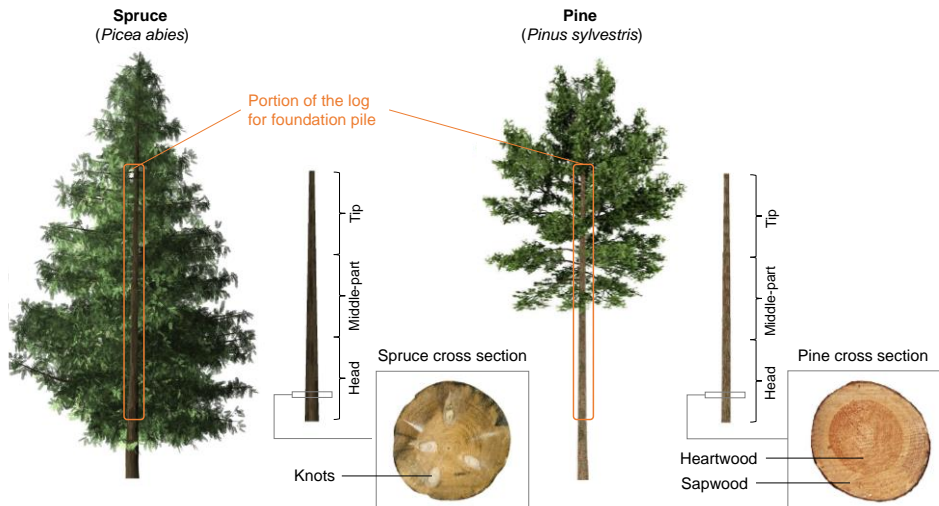


Figure 2.18: Wooden pile extracted from spruce and pine trees; distribution of the crown and cross section.

Knots result to have a large influence on the mechanical properties of wood, reducing the compressive strength parallel to the grain [73], [115], [116]. The density of a knot in softwoods is roughly twice the density of a free-knot area [110],[114], which can imply different stress distribution in the pile's cross section.

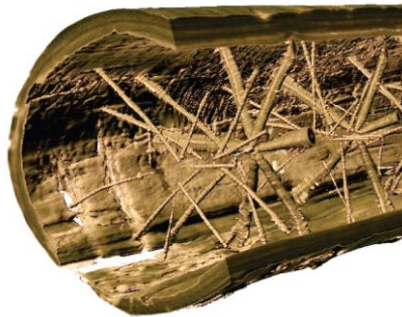


Figure 2.19: Result from a CT scan of a log with knots originating from the pith from [113].

In the case of a wooden pile subjected to axial load during its service life, the presence of knots can be governing for the capacity of the pile [58]-[69], [73]. This is because the grain deviation caused by a knot implies that the fibres in and immediately around the knot are oriented in the direction perpendicular to the axial direction of the tree (Figure 2.20). This has also an impact on the stiffness of wood around knots, where the modulus of elasticity perpendicular to the grain of the pile is 30 times smaller than that parallel to the grain ($E_{c,90} = 1/30 E_{c,0}$), EN 338 (2016) [125]. Thus, when a compression load is applied in the axial direction of a pile, only a very small amount of the load is taken up by the knots, since the stress flow follows the wood fibre around the knots (Figure 2.20), where the inclination of the wood fibres imply a lower modulus of elasticity. However, the effect of

wood knots on the strength and stiffness of wooden piles has not been widely studied and it is not easy to quantify, since it depends on the size, number, and distribution of knots.

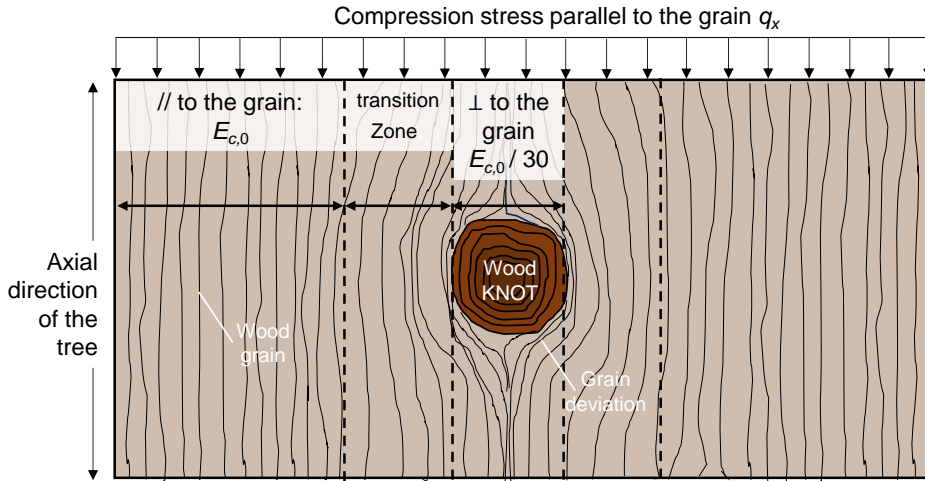


Figure 2.20: representation of a section of a timber pile with a knot and grain deviation around it.

In order to quantify the effect of knots on the compressive strength and stiffness of a timber pile, a knot ratio (KR) is commonly used (i.e. the ratio between the sum of the knot diameters perpendicular to the longitudinal axis of the log, over a 150 mm length, and the circumference of the log in that section) to account for the presence of knots according to the Dutch grading standard NEN 5491 (2010) [20]. The provisions given in NEN 5491 are based on experimental analysis of saturated round wood (van de Kuilen [33]), and provide a threshold of $KR = 0.5$. Even if no correlation was found in [33] between KR and the saturated compressive strength, and given that no piles with a KR greater than 0.5 were tested, a boundary ($KR = 0.5$) was established. However, given the limited dataset in [33], further research needs to be conducted on the relationship between KR and saturated compressive strength.

Compression wood

When a tree is subjected to mechanical stress or environmental factors, such as gravity, wind, or uneven growth conditions, the woody tissues produce reaction wood (Figure 2.21). In softwoods, reaction wood is referred to as compression wood [37]. It develops on the underside of branches (Figure 2.21a), but also underside of leaning trees and on the leeward side of trees that can be bent by wind forces (Figure 2.21c), or forced out of their normal growth pattern due to environmental/induced alterations [101]. Compression wood in piles can be identified by the presence of eccentric growth rings and a more gradual shift from earlywood to latewood, which differs from the sharper contrast seen in normal wood (Figure 2.21b).

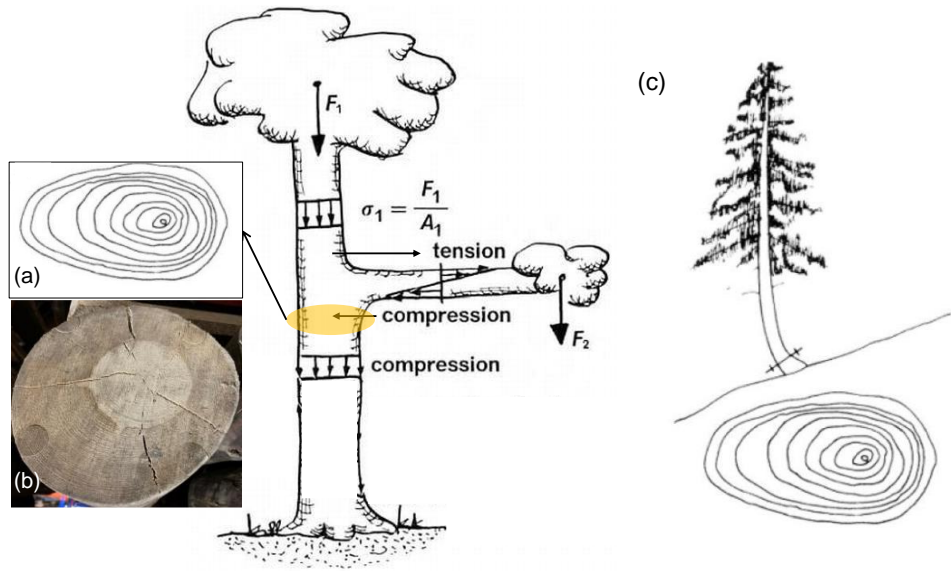


Figure 2.21: (a) Compression wood generating under a branch of a softwood tree (Adaptation from [39]), cross-sectional sketch of compression wood; (b) eccentric portion of stem cross section in pine (*Pinus sylvestris*); (c) compression wood generating in a softwood tree by a non-vertical orientation of the trunk (Adaptation from [38]).

A significant presence of compression wood within a timber pile is generally seen as unfavorable for any structural application. This is because the density of compression wood can be 20% to 40% higher than 'normal wood', generating an unbalanced distribution of density within the cross section and longitudinally along the wooden pile [101],[106],[117],[118]. This can result in an uneven stress distribution in an axially loaded pile with compression wood, leading to poorer mechanical behaviors.

Slope of grain

Grain deviation can occur in a tree due to irregularities in grain patterns developed during the tree's growth [119]. Spiral grains can be caused by winding or spiral growth of wood fibers within the trunk, deviating from vertical growth. Spiral grains lie in the tangential plane of the growth rings, rather than parallel to the longitudinal axis of the timber pile [96],[120]. In particular, this happens when factors such as wind and phototropism (orientation of a tree in response to light) influence the tree growth, generating spiral grain.

In literature, the mechanical properties of small wood samples with various grain slopes were studied [96]. Table 2.1 shows that the wood compressive strength parallel to the grain remained unaltered under a threshold of the slope of the grain (SoG) equal to a ratio of 1:10 ($\alpha = 5.7^\circ$). This value is also considered the current highest acceptable value for strength grading for round wood according to the prEN 1995-1-1/NB/2023.

2.4 Structure of softwoods

Table 2.1: Strength of wood members with various grain slopes compared with strength of a straight-grained member (Impact bending is height of drop causing complete failure (22.7-kg hammer); compression parallel to grain is maximum crushing strength. Adaptation from [96].

Maximum slope of grain in member		Modulus of rupture	Impact bending	Compression parallel to grain
Ratio	Degrees	%	%	%
Straight-grained	0°	100	100	100
1 in 25	2.3°	96	95	100
1 in 20	2.8°	93	90	100
1 in 15	3.8°	89	81	100
1 in 10	5.7°	81	62	99
1 in 5	11.4°	55	36	93

2.5 Mechanical properties of timber piles

The mechanical properties of timber piles are dependent on moisture content [37]. Since timber foundation piles are only used in saturated conditions, high moisture levels result in lower compressive strength and stiffness parallel to the grain [96],[101],[106]. This effect is explained by two reasons: when the water penetrates the wood cell walls weakens the hydrogen bonds responsible for holding together the cell wall (See Paragraph 2.4.1 and 2.4.3). Moreover, the cell walls swell, resulting in less cell wall material available per unit [37],[106].

In this context, the saturated mechanical properties of timber piles have not been widely studied in the literature, and little or no design guidance can be found in design standards. The literature available is not fully comprehensive for a correct design or assessment of timber piles, since it is based on a limited database, without providing grading boundaries and strength parameters spanning from the head to the tip of the pile.

Currently, the design standards [19] for timber piles are based on one “dry” (MC = 12%) characteristic compressive strength value ($f_{c,0,k,dry}$) applicable to all softwood piles, without differentiating strength classes or grading criteria. The saturated compressive strength (effect of high moisture contents) is calculated from $f_{c,0,k,dry}$ with reduction factors (k_{mod}) from the Dutch code NEN 6760 [127]. The k_{mod} -factors were calculated on the basis of edgewise bending tests of timber boards, which may have different behaviour in compression and bending than round wood as timber piles.

Thus, in order to enable engineers to adequately design timber foundation piles, reliable saturated mechanical properties and grading specifications are required. These aspects have to be considered alongside the fact that wooden foundation piles used under buildings, bridges and quay walls, remain submerged under the water table for their whole service life, enduring high moisture levels.

In this Section, the available saturated mechanical properties of wooden piles from literature and European design codes are presented, highlighting the knowledge gaps that pose a significant challenge in the design of wooden foundation piles.

2.5.1 Overview of the literature review on saturated compressive strength of timber piles

The literature available regarding the saturated compressive strength of timber piles is limited to three main research studies which investigated different aspects:

- a) (Paragraph 2.5.2): The saturated compressive strength of 57 spruce, 20 larch, and 18 Douglas fir full-scale piles was determined in saturated conditions in 1982 [32], with full-scale compression tests. This represented the only large-scale experimental campaign conducted in Europe to characterize the saturated compressive strength of softwood piles. However, the database was too limited to determine reliable values for the saturated compressive strength and making potential distinction in multiple strength classes. Only the knot ratio of the piles was measured, but the other physical properties (density, age, rate of growth,

slope of the grain, etc.) were not reported. No correlation between knot ratio and saturated compressive strength was found. The data was subsequently analysed in 1994 [33], where wet characteristic compression strength values were derived based on the test data in [32]. The values derived in the statistical analysis in [33] were standardized for the first time in 1997 in the Dutch design code for Timber Structures NEN 6760 1997 [147].

- b) (Paragraph 2.5.3) The distribution of saturated mechanical properties along the length of full-size American Douglas fir and Southern pine were characterized in 1968 [59] in the United States. This research highlighted the high variability of the saturated compressive strength from the head to the tip of 30 southern pine and 30 Douglas fir piles, characterized by means of full-scale compression tests. It also highlighted that the variability in the saturated compressive strength is related to growth characteristics of the piles (such as number and size of knots, and number of annual rings).
- c) (Paragraph 2.5.4): The influence of moisture content on the compressive strength was studied in [36] (2016), where 17 dry and 17 saturated spruce piles were characterized by means of full-scale compression tests. To account for the compressive strength of timber piles from dry to wet conditions, a reduction factor of $k_{\text{moist}} = 0.65$ was experimentally derived. This research revealed that the $k_{\text{mod}} = 0.82$ provided in the standards [19] is not adequate to account for the effect of high moisture content on the dry compressive strength of saturated timber piles.

Table 2.2 presents an overview of the three main research studies conducted in literature to characterize of the saturated compressive strength of timber foundation piles. The results are presented and discussed in detail in the following paragraphs.

Table 2.2: Mechanical properties in compression parallel to the grain in wet (MC > 30%) conditions for round spruce (*Picea abies*), Douglas fir (*Abies alba*), larch (*Larix decidua*) and southern pine reported in literature (Van de Kuilen 1994 [33]; Aicher 2016 [36], Wilkinson 1968 [59]).

Category	Reference	Dry (MC \approx 12%)							Wet (MC > 30%)						
		Diameter (mm)		No.	$E_{c,0}$ (GPa)		$f_{c,0}$ (MPa)		No.	$E_{c,0,wet}$ (GPa)	$f_{c,0,wet}$ (MPa)		$f_{c,0,k,wet}$ (MPa)		
		mean	SD	-	mean	SD	mean		SD	-	mean	SD	mean	SD	$\times 0.5$
Southern pine heads and tips (treated and steam-conditioned)	Wilkinson (1968) [59]	260	-	-	-	-	-	-	-	30	10.0	-	16.4	4.3	8.4
Treated southern pine – saturated – (1 to 6)	Wilkinson (1968) [59]	250	15	-	-	-	-	-	-	30	11.7	1.8	26.7	3.0	21.2
Spruce	Van de Kuilen (1994) [33]	113	28	-	-	-	-	-	-	57	-	-	20.0	2.2	16.3
	Aicher (2016) [36]	200	-	17	12.1	1.9	30.8 ($f_{c,0,k} = 20.3$)	6.1	17	10.7	1.6	17.6	2.3	13.4	
Douglas fir	Van de Kuilen (1994) [33]	148	22	-	-	-	-	-	-	16	-	-	21.8	1.7	18.4
Douglas fir heads and tips (treated and steam-conditioned)	Wilkinson (1968) [59]	265	-	-	-	-	-	-	-	30	13.5	-	22.6	3.9	15.4
Larch	Van de Kuilen (1994) [33]	141	26	-	-	-	-	-	-	19	-	-	22.9	2.9	17.1

2.5.2 Saturated compressive strength

In 1982, the initial step in assessing the mechanical properties of saturated timber piles was carried out in Buiten and Rijdsdijk [32], where axial compression tests parallel to the grain were performed on 95 wet, debarked, full-scale pile segments. More specifically, wet compressive strength values ($f_{c,0,wet}$) were determined for 57 European spruce (*Picea abies*), 18 Douglas fir (*Pseudotsuga menziesii*), and 20 larch (*Larix decidua*) piles, with an average diameter of 140 mm, a length of 900 mm (ratio 1:6:4, close to 1:6 in accordance with EN 408 2010 [122] and EN 14251 2003 [124]). The piles were fully saturated, with an average moisture content (MC) of 100% at the moment of the test.

Based on these data, a statistical analysis was subsequently conducted in [33], from which the characteristic wet compressive strength parallel to the grain was derived (See Table 2.2). Depending on the grade requirements (listed at the time in NEN 5491 1999 [20]), which provided limits of 50 mm for the biggest knot, and 0.5 for KR, 37 out of 95 specimens were excluded from strength grading in [33], leaving 58 standardized specimens. The results of all samples and standardized samples (58) are shown in Table 2. 3.

Table 2. 3: Mean wet compressive strength ($f_{c,0,wet,mean}$) and standard deviation (SD) of all the 95 timber piles tested in compression and 58/95 timber piles complying with grade requirements in NEN 5491 2010. Average MC = 100%. Adaptation from [32].

Wood species	All 95 timber piles			58 standardized timber piles according to NEN 5491		
	No.	$f_{c,0,wet,mean}$	SD	No.	$f_{c,0,wet,mean}$	SD
Larch	20	24.0	3.9	13	24.8	2.9
Douglas fir	18	22.9	2.8	17	22.5	2.1
Spruce	57	20.0	2.2	28	20.0	2.3

The difference in saturated compressive strength values among the three wood species was not large enough for strength sorting by wood species, given the limited number of larch and Douglas fir piles. Furthermore, in order to prevent the batch of spruce piles from being assigned to a too high strength value, the characteristic value was derived based only on the saturated compressive strength ($f_{c,0,mean,wet}$) of the 57 spruce piles. Thus, from $f_{c,0,mean,wet} = 20 \pm 2.2$ MPa of the 57 spruce piles, a corresponding characteristic wet compressive strength, $f_{c,0,k,wet} = 16.3$ MPa, was derived in [33]. $f_{c,0,k,wet} = 16.3$ MPa served as a basis to standardize the design and the 'dry' compressive strength for a single wooden pile ($f_{c,0,rep} = 19.8$ MPa) by applying a combination of $k_{mod} = 0.85/0.7$ for short term strength in dry/wet conditions, respectively (Paragraph 2.5.5).

The report did not specify the location within the tree from which the 900-mm piles were extracted. Based on the average diameter of 140 mm, an assumption can be made that the 900-mm-piles were extracted from the tip of the tree trunk used as foundation pile, as this dimension is close to the minimum diameter of 150 mm typically associated with the pile tips used in practical foundation pile applications (Section 2.3). However, important parameters for the wood quality, such as rate of growth and age of the piles, were not

provided. The knot ratio (KR) of the piles was measured between 0.2 and 0.6. Differently from the literature [34],[35],[59], the expected correlation between $f_{c,0,wet}$ and KR of the piles was not found (Figure 2.22a). A very weak correlation was also found between $f_{c,0,wet}$ and the diameter (Figure 2.22b). The modulus of elasticity and density were not measured.

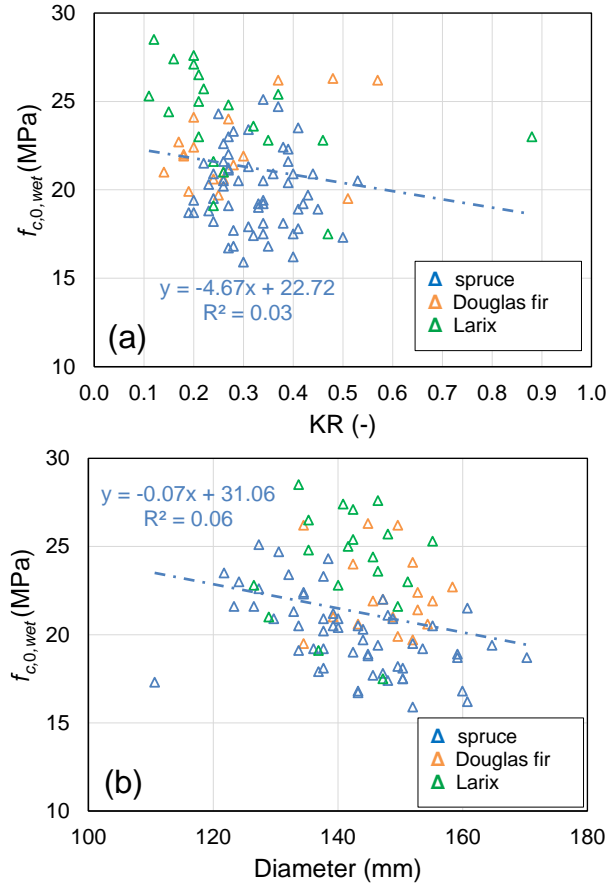


Figure 2.22: Very weak correlation found in [33] between the saturated compressive strength and (a) KR; (b) Diameter of spruce, Douglas fir, and larch piles.

2.5.3 Variability of the saturated strength properties along timber piles

The research conducted by the U.S. Department of Agriculture in 1968 [59] involved axial mechanical testing of 900-mm segments extracted from the head and the tip of 15-m-long southern pine and 15-m-long Douglas fir piles, with average tip diameters of 195-220 mm, and head diameter of 300-330 mm, tested according to the standard ASTM D198-67 (1967) [60]. These piles were meant to be used as marine piles. Thus, prior to testing, all the piles were subjected to steam conditioning to soften the outer fibers and allow penetration of the creosote. This conditioning has been reported to reduce the strength properties of southern pine [59]. The sapwood was completely penetrated in both southern pine and Douglas fir piles. Based on this, the strength properties reported in this study might not be fully representative for untreated wooden foundation piles.

It is important to note that in the literature, controversial findings are reported on the influence of preservative treatment on timber piles. In [63], preservative treatment with creosote revealed to have no chemical influence that would affect the strength of wood. From tests of Douglas fir and southern pine full- and small-sized marine piles treated with preservatives according to the American standards [65], [66], it was demonstrated in [62], that the compression strength and stiffness parallel to the grain were not affected in either species by preservative treatment including creosote. Contrarily, significant reductions in mechanical properties may be observed if the treating processes is not controlled within acceptable limits [63]. Also the Eurocode 5 [18] reports that preservative treatment may affect the strength and stiffness properties; no indications are given on the treating process.

The compressive strength parallel to the fiber was calculated from the maximum force reached in compression. Figure 2.23 shows the position within the pile of all the tested piles, including the discs extracted for the moisture content determination by oven-drying (See Paragraph 2.4.3).

All samples had a moisture content above fiber saturation at the test time ($MC > 59\%$). The specific gravity was determined from the oven-dry weight and green volume of the specimens. The Douglas-fir and southern pine piles were debarked and had an average tapering of 7-10 mm/m. All piles met the requirements for straightness according to ASTM Standard D 25-58 [67].

All knots were measured, and the calculated KR (i.e. the ratio between the sum of the knot diameters perpendicular to the longitudinal axis of the log, over a 150 mm length, and the circumference of the log in that section) ranged at 0.08-0.48. The annual rings, from the pith to the bark were also measured (See Paragraph 2.4.2).

The piles were also examined for spiral grain, with neglectable values that were considered to have no effect on the mechanical properties of the piles.

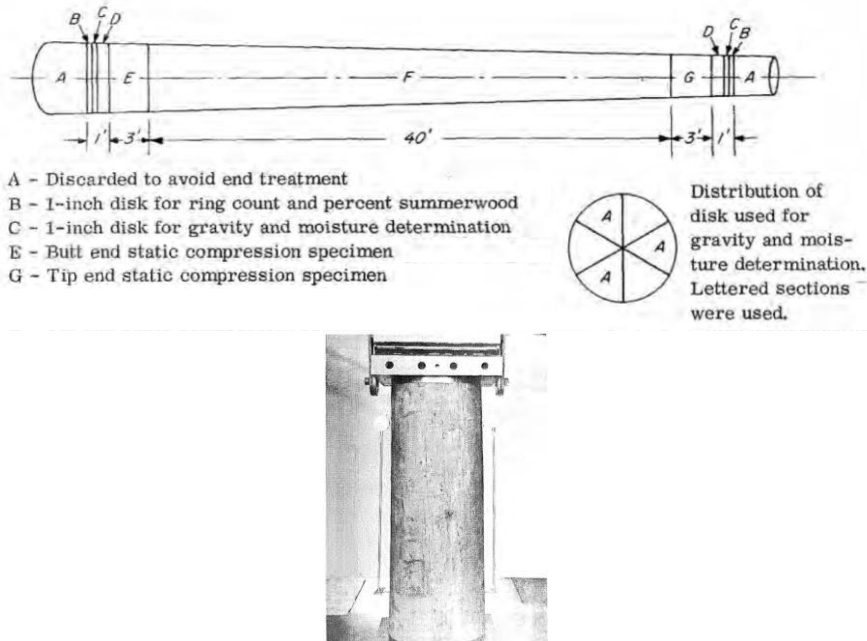


Figure 2.23. Cutting scheme and compression tests performed on 900-mm-samples (Adapted from [59]). The dimensions of the pile-parts are in inches.

The results of saturated mean static modulus of elasticity $E_{c,0,wet,mean}$, compressive strength $f_{c,0,wet,mean}$, specific gravity, and moisture content (MC) determined for the 900-mm-segments extracted from the head and tip of the 15-m-piles, are shown in Table 2.4.

A significant difference between the mechanical properties of the head and tip of the pile was found. In particular, the compressive strength decreased up to 40% from head to tip in southern pine. The lower strength values in the southern pine were possibly attributed to the steam-conditioning to which piles were subjected for 15 hours at 245° F (118 °C). However, the influence of this was not proven in [59].

Considering all the tested pile-segments, the variability of the mechanical properties from head to tip was attributed to the different specific gravity values between the head and tip (Table 2.4). Also KR resulted to be correlated with the $f_{c,0,wet}$ (Figure 2.24a) differently from [33] where a very weak correlation was found. Unfortunately, KR was not measured specifically for tips and heads, but only the maximum KR value and position were reported along the pile. Based on the position of the maximum KR, it was then associated with head or tip in Figure 2.24a. However, in most of the cases, the KR values were associated to tips, both because of the higher number and larger size of knots compared to the rest of the pile, which possibly contributed to the lower compressive strength of the 900-mm pile segments. Further research needs to be conducted to investigate this correlation. The saturated compressive strength was moderately correlated with the

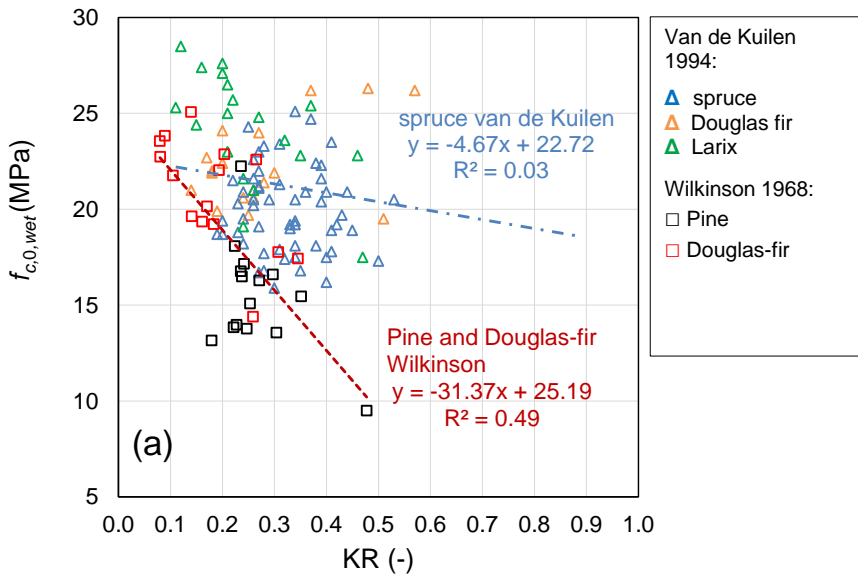
diameter, with a clear distinction between head and tips in both southern pine and Douglas-fir (Figure 2.24b).

The good correlation between $f_{c,0,wet}$ and the number of annual rings (age) was shown in Figure 2.25a, suggesting that independently from head and tip, the age of the pile may be a good indicator for the compressive strength, since older trees have intrinsic higher density, increasing from the top to the butt of the tree (Paragraph 2.4.3). This was applicable to the individual pile, where the specific gravity of the tip was always lower than the head. However, when looking at the whole dataset, a very weak correlation was found between $f_{c,0,wet}$ and specific gravity (Figure 2.25b).

Finally, a strong correlation was found between $f_{c,0,wet}$ and the saturated modulus of elasticity ($E_{c,0,wet}$) in Figure 2.26, indicating that this parameter may be useful to predict the saturated compressive strength of the piles.

Table 2.4: Mean mechanical properties of treated 900-mm-piles loaded statically in [59].

Wood species	30 large-scale 900-mm-piles (15 head-sections + 15 tip-sections)									
	Diameter mean (mm)		$E_{c,0,wet,mean}$ (MPa)		$f_{c,0,wet,mean}$ (MPa)		Specific gravity mean (kg/m ³)		MC mean (%)	
	Head	Tip	Head	Tip	Head	Tip	Head	Tip	Head	Tip
Douglas fir	312	222	15200	11800	24.7	20.4	510	470	59	74
Southern pine	328	195	12500	7600	20.3	12.5	530	480	93	100



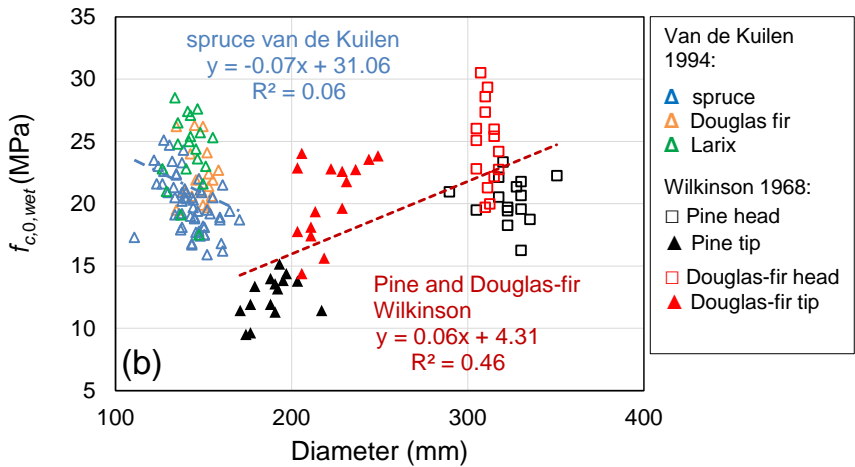


Figure 2.24: Correlation between wet compressive strength ($f_{c,0,wet}$) and (a) KR; (b) Diameter for 900-mm heads and tips of treated southern pine and Dougals fir tested in [59] superimposed with the results in [33].

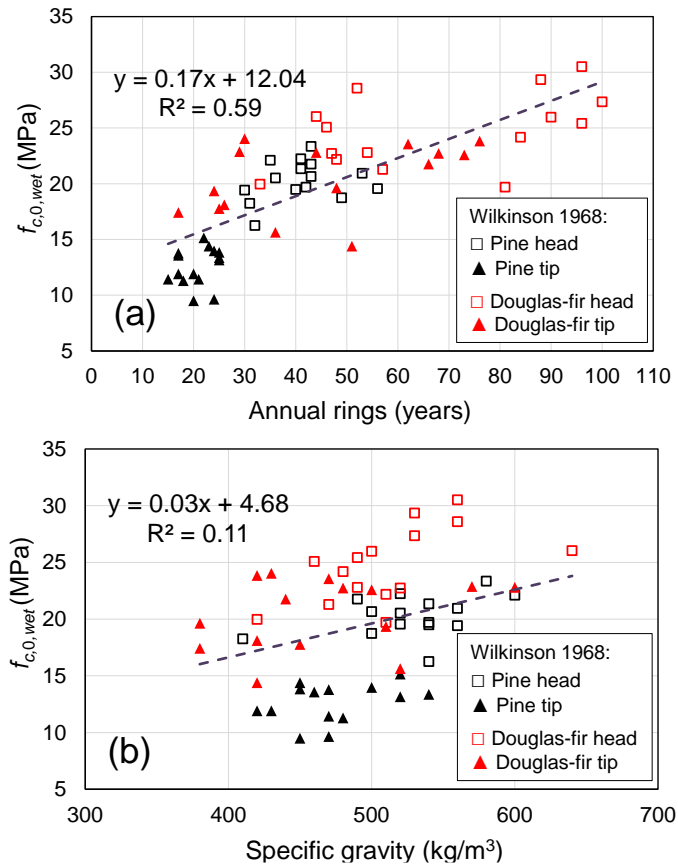


Figure 2.25: Correlation between wet compressive strength ($f_{c,0,wet}$) and (a) number of annual rings; (b) Specific gravity for heads and tips of treated southern pine and Dougals fir tested in [59].

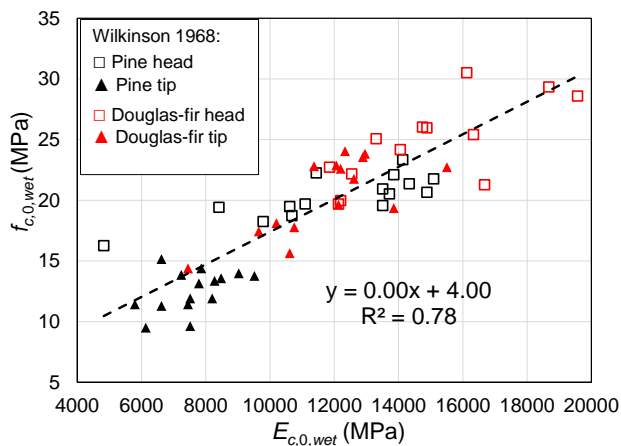


Figure 2.26: Correlation between wet compressive strength ($f_{c,0,wet}$) and modulus of elasticity ($E_{c,0,wet}$) for heads and tips of treated southern pine and Dougals fir tested in [59].

The second part of the research outlined in [59] investigated the mechanical properties of saturated 1500-mm-pile segments extracted along the length of 15 southern pile piles. The full-length piles were approximately 9-m long. However, these piles were not steam-conditioned, but dried to a MC = 23-24 % and then treated with creosote. This was done to study the impact of steam conditioning on the mechanical properties. For the interest of this thesis, only the trend of the mechanical properties along the length of the piles was considered relevant. Therefore, the mechanical properties reported for these piles might not be fully representative of untreated wooden foundation piles.

The saturated compression strength was determined all along the length of the southern pine piles. A total of 30 pile-sections were extracted according to Figure 2.27 from 1 (tip) to 6 (head). The fully saturated piles were kept submerged in water for 30 days, assuming a moisture content above fiber saturation. However, the precise moisture content values were not reported. The KR_s were not reported per pile but only the overall maximum KR_s = 0.25 was mentioned.

In addition to this, 30 declared “kiln-dried” and 30 “kiln-dried and treated” (with creosote) pile segments were also extracted from the piles. The “kiln-dried” piles had an average MC = 24%, and the “kiln-dried and treated” a MC = 23%. The “kiln-dried” piles were not tested at dry conditions (MC = 0%) or the standardized MC = 12%. Therefore, it is important to note that the term kiln-dried in [59] refers to moisture contents at 23-24%, almost at the threshold of fully saturated status (See Paragraph 2.4.3).

The overall distribution of the mechanical properties along the tested piles (1 to 6) is shown in Table 2.5. The results provide good insight into the variability of the mechanical properties along the pile, showing up to 20% lower strength and stiffness from the head to the tip (Figure 2.28). The tip (part 1) showed slightly higher $f_{c,0,wet}$ than the adjacent part 2; however, a high standard deviation was associated with tips.

The moisture content of the kiln-dried and kiln-dried and treated piles ranged from 23-24%, close to the fiber saturation point according to [96]. No significant difference was found between the average mechanical properties of “kiln-dried and treated” and saturated pile sections. However, the effect of treatment with creosote was not clearly investigated. On the other hand, the mechanical properties of the “kiln-dried” piles revealed to be up to 20% lower than the saturated pile sections, for similar density and diameters. The reduction in strength of kiln-dried piles was attributed in [59] to the kiln-drying process or to the natural variability of the mechanical properties from segment to segment related to possible higher KR_s. However, the results remain unclear.

For the interest of this study, it is important to notice that the timber piles exhibit a variability of the mechanical properties from head to tip. The tip is especially critical as it can feature the lowest mechanical properties. Thus, depending on soil conditions, the tip of a wooden foundation pile corresponds to the critical cross section of the pile during service, primarily due to the high stresses associated with its smaller cross section.

2.5 Mechanical properties of timber piles

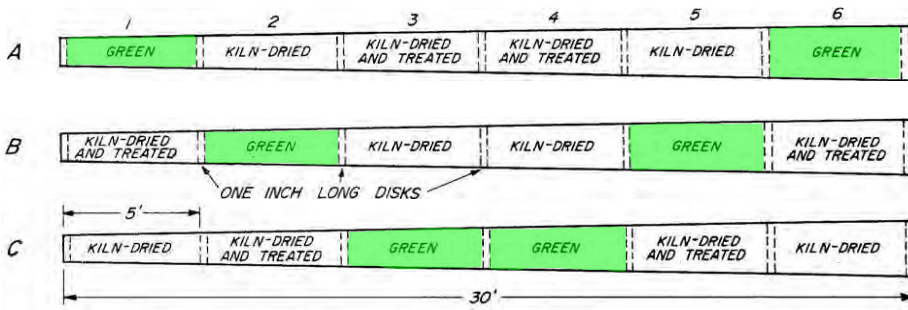


Figure 2.27: Cutting scheme of green (fully saturated) 1500-mm-long pile sections extracted along southern pine piles with full-length of ca. 9 m. Adaptation from [59].

Table 2.5: Distribution of the mechanical properties for saturated 1500-mm-pile sections tested in compression in [59], extracted along 9-m-long southern pine piles from head (6) to tip (1) according to the cutting scheme in Figure 2.27.

Large-scale saturated 1500-mm-piles										
Southern pine parts	No.	Category	$E_{c,0,wet}$ (MPa)		$f_{c,0,wet}$ (MPa)		Specific gravity (kg/m ³)		Diameter (mm)	
			mean	SD	mean	SD	mean	SD	mean	SD
All parts (1 to 6)	30	Saturated	11700	2052	26.7	3.0	540	40	250	26
All parts (1 to 6)	30	K-D	11400	1779	23.7	2.6	540	33	250	24
All parts (1 to 6)	30	K-D treated	11500	1833	27.2	3.2	540	35	250	26
6 (head)	5	Saturated	13100	1374	29.8	1.9	590	28	270	9
5	5	Saturated	12600	2070	28.7	2.3	550	34	268	16
4	5	Saturated	12600	2362	27.2	1.9	540	29	259	19
3	5	Saturated	11800	2122	26.1	1.8	530	31	254	27
2	5	Saturated	9900	1588	23.8	1.8	500	42	228	11
1 (tip)	5	Saturated	10400	1035	24.6	3.3	520	35	212	9

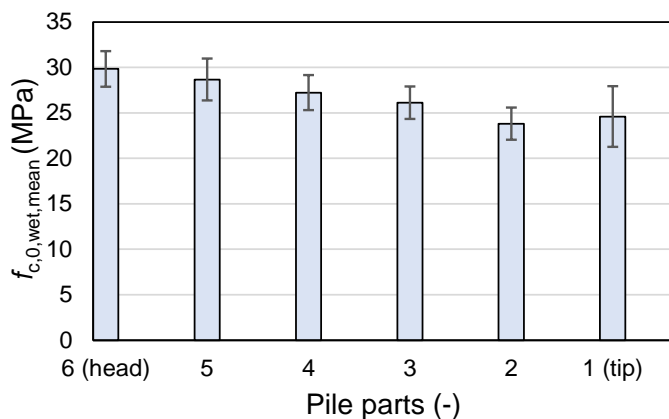


Figure 2.28: Visual distribution of the saturated compressive strength along 9-m-long southern pine piles. The bars represent the average values, the lines show the standard deviation.

2.5.4 Influence of moisture content on the compressive strength

In order to study the effect of high moisture contents on the compressive strength of timber piles, the compressive strength of 17 saturated and 17 dry spruce piles was determined by means of full-scale compression tests in Aicher [36] (Figure 2.29). The saturated piles were tested with an average MC = 89%.

The piles had an average mid-length diameter of 197 mm and a length of 6 times the smallest diameter of the conical log sections in accordance with EN 408 (2010) and EN 14251 (2003). The grade of the log segments complied with NEN 5491 (2016), with maximum knot diameters of 19 mm to 42 mm and knot area ratios of 0.11 to 0.31. The full results are shown in Table 2.2..

From the dry and wet compressive strength (on the 5% quantile level), a reduction factor $k_{moist} = 0.65$ was derived, confirming the findings in Kollmann [37], who suggested that reduction factors related to fiber saturation extend beyond the chosen fiber saturation limit of MC \approx 25% (See also Paragraph 2.4.3). This showed that the moisture modification factor of 0.82, provided by the NEN-EN 1995-1-1 NB (2011) for converting from dry to wet compressive strength, is not appropriate for considering the reduction of the compression strength of spruce in wet conditions.

This highlights the need for compressive strength values in saturated conditions, or, when not available, adequate moisture modification factors should be adopted, such as $k_{moist} = 0.65$ derived in [36].

Furthermore, it suggests that the k_{mod} factors, defined on the basis of edgewise bending tests of timber boards, are not adequate for timber piles.

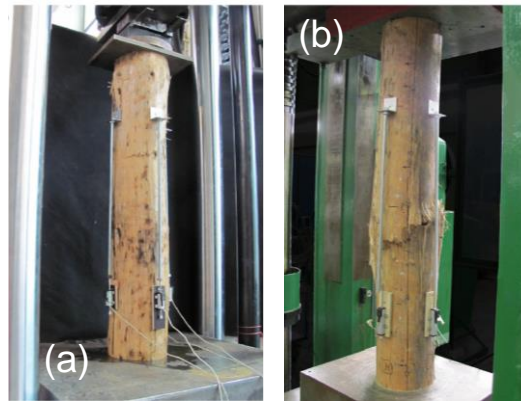


Figure 2.29: Full-scale compression tests on (a) saturated spruce pile; (b) dry spruce pile (Adaptation from [36]).

2.5.5 Design codes

In this paragraph, an overview of the design codes for timber foundation piles is given, explaining the problems related to design values and calculation methods provided in the standards. The new approach given in the new Eurocode 5 2023 is presented, as a basis for the new European design of timber piles used only in saturated conditions.

The first inclusion of compressive strength values for timber piles was reported in the Dutch design code for Timber Structures NEN 6760:1997 [127], with a declared ‘dry’ characteristic compressive strength value for a single wooden pile $f_{c,0,rep} = 19.8$ MPa (at 12% moisture content). This value was derived from the statistical analysis in [33] (See Paragraph 2.5.2), based on compression tests carried out for saturated European spruce, Douglas fir, and larch piles.

The mentioned characteristic value $f_{c,0,rep}$ was recalculated from wet to dry with the k_{mod} values from the Dutch code NEN 6760 with Equation 2.5, aligning it with the design practice, where the verification starts from the material properties at MC = 12%, factoring in climate conditions and load durations using codified modification factors (k_{mod}) in the calculation. All the values and the factors used are listed in Table 2.6.

$$f_{c,0,d} = \frac{f_{c,0,rep} * k_{mod}}{\gamma_M} \quad (2.4)$$

Subsequently, $f_{c,0,rep} = 19.8$ MPa was reported in 2007 in the Dutch National Annex to the Eurocode 5 (EN 1995-1-1/NB:2007). The $k_{mod} = 0.5$ for long-term loading and the $\gamma_M = 1.3$ adopted for this Standard, resulted in a lower design compressive strength value (calculated with Equation 2.5 for short-term and long-term loading) as shown in Table 2.6.

Currently, in the European Standard – Eurocode 5 [18] – timber piles are not mentioned. In the Netherlands, the present NEN-EN 1995-1-1/NB:2013 [19] does not report the former characteristic strength value $f_{c,0,k} = 19.8$ MPa from EN1995-1-1/NB:2007, but provides only design compressive strength values for short-term load application $f_{c,0,d,short} = 11.5$ MPa and for long-term loading $f_{c,0,d,long} = 9.8$ MPa, stating that the system strength factor $k_{sys} = 1.1$ for a minimum of 3 piles in a foundation are already applied in the values. Additionally,

grading rules for timber piles and their application in soil are reported. However, contrary to what was stated in the Dutch National Annex to NEN-EN 1995-1-1 NB:2013, the k_{sys} were not included in the proposed design values. This is because, the reported design values ($f_{c,0,d,short} = 11.5$ MPa; $f_{c,0,d,long} = 9.8$ MPa) were obtained by applying to characteristic strength value $f_{c,0,k} = 19.8$ MPa, the k_{mod} (0.7 for short- and 0.6 long-term loading, respectively) and $\gamma_M = 1.2$, as in Equation 2.5.1.

The NEN 8707:2018 [23], which reports guidelines for the assessment of existing wooden foundation piles in case of reconstruction and disapproval (Geotechnical structures), provides design compressive strength values for timber piles: $f_{c,0,d,short} = 12.6$ MPa and $f_{c,0,d,long} = 10.8$ MPa. The NEN 8707:2023 specifies that the values include factor $k_{sys} = 1.1$ and are calculated with $k_{mod,short} = 0.6$ and $k_{mod,long} = 0.7$, as listed in Table 2.6. The values reported in the NEN 8708:2018 were consistent with those provided in the NEN 6760:1997, and they serve as a confirmation of the inaccuracy reported in the Dutch National Annex to EC5, NEN-EN 1995-1-1/NB:2013, where the k_{sys} was actually not included in the design values.

Table 2.6: Compressive strength values for wooden foundation piles adopted in the Dutch standards from 1997 to 2023.

Standards	$f_{c,0,rep}$ (MPa)	k_{mod}	k_{mod}	γ_M	k_{sys} (or k_n)	$f_{c,0,d,short}$	$f_{c,0,d,long}$	$f_{c,0,d,short} * k_{sys}$ (MPa)	$f_{c,0,d,long} * k_{sys}$ (MPa)
	dry MC =12%	short- term	long- term	ULS	system strength factor	short- term	long- term	short- term	long- term
NEN 6760 1997 ^a	19.8	0.7	0.6	1.2	1.09	11.6	9.9	12.6	10.8
NEN-EN 1995-1-1/NB:2007	19.8	0.7	0.5	1.3	1.1	10.7	7.6	11.7	8.4
NEN-EN 1995-1-1/NB:2013								11.5	9.8
NEN 8707:2018+C2:2023		0.7	0.6					12.6	10.8

^a the same values are reported in NEN 6760:2008.

Since timber foundation piles are only used in saturated conditions, a new approach is chosen in the draft of the new Eurocode 5, prEN 1995-1-1:2023 [21], where saturated compressive strength values are to be determined for timber piles. The given k_{mod} values are only to be used for load duration effects in the newly defined service class 4. In the Annex P of the draft EC 5, verification rules and specifications are provided for the utilization of these material properties, while Annex Q outlines requirements for timber foundation piles to which Annex P applies. The Annex P is partly based on the Dutch grading standard for timber foundation piles NEN 5491 2010.

In addition, indications regarding the mean and compressive modulus of elasticity parallel to grain ($E_{c,0,mean,sat}$; $E_{c,0,k,sat}$) of timber foundation piles are reported, indicating that they should be taken as the respective values of the timber logs used as foundation piles in fully saturated condition (MC \geq 50%). Indications are given on how to determine mean and characteristic values for both $f_{c,0,sat}$ and $E_{c,0,sat}$. More specifically, the compressive strength and stiffness parallel to the grain of timber logs to be used as foundation piles can be determined by means of compression tests parallel to grain in fully saturated condition according to EN 14251 (2003) [124]. The characteristic compressive strength and stiffness parallel to grain $f_{c,0,k,sat}$ and $E_{c,0,k,sat}$ can be calculated as specified in EN 14358 [150].

2.5 Mechanical properties of timber piles

Verification of ultimate limit states shall include short-term, long-term and permanent loading situations, by calculating the design compressive strength parallel to the grain with Equation 2.5. A $k_{mod,sat}$ is introduced (see Table 2.7), only accounting for the effect of the duration of load in a timber pile, since the effect of moisture is already accounted in $f_{c,0,k,sat}$ for fully-saturated condition. The partial factors for resistances of timber piles $\gamma_M = 1.3$ is adopted for ULS.

$$f_{c,0,d} = \frac{f_{c,0,k,sat} * k_{mod,sat}}{\gamma_M} \quad (2.5)$$

Table 2.7: Values of $k_{mod,sat}$ for timber foundation piles in prEN 1995-1-1/NB:2023

Material	Standard or EAD	Service class	Load-duration of action				
			Permanent	Long-term	Medium-term	Short-term	Instantaneous
Coniferous timber logs in fully saturated condition used as foundation piles	-	4	0.6	0.7	0.8	0.9	1.1

2.5.6 Conclusions

All the studies available in literature regarding the saturated mechanical properties of timber piles revealed high variability among the saturated compressive strength values, as reported in Table 2.8.

Table 2.8: Summary of the mean and characteristic saturated compressive strength values for timber piles in literature.

Category	Reference	Sample size	$f_{c,0,wet}$ (MPa)		$f_{c,0,k,wet}$ (MPa)
		No.	mean	SD	$\times 0.5$
Southern pine heads and tips (treated and steam-conditioned)	Wilkinson (1968) [59]	30	16.4	4.3	8.4
Treated southern pine – saturated – (1 to 6)	Wilkinson (1968) [59]	30	26.7	3.0	21.2
Spruce	Van de Kuilen (1994) [33]	57	20.0	2.2	16.3
	Aicher (2016) [36]	17	17.6	2.3	13.4
Douglas fir	Van de Kuilen (1994) [33]	16	21.8	1.7	18.4
Douglas fir heads and tips (treated and steam-conditioned)	Wilkinson (1968) [59]	30	22.6	3.9	15.4
Larch	Van de Kuilen (1994) [33]	19	22.9	2.9	17.1

The following key points underline the relevance and the several knowledge gaps associated with the studies conducted in the literature:

- a) The saturated strength parameters for spruce, Douglas fir and larch reported in Buiten [32] and statistically analysed in Van de Kuilen [33], represented a relevant experimental campaign conducted in Europe to characterize the saturated properties of timber piles. However, saturated compressive strength values were determined only for piles with average diameter of 140 mm, extracted only from the tip of the piles, assuming the tip section was the weakest one within the tapered pile, due to its smaller cross section. This prevented the understanding of the mechanical properties along timber piles, which were not characterized from head to tip. The density and stiffness values of the tested piles were not determined. Moreover, parameters such as age (number of annual rings) and growth rate, which can give indications about wood quality, were not reported. Finally, no correlation was found between compressive strength and KR. The aforementioned limitations in the database prevented from an adequate understanding of the behaviour of saturated timber piles in compression in relation to physical and material properties that may affect their saturated compressive strength.
- b) The mechanical properties characterized along the length of preservative-treated southern pine and Douglas fir piles [59], provided useful insights into the variability of saturated compressive strength, stiffness, density and age, from the head to the tip of the pile. The saturated compressive strength revealed to be well correlated with age and KR, suggesting that these two parameters can be used for possible strength grading of the piles. The tip of the piles always exhibited the lowest compression strength compared to the rest of the pile. This aspect is particularly significant in axially-loaded wooden foundation piles in the soil, where the tip may be the critical section, since it is subjected to higher stresses due to its smaller cross-section compared to the rest of the pile. This highlighted the importance of characterizing the mechanical properties all along the length of the piles.
However, the saturated strength values determined in [59] might not be fully representative for (untreated) wooden foundation piles, due to the steam-conditioning, kiln-drying and preservative treatment with creosote processes applied to the southern pine and Douglas fir piles. Furthermore, the results in [59] may not be comparable with saturated European Douglas fir studied in [32].
- c) The mechanical properties determined in [36], for 17 dry and 17 saturated spruce piles, revealed very useful insights on the influence of high moisture contents on the compressive strength of spruce piles, where a moisture modification factor $k_{\text{moist}} = 0.65$ from dry to wet was derived. This study highlighted that the $k_{\text{mod}} = 0.82$, currently used in the design standards to account for high moisture contents, is not applicable to timber piles, since it was calculated on the basis of edgewise bending tests of timber boards, not representative of the behaviour of timber piles. However, it should be noted that a limited number of piles were investigated.

In order to overcome the lack of compressive strength values along saturated wooden piles, a large experimental campaign is presented in this study with the purpose of characterizing the mechanical properties of head, middle-part, and tip of saturated full-sized spruce (*Picea abies*) and pine (*Pinus sylvestris*) foundation piles.

The tested piles had an average total length of 12 m, and different diameters were investigated, ranging from 130 mm to 280 mm. The visually detectable characteristics of timber, such as diameter, knot-related parameters, annual rings, rate of growth, slope of the grain, and tapering, which may influence strength and stiffness, were visually graded with the objective of finding correlations with the saturated compressive strength of the piles, and assign possible strength classes to visual grades.

The results provide a basis for the design and engineering assessment of wooden foundation piles and they can be used together with the provisions given in the draft of the new Eurocode 5 prEN 1995-1-1:2023 [10].

2.6 Biological degradation in timber foundation piles

2.6.1 Introduction

Since wood is a natural material, its durability is strongly related to exposure to the surrounding natural environment [37],[38]. Wooden foundation piles used under buildings, bridges, and quay walls, remain submerged under the water table for their whole service life, enduring high moisture levels. This makes them insusceptible to fungal decay [5]-[8],[37], which cannot develop underwater due to the absence of oxygen [12],[13]. However, submerged timber piles may be susceptible to biological decay, proceeding at a very slow rate, allowing the piles to perform their function for centuries before showing a substantial reduction of the load-bearing capacity [1],[3],[5]-[1], leading to safety issues in the supported buildings.

Biological decay in waterlogged soils can be caused by either soft rot fungi (in low-oxygen conditions), or bacteria (even in anoxic conditions), in Figure 2. 30, as initially studied by Variosseau in 1949 [143] and followed by [10],[11],[1],[25].

Bacteria can be divided into erosion bacteria, on the basis of their way of eroding the wood fiber cell walls [139],[140] (Figure 2.31), or tunnelling bacteria, digging tunnels in the cell wall (Figure 2.31b), penetrating and degrading the middle lamellae or primary structure of bordered pits in softwoods [25]. These bacteria are responsible for wood degradation in all types of waterlogged anaerobic terrestrial and marine environments worldwide [12],[139],[140],[143].

Bacteria usually start wood colonization from the rays, and later they enter other parts of the wood via pits or from cell to cell, boring holes through cell walls [141],[143] (See Paragraph 2.4.1).



Figure 2. 30: Damage to timber piles under buildings in the Netherlands due to biological wood decay (soft rot fungi and/or erosion bacteria). (Adaptation from [145]).

In particular, softwood foundation piles degraded by bacteria appear unaffected when examined on-site, since their surface, layer, colour, and original dimensions are maintained in wet conditions [11] (Figure 2.32). However, the outer layer of the cross section could often be soft and spongy because of degradation, which always starts from the non-durable sapwood (See Paragraph 2.4.2), whereas the inner part of the pile, including heartwood, might be less decayed or even sound [3]-[8],[10]-[1].

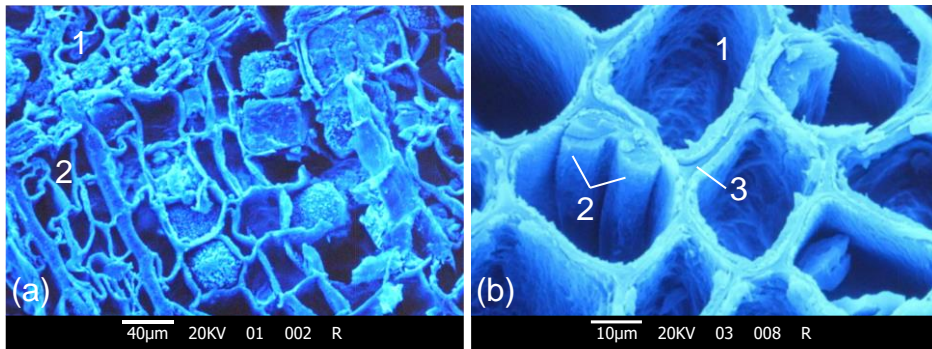


Figure 2.31: Scanning Electron Microscope (SEM) picture of a larch pile (*Larix decidua* Mill.), characterized by collapsed cells with thin walls in the (a1) latewood and (a2) earlywood, showing severe degradation. (b1) Signs of tunnelling in the cell, suggesting the attack of tunnelling bacteria; (b2) accumulation of silty and clayey material; (b3) detachments of cell wall from the compound middle lamella, indicating the effect of erosion bacteria.

The variations in degradation within the cross-section cause pronounced variations of compressive strength, stiffness, density, and moisture content, all factors influencing the global load-bearing capacity of the piles. When bacterial decay progresses to the extent that most of the cell walls are eroded, a strong reduction of density and compressive strength occurs, linked to an increase in moisture content [1],[3],[5],[10],[11].



Figure 2.32: A cross-sectional view of a pile retrieved under a bridge after ca. 300 years of service life with the severe effect of bacterial decay. The effects of bacterial decay are not visually distinguishable in the cross section.

In the city of Amsterdam, spruce, pine, and occasionally fir piles, have been dominantly employed to realize foundation structures [3],[5],[145]. The local soil is mainly composed of peat and clay layers, resting on a sand layer at a depth of 11–12 m, and the groundwater is mainly brackish [3] (See Section 2.2).

Given the essential function of these foundations and their widespread presence in the historic city center of Amsterdam, estimating the impact of bacterial decay on the material and mechanical properties of the piles is crucial for arranging timely maintenance interventions.



Figure 2.33: Degraded parts of a wooden foundation: (a) disintegration of the tip of a wooden pile due to bacterial decay; (b) biodegradation of an horizontal portion of the foundation (visible detail of vertical wooden connectors for piles attached to the beam); (c) cross-sectional portion of a pile with severe effect of bacterial decay, where it is not possible to visually distinguish the effects of bacterial decay.

2.6.2 Research studies on biological degradation

At the end of the 1980s, growing emphasis was put on analysing the current condition of timber pile foundations in relation to biological activity [49],[51],[54],[55]. This was driven by growing concern about many Dutch buildings, ca. 100 years old, showing cracks due to settlements of the foundations [145].

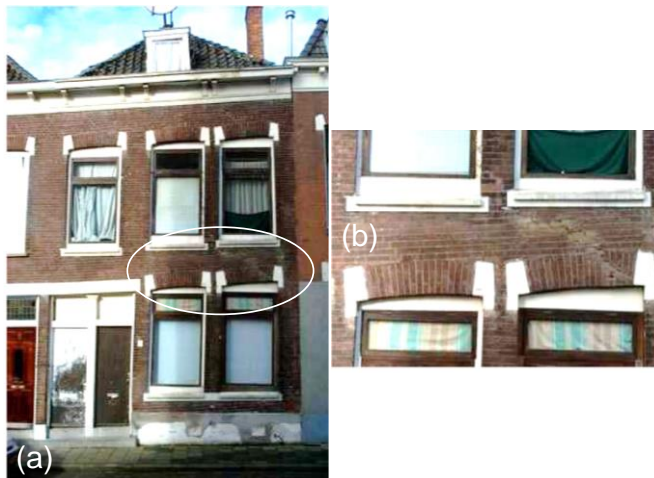


Figure 2.34: (a) Dutch house showing differential settlements (more than 20 cm) between right and left wall causing (b) cracks in the wall and structural damage to the house (Adaptation from [145]).

The first studies in the Netherlands on the remaining compressive strength of spruce piles retrieved from a lock gate in Weesp (NL) (Figure 2.35) [144], revealed that after 113 of time in service, the remaining short-term compressive strength in the spruce sapwood was roughly half of that in the heartwood. Although the piles remained under the water table for their whole service life, they showed severe degradations, indicating a possible presence of bacterial decay in the sapwood. More specifically, spruce sapwood had a

$f_{c,0,\text{mean,wet}} = 7.4 \pm 1.9$ MPa, and heartwood $f_{c,0,\text{mean,wet}} = 14.3 \pm 1.4$ MPa, determined on the basis of small-scale compression tests on 3 samples extracted from heartwood and 9 from sapwood, in fully saturated conditions ($\text{MC} > 100\%$).

Similar problems occurred in other Dutch cities as well [5], revealing that timber pile foundations situated beneath the groundwater table for a century or more may undergo significant deterioration.

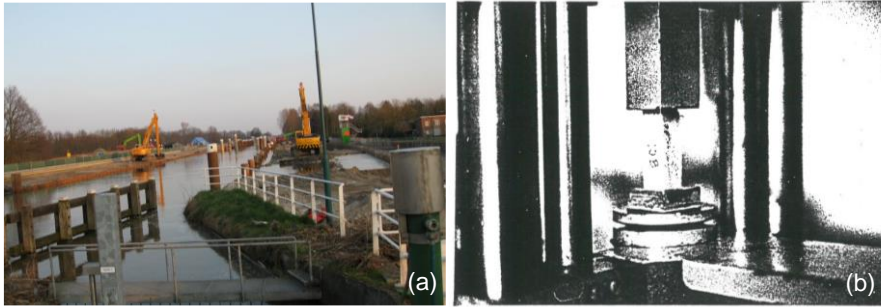


Figure 2.35: (a) lock gate in Weesp originally built in 1874, from which 5 spruce piles were extracted (photo taken in 2008 during renovation work; (b) compression tests on small-scale samples from heartwood and sapwood of pile heads (Adapted from [144]).

In this context, at the beginning of 1990s, the assessment of the material status of timber foundation piles in The Netherlands became important. The assessment was conducted by extracting drill cores from the head of wooden foundation piles [54],[55],[145]. The cores were collected radially from the exterior toward the centre of the pile. However, these tests were mainly fragmented among institutes and companies that conducted the measurements, and no standardized characterization of the biodegradation of timber piles was available.

To this end, the European Commission funded in 2002 a scientific project commonly known as “Bacpoles” [145], with the aim of providing general knowledge on bacterial decay of wood in foundation piles, and developing practical preservation methods for wooden foundations. Wood and soil science experts, alongside microbiologists, archaeologists, and geophysicists from 5 collaborating countries, Germany, Great Britain, Italy, The Netherlands, and Sweden, joined forces for this collaborative project. The universities and research institutes focused on foundational research, while the companies took charge of on-site examinations of wooden foundations and integrating innovative wood preservation technologies into established techniques. The characterization was established through visual observations and field measurements such as Pilodyn [146] and the aforementioned drill-cores.

On the basis of the dataset collected during the Bacpoles project [145], a model for the prediction of the saturated compressive strength was made [5], based on the maximum moisture content of a large number of small-scale samples extracted along pine piles with different degradation, from sound to total disrupted wood structure (Figure 2.36) [5]. In total, the model comprised 5 “new” pine piles sourced from the Netherlands, and 13 pine piles retrieved from foundations of approximately 100-year-old buildings from different

cities in the Netherlands (including Amsterdam). The decay classification was conducted with microscopic analysis according to Varossieau (1949) [143], where 4 decay classes were used: sound, weak, moderate, and severe (Figure 2.36).

On the basis of the model developed in [5] and the extraction of drill cores from the head of timber piles, a standardized method was made for the assessment of wooden piles in the Netherlands. This inspection method was incorporated in the Dutch F3O guidelines [22] and the Dutch standard NEN 8707 [23].

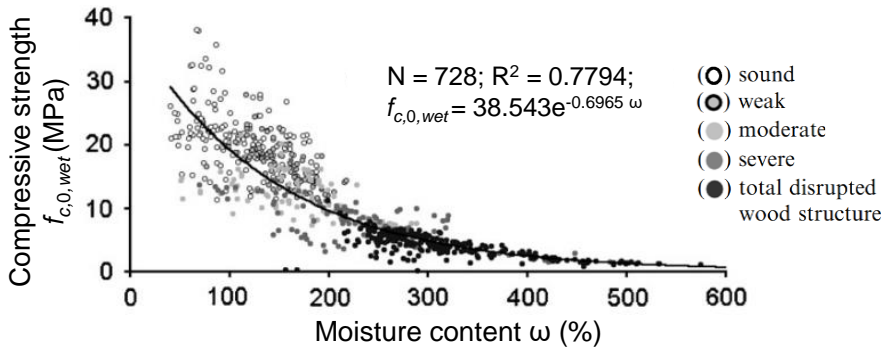


Figure 2.36: Relationship between compression strength and moisture content determined from small-scale compression tests of pine (Adaptation from [5]).

In the Netherlands, more than 2000 wooden foundation piles were sampled and assessed [155]. The majority of these samples were derived from the underpinnings of historical structures, primarily located in Amsterdam but also in other cities across the Netherlands. The results of these investigations on biological decay are shown in Figure 2.37.

From this large project, it emerged that:

- Wooden foundation piles, approximately 100 years old and located below the groundwater level, exhibited biological decay primarily in their outermost layer.
- The degradation process initiates externally in the non-durable sapwood and gradually diminishes towards the centre of the pile.
- Spruce sapwood demonstrated higher resistance to bacterial degradation compared to pine sapwood and alder (Figure 2.37). In pine, degradation was only present in sapwood and never present in heartwood which appeared notably resilient. Sapwood was measured only for pine, thus, no conclusions can be made for spruce, fir, and alder. Despite this general trend, cases have been documented where 100-year-old spruce piles experienced severe degradation, while some 100-year-old pine piles showed no signs of decay.
- Severe bacterial attacks tend to occur more frequently in permeable soils like sand, while attacks are less prevalent in non-permeable soils such as clay and peat.

This research gave a good general overview of the state of conservation of the timber foundation piles. However, several uncertainties emerged due to the fact that the drill cores were only extracted from the pile head, without giving a detailed analysis of decay

along the pile. Moreover, the drill core extraction is a localized analysis, which could not fully capture the distribution of decay around the cross section.

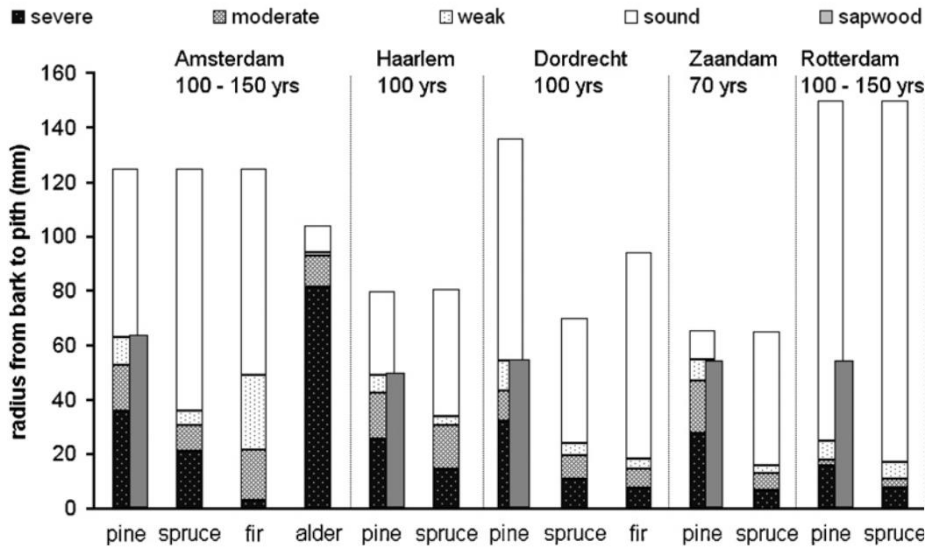


Figure 2.37: Average degree of biological decay in pile heads from five Dutch cities (Amsterdam, Rotterdam, 100–150 years; Dordrecht and Haarlem, ca. 100 years; Zaandam, ca. 70 years) The amount of sapwood is only given for pine (Adaptation from [5]).

2.6.3 Assessment of wooden piles in Amsterdam

In the last 10 years, the city of Amsterdam has carried out a research and monitoring project, aimed at assessing the current state of the timber pile foundations. The inspection techniques involved the extraction of drill cores (with a diameter of 10 mm and a length of roughly half the pile diameter) from the head of the wooden piles, ca. 50 cm below the pile head.

This was done according to F3O guidelines [22] and the Dutch standard NEN 8707 [23], incorporating the principles explained in Paragraph 2.6.2. A total of 3713 drill cores were taken from the wooden piles of 181 bridges in Amsterdam (Figure 2.39a), built across various historical periods, spanning from 50- to 400-year-old piles.

The drill cores were extracted by divers with a hand-driven increment borer (Ø10 mm), and collected in plastic tubes filled with water (Figure 2.38c), to preserve their physical properties.



Figure 2.38: Extraction of a drill core from a timber foundation pile collected in a plastic tube filled with water.

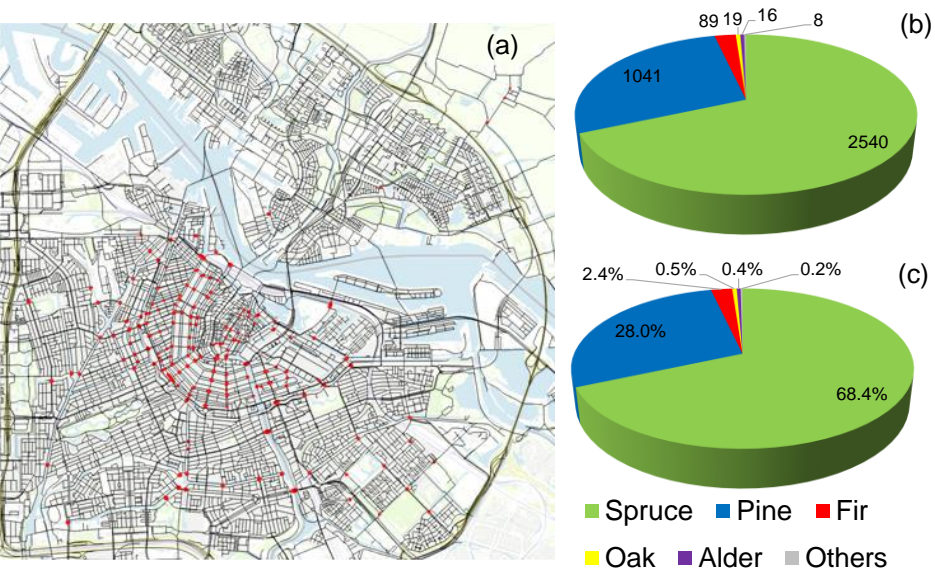


Figure 2.39: (a) Map of Amsterdam with locations (in red) of the bridges in which drill cores were taken from the wooden piles. (b) Wood species distribution of 3713 samples per number of drill cores; (c) per percentage of wood species.

Subsequently, the drill cores were segmented into sub-sections and visually examined: the wood species, the type, and the degree of deterioration were determined under the microscope according to [5],[143] (Paragraph 2.6.2). The wood species mainly involved spruce, pine, and fir, with a smaller proportion of alder and oak (Figure 2.39b-c). The diameter of the pile head was also measured for all the investigated piles. The range of head diameters, mostly 200-300 mm, is presented for the most used wood species: spruce (Figure 2.40a), pine (Figure 2.40b), and fir (Figure 2.40c).

From the analysis of the decay of the drill cores, it was concluded that bacterial decay was present in a significant number of piles. Subsequently, the remaining compression strength of the piles was estimated by using the maximum moisture content that a sub-section of the drill core could absorb, according to the model for pine piles in [5] (Paragraph 2.6.2), where high moisture contents above ca. MC= 230% are correlated to total disrupted wood structure (See Figure 2.36).

Using this model, the city of Amsterdam considered every sub-section of the drill core with a predicted compression strength lower than 8 N/mm² (correspondent to disrupted wood structure, MC = 230%), as being part of a so-called “soft shell”: the degraded part of the cross section to which no strength is assigned. Assuming that the detected soft shell (mm) is constant for the whole cross section, the percentage of the remaining sound cross section was calculated, by subtracting the soft shell from the whole cross section.

Based on the remaining cross section, the following decay classes were made by the Author to give an overview of the extent of decay within the cross section of the piles assessed in Amsterdam:

- Remaining cross section $\geq 85\%$: sound pile;
- $65\% \leq$ Remaining cross section $< 85\%$: moderately decayed pile;
- Remaining cross section $< 65\%$: severely decayed pile.

The soft shell detected from the drill cores was related to the parameters time in service and wood species in Figure 2.41a and Figure 2.41b.

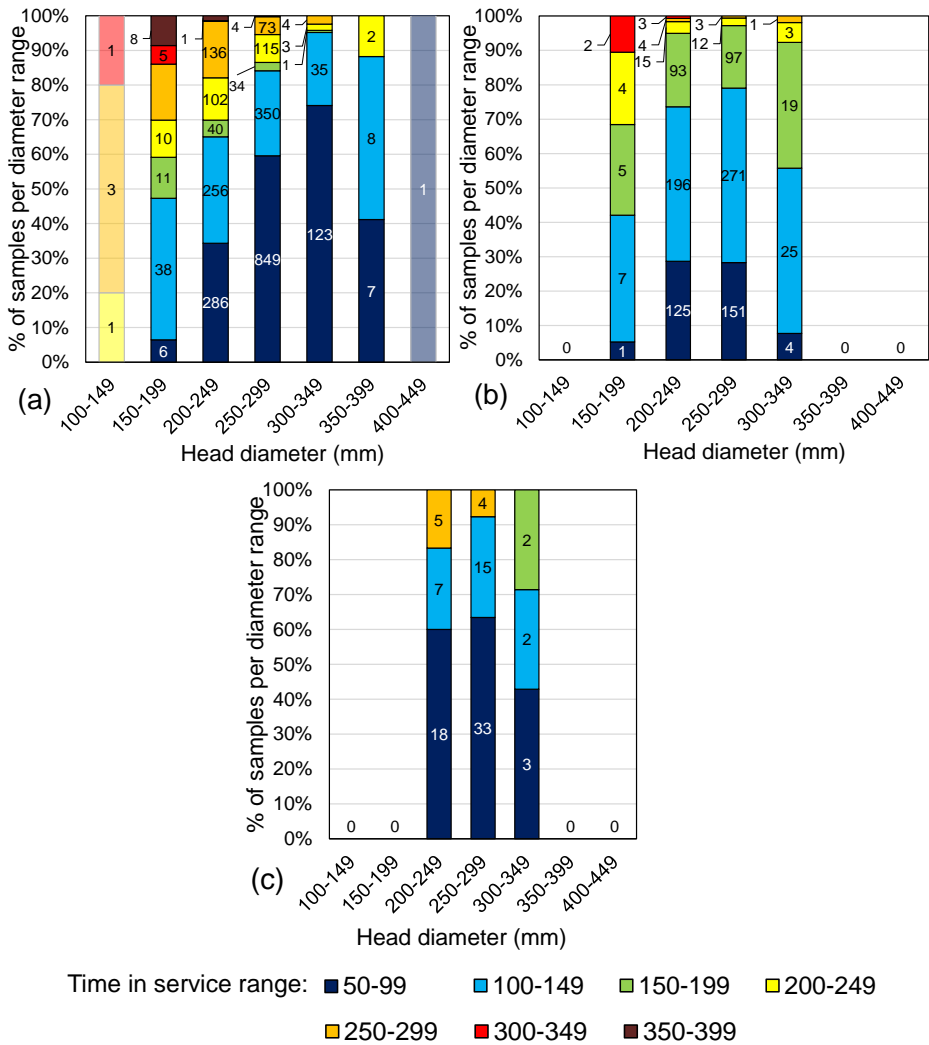


Figure 2.40: Distribution of the % of (a) spruce; (b) pine; (c) fir samples, based on head diameter of the piles for 7 ranges of time in service. The number in the rectangles represents the sample number of each range.

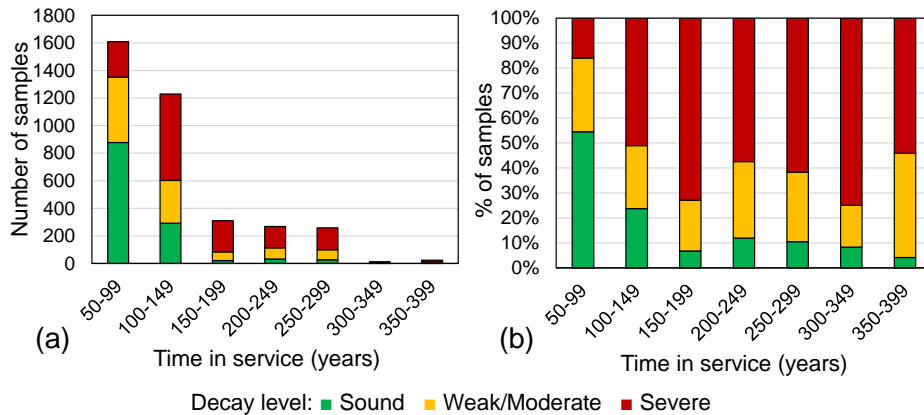


Figure 2.41: Decay classification for 3711 drill cores: (a) number of samples; (b) percentage of samples for each time-in-service group.

In order to calculate the remaining load-bearing capacity of the piles, the compression strength for “new” piles provided in the National Annex to Eurocode 5 NEN-EN-1-1/NB:2013 [19] and NEN 8707 [23] was assigned to the remaining assumed sound part, deriving the design compression force according to the modification factors (k_{mod}) used in the Eurocode 5 EN 1995-1-1 [18] (See Paragraph 2.5.5). However, the derived compressive strength values of the piles could not be validated with the compressive forces acting on the piles that have been in service, since only very limited data was available.

In Amsterdam, the aforementioned inspection technique, which relies on the analysis of drill cores (Paragraph 2.6.2), facilitated the sampling of numerous piles within the city, providing an overview of the amount of decay present in the piles. However, the drill-core analysis revealed several issues, as anticipated in Paragraph 2.6.2:

- Drill-core analysis was based on local measurements conducted at a specific localized spot, limited to the pile head and dependent on the diver’s expertise. Thus, a continuous representation over the cross section of the pile was not given.
- The analysis of the possible decay of the drill cores required specific expertise and extensive investigations, since after the extraction, microscopic analyses and application of experimental models needed to be conducted.

In order to address the knowledge gap concerning the impact of biological decay on the mechanical properties of wooden foundation piles and to explore assessment techniques for efficiently mapping the radial distribution of decay within these piles, an extensive experimental campaign was initiated in collaboration with the TU Delft and the municipality of Amsterdam. The main objectives are:

1. Characterizing the present condition of wooden foundation piles driven into the soil in 3 different time periods (1727, 1886, 1922), retrieved from two bridges in Amsterdam that were demolished and replaced, through a large testing campaign involving mechanical tests on full-size specimens.

2. Exploring the applicability of a more effective inspection technique to be used in practice.

Among the available non-destructive techniques for assessing the material condition of timber piles, micro-drilling stands out as a promising method, offering the advantage of enabling extensive in-situ sampling across a large number of piles [26]-[29],[152],[153].

2.6.4 Conclusions

In the city of Amsterdam, many wooden foundation piles exhibited moderate and severe decay due to bacterial decay, influencing their load-bearing capacity and leading to possible safety issues. The assessment techniques currently adopted in Amsterdam are based on the extraction and analysis of drill cores retrieved from the head of the timber piles. However, several drawbacks emerged from this approach: firstly, the derived compressive strength values of the piles could not be validated with the compressive strength of the piles that have been in service, since these data were not available. Secondly, the analysis of the drill cores is often cumbersome and the analysis is dependent on the technician's expertise. Finally, the analysis does not give a continuous representation over the cross section.

In order to address the knowledge gap concerning the impact of bacterial decay on the mechanical properties of wooden foundation piles and to explore assessment techniques for efficiently mapping the radial distribution of decay in their cross section, 60 wooden foundation piles with different levels of decay were investigated. The historical piles were retrieved from two bridges in Amsterdam after a time in service between 100-300 years.

Micro-drilling was adopted to assess the amount of bacterial decay within the historical wooden piles. Micro drilling allows inspecting the material status throughout the whole cross section of the pile, involving the utilization of a drilling tool, where a drilling needle is pushed into the material with a chosen drill and feed speed, resulting in a graphical representation of the resistance encountered during the drilling process (Figure 2.42). The resistance profile can be directly evaluated in situ, allowing to check if the measurement is successful or has to be repeated. The measurements can be performed underwater by divers in different positions and directions, resulting in more available measurements, increased accuracy, faster in-situ testing, reducing costs and applicability.

The primary objectives of this thesis include characterizing the present condition of wooden foundation piles with micro-drilling measurements, as an alternative to the current method of extraction of drill cores to determine the soft shell – the degraded portion of the cross section. Secondly, investigate correlations between the remaining *short-term* mechanical properties of the piles and the micro-drilling signals, to check the reliability of micro-drilling measurements in identifying decay from both a qualitative and quantitative point of view.

Short-term mechanical properties refer to e.g. the saturated compressive strength of wooden piles, determined at the moment of the test in a specific timeframe during the lifetime of a pile, without considering the material history over extended periods of time under specific sustained loads or stress conditions. This also includes mechanical

degradation due to the duration of load effect, to which timber piles loaded for centuries may be subjected. However, mechanical damage was not investigated in this study.



Figure 2.42: Micro-drilling performed throughout a spruce cross section exhibiting decay on the outer part. The degraded portion of the cross section is visible in the signal due to the considerable reduction in the resistance profile compared to the sound core.

Materials and Methods

3.1 Introduction

The literature review in Chapter 2 has unveiled several knowledge gaps concerning the material and mechanical properties of saturated timber piles, and their utilization in engineering practice.

The materials used in this research are presented in Section 3.2, involving “new” timber piles and historic timber piles. All piles are preliminary tested, as described in Section 3.3, and subdivided into segments (Section 3.4) to be subjected to mechanical testing.

Full-length “new” softwood piles are characterized in Section 3.5 and Section 3.6. Visually graded properties that could influence the saturated compressive strength of “new” piles are investigated (Section 3.7), with the goal of defining visual grading limits for possible strength classes for spruce and pine piles (Section 3.8 and Appendix A3), to be used in practice together with the provisions reported in the draft of the new Eurocode 5 2023 [21].

The effect of decay on the mechanical properties of historical spruce and fir piles is investigated, by analysing piles with different decay levels, retrieved from 2 bridges in Amsterdam after a time in service between 100-300 years. The material properties along the piles are characterized in Section 3.5 and their remaining short-term compressive strength is determined with compression tests in Section 3.6. The amount of bacterial decay in the historical piles is assessed with micro-drilling measurements (Section 3.9). The influence of different moisture contents on the assessment of decay levels with micro-drilling is also investigated in Section 3.10, to check the reliability of micro-drilling in detecting decay at different moisture contents. Subsequently, small-scale mechanical testing at cross-sectional level is conducted on historical piles (Section 3.11), to relate micro-drilling to the distribution of decay and density within their cross section. The density distribution within the cross-section is further investigated with Computed Tomography (CT) scanning, conducted in correspondence to the micro-drilled section (Section 3.12). CT scanning is also used to assess the extent of decay within sapwood and heartwood in the cross section. To support this, light microscopy observations are conducted to assess the presence of bacterial decay in sapwood and heartwood of selected severely decayed piles (Section 3.13).

A comprehensive overview of the methodology adopted in this research is showcased in Figure 3.1, to help the reader understand the different steps carried out.

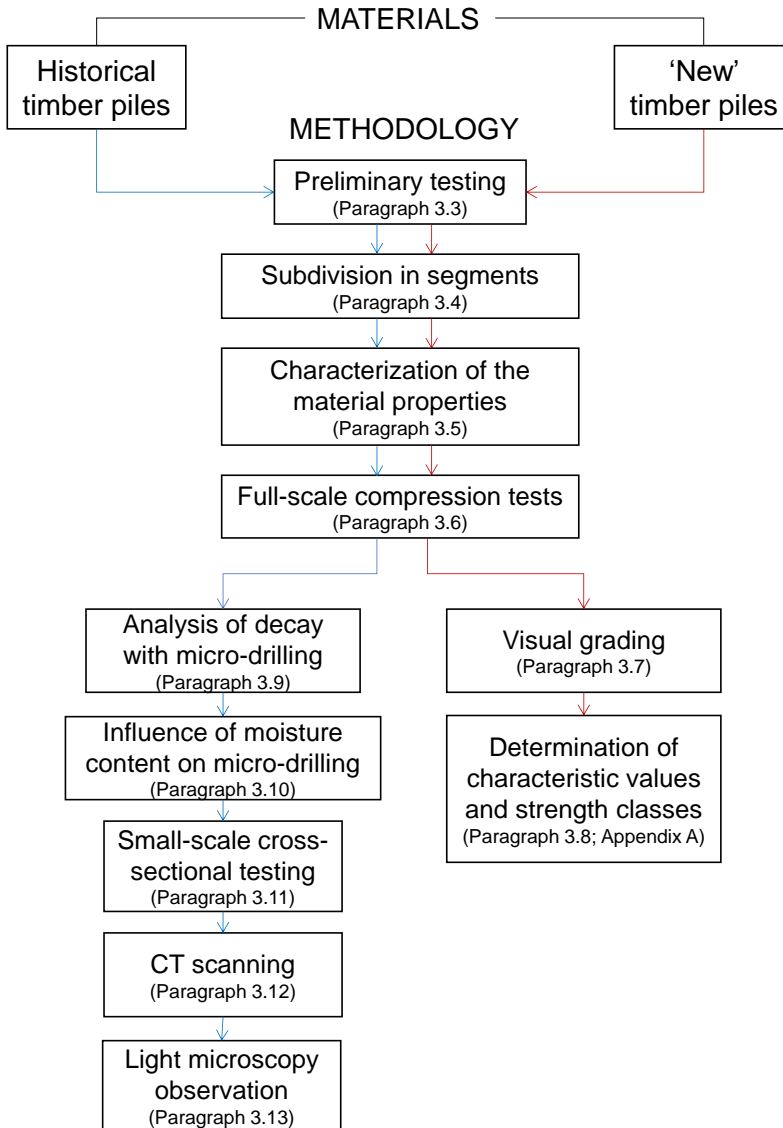


Figure 3.1: Comprehensive overview of the methodology adopted in Chapter 3.

3.2 Materials

In order to characterize the mechanical properties of wooden foundation piles, destructive and non-destructive tests are conducted on 130 full-scale piles categorized into two distinct groups:

- “New” timber piles with average length of 14 m, mean head diameter (D_{head}) of 290 mm, and a mean tip diameter (D_{tip}) of 135 mm, felled in 2019, comprising:
 - 38 spruce (*Picea abies*) piles felled in a forest in Holterberg, The Netherlands;
 - 32 pine (*Pinus sylvestris*) piles felled in a forest in Nuremberg, Germany.Detailed properties of the “new” full-length piles are provided in Table 3.1 (Paragraph 3.2.1).
- Timber piles retrieved under bridges in Amsterdam, driven into the soil in 1727, 1886 and 1922, with average length ranging from 9.5 m to 13.5 m, with an average head diameter of 230 mm and average tip diameter of 145 mm, comprising:
 - 55 spruce (*Picea abies*) piles;
 - 5 fir (*Abies*) piles.Detailed properties of the historic full-length piles are provided in Table 3.2 (Paragraph 3.2.2).



Figure 3.2: wooden foundation piles: (a) batch of “new” timber piles; (b) timber piles retrieved under a bridge in Amsterdam, the pile tip is smashed due to loading in the ground.

3.2.1 “New” wooden piles felled in 2019

The first category, namely “new” timber piles—denoting that they were felled and never used as foundation piles—comprised 70 logs that were harvested in the year 2019, with a mean length of 15 meters, mean head diameter (D_{head}) of 290 mm, and a mean tip diameter (D_{tip}) of 135 mm.

Out of a total of 70 piles, 27 piles (18 spruce and 9 pine) were driven into the soil in 2019 in a test field in Over Amstel, Amsterdam (NL), as part of a geotechnical project handled by the city of Amsterdam. Subsequently, 18 of these piles (13 spruce and 5 pine), named DL (*Driven and Loaded*), were subjected to short-term in-situ loading with the goal of assessing the maximum geotechnical failure load, correspondent to a maximum displacement of the head of the pile equal to 10% of the head diameter, in accordance with

3.2 Materials

NEN 9997-1+C2:2017 [147]. The loading procedure was carried out within a day, with a maximum stress of 6.3 MPa calculated on the pile head. It should be noted that the failure did not correspond to the material failure, but to the failure with respect to the soil settlement. After this, the load was removed from the 18 piles, except for 2 spruce piles (DL-1) that were loaded to 80% of the failure load for 22 days. The other 9/27 piles (5 spruce and 4 pine), named D (*Driven*), were driven but never loaded. Subsequently, all the piles were extracted from the soil and treated in the same manner as the other 43 non-driven piles, named ND (*Never Driven*), which involved cutting each pile into three parts (head, middle-part and tip), and submerging all the parts in water in containers. Figure 3.3 shows the workflow of the piles and the different categories of piles used in this research. Table 3.1 lists the preliminary data of each pile category and the average maximum stress levels reached on the pile head during the loading operation.

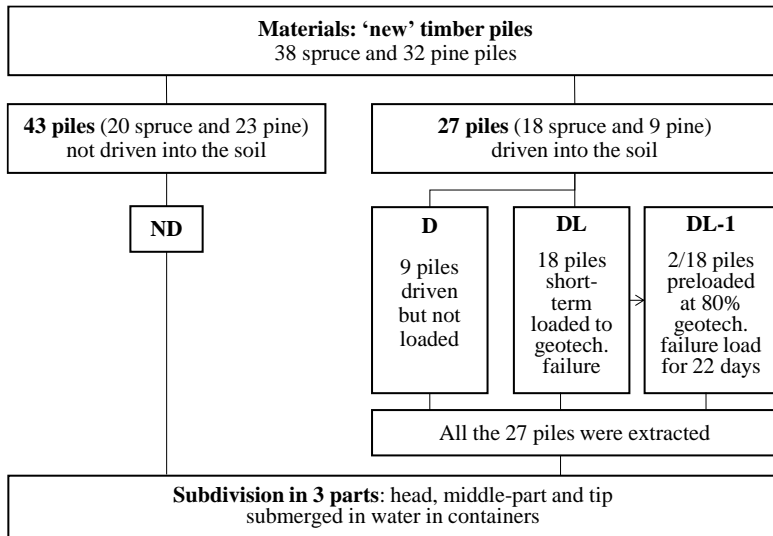


Figure 3.3: Workflow of the materials used in this research

Table 3.1: Preliminary data of full-scale piles and in-situ applied stress (standard deviation reported in brackets)

Pile Categories	No.	Length mean m	D _{head} mean mm	D _{tip} mean mm	Avg. tapering mm/m	Max stress on pile head MPa
ND	20 ^a 23 ^b	15.1 (0.16)	290 (27)	135 (13)	8.6 (2.5)	-
D	5 ^a 4 ^b	15.1 (0.12)	290 (30)	135 (12)	10.1 (2.7)	-
DL	13 ^a 5 ^b	15.1 (0.11)	300 (26)	135 (13)	10.6 (2.1)	6.3
DL-1 ^c	2 ^a	15.1 (0.06)	310 (8)	130 (9)	11.9 (1.1)	4.5

^a Spruce piles (*Picea abies*)

^b Pine (*Pinus sylvestris*)

^c Piles DL-1 are a sub-category of 2/18 piles included in DL

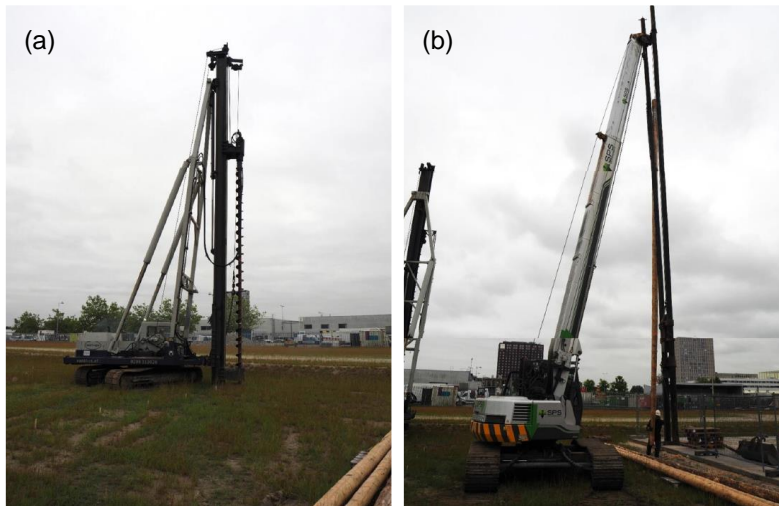


Figure 3.4: Driving of the piles in Overamstel: (a) predrilling operations; (b) timber pile driving.

3.2.2 Historical timber piles from bridges in Amsterdam

The second category of investigated piles involved 55 spruce (*Picea abies*) and 5 fir (*Abies alba*) piles, which were part of the foundation system of the piers of two bridges in the city of Amsterdam (Figure 3.5). More specifically, 28 piles were retrieved from *bridge 30* (De Isa van Eeghenbrug) in Figure 3.6, and 32 piles from *bridge 41* (Johanna Borskibrug) in Figure 3.7. A total of 48 piles were extracted from the external rows of the bridge foundations (exposed to water flow), while only 12 were extracted from the internal rows. The piles were dated back to 1727 (30 piles), 1886 (16 piles), and 1922 (14 piles), the fir piles were all driven in 1886. The full-length specimens ranged from 9.5 m to 13.5 m, with an average head diameter of 230 mm and average tip diameter of 145 mm (Table 3.2).

After the extraction, the full-length timber piles were placed underwater in barges and transported to the storage location of the municipality of Amsterdam, next to the harbour. At the storage location, all full-length piles were measured and tested over the whole length according to Section 3.3. After this, the 60 piles were cut into three parts (head, middle-part and tip) and submerged underwater in containers.

Based on the studies on the dendroprovenancing of timber piles used for foundations in The Netherlands [78], on 8 historic Dutch buildings in 6 different cities, mostly ranging from the end of the 19th century until the 1930s, and one (Maritime Museum, Amsterdam) dated back to the mid-17th century, it was found that: (a) spruce piles originated from south Germany and Sweden. (b) All spruce piles differed considerably in age, between 55-114 years old. (c) Different quality of wood was found for similar diameters. As spruce was imported into the Netherlands and was transported either from Germany by floating up the Rhine or from Scandinavia by boat, the logs would have gone through different stages of selection, classification, and assortment in timber yards. This might partly explain the different diameters of the piles (Table 3.2) and the different number of annual rings (indicators of the tree's age) of the piles (see Paragraphs 3.5.2 and 5.2.3), especially between those from 1727 and those from 1886 and 1922.

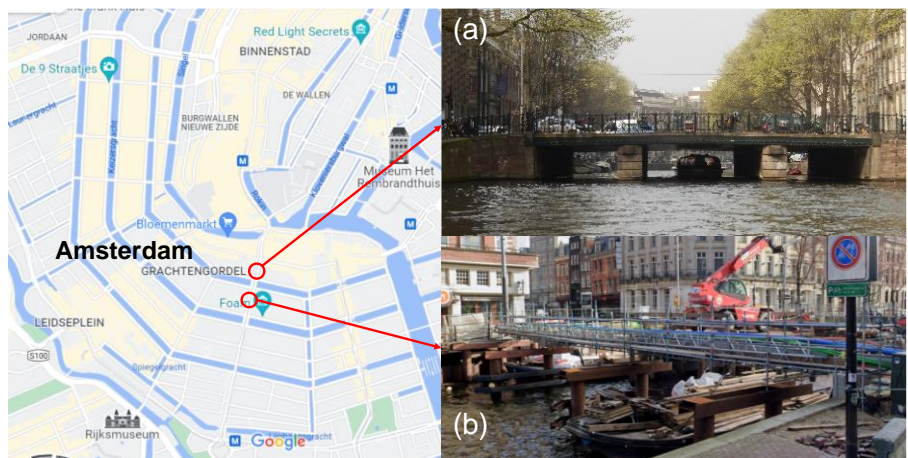


Figure 3.5: Location of (a) bridge 30 and (b) bridge 41 in the historical centre of Amsterdam from which the timber piles were extracted.

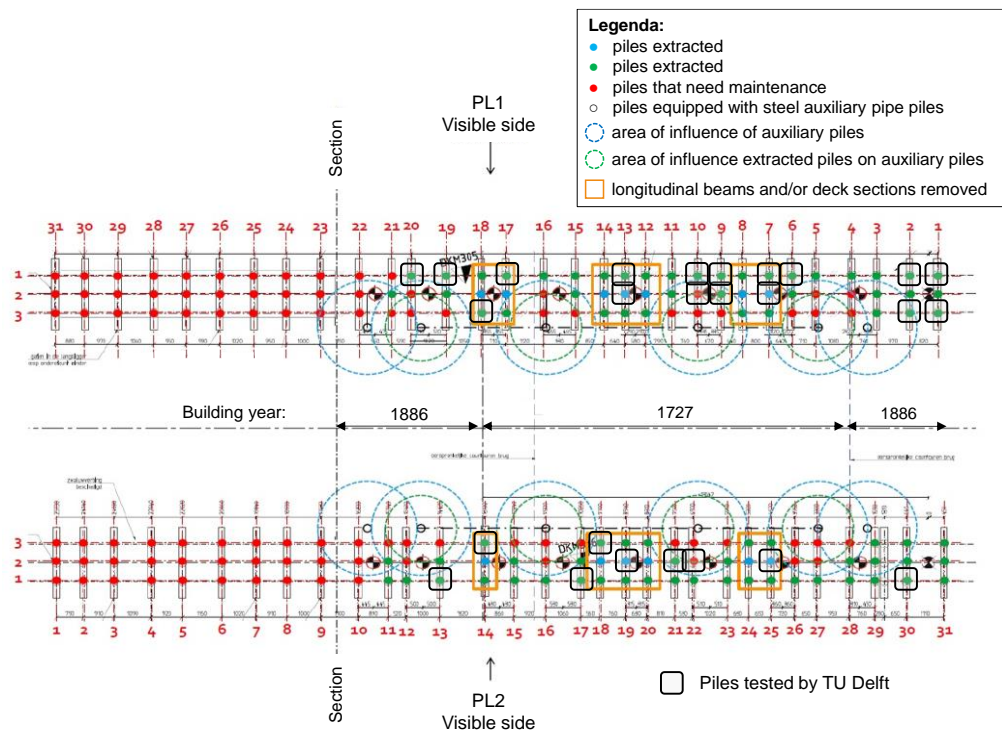


Figure 3.6: Plan of piles layout of bridge 30 in Amsterdam.

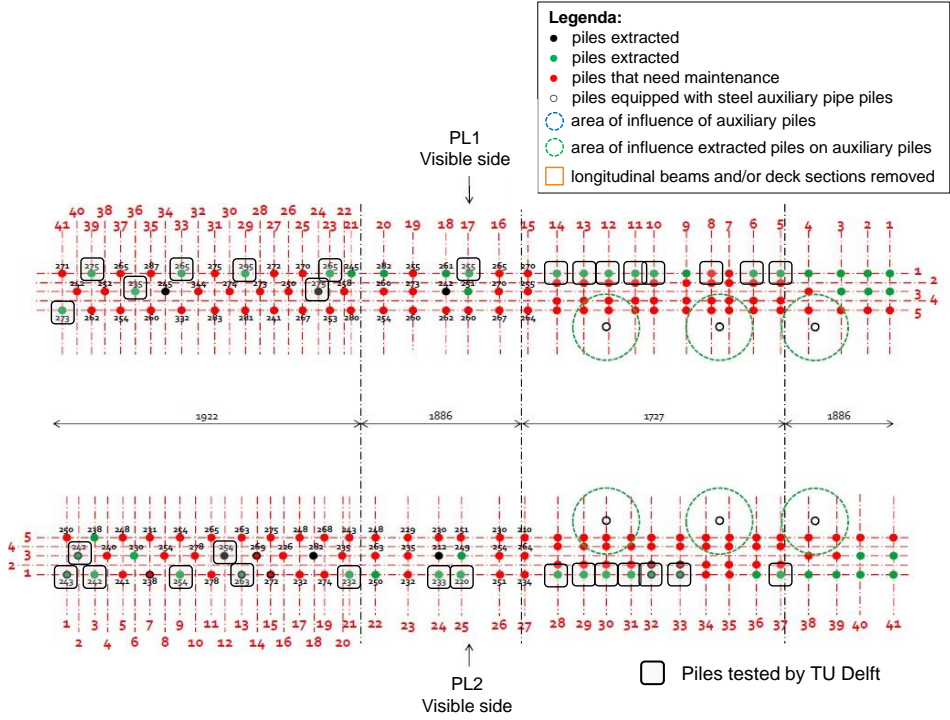


Figure 3.7: Plan of piles layout of bridge 41 in Amsterdam.

Table 3.2: Preliminary data of full-scale piles retrieved from bridges in Amsterdam (Standard deviation reported in brackets)

Building year	No.	Length	D _{head}	D _{tip}	Avg.
		mean	mean	mean	tapering
		m	mm	mm	mm/m
1922	14	12.6 (0.8)	256 (12)	170 (16)	6.9 (1.5)
1886	16	12.0 (1.9)	248 (10)	172 (23)	6.4 (2)
1727	30	10.7 (1.1)	220 (39)	129 (29)	8.5 (2.9)

3.3 Preliminary in-situ testing on full-length piles

In-situ preliminary tests were conducted on the full-length piles (both “new” and historical) at the storage location of the municipality of Amsterdam. The objective was to characterize the full-length pile properties before their subdivision into segments (Paragraph 3.4).

All the full-length piles were labelled and enumerated by dimensions and weight. The circumference of each pile (O_{avg}) was measured by averaging the pile’s circumference over 4 points along the pile, starting from the pile-head and repeating the measurement approximately every 4 meters (l_2, l_3, l_4) until the pile-tip as shown in Figure 3.8. From the length (L) and O_{avg} , the wet volume (V_{wet}) of the whole pile was calculated with Equation 3.1. Subsequently, the wet density (ρ_{wet}) was determined with Equation 3.2. Furthermore,

3.3 Preliminary in-situ testing on full-length piles

the dynamic modulus of elasticity parallel to the grain ($E_{c,0,dyn,wet}$) was evaluated through the frequency response method using a Brookhuis Timber Grader MTG [161]. From this, the natural frequency of the pile (f) could be determined. By using ρ_{wet} and f , $E_{c,0,dyn,wet}$ could be calculated with Equation 3.3.

$$V_{wet} = \pi \left(\frac{O_{avg}}{2\pi} \right)^2 * L \quad (3.1)$$

$$\rho_{wet} = m_{wet} / V_{wet} \quad (3.2)$$

$$E_{c,0,dyn,wet} = 4 \rho_{wet} f^2 L^2 \quad (3.3)$$

Where: L = full length of the pile; m_{wet} = wet mass; V_{wet} = wet volume; f = frequency determined with MTG grader.

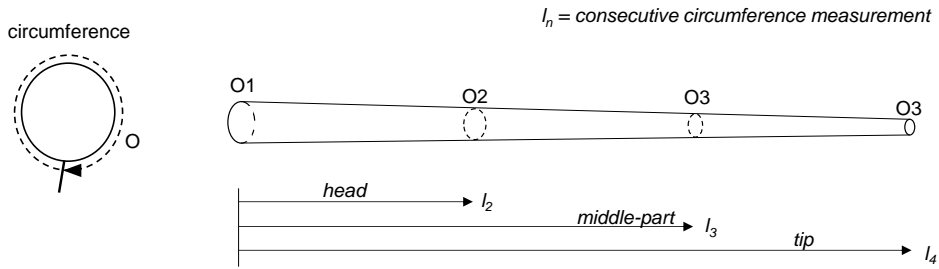


Figure 3.8: Measurements of the circumference (O_{avg}) as average of the circumference ($O_{1,2,3,4}$) measured over 4 points along the length of full-length timber piles.

For piles ND, it was not possible to determine $E_{c,0,dyn,wet}$ along the whole pile, since prior to testing (after the debarking process), they were already subdivided in head, middle-part and tip. Thus, for each pile ND, $E_{c,0,dyn,wet}$ was determined separately for head, middle-part and tip, and estimated for the complete pile as average $E_{c,0,dyn,wet}$ value of the three parts.

After these preliminary tests, the full-length piles were subdivided in three parts: head, middle-part, and tip, each approximately 4-m long. This was done to facilitate storage and handling operations and to provide already 3 parts from which the pile segments were to be extracted (Paragraph 3.4). The 4-m parts were stored underwater in containers to preserve the fully-saturated conditions of the piles in-situ, where they remain fully submerged under the water table. The containers were kept filled with water until shipping to the TU Delft was possible. Subsequently, upon request, the water was drained and the containers with piles were sent to the TU Delft Stevin 2 laboratory for the characterization of their material and mechanical properties.



Figure 3.9: a) preliminary testing of timber piles; b) frequency response measurements with a Timber Grader MTG.

3.4 Subdivision of the piles into segments

At the arrival of every batch of piles, each 4-m pile part (head, middle, and tip) was sawn in segments (Figure 3.10) with a length of approximately 6 times the smallest diameter of the conical log sections according to EN 408 (2010). This was done to characterize the mechanical properties of standardized specimens undergoing compression tests parallel to the grain, along the length of the pile. All the piles (both “new” and historic) were subdivided into segments.

The cutting process was executed using a laser positioning system (Figure 3.11a) with the pile meticulously aligned within a wooden frame to achieve a straight orientation. After that, a frame-guided chainsaw was used to obtain a parallel plane on the ends, with a laser line indicating the exact position of the cut (Figure 3.11b).

Three length categories were established: 900 mm (pile diameter $D < 160$ mm), 1350 mm ($160 \text{ mm} \leq D \leq 240$ mm) and 1800 mm ($D > 240$ mm). In this way, the cutting process resulted to be faster, given the large amount of pile segments, approximately respecting the length-diameter ratio of 1:6 in accordance with EN 408 (2010).

During handling and cutting procedures, the piles were kept in wet condition to avoid drying and consequent cracking (potentially influencing the mechanical properties in compression), with a minimum moisture content value of 50%, well above fiber saturation point. This was done to obtain the same in-soil conditions, where the piles are fully under the water table, in order to determine comparable mechanical and physical properties during testing.

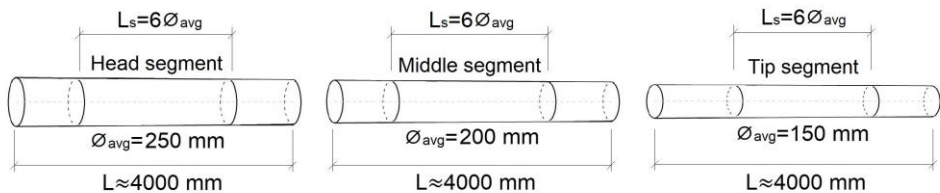


Figure 3.10: Subdivision of a timber pile in head, middle-part and tip and pile segments



Figure 3.11: Procedure for cutting the pile segments from head, middle-part and tip: (a) laser positioning system; (b) frame-guided sawing.

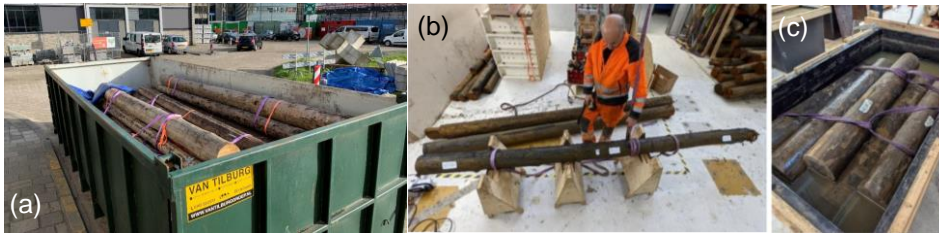


Figure 3.12: (a) Container with timber piles divided in parts (head, middle-part and tip); (b) cutting of pile segments from each part; (c) batch of pile segments submerged in water after cutting.

3.5 Characterization of the material properties

The material properties of all the pile segments were characterized in order to find their correlations with the saturated compressive strength of the piles. The material properties included:

- Experimentally-determined properties (Paragraph 3.5.1): moisture content (MC), wet density (ρ_{wet}), dry density (ρ_{dry}), dynamic modulus of elasticity ($E_{c,0,dyn,wet}$).
- Visually-determined growth characteristics (Paragraph 3.5.2): diameter (D), number of annual rings (Age), rate of growth (RoG), maximum knot-ratio at the failure section (KR), slope of the grain (SoG) and tapering.

3.5.1 Experimentally-determined properties

The moisture content (MC) was determined with the oven-dry method, according to EN 13183 2002 [148], for two 30-mm-thick discs taken from both sides of each selected segment (Figure 3.13). The discs were oven-dried at a temperature of 103 °C until a constant mass was achieved. MC was then determined from the ratio between the difference between wet and dry mass, and dry mass of the discs (Equation 3.4).

The global MC of the whole cross section was determined. The global MC values were related to global large-scale mechanical testing performed on the pile segments

Materials and Methods

(Paragraph 3.6), where the mechanical properties were determined in relation to the full cross-section of the pile. MC was therefore assumed to be comparable to that of the in-situ piles fully submerged under the water table.

$$MC = \frac{m_{wet,disc} - m_{dry,disc}}{m_{dry,disc}} \quad (3.4)$$

Where: $m_{wet,disc}$ is the mass of the disc at a given MC; $m_{dry,disc}$ is the mass of the oven-dry disc (MC = 0%).

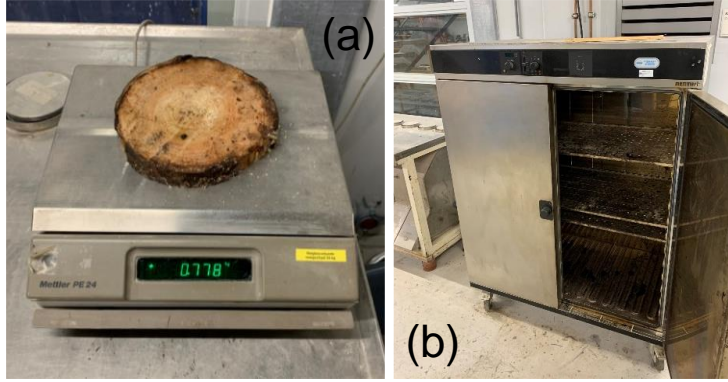


Figure 3.13: (a) weighing of a 30-mm-thick disc after the cut; (b) oven used for drying the samples at 103°C.

The wet density ρ_{wet} of the segments was calculated from the ratio between m_{wet} of the pile segment and the wet volume (V_{wet}) of the pile segment at test MC. m_{wet} and V_{wet} were calculated immediately after the calculation of MC of the discs. In this way the MC of the discs could be precisely related to the MC of the pile segment.

The dry density ρ_{dry} (at MC = 0%) of the segments was also calculated, from the ratio between the dry mass of the pile segment (m_{dry}) and the dry volume of the pile segment (V_{dry}), according to Equation 3.5.

The pile segments were not oven-dried due to their large dimensions and number (in total 454 samples, with average length of 1.5 m); thus, V_{dry} was calculated from V_{wet} , assuming an average 12% volumetric shrinkage from green to oven-dry MC for both spruce, pine and fir, according to [96].

$$\rho_{dry} = \frac{m_{wet} / (MC+1)}{V_{dry}} \quad (3.5)$$

In addition to this, the density at MC = 12% (ρ_{12}) was calculated, in order to have a standardized value comparable with results in the standards and literature, where ρ_{12} is reported for the density. ρ_{12} was determined in Equation 3.6 from the calculated mass m_{12} (Eq. 3.7) and the volume V_{12} at MC = 12% (Eq. 3.8). In order to determine V_{12} , the

3.5 Characterization of the material properties

volumetric shrinkage at MC = 12% was calculated on the basis of the following three assumptions according to [96]:

- shrinkage starts at the fiber saturation point (MC = 30%);
- the dimensions of the pile decrease linearly with decreasing MC;
- variability in volumetric shrinkage can be expressed using a coefficient of variation of approximately COV = 15 %, accounting for wood's intrinsic growth characteristics.

Based on this, Equation 3.8 was used to calculate the volume V_{12} at MC = 12%.

$$\rho_{12} = m_{12} / V_{12} \quad (3.6)$$

$$m_{12} = m_{\text{dry}} (1 + u_{\text{ref}}) \quad (3.7)$$

$$V_{12} = V_{\text{wet}} \cdot (1 - S_0) \cdot (1 - u_{\text{ref}} / u_{30}) \quad (3.8)$$

Where:

V_{wet}	volume at test moisture content.
$u_{30} = 30\%$	moisture content at fiber saturation point (assumed equal to 30% [96]).
$u_{\text{ref}} = 12\%$	moisture content at 12%.
$S_0 = 12\%$	volumetric shrinkage from green (MC = 30%) to oven-dry (MC = 0%) assumed to be 12% [96] for both pine and spruce.

Finally, the dynamic modulus of elasticity $E_{c,0,\text{dyn,wet}}$ was determined through the frequency response method, using a Timber Grader (MTG) tool (Figure 3.14). This measurement was performed on every segment of the pile, prior to mechanical testing when all the specimens were above fiber saturation, with an average MC higher than 70%. $E_{c,0,\text{dyn,wet}}$ was calculated with Equation 3.5.

$$E_{c,0,\text{dyn,wet}} = 4 \rho_{\text{wet}} f^2 L_s^2 \quad (3.9)$$

with ρ_{wet} = wet density, f = frequency and L_s = length of the segment.



Figure 3.14: Frequency response measurements performed on a timber pile segment with an MTG Timber Grader.

3.5.2 Visually-determined growth characteristics

The diameter, number of annual rings (Age), rate of growth (RoG), maximum knot-ratio at the failure section (KR), slope of the grain (SoG), and tapering, can give information on the wood quality influencing strength, stiffness, and density [71], [72] (Section 2.4).

For every pile, RoG was calculated by counting the number of growth rings over the outer 75% of the radius of the cross section, in accordance with NEN-EN 1309-3 (2018) [149]. An example is provided in Figure 3.15, where the pith is eccentric: the length equal to 75% of the radius was divided by the number of growth rings counted, RoG was expressed in millimeters. After this, Age was calculated over the radius R , by counting the annual rings. In some cases it was difficult to count all the rings, especially close to the outer side of the cross section, therefore a measurement error of 5-10% should be considered.

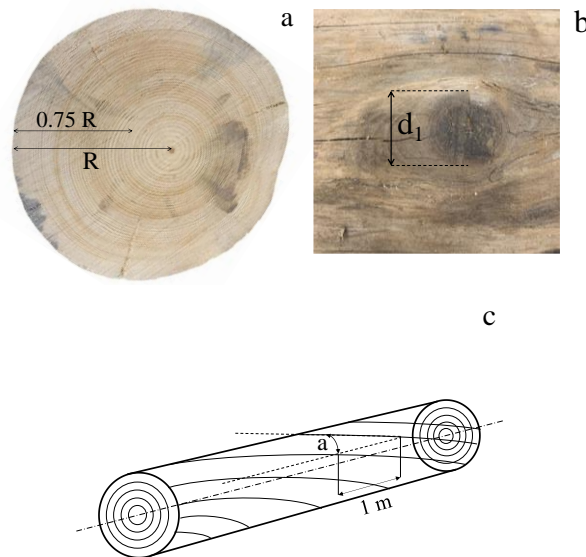


Figure 3.15: (a) Rate of growth calculation over $0.75 R$, and annual rings over R , for a cross section where the pith is eccentric; (b) measurement of the diameter d_1 of a knot perpendicular to the longitudinal direction of the log; (c) slope of the grain measurement over a distance of 1 meter.

The knot ratio (KR) was measured according to NEN 5491 (2010), i.e. the ratio between the sum of the knot diameters perpendicular to the longitudinal axis of the log, over a 150 mm length, and the circumference of the log in that section. The knots are wood defects where the fiber deviates, potentially reducing the compressive strength of the pile-segment in the section where they occur (see paragraph 2.4.4). Therefore, the correlation between compressive strength and KR where failure occurred was studied. In order to comply with the strength grading requirements provided in the standard NEN 5491 (2010), KR of round wood has to be less than or equal to 0.5, while the largest knot has to be less than or equal to 50 mm or $1/12$ of the circumference. These suggestions given in NEN 5491 (2010) for timber piles grading were taken into account. However, the samples with $KR > 0.5$ were not excluded from the analysis; all the measured KRs were considered for the correlation with the compressive strength.

The slope of the grain (SoG) was determined in accordance with NEN-EN 1309-3 (2018), (Figure 3.15). The values were reported in the following increments: 1/4, 1/6, 1/8, 1/10, 1/12, etcetera, to analyse the effect of SoG on the mechanical properties, where $\text{SoG} = 1/10$ ($\alpha = 5.7^\circ$) is considered as the current highest acceptable value for strength grading according to the draft of prEN 1995-1-1 (2023). However, all the SoG values were considered to study their influence on the mechanical properties. Given the fact that it is difficult to visually measure SoG of wet piles, the measurements were conducted after drying, with MC ranging at 7-20%, when most of the specimens showed visible surface cracks.

The diameter of the pile at the head and the tip is measured, and classified in sizes. Based on the minimum tip diameter selected for pile, the new Eurocode 5 2023 [21] provides sizes for the piles ranging from 8 – 16, from a minimum diameter of ca. 75 mm (circumference 240 mm), up to a diameter of 155 mm (circumference of 490 mm).

The effect of tapering on the mechanical properties was analysed, by measuring the ratio between the difference in diameter of head and tip of the pile segment and its length. The influence on the mechanical properties was investigated considering that a constant taper limited to a maximum of 15 mm/m over the whole length complies with the pile grade requirements specified in NEN 5491 (2010). Below this threshold, it was found that the bearing capacity of the piles remains unaffected [82].

Finally, the cutting procedure of the piles was performed in such way that the straightness of all the pile segments selected did not deviate from the straight line more than 1% of the length.

3.6 Full-scale compression tests

Mechanical testing was performed to determine the short-term strength and stiffness parallel to the grain, all over the length of the timber piles, by testing in compression the pile segments. From the test, the wet compressive strength ($f_{c,0,\text{wet}}$) and static modulus of elasticity ($E_{c,0,\text{wet}}$) parallel to the grain were determined. This test was applied to all the piles, both “new” piles and historical piles.

Prior to conducting full-scale mechanical testing on the pile segments, the wet density of each pile was determined by measuring wet mass and volume. For the mechanical tests, a displacement-controlled set-up was used (Figure 3.16), where the specimens were subjected to an axial load in direction parallel to the grain in accordance with EN 408 (2010) and EN 14251 (2003). The precise displacement between the two steel plates during the mechanical testing was monitored using four linear potentiometers (S-sensors), which were placed on the four edges of the top plate and connected to the bottom plate. The deformation of the specimens was measured with four linear potentiometers that were attached to the surface of the pile (P-sensors), positioned at 90° intervals on each side of the pile, with a variable length equal to two-thirds of the length of the specimen. Given the short stroke of the four P-sensors placed on the pile, they were removed right after the peak load to avoid damages. The post-peak softening was monitored only by the S-potentiometers attached to the top and bottom steel plates of the compression machine. In addition, a hinge, mounted on a steel plate, was placed on top of the specimen to have a uniformly distributed compression load on the pile. The tests were conducted at a displacement rate of 0.02 mm/s until the peak load was reached. After the peak load

(reached at approximately 5 minutes according to EN 408), the test continued at a higher speed until the cracks were visible, and to show the post-peak behaviour of the pile (EN 14251 2003).

Upon completion of the test, $f_{c,0,wet}$ was calculated by taking the ratio of the maximum force achieved in compression by the specimen and the average cross-sectional area of the pile. The global behaviour of the piles was studied with the average stress-strain curve of the four linear potentiometers connected to the compression test machine; the strains were calculated considering the length of the specimen. $E_{c,0,wet}$ was calculated from the stress variation ($\Delta\sigma$) divided by the strain variation ($\Delta\varepsilon$), between 10% and 40% in the slope of the linear elastic portion of the stress-strain curve according to NEN-EN 408:2010 (Equation 3.10).

$$E_{c,0,wet} = \Delta\sigma / \Delta\varepsilon = (\sigma_2 - \sigma_1) / (\varepsilon_2 - \varepsilon_1) = (\Delta F / \Delta L) / (L_0 / A_r) \quad (3.10)$$

With:

$\Delta\sigma$ = stress variation between points σ_2 and σ_1 ;

$\Delta\varepsilon$ = strain variation between points ε_2 and ε_1 ;

ΔF = force variation between points ($F_2 = 0.4 F_{max}$ and $F_1 = 0.1 F_{max}$);

ΔL = deformation variation corresponding to points F_2 and F_1 ;

L_0 = length of the linear potentiometers screwed on the pile (mm),

A_r = cross-sectional area (mm).

Finally, in order to study the expected failure mechanisms, pictures were taken after reaching the peak load during the compression test, where compression wrinkles and horizontal cracks are visible around the failure area, accompanied by and longitudinal cracks in correspondence of a knot or sections with multiple knots (whorl).

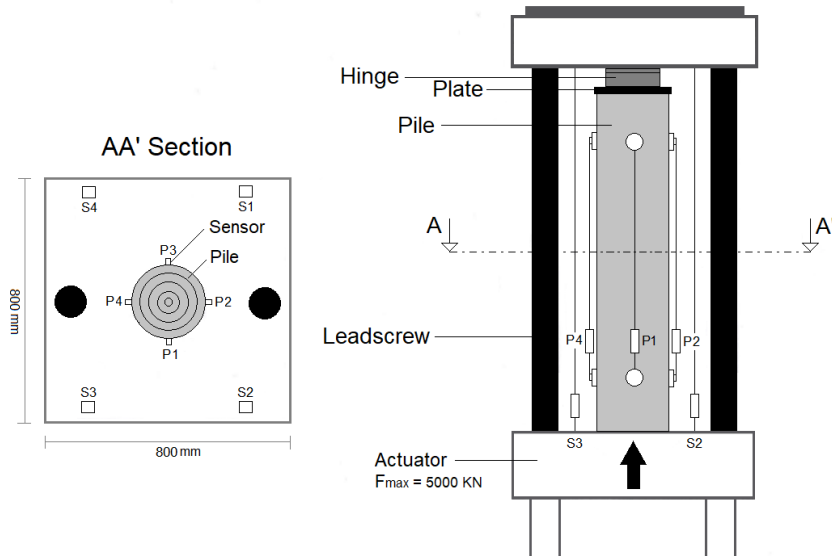


Figure 3.16: Sensors positioning and set-up for the compression test of pile segments.

Table 3.3: Description of the sensors used for the compression test.

Name	Description	Sensor Type	Stroke (mm)
Actuator	Vertical actuator. Max force 5000 kN.	Hydraulic actuator	+/- 100
S ₁ , S ₂ , S ₃ , S ₄	Vertical displacement between top and bottom steel plates of the compression machine	Linear potentiometers	+/-50
P ₁ , P ₂ , P ₃ , P ₄	Deformation of the wooden pile measured on each side of the pile. The sensors span 2/3 of the length of the pile.	Linear potentiometers	+/-20

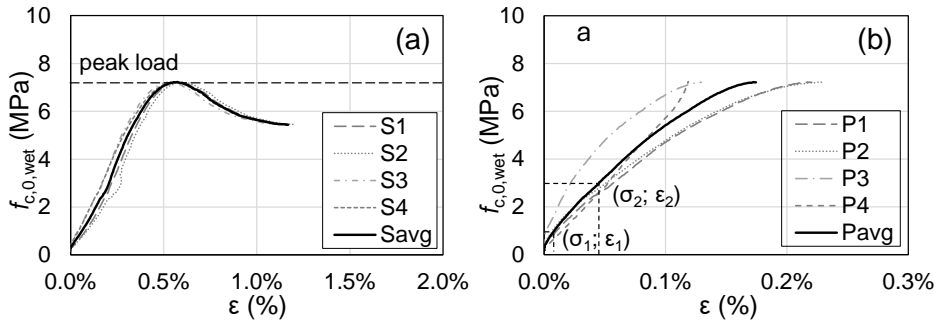


Figure 3.17: Example of axial compression tests of a water-saturated pile segment: a) global behaviour of the pile, stress-strain curves measured by S-sensors; b) stress-strain curves measured by P-sensors to determine the $E_{c,0,wet}$.

3.7 Visual grading of “new” wooden foundation piles

There are currently two types of strength grading systems in use in Europe, adopted for sawn timber: visual grading and machine grading [172].

Visual grading is carried out by means of visual inspection, (i.e. boards visually examined by humans or optical scanners) to ensure that certain visible defects (such as knots, slope of grain, etc.) do not exceed limits specified in the grading rules EN 14081-1 2016. Machine grading includes parameters (e.g., dynamic modulus of elasticity), which cannot be determined by means of visual analysis. The determination of these parameters is carried out using an approved grading machine (e.g. Brookhuis MTG Timber Grader used in this study), or a combination of machines, directly measuring one or several board properties non-destructively, to predict their strength, stiffness, and density.

The strength grading of round timber is not as developed as for sawn timber. Visual grading rules are provided in the Dutch grading standard for timber foundation piles (NEN 5491 2010) leading to a single strength grade for spruce, larch and Douglas fir based on $KR < 0.5$ (NEN 6760:1997). Previous studies have analysed the possibility and effectiveness of strength grading round timber, mainly by visual methods but only in dry conditions [172]–[179]. Some research was conducted also with machine grading, but only

limited to the investigation of the effectiveness of predicting the mechanical properties of wood by non-destructive measurements [172],[175],[178].

On this basis, possible strength grades and grade boundaries were determined based on visually-graded parameters for the “new” spruce and pine piles tested in this research. The potential benefit of having more than one grade for the application of softwood foundation piles depends on how much the strength values differ between grades compared to the actual effort in engineering practice and a potential increase in rejected piles. The benefit of having multiple strength classes can aid engineering design by allowing for more precise material selection based on specific strength requirements. This may enable engineers to optimize designs, potentially reducing material usage and costs while improving overall performance and safety.

The visual grading was carried out according to Annex P of the draft of the Eurocode 5 2023, partly based on the Dutch grading standard for timber foundation piles NEN 5491 2010. The correlation between visual grading (according to Annex Q of draft EC5 2023) and the saturated compressive strength was studied along the spruce and pine piles, in order to derive possible strength classes for an adequate design of timber piles. Only the saturated compressive strength of “new” spruce and pine piles was taken into account for visual grading, since timber foundation piles are only used in saturated conditions. This is also specified in the draft EC5 2023 where *“timber foundation piles should be calculated based on the characteristic compressive strength parallel to the grain of piles which are in fully saturated condition as specified in EN 14358”* [150].

Thus, a new approach for grading saturated timber piles is proposed in this thesis, according to the guidelines outlined in the draft of the EC 5 (EN 1995-1-1 2023). The visually-graded properties were used to calculate one or several Indicating Properties (IPs) by means of regression analyses (explained in Appendix A). By choosing predefined limits for the IPs, the pile segment is either assigned to a graded class or rejected. Development and evaluation of a visual grading method consist of two parts (fully showcased in Appendix A). The first one concerns definitions and calculations of IPs by means of regression analysis. The second part consists of determining limits for the IPs for the calculation of characteristic values for the wet compressive strength of spruce and pile segments to be assigned to possible grading classes.

The grading of the tested pile segments was done by measuring visually graded characteristics that could possibly relate to the saturated compressive strength along the length of the pile (Section 4.3). These included visual grades of: number of annual rings (Age), rate of growth (RoG), maximum knot-ratio at the failure section (KR) which revealed to be the parameters with the larger influence on the compressive strength.

3.8 Determination of characteristic values

Characteristic values (mean $E_{c,0,wet}$ and the 5-percentile value of $f_{c,0,wet}$ and ρ_{12}) were determined for “new” spruce and pine piles, according to the parametric calculation in NEN-EN 14358 [150]. The goal was to provide characteristic compressive strength and stiffness parallel to the grain for saturated “new” spruce and pine piles to be used for

visually graded piles together with the provisions given in prEN 1995-1-1/NB:2023 [10]. The procedure for the derivation of characteristic values is explained in detail in Appendix A3.

3.9 Assessment of decay with micro-drilling measurements

Micro-drilling measurements fall within the non-destructive techniques used for wood inspection. Micro-drilling measurements were adopted in this research as an assessment technique to investigate the (potential) amount of decay within the cross section of historical timber piles. Micro-drilling was not adopted for “new” timber piles, since they were not decayed.

In this study, a IML-RESI PD 400 tool was used to conduct micro-drilling measurements on the historical spruce and fir piles. During micro-drilling, a drilling needle is pushed into the pile’s cross-section with a drill speed of 2500 r/min and a feed speed of 150 cm/min. These settings were kept for all the conducted measurements in this study. The drill bit used for the measurements was 400 mm long, with a thin shaft of 1.5 mm in diameter and a 3.1 mm wide triangular-shaped cutting part, with hard chrome coating. The acquired data, recorded every 0.1 mm of the drilling depth, was plotted as amplitude vs distance. The amplitude is expressed as the percentage of the maximum drilling power of the engine, employed while drilling through the material with the aforementioned settings of drill and feed speed.

All the 60 historical timber piles were subdivided in segments and tested with micro-drilling measurements at the TU Delft laboratory. Two micro-drilling measurements were performed through the cross-section of each pile segment (in head, middle-part and tip), approximately 90 degrees to each other and 300 mm from the head of the segment itself (Figure 3.18). In this way, it was possible to map the amount of decay within the cross section and along the whole length of the pile, assuming linear interpolation between the analysed cross sections.

Each measurement was performed before testing the specimens in compression, in order to have the most accurate correlation between the material status and the derived remaining short-term compressive strength.

By observing the resistance profile of each micro-drilling signal, it is possible to map the annual rings, with maximum amplitudes, corresponding to latewood rings, and minimum amplitudes, representing early-wood (as exemplified in Figure 3.18). All these parameters were considered, including isolated peaks or lower values detected in the resistance profile related to:

- wood knots and other high-density anatomical variations of the material (i.e. compression wood);
- piths and cracks in the cross-section, creating voids through which the drilling tool records zero or very low resistance.

Figure 3.18 shows drilling signals A and B of a pile that exhibits degradation in the outer 20-30 mm of the cross-section: the two drilling signals A and B are not perfectly superimposable, this is because the degradation pattern around the cross section can vary.

To this end, a detailed procedure is presented in Paragraph 3.9.1, to determine the decayed portion of the cross section (called “soft shell”) of historical timber piles.

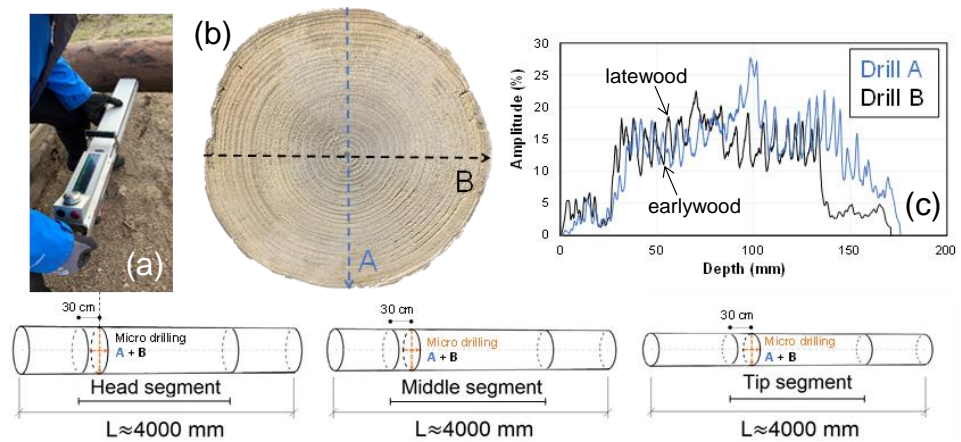


Figure 3.18: (a) Micro-drilling measurements on a wooden pile; (b) drill A and B performed 30 cm from the head of the pile segment; (c) micro-drilling signal plotted as resistance (amplitude: percentage of the maximum engine power during drilling) vs distance (in mm).

3.9.1 Determination of the soft shell with micro-drilling

In order to evaluate the degraded portion of the cross section of the historical piles, the micro-drilling signals A and B performed on each pile segment were analysed with an algorithm developed by the TU Delft (fully reported in Appendix E). The purpose of the algorithm is to analyse the micro-drilling signal and to subdivide it into zones based on the signal amplitude. The algorithm is based on the differences in signal values and not on absolute values, starting from the assumption that the wood in the centre of the pile is sound.

First, the signal is smoothened to a Drilling Moving Average (Drill_MA), giving the average of the length of the signal between 5 mm before and 5 mm after a specific signal point. This process involves calculating the average value of the drilling amplitude (y-axis in Figure 3.19) over a specific range, specifically from 5 mm before to 5 mm after a given point along the drilling depth (x-axis in Figure 3.19). This results in a smoother signal by averaging fluctuations (drops and peaks). Subsequently, an Incremental Outwards Moving Average (IOMA) is calculated for both sides starting from the centre of the signal. This involves computing the average of the Moving Average values incrementally outward from the centre point, for every signal point, on both sides of the signal, gradually including more data points in the calculation as moving outward from the centre. The maximum IOMA value on both sides is considered to be the value for sound wood. From this, 4 zones are determined through chosen ratios between the regular moving average of the signal and the maximum value of the IOMA. Zones 1, 2, 3, 4 on each side correspond to the point in which the Moving Average, seen from the outside part, reaches 20%, 40%, 60%, and 80% of the maximum value of the IOMA on that side (Figure 3.19).

The soft shell – the degraded portion of the cross section – is finally calculated as the sum of a number of zones, which number is determined according to Paragraph 3.9.2 and presented in Paragraph 5.3. In Figure 3.19, an example is given when the soft shell is assigned to zones 1+2. In this way, for each micro-drilling measurement, it was possible to assess the zone allocation in a relative way.

It should be noted that micro-drilling is a local measurement, thus, it may happen that the soft shell determined in a specific cross section of the pile may differ if measured in other positions over the length of the specimen. In order to minimize this effect, all the micro-drilling measurements were performed in positions without visible defects or irregularities in the material. The total soft shell of a decayed cross section was calculated as the average of the 4 lengths of the soft shell (SS), determined according to the next paragraph, corresponding to left and right sides of micro-drilling signal A + B. From this, the average length of the soft shell (al_{ss}) was calculated with Equation 3.15. Subsequently, the remaining sound cross-sectional area (A_{sound}), i.e. the part of the cross section that did not exhibit degradation, was calculated by subtracting al_{ss} to the radius (r) of the whole cross-section, and expressed as a percentage of the full cross-sectional area (A_{tot}) in Equation 3.16.

$$\text{Average soft shell length (mm)} = al_{ss} = (SS_{A,left} + SS_{A,right} + SS_{B,left} + SS_{B,right})/4 \quad (3.11)$$

$$A_{sound} (\%) = A_{sound} / A_{tot} (\%) = [\pi(r - al_{ss})^2 / \pi r^2] * 100 \quad (3.12)$$

It should be noted that micro-drilling is a local measurement. Thus the soft shell measured in a cross section may differ if measured in other positions over the length of the specimen. In order to minimize this effect, all the micro-drilling measurements were performed in positions without visible defects or irregularities in the material.

The average length of the soft shell was calculated as the average of the 4 lengths of the soft shell (the left and right sides of measurements A + B) and expressed in terms of the average length of the soft shell (al_{ss}) in mm (Figure 3.20). Subsequently, the average soft shell area was calculated according to Equation 3.9.

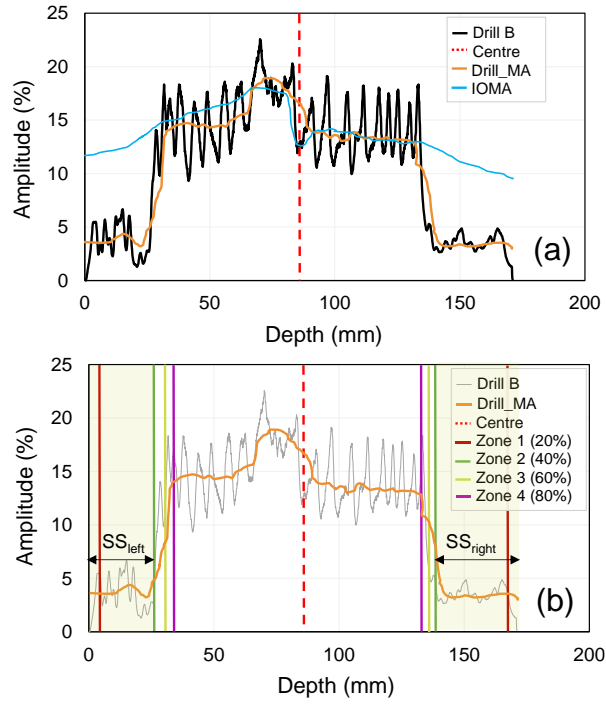


Figure 3.19: Example of the analysis of the drilling signal (*Drill B*) for the decayed spruce pile shown in Figure 2: (a) drilling moving average (*Drill_MA*) and IOMA from which the zones are calculated; (b) 4 zones and soft shell (SS_{left} and SS_{right}) associated to zone 1+2.

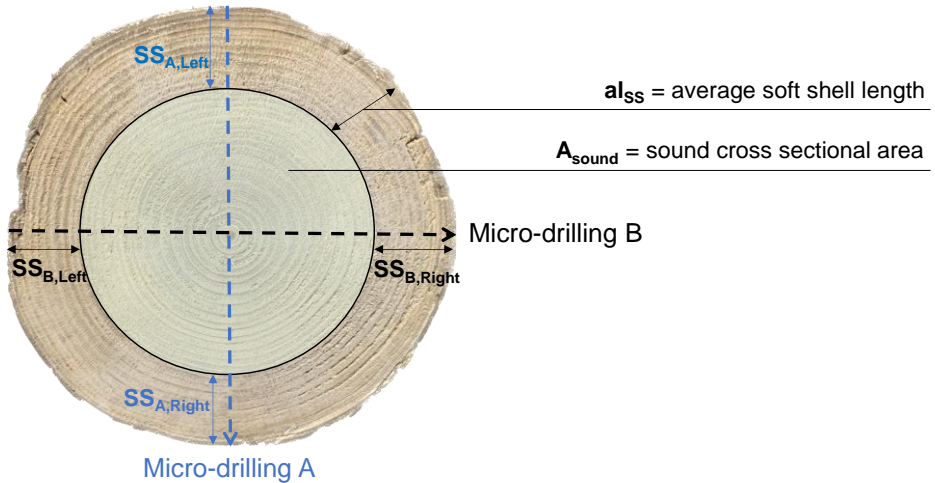


Figure 3.20: Average soft shell length (a_{ss}) calculated considering the average of 4 soft shell lengths as in Equation 3.11 measured with micro-drilling measurements A and B, and analysed with the 'soft shell calculator'.

3.9.2 Validation of the zones associated with the soft shell based on the results of mechanical testing

In order to validate the zones correlated to the soft shell (to which zero compression strength is assigned), the following procedure was followed:

- A. The pile segments extracted from the retrieved piles that did not exhibit decay, according to the micro-drilling analysis in Section 3.9.1, were identified. These sound segments revealed a sound cross-sectional area (A_{sound}) between 95-100% of the full cross-sectional area (A_{tot}). This means that the sum of zones 1+2+3 of both sides was less than 5% of the diameter of the pile. The full cross-sectional area was used to calculate the average sound compression strength ($f_{c,0,wet,sound}$) of these segments, for head, middle-part and tip.
- B. The selected sound segments only belonged to 1922 and 1886. Thus, the average $f_{c,0,wet,sound}$, i.e. the sound compressive strength of non-decayed piles, was taken from the test results of a total of 62 pile segments from 1922 and 1886.
- C. For all piles from 1922 and 1886, $F_{c,0,mod}$ was calculated according to Equation 3.13, with the average $f_{c,0,wet,sound}$ of the 62 pile segments and A_{sound} of each pile, determined by subtracting al_{ss} (Eq. 3.11) to the full pile radius (r), calculated with Zone 1, Zone 1+2, and Zone 1+2+3, respectively.

$$F_{c,0,mod} = f_{c,0,wet,sound} * A_{sound} = f_{c,0,wet,sound} * \pi(r - al_{ss})^2 \quad (3.13)$$

- D. A correlation analysis was conducted between the maximum force measured with compression tests of the pile segments ($F_{c,0,test}$) and the force ($F_{c,0,mod}$) calculated with Zone 1, Zone 1+2, and Zone 1+2+3, respectively. With this, the number of zones describing the soft shell are determined.
- E. With the chosen number of zones associated with the soft shell, which revealed to be zones 1+2 (Paragraph 5.3), the soft shell is calculated for all segments including those from 1727. Also, for segments with a sound cross section above 95%, the soft shell is calculated. The soft shell of each pile is subtracted from the whole cross section, resulting in the final sound compressive strength, including all piles, also from 1727. This is named equivalent sound compressive strength (EQ $f_{c,0,wet,sound}$) derived for every building year and for head, middle and tip. Hereby the assumption is made that the soft shell will not take up forces and zero strength and stiffness are allocated to this part. This means that the entire force is taken up by the remaining sound cross-sectional area A_{sound} .
- F. Finally, $F_{c,0,mod}$ was calculated, by applying Equation 3.14 to all pile segments, with the soft shell corresponding to zones 1+2, and plotted against all $F_{c,0,test}$ values.

$$F_{c,0,mod} = EQ f_{c,0,wet,sound} * A_{sound} = EQ f_{c,0,wet,sound} * \pi(r - al_{ss,zone1+2})^2 \quad (3.14)$$

3.10 Influence of moisture content variation on micro-drilling signals

Micro-drilling measurements were conducted on wooden piles at varying moisture content levels to evaluate the technique's reliability in assessing decay levels

independently of moisture variations. This part of the methodology was developed in collaboration with my colleague dr. Michele Mirra [31].

This validation aimed to:

- Assess the reliability of micro-drilling in accurately capturing cross-sectional features, such as sound or decayed sapwood and knots, across different moisture content values.
- Establish a correlation between laboratory and in situ measurements, demonstrating that the micro-drilling data obtained from tested piles can be reliably compared to in situ measurements performed on pile heads.

By integrating micro-drilling as an alternative or support to the current method of extracting drill cores for soft shell determination, this approach offers several advantages. It enables comprehensive inspections of the material condition across the entire pile cross-section at multiple positions and orientations. Additionally, it provides a greater volume of data, facilitates faster in situ assessments, and reduces both costs and practical limitations associated with traditional core extraction methods.

A total of 24 segments from wooden foundation piles with a time in service (TS) ranging from 2 to 294 years (with reference to 2021 – when their extraction took place) were selected, and micro-drilling measurements were conducted at varying MC values between 7% and 212% (Table 3. 4). The outcomes from micro-drilling measurements were studied, with reference to different parameters besides MC itself, such as drill and feed speed, drilling depth, wood species, all factors influencing the shaft friction along the drill [159]-[160].

This analysis was conducted considering the following two scenarios:

- Assessment of the possible influence of different MC values referred to a whole segment on the corresponding drilling resistance (DR), thus an analysis at the global segment level;
- Evaluation, with reference to submerged conditions, of the possible influence of the MC gradient along the drilling depth on the micro-drilling signals, thus an analysis at the cross-sectional level.

Table 3. 4: Overview of the time in service (TS) and moisture content (MC) of the tested pile segments.

Number of segments	TS (years)	MC range (%)
6	294	13-212
6	135	8-57
6	99	12-100
6	2	7-84

The micro-drilling measurements were conducted with an IMLRESI PD400 drill. All measurements were taken 30 cm below the top of each segment, in two orthogonal directions (A and B) and with the same settings reported in Paragraph 3.9. The first two (A+B) micro-drilling measurements were executed on each segment in submerged

conditions, immediately prior to its compression test. Other four micro-drilling measurement (A+B) were then taken during the drying process of each segment after the compression test, recording every time the weight of the segment and determining the corresponding global MC. A total of 240 micro-drilling measurements were conducted.

After testing the segments in submerged conditions, the corresponding MC gradient along the drilling depth was determined as well, by retrieving five small prisms of dimensions $20 \times 20 \times 120 \text{ mm}^3$ (Figure 3.21). Sample 3 was taken in correspondence to the pith, approximately within the first 10 annual rings. Samples 1 and 5, were taken from the outer part of the cross section, including sapwood. These prisms allowed to detect the MC variations along the drilling depth: in this way, the influence of such variations on drilling resistance profiles could be evaluated for pile segments with different amounts of decay.



Figure 3.21: Procedure conducted from micro-drilling measurements to the cutting of the disc, from which 5 prisms were obtained.

3.11 Determination of material and mechanical properties of small-scale prismatic samples

Small-scale material and compressive tests were performed on prisms cut along the cross section of tested “new” and historical pile segments. This part of the methodology was developed in collaboration with my colleagues dr. Michele Mirra and ir. Michael Lee [184].

The goal was to:

- Investigate the distribution of the material properties within the cross section of piles with different amounts of decay, in order to determine the remaining material properties of the degraded part and the sound part.
- Characterize the compressive strength of sapwood, heartwood, and juvenile wood, in order to understand the distribution of the compressive strength within the cross section.
- Establish correlations between the material properties of prismatic samples extracted throughout the cross section and micro-drilling measurements executed next to the prisms themselves. The correlations between the material and mechanical properties of the prisms and the micro-drilling signals, to check whether it was possible to predict the material and mechanical properties of a cross section of a pile from its micro-drilling signal.
- Characterize the distribution of decay in the cross-section, and its extension within the cross-section, by means of CT scans (Paragraph 3.12).

To this end, a total of 9 full-length piles were selected, dated back to 1727 (3 piles), 1886 (4 piles), and 1922 (2 piles).

The length of the piles was approximately 12 m, their head diameter ranged from 175 to 260 mm, while their tip diameter ranged from 125 to 210 mm. All piles were made of spruce (*Picea abies*), with the exception of one from 1886, made of fir (*Abies*).

The segments were coded in the form “year-number-pile part” (e.g. 1727–1–head), and were subdivided into two groups of specimens, hereinafter referred to as *group 1* and *group 2* (Figure 3.22), for different purposes:

- *Group 1*: consisted of 15 segments from 5 piles (Fig. 1): 9 segments from 1727, 3 from 1886, and 3 from 1922, in water-saturated conditions.

The main target for the segments in group 1 was the characterisation of material and mechanical properties along the cross section. To this end, a disc was first taken from the pile segments, from which smaller longitudinal prismatic samples were retrieved. For all segments, a location without knots was identified, and before cutting the prisms, two micro-drilling measurements were conducted in the same direction along which the prisms were taken within the cross section, right above and below the prisms themselves (Figure 3.24). Next, 5 20×20×120 mm³ prisms were retrieved from the cross section to test their material and mechanical properties (Figure 3.23), in agreement with EN 408. Additionally, for head, middle part and tip of samples 1727–1, 1886–1 and 1922–1, other 5 20×20×60 mm³ prisms were taken, to assess whether a possible influence of size effect was present. In this way, it was possible to determine the physical, material and mechanical properties of the prisms, and to establish their correlations with micro-drilling measurements. A total of 120 prisms were tested, and 48 micro-drilling measurements were taken.

- *Group 2*: 18 consisted of 18 segments. The main aim was a more detailed characterisation of bacterial decay. Group 2 also included six segments from 1727 which were part of group 1 (Figure 3.22), to ensure a complete characterisation of the piles with the longest exposure time.

Two micro-drilling measurements perpendicular to each other were taken and CT scans (Paragraph 3.12), in correspondence to the micro-drilling measurements were performed. A total of 36 micro-drilling measurements and 18 CT scans were executed. The outcomes from the tests performed on the segments of group 2 allowed to characterise their decay and main features, as well as to obtain their density profiles, retrieved from CT scans. As a final step, the reconstruction of density profiles by means of micro-drilling measurements was also evaluated, thus combining the outcomes of group 1 and group 2.

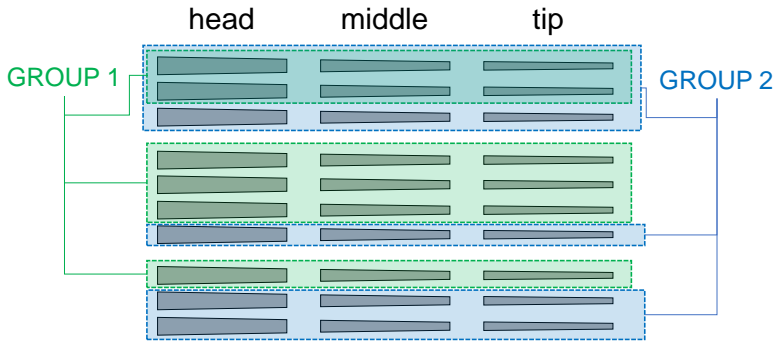


Figure 3.22: Overview of the 2 groups of piles investigated.

In general, the 5 prisms retrieved along the cross section were subdivided into: 2 prisms from the outermost part (1 and 5, containing sapwood and possibly subjected to bacterial decay), 2 containing heartwood (2 and 4), and one on the pith location (3) as illustrated in Figure 3.23. Volume and weight of the prisms for deriving their wet density were subsequently measured by means of a calliper and a scale. For the small-scale compression tests, the application of a compressive load without inducing bending was ensured by means of a hinge. The tests were conducted at a displacement rate of 0.02 mm/s, and both compressive strength $f_{c,0,wet,prism}$ and modulus of elasticity $E_{c,0,wet,prism}$ of the prisms were determined.

After testing, the moisture content of the prisms was determined with the oven-dry method, and their weight and volume for deriving their dry density were also measured by means of a calliper and a scale. In this way, from these experiments, it was possible to reconstruct the density, compressive strength, and stiffness profiles, as well as moisture content gradients along the cross sections of the segments.

It should be noted that all the full segments were already tested with micro-drilling before the compression test, where two measurements were taken 30 cm below the head of each sample, in the two orthogonal directions A and B.

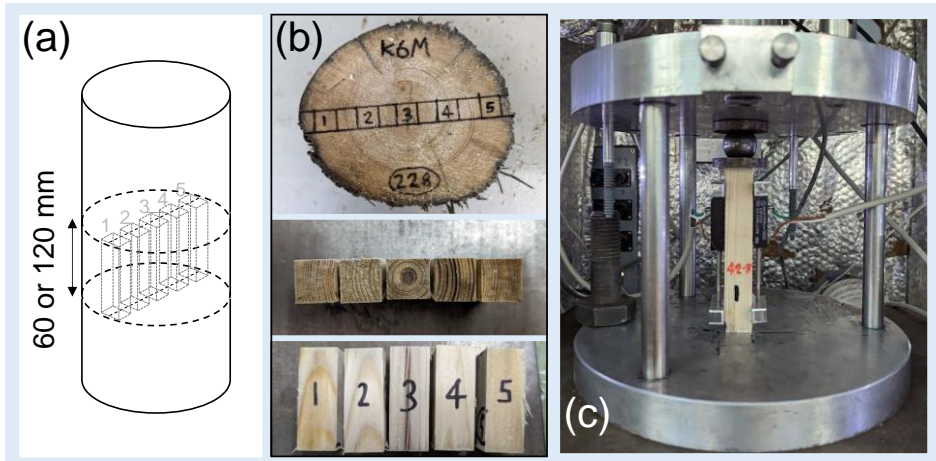


Figure 3.23: (a) extraction of the 60-mm or 12-mm discs from the pile; (b) 5 prisms are extracted along the disc; (c) setup for compression tests of prismatic samples.

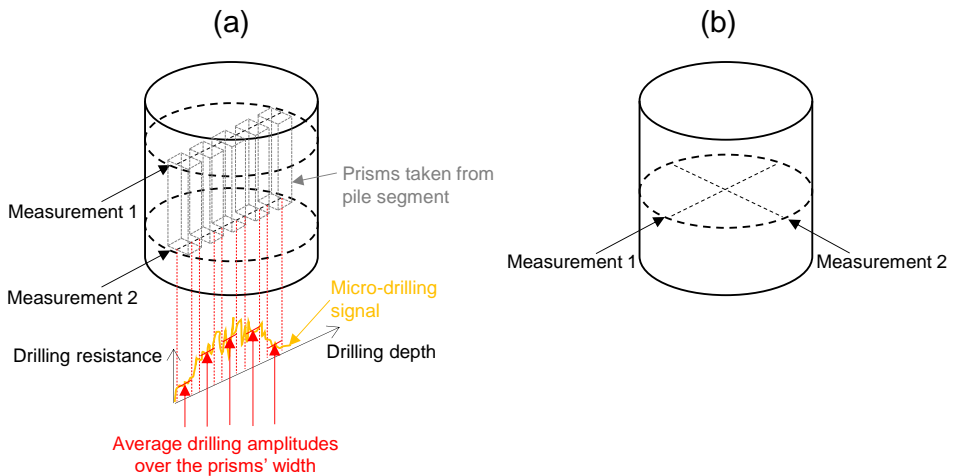


Figure 3.24: Principle for execution of micro-drilling measurements for the first (a) and second group of pile segments (b).

3.12 Computed Tomography (CT) scanning

The application of CT scanning technology in wood science allows the digital extraction of three-dimensional data to perform wood density estimation and radial pattern analysis. The device available at Delft University of Technology, a *Siemens Somatom Definition CT scanner* is shown in Figure 3.25. The CT scanner generates images of the samples via X-ray by measuring the reflected radiations with a 0.6 mm sampling resolution. The obtained images are displayed in grey values reported in Hounsfield units (HU) [158]. In CT, the density of a tissue is always represented using the Hounsfield scale, with water having a value of 0 HU, tissues denser than water having positive values, and tissues less dense than water having negative values [158], up to -1000 HU for air. When using grey values, low-density tissues appear as darker (black) and high-density structures as brighter

(whiter) colours (Figure 3.26). With reference to wooden elements, this representation is associated with brighter colours in correspondence of e.g. knots, and darker colours around low-density or degraded areas [43]. In this way, the difference in densities in cross sections and in whole pile segments could be characterized and reconstructed. For the postprocessing of the scans, conducted with myVGL 2022.1 software, the grey values and associated dried densities were subdivided in ranges, each one of which was assigned a representative colour:

- Red for 90-180 kg/m³
- Orange for 180-270 kg/m³
- Yellow for 270-360 kg/m³
- Green for 360-450 kg/m³ (expected average reference for sound spruce/pine wood)
- Blue for 450-540 kg/m³ (dense sound wood, or knots/compression wood)

Thus, the less dense decayed areas could appear as red-orange, the sound wood as green (or blue, for denser tissue).



Figure 3.25: CT scanning of a historical spruce pile segment from 1727 at Delft University of Technology.

The obtained density profiles from the CT, were used to validate:

- a) The density throughout the cross section of 18 pile segments belonging to group 2 (Section 3.11), dried in indoor conditions for at least three months, in order to optimally capture the variations in measured dried density. CT scans were done in correspondence of the cross-section where micro-drilling was conducted, in order to validate the correlation between micro-drilling and the density determined with small-scale tests on prisms (Section 3.11).
- b) The proportion of sapwood and heartwood in historical spruce and fir piles, where the heartwood and sapwood are not visually distinguishable [75], as explained in Section 2.4. CT scanning allows to experimentally determine the boundary between less-dense heartwood and more-dense sapwood [162],[163], (Figure 3.26). The knowledge on the distribution of sapwood and heartwood within decayed piles, allows to understand the extension of biological decay within the cross section, in order to analyse whether decay is only limited to sapwood or whether it could reach the heartwood. To this end, 45 discs, extracted from their respective

“new”, sound and decayed spruce pile segments, were scanned with CT (Paragraph 3.12.1). The depth of sapwood was compared with the length of the soft shell (determined with micro-drilling), to assess the extension of decay in the sapwood region, and possibly in the heartwood.

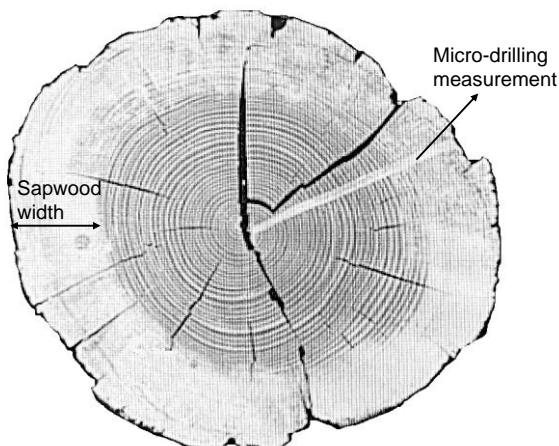


Figure 3.26: Example of identification of sapwood (brighter) and heartwood (darker) in a CT-scanned spruce disc, in correspondence to the section where micro-drilling was conducted.

3.12.1 Determination of the proportion of sapwood and heartwood of spruce piles

The bacterial degradation proceeds radially inward within the pile’s cross section, at first affecting the non-durable sapwood, while the inner part of the cross section of the pile, including the heartwood, tends to exhibit a lower degree of decay or remains sound [8],[10]-[12]. Thus, the proportion of sapwood and heartwood in a timber pile can significantly influence the amount of bacterial decay present within the cross section.

In the case of spruce and fir piles, the proportion of sapwood and heartwood cannot be visually measured (Section 2.4). The boundary between these two parts cannot be distinguished, as the colour is uniform throughout the cross section. To this end, existing models from literature were employed [181], allowing to estimate the sapwood width (W_s) on the basis of diameter d (mm), number of annual rings (Age) and average radial growth rate RoG (mm/year) of a segment (Equation 3.15).

$$W_s (cm) = (3.48 \times RoG^{1.07}) / (1 + 6.82 \times e^{-0.064 Age}) \quad (3.15)$$

Age and RoG were calculated according to Paragraph 3.5.2. However, in the case of extensive bacterial decay, especially encountered in piles from 1727, it was difficult to count the number of annual rings (Age), especially on the outer side of the cross section. Therefore, a measurement error of 5-10% should be considered.

The experimental equation (Eq. 3.15) was validated with CT-scanning of 45 spruce discs, extracted from the same position from which the Age and RoG of the piles were calculated for Equation 3.15. The validation is presented in Appendix D.

CT scanning can provide a reliable picture of the proportion between sapwood and heartwood in the segments. This is because of two properties of sapwood: a higher density compared to heartwood, and a larger moisture content as well in green segments [101]-[103], [106], resulting in a recognizable difference in grey values between the two (brighter colour = higher density; darker colour = lower density) (Figure 3.26 in Section 3.12). This is related to the different water-absorption coefficient along the grain of sapwood compared to heartwood [164]-[166] in the longitudinal direction, (i.e. the one of interest for the discs examined in this study), where spruce sapwood can have a water absorption coefficient up to five times larger than that of heartwood [164]. It should be noticed that when spruce dries, the pits among the cells close [167], possibly leading to variations in the water-absorption coefficient. Yet, when examining moisture contents of wet spruce pile segments, it was noticed that the moisture content gradient along their cross section was very similar to logs in green conditions, thus it should be possible to observe clearly the sapwood/heartwood differentiation.

To this end, each disc was submerged underwater 12 hours prior to CT scanning (Figure 3.27), to allow sapwood to absorb enough water, and then scanned to assess whether in such conditions the CT images allowed to distinguish sapwood and heartwood.

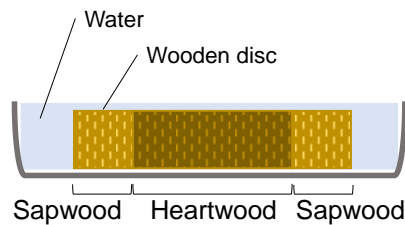


Figure 3.27: Setup for CT scans for determining sapwood and heartwood of pile discs

3.13 Light microscopy observation

To complete the characterisation of biodegradation for the pile segments of group 2 (see Section 3.11), light microscopy observations were performed. This part of the methodology was developed in collaboration with my colleague dr. Michele Mirra [184]. In this way, the extent of decay from the wood surface inwards was assessed. To this end, radial sections with a thickness of 20 μm suitable for microscopic observations were retrieved from the locations where micro-drilling measurements were executed. These radial sections were cut with a *Leica HistoCore Multicut R* microtome, and examined under polarised light with a *Keyence VHX 6000* digital microscope. The use of polarized light enabled the detection of birefringence, a typical feature of cellulose: once this is degraded by bacteria, a loss of birefringence is observed [5],[7],[8]. Bacterial decay was also evaluated by considering wood microanatomical features (presence of erosion channels, degraded cell walls), associated with corresponding decay levels, similar to the classification provided in reference literature for wooden foundation piles [5],[11]:

- No decay: All cell walls are smooth, and show clear, intensive birefringence under polarised light (Figure 3.29 -A1).
- Light decay: In earlywood, isolated tracheid cell walls are degraded, showing grooved-like erosion; in latewood, tracheids are free of degradation; Rare attacks visible on longitudinal cell walls (Figure 3.28a).
- Moderate decay: Diffuse isolated degraded tracheids in a matrix of sound cells can be observed; in most earlywood tracheids, grooved-like eroded areas following the microfibrils angle are present, and these areas are sharply separated from sound cell walls. Latewood tracheids feature triangular-shaped notches (Figure 3.28b and Figure 3.29 -A2);
- Severe decay: The majority of cell walls are decayed. Isolated sound cells in a matrix of degraded cells can be observed, with almost all tracheid cell walls fully eroded (Figure 3.28c); in earlywood, grooved-like erosion channels in cell walls are present, following the microfibril angle. Since almost all cell walls are eroded, no birefringence is observed in them (Figure 3.29-A3).

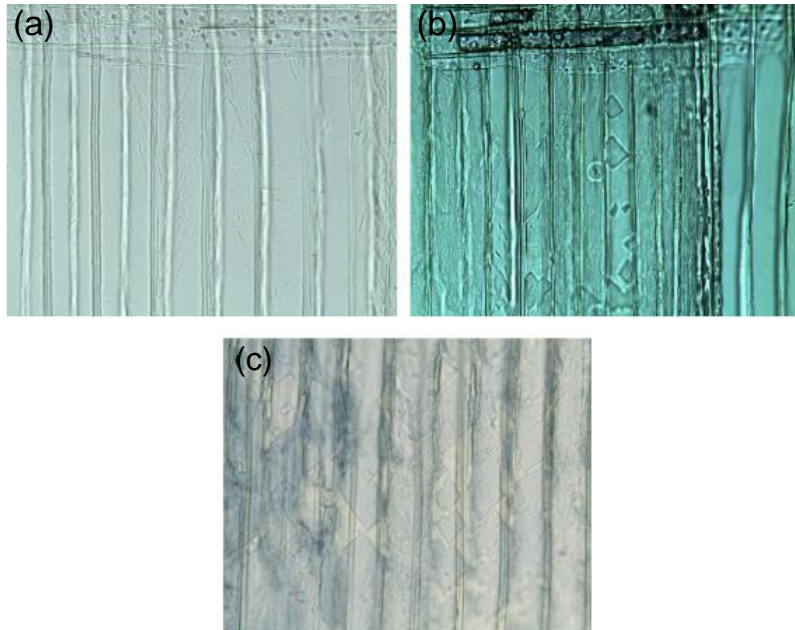


Figure 3.28: Adaptation from [5]: Radial sections of spruce (*Picea abies*) showing (a) possible weak signs of erosion bacteria, earlywood tracheids with groove-like erosion (200x); (b) moderate signs of erosion bacteria in the earlywood tracheids, with darker triangular-shaped notches caused by bacterial degradation (100x); (c) severe degradation in the latewood tracheids fully degraded (darker coloured), some remaining sound cell wall between coalescing of V-shaped notches (200x).

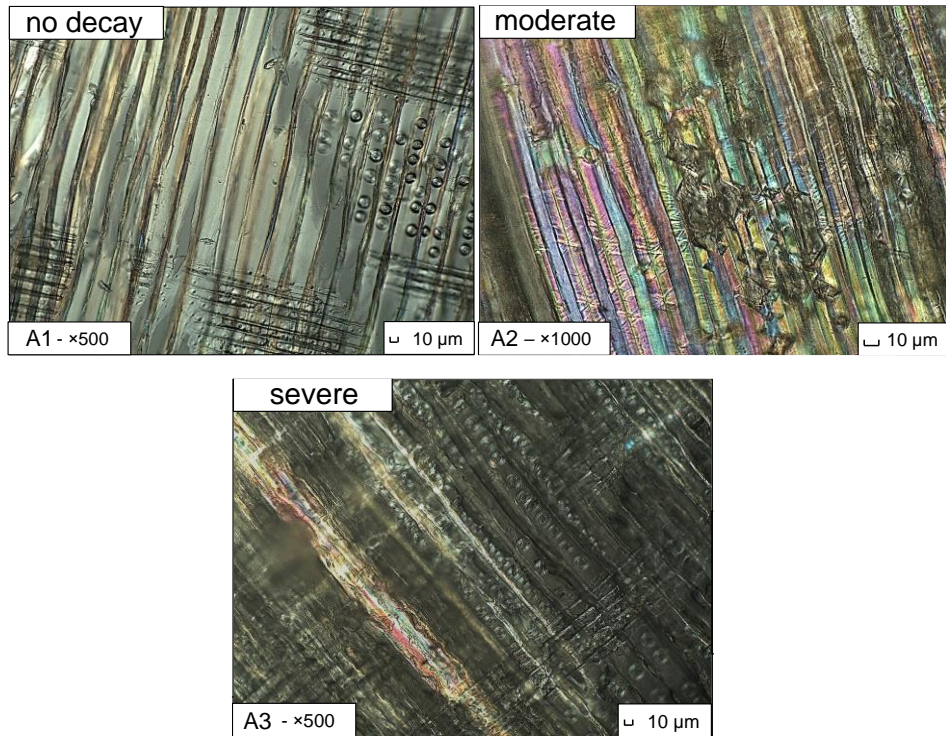


Figure 3.29: In radial section A1 smooth cell walls and intensive birefringence can be observed, corresponding to the absence of decay. In radial section A2, a matrix of sound cells showing birefringence is observed, but with some tracheids showing darker triangular-shaped notches caused by bacterial degradation, corresponding to possible moderate decay. In radial section A3, only few sound cells showing birefringence are present, whereas the other tracheids are fully degraded and do not exhibit birefringence, corresponding to severe decay.

4

Experimental results of “new” wooden foundation piles

4.1 Introduction

Chapter 4 presents the results of the material and mechanical characterization along “new” saturated spruce and pine foundation piles, categorized into three groups: ND, D, and DL, as outlined in Section 4.2.

Section 4.3 describes the behaviour of the piles under compression and their failure mechanisms. The results of the compression tests on head, middle-part, and tip of the piles are presented, to characterize their saturated compressive strength and stiffness parallel to the grain. The material properties of the piles, characterized by machine and visual grading, are finally reported for each part of the pile.

Section 4.3 details the results of the correlation analysis between the saturated compressive strength and material properties of the piles, identifying the most influencing parameters on their saturated compressive strength. Section 4.4 discusses the effect of pile driving and in-situ loading, concluding that variations in saturated compressive strength between the groups are not due to pile driving or loading, but rather differences in material properties.

In Section 4.5, the calculation of characteristic values for visual grades—such as knot ratio, annual rings, and growth rate—is reported for both spruce and pine piles, following the guidelines in prEN 1995-1-1 (2023). Section 4.6 proposes a method for calculating compressive strength design values based on the characteristic values derived from the material characterization of all piles, in accordance with prEN 1995-1-1 (2023). In addition, strength classes are proposed both for spruce and pine piles, separately, and for one category of combined spruce and pine species. Finally, Section 4.7 provides a summary of the test results.

4.2 Results from material and mechanical characterization of saturated spruce and pine piles

4.2.1 Preliminary results on full-length piles

The results of the preliminary tests conducted on full-length piles are presented in Table 4.1 and Table 4.2, for spruce and pine in the 4 different categories D, DL, DL-1, and ND (See Section 3.2). The full-pile sizes were between 13-16 (according to Annex Q of prEN 1995-1-1 2023), with a minimum tip diameter of 130 mm (Class 13) and a maximum tip diameter of 166 mm (Class 16).

For piles ND, it was not possible to determine $E_{c,0,dyn,wet}$ along the whole piles, since they were subdivided into head, middle-part, and tip after the debarking process. Thus, for each pile ND, $E_{c,0,dyn,wet}$ was determined separately for head, middle-part and tip, and reported as the averaged value of the 3 parts. In order to have a comparison of the averaged values of $E_{c,0,dyn,wet}$ for all the categories, the averaging was done also for D, DL, and DL-1, showing differences between $E_{c,0,dyn,wet}$ and $E_{c,0,dyn,wet}$ avg. H-M-T, generally within $\pm 10\%$ (see Table 4.1).

Table 4.1: Preliminary material properties of full-length spruce and pine piles category D, DL and DL-1.

Cat.	ID	ID site	species	year	Length (mm)	D _{head} (mm)	D _{tip} (mm)	D _{avg} (mm)	ρ_{wet} (kg/m ³)	$E_{c,0,dyn,wet}$ (MPa)	$E_{c,0,dyn,wet}$ avg. H-M-T (MPa)
D	10570	OAM-P1.7	spruce	2019	13780	286	137	216	930	14300	12600
	10172	OAM-P1.8	spruce	2019	13900	242	146	202	900	14000	11700
	10399	OAM-P1.9	spruce	2019	13980	248	143	204	890	14800	13700
	10187	OAM-P1.10	spruce	2019	13830	286	143	217	910	12100	11000
	10162	OAM-P1.12	spruce	2019	13600	309	146	224	810	12100	11300
	10581	OAM-P2.11	pine	2019	14030	232	153	190	900	13200	13000
	10595	OAM-P2.12	pine	2019	14080	210	134	174	800	12000	11500
	10596	OAM-P3.10	pine	2019	14220	223	153	185	755	9900	9800
	10590	OAM-P3.12	pine	2019	14300	216	146	177	790	10400	10200
DL	10398	OAM-P1.1	spruce	2019	12700	245	143	197	795	11700	11100
	10179	OAM-P1.2	spruce	2019	12410	274	153	221	860	11300	11900
	10572	OAM-P1.3	spruce	2019	13600	309	153	243	735	10200	9400
	10397	OAM-P1.4	spruce	2019	13700	283	140	221	900	11700	9600
	10195	OAM-P1.5	spruce	2019	13680	251	137	217	760	9900	8900
	10183	OAM-P1.6	spruce	2019	13710	283	166	224	800	10500	9700
	10164	OAM-P2.1	spruce	2019	13830	245	127	197	780	11300	12100
	10191	OAM-P2.2	spruce	2019	13390	280	140	223	780	11300	10500
	10177	OAM-P2.3	spruce	2019	12440	277	150	229	720	9600	11300
	10564	OAM-P2.4	spruce	2019	12630	248	130	198	1020	13800	12100
	10175	OAM-P2.5	spruce	2019	13400	286	146	217	850	12300	11000
	10643	OAM-P2.6	pine	2019	13980	236	146	180	740	10100	10800
	10573	OAM-P2.7	pine	2019	14000	258	159	209	810	11100	11200
	10594	OAM-P2.8	pine	2019	14230	229	143	183	790	8800	9200
	10592	OAM-P2.9	pine	2019	13320	242	140	196	810	10700	11500
DL1	10576	OAM-P2.10	pine	2019	13940	216	153	177	760	11100	12000
	10566	OAM-P1.11	spruce	2019	13660	226	134	192	930	14000	10500
	10567	OAM-P3.11	spruce	2019	13980	271	143	206	980	14300	11500

Table 4.2: Preliminary material properties of full-length spruce and pine piles category ND.

Cat.	ID	ID Hierden	species	year	Length (mm)	D _{head} (mm)	D _{tip} (mm)	D _{avg} (mm)	ρ_{wet} (kg/m ³)	$E_{c,0,dyn,wet}$ avg. H-M-T (MPa)
ND	10392	HIE-P10392	Pine	2019	15045	252	137	194	730	10000
	10574	HIE-P10574	Pine	2019	15050	255	146	201	670	10600
	10575	HIE-P10575	Pine	2019	15020	282	142	212	760	9700
	10577	HIE-P10577	Pine	2019	15070	265	143	204	600	8800
	10579	HIE-P10579	Pine	2019	15040	185	145	165	620	11400
	10580	HIE-P10580	Pine	2019	15040	257	159	208	720	11400
	10582	HIE-P10582	Pine	2019	14980	241	148	195	820	12400
	10583	HIE-P10583	Pine	2019	15045	312	148	230	710	9900
	10584	HIE-P10584	Pine	2019	15010	264	148	206	860	12200
	10585	HIE-P10585	Pine	2019	15070	302	161	232	730	10500
	10587	HIE-P10587	Pine	2019	14975	278	151	214	690	9400
	10589	HIE-P10589	Pine	2019	14975	300	166	233	820	8000
	10591	HIE-P10591	Pine	2019	15050	213	151	182	710	10500
	10593	HIE-P10593	Pine	2019	15120	236	143	189	610	9500
	10597	HIE-P10597	Pine	2019	14999	246	145	196	700	11200
	10598	HIE-P10598	Pine	2019	15010	302	150	226	650	10500
	10640	HIE-P10640	Pine	2019	14960	246	140	193	910	12500
	10641	HIE-P10641	Pine	2019	15190	306	150	228	730	13400
	10642	HIE-P10642	Pine	2019	15031	299	140	220	770	12100
	10644	HIE-P10644	Pine	2019	15035	247	142	194	780	13400
	10645	HIE-P10645	Pine	2019	15060	271	159	215	680	10100
	10646	HIE-P10646	Pine	2019	15070	236	148	192	720	11400
	10586bis	HIE-P10586bis	Pine	2019	15010	213	132	173	770	11800
	3801	HIE-P03801	Spruce	2019	15080	208	134	171	730	10300
	3802	HIE-P03802	Spruce	2019	15000	290	127	209	630	9300
	10169	HIE-P10169	Spruce	2019	13240	321	151	236	740	11500
	10178	HIE-P10178	Spruce	2019	15000	296	133	205	710	11800
	10181	HIE-P10181	Spruce	2019	14975	299	135	217	650	11300
	10185	HIE-P10185	Spruce	2019	14800	328	124	226	830	13100
	10192	HIE-P10192	Spruce	2019	15340	291	154	223	590	10600
	10193	HIE-P10193	Spruce	2019	14990	296	145	220	600	9800
	10196	HIE-P10196	Spruce	2019	15000	220	146	183	710	11700
	10393	HIE-P10393	Spruce	2019	15000	223	143	183	660	10900
	10394	HIE-P10394	Spruce	2019	15000	286	133	193	660	10500
	10396	HIE-P10396	Spruce	2019	14690	299	130	213	700	13500
	10561	HIE-P10561	Spruce	2019	15010	318	135	227	780	13600
	10562	HIE-P10562	Spruce	2019	15040	271	146	208	680	13300
	10563	HIE-P10563	Spruce	2019	15141	312	142	227	700	10600
	10565	HIE-P10565	Spruce	2019	14870	290	134	212	730	9800
	10569	HIE-P10569	Spruce	2019	14970	280	130	203	680	9900
	10571	HIE-P10571	Spruce	2019	14970	293	140	216	680	12000
	10586	HIE-P10586	Spruce	2019	15050	251	134	193	700	12000
	10588	HIE-P10588	Spruce	2019	14910	261	150	206	870	11600

4.2.2 Results of the compression tests on pile segments

The load-displacement behaviour of the saturated spruce and pine specimens tested in compression exhibited linearity up to 70% - 80% of the maximum compression load, followed by non-linear behaviour until peak load, as in Figure 4.3 (head), Figure 4.2 (middle-part), Figure 4.3 (tip), (See Appendix B1 for a complete overview of compression tests). When softening started, the load gradually decreased showing a quasi-plastic load plateau. In approximately 70% of the cases, a failure mechanism for local buckling of fibres was observed in the section with the highest KR. In this case, when the softening starts,

wrinkles appear around the compression failure area, followed by cracks on the bottom or top part of the section with the highest KR as in Figure 4.4b. For the other cases, a failure for crushing was detected, occurring mostly in the top or bottom part of the pile, typically observed in pile segments with $KR < 0.1$ (Figure 4.4a).

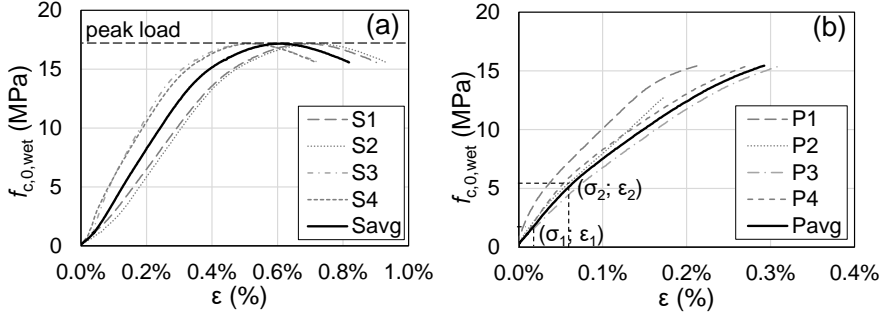


Figure 4.1: Results of the axial compression test of head-segment K1.1M: a) global behaviour with stress-strain curves measured by S1, S2, S3, S4; b) stress-strain curves measured by P1, P2, P3, P4 to determine $E_{c,0,wet}$.

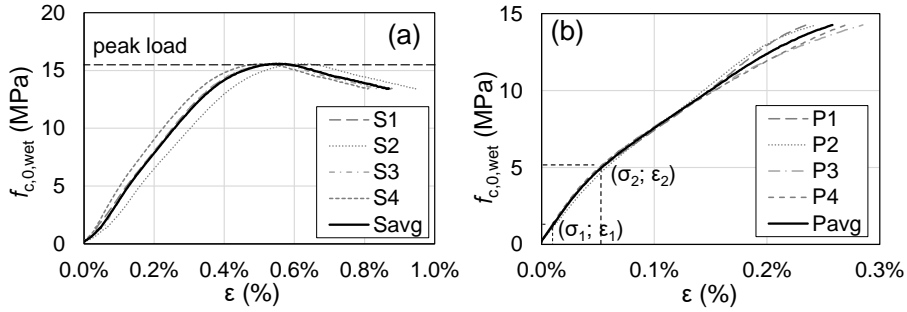


Figure 4.2: Results of the axial compression test of middle-part segment V1.1Va: a) global behaviour with stress-strain curves measured by S1, S2, S3, S4; b) stress-strain curves measured by P1, P2, P3, P4 to determine $E_{c,0,wet}$.

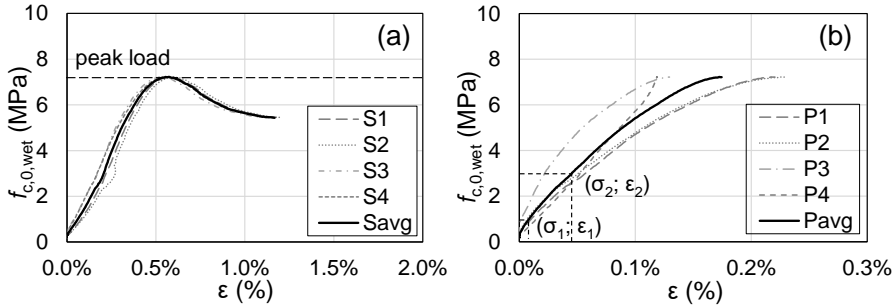


Figure 4.3: Results of the axial compression test of tip segment V1.1Va: a) global behaviour with stress-strain curves measured by S1, S2, S3, S4; b) stress-strain curves measured by P1, P2, P3, P4 to determine $E_{c,0,wet}$.

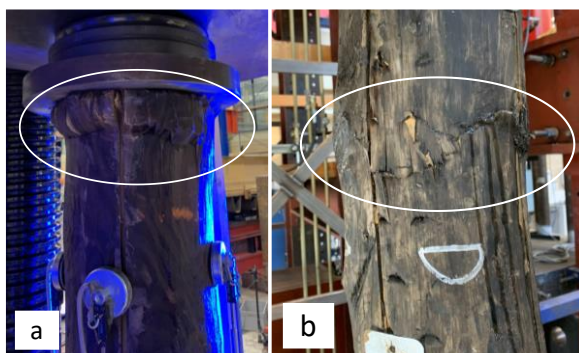


Figure 4.4: Failure mechanisms in compression: (a) failure for crushing on top of the pile segment M2.12M; (b) failure for buckling of segment V1.1Va.

The saturated short-term compressive strength ($f_{c,0,wet}$) and modulus of elasticity ($E_{c,0,wet}$) parallel to the grain of 253 pile segments, divided into head, middle-part, and tip, were characterized in Table 4.3. The results are subdivided based on the pile categories ND, D, DL, and DL-1, and wood species: spruce and pine. In addition, the characteristic wet compressive strength ($f_{c,0,k,wet}$) is reported, calculated according to the parametric calculation in NEN-EN 14358 (2016) explained in Section 3.8. All the values refer to an average moisture content of the samples between 70-100%.

The cumulative distributions of the $f_{c,0,wet}$ and $E_{c,0,wet}$ for pile segments ND, D, and DL are presented in Figure 4.5 for spruce, and Figure 4.6 for pine, based on the results listed in Table 4.3. The markers represent the individual data points, the continuous lines are the cumulative distributions determined with the mean standard deviation listed in Table 4.3.

In Figure 4.7, the cumulative distributions of $f_{c,0,wet}$ of spruce and pine piles (ND) studied in this research are plotted together with all the data on saturated $f_{c,0,wet}$ from literature: spruce, Douglas fir, and larch from Van de Kuilen [33]; southern pine and Douglas fir in Wilkinson 1968 [59]. While the data available from the literature presented in Figure 4.7 are all softwood piles characterized in fully-saturated conditions, they show a large range of $f_{c,0,wet}$, often associated with limited sample sizes.

This highlights the contribution provided by this research, in enlarging the database for the saturated compressive strength of spruce and pine piles. Moreover, $f_{c,0,wet}$ was characterized along the length of the pile, showing the difference in the saturated compressive strength along the pile, suitable to be considered for design practice and grading criteria (See Section 4.5).

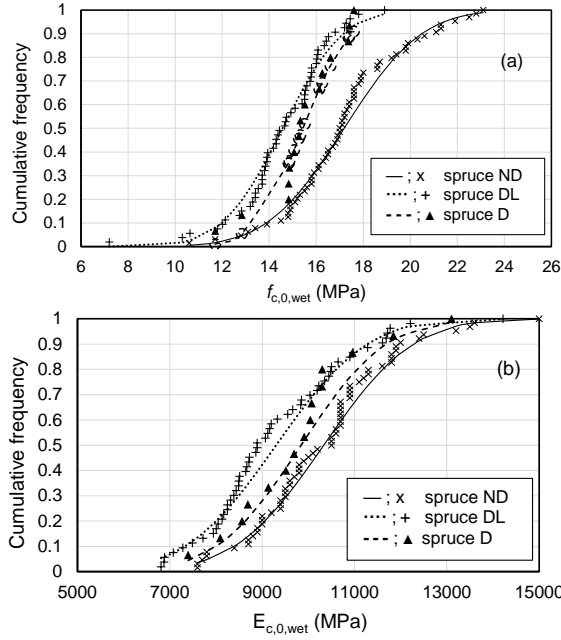


Figure 4.5: Cumulative distributions of $f_{c,0,wet}$ (a) and $E_{c,0,wet}$ (b) parallel to the grain for spruce pile segments ND, DL and D tested according to EN 408 (2010) in wet status ($MC_{mean} > 70\%$). The lines show the normal distribution fitted to the data.

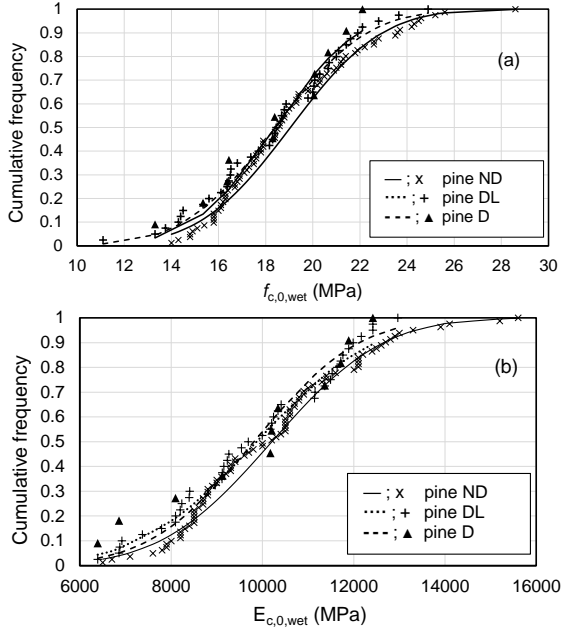


Figure 4.6: Cumulative distributions of $f_{c,0,wet}$ (a) and $E_{c,0,wet}$ (b) parallel to the grain for pine pile segments ND, DL and D tested according to EN 408 (2010) in wet status ($MC_{mean} > 70\%$). The lines show the normal distribution fitted to the data.

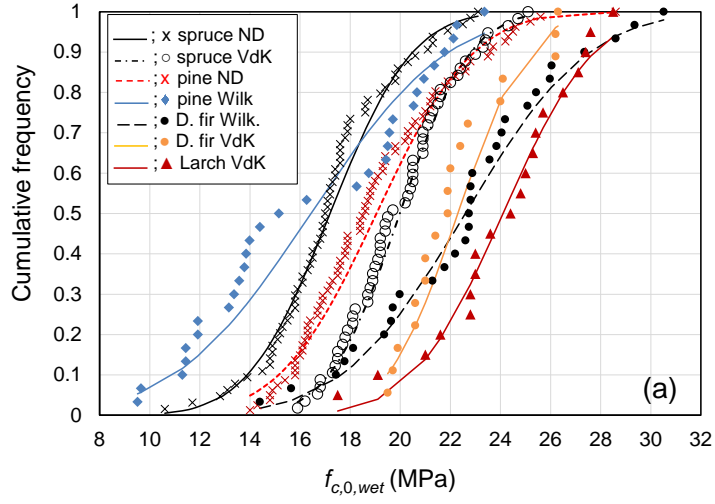


Figure 4.7: Cumulative distributions of $f_{c,0,wet}$ for spruce and pine ND, together with the data from literature: spruce, Douglas-fir (D. fir) and larch in Van de Kuilen (VdK) 1994 [33]; southern pine and Douglas-fir (D. fir) in Wilkinson (Wilk.) 1968 [59]. The lines show the normal distribution fitted to the data.

4.2 Results from material and mechanical characterization of saturated spruce and pine piles

Table 4.3: Results for spruce and pine pile segments tested in compression parallel to the fiber in wet state according to EN 408. The 5-percentile characteristic values correspond to $70\% < MC < 100\%$ (at test time).

Category	Segment	Sample size (No.)	D (mm)		$f_{c,0,wet}$ (MPa)		$E_{c,0,wet}$ (MPa)		ρ_{wet} (kg/m ³)		$f_{c,0,k,wet}$ (MPa)
			mean	SD	mean	SD	mean	SD	mean	SD	$\chi_{0.05}$
spruce + pine ND	All	145	210	40	18.3	3.0	10300	1700	780	80	13.0
spruce + pine D	All	26	210	35	16.7	2.6	9900	1600	730	62	12.0
spruce + pine DL	All	82	210	35	16.0	3.1	9500	1700	710	63	10.2
spruce DL-1	All	6	230	30	14.8	1.3	9600	1000	690	56	11.8
spruce ND	All	64	210	38	17.2	2.6	10300	1500	740	75	12.5
	Head	20	260	20	18.9	2.3	11400	1300	740	75	14.5
	Middle	20	220	15	17.8	2.0	10500	1100	740	85	14.0
	Tip	24	180	15	15.4	2.0	9200	1200	760	70	11.6
spruce D	All	15	220	36	15.5	1.6	9900	1400	720	62	12.3
	Head	5	260	18	14.8	2.4	10400	1600	770	44	-
	Middle	5	230	10	16.6	1.0	10600	900	720	66	-
	Tip	5	180	6	15.1	0.3	8700	2800	680	51	-
spruce DL	All	53	220	37	14.6	2.0	9400	1500	690	61	10.9
	Head	15	260	22	15.6	1.9	10400	1500	730	65	11.9
	Middle	16	230	15	15.3	1.1	9600	1200	700	47	13.2
	Tip	22	180	18	13.4	2.1	8500	1200	670	61	9.4
spruce DL-1	All	6	230	30	14.8	1.3	9600	1000	690	56	11.8
	Head	2	250	24	15.0	2.0	10500	300	750	57	-
	Middle	2	230	3	15.2	1.2	9900	1000	680	20	-
	Tip	2	190	9	14.1	0.9	8500	40	640	0	-
pine ND	All	81	200	35	19.1	3.0	10200	1900	810	75	13.6
	Head	23	230	20	21.9	2.7	12100	1600	820	90	16.8
	Middle	25	200	20	19.4	2.5	10400	1300	780	80	14.8
	Tip	33	170	15	16.9	1.7	8700	1100	800	60	13.8
pine D	All	11	190	25	18.5	2.8	9900	2000	720	65	12.8
	Head	4	210	15	21.0	1.0	11600	900	740	90	-
	Middle	4	190	5	18.0	2.0	9700	1400	700	50	-
	Tip	3	160	10	15.7	2.6	7800	2100	690	40	-
pine DL	All	29	180	25	18.5	3.2	9800	1800	720	60	12.5
	Head	8	210	10	21.4	2.3	11200	1200	760	70	16.3
	Middle	8	190	15	18.9	2.1	10400	1400	750	50	14.3
	Tip	13	160	15	16.3	2.8	8600	1300	690	40	10.7

4.2.3 Results from the characterization of the material properties of pile segments

The material properties characterized according to Section 3.5, were reported in Table 4.4.

All the tested pile segments had a slope of grain $SoG < 1:10$. Higher deviation of grain direction was not measured. Hence, this parameter was not included in the results.

The density calculated at $MC = 12\%$ (ρ_{12}) according to Paragraph 3.5.1, was also included in order to have a standardized parameter for the density.

The spruce piles (from trees in the Netherlands) showed lower age and higher rate of growth compared to pine piles (from trees in Nuremberg, Germany). As explained in Section 2.3, this could be attributed to the different environmental factors, soil conditions, and forestry management. For example, the temperate climate of The Netherlands (classified as Cfb according to Köppen-Geiger climate classification [61]), can result in faster tree growth, leading to a higher rate of growth and larger pile taper [60]. Contrarily, the colder climate in Nuremberg, (classified as Dfb according to Köppen-Geiger climate classification [61]), can lead to slower tree growth, resulting in a lower rate of growth for the same age and diameter.

Table 4 4: Results of material properties determined for each category of spruce and pine piles for head, middle-part and tip.

Category	Segment	Sample size (No.)	D (mm)		ρ_{wet} (kg/m ³)		ρ_{12} (kg/m ³)		$E_{c,0,dyn,wet}$ (MPa)		KR (-)		Age (years)		RoG (mm/year)		MC (%)	
			mean	SD	mean	SD	mean	SD	mean	SD	mean	SD	mean	SD	mean	SD	mean	SD
spruce + pine (ND)	All	145	210	40	780	80	500	49	10900	1800	0.16	0.12	54	20	2.2	1.0	90	16
spruce + pine (D)	All	26	210	35	730	62	480	44	10600	2000	0.25	0.12	52	18	2.3	0.8	80	13
spruce + pine (DL)	All	82	210	35	710	63	460	47	10100	1700	0.22	0.09	43	17	2.8	1.0	80	14
spruce (DL-1)	All	6	230	30	690	56	460	14	10200	700	0.22	0.08	44	17	2.9	1.0	80	12
spruce (ND)	All	64	210	38	740	75	500	49	10800	1600	0.19	0.12	43	17	2.9	1.1	80	16
	Head	20	260	20	740	75	520	54	12000	1400	0.12	0.07	57	17	2.5	0.8	80	10
	Middle	20	220	15	740	85	500	39	11200	1300	0.16	0.07	43	13	2.8	1.0	80	15
	Tip	24	180	15	760	70	490	52	9600	1200	0.28	0.12	32	12	3.2	1.2	90	20
spruce (D)	All	15	220	36	720	62	480	31	10800	1900	0.20	0.06	43	15	2.8	0.7	80	15
	Head	5	260	18	770	44	480	39	11500	2700	0.14	0.02	55	17	2.6	0.8	90	21
	Middle	5	230	10	720	66	490	22	11400	1100	0.21	0.05	44	10	2.7	0.6	80	11
	Tip	5	180	6	680	51	470	32	9600	3200	0.25	0.02	31	7	3.1	0.7	80	3
spruce (DL)	All	53	220	37	690	61	450	40	9900	1300	0.25	0.08	36	14	3.3	0.8	90	15
	Head	15	260	22	730	65	470	47	10800	1400	0.19	0.04	51	11	2.7	0.6	90	14
	Middle	16	230	15	700	47	440	36	10200	1100	0.23	0.04	36	7	3.3	0.7	90	18
	Tip	22	180	18	670	61	440	34	9000	1000	0.31	0.07	26	7	3.8	0.7	80	13
spruce (DL-1)	All	6	230	30	690	56	460	14	10200	800	0.22	0.09	44	17	2.9	1.0	80	12
	Head	2	250	24	750	57	460	12	11000	0	0.16	0.01	56	22	2.6	1.2	100	10
	Middle	2	230	3	680	20	470	8	10300	400	0.17	0.00	44	18	2.9	1.2	70	3
	Tip	2	190	9	640	0	440	13	9300	60	0.34	0.03	34	15	3.2	1.3	70	5
pine (ND)	All	81	200	35	810	75	500	49	10800	1900	0.13	0.11	62	17	1.7	0.6	90	15
	Head	23	230	20	820	90	540	47	12700	1700	0.05	0.05	80	13	1.5	0.5	80	10
	Middle	25	200	20	780	80	500	43	11100	1400	0.10	0.06	64	11	1.7	0.5	90	10
	Tip	33	170	15	800	60	480	38	9200	1200	0.20	0.11	48	10	1.9	0.7	100	15
pine (D)	All	11	190	25	720	65	490	60	10300	2200	0.14	0.10	64	16	1.6	0.2	70	10
	Head	4	210	15	740	90	500	93	12000	900	0.04	0.07	81	5	1.4	0.1	70	15
	Middle	4	190	5	700	50	490	36	10400	1800	0.15	0.01	62	7	1.6	0.2	70	1
	Tip	3	160	10	690	40	460	38	7900	2200	0.25	0.08	46	10	1.8	0.3	80	10
pine (DL)	All	29	180	25	720	60	490	49	10400	2000	0.17	0.09	55	16	1.8	0.4	80	10
	Head	8	210	10	760	70	530	52	12100	1700	0.09	0.07	76	7	1.4	0.1	70	10
	Middle	8	190	15	750	50	480	33	10800	1500	0.16	0.08	56	6	1.7	0.2	80	10
	Tip	13	160	15	690	40	460	35	9100	1300	0.22	0.07	41	6	2.1	0.3	80	10

4.3 Correlations between strength and visually- and experimentally-determined parameters

The correlation analysis was conducted for all the experimentally- and visually-determined properties well above fiber saturation. This was done to analyse the parameters that have a significant influence on the compressive strength of the pile. The correlation matrix was presented both for spruce piles (Table 4.5) and for pine piles (Table 4.6). Knot ratio (KR), annual rings (Age) and growth rate (RoG) resulted to be the visually-graded parameters with the highest influence on $f_{c,0,wet}$.

While diameter and tapering exhibited a very low correlation. $f_{c,0,wet}$ and $E_{c,0,wet}$ revealed to be strongly correlated. The density ρ_{12} had a moderate positive correlation with the $f_{c,0,wet}$, higher than the wet density ρ_{wet} . The moisture content (MC) exhibited in both spruce and pine a weak negative correlation with $f_{c,0,wet}$.

More specifically, the age showed a clear positive correlation with both $E_{c,0,wet}$ and $f_{c,0,wet}$. However, KR had a strong negative correlations with mechanical properties, both in spruce and pine piles. The same negative correlation was found between RoG and the mechanical properties, strong in the case of spruce piles and moderate in pine piles. The tapering of the piles exhibited in both spruce and pine a weak negative correlation with the mechanical properties.

Finally, the diameter had a weak positive correlation with $f_{c,0,wet}$ in spruce piles, and positive moderate correlation in pine piles. In addition, the diameter exhibited a moderate negative correlation with the KR. In general, age was strongly correlated with KR in both spruce and pine; a moderate positive correlation was observed between KR and RoG.

Table 4.5: Correlation matrix for all spruce piles

	$f_{c,0,wet}$	$E_{c,0,wet}$	ρ_{wet}	ρ_{12}	Age	KR	RoG	MC	Tapering	D
$f_{c,0,wet}$	1									
$E_{c,0,wet}$	0.76	1								
ρ_{wet}	0.41	0.37	1							
ρ_{12}	0.53	0.54	0.62	1						
Age	0.72	0.63	0.34	0.35	1					
KR	-0.60	-0.48	-0.24	-0.24	-0.66	1				
RoG	-0.68	-0.54	-0.28	-0.29	-0.86	0.53	1			
MC	-0.14	-0.19	0.36	-0.49	-0.02	0.02	0.00	1		
Tapering	-0.22	-0.34	0.01	0.04	-0.34	0.37	0.23	-0.05	1	
D	0.27	0.34	0.11	0.10	0.44	-0.48	-0.12	0.01	-0.26	1

4.3 Correlations between strength and visually- and experimentally-determined parameters

Table 4.6: Correlation matrix for all pine piles

	$f_{c,0,wet}$	$E_{c,0,wet}$	ρ_{wet}	ρ_{12}	Age	KR	RoG	MC	Tapering	D
$f_{c,0,wet}$	1									
$E_{c,0,wet}$	0.89	1								
ρ_{wet}	0.42	0.39	1							
ρ_{12}	0.64	0.70	0.70	1						
Age	0.76	0.74	0.24	0.49	1					
KR	-0.72	-0.66	-0.28	-0.46	-0.71	1				
RoG	-0.52	-0.47	-0.20	-0.32	-0.73	0.52	1			
MC	-0.24	-0.36	0.47	-0.28	-0.31	0.21	0.14	1		
Tapering	-0.31	-0.32	0.06	-0.17	-0.41	0.38	0.30	0.34	1	
D	0.46	0.46	0.06	0.29	0.64	-0.49	-0.09	-0.28	-0.32	1

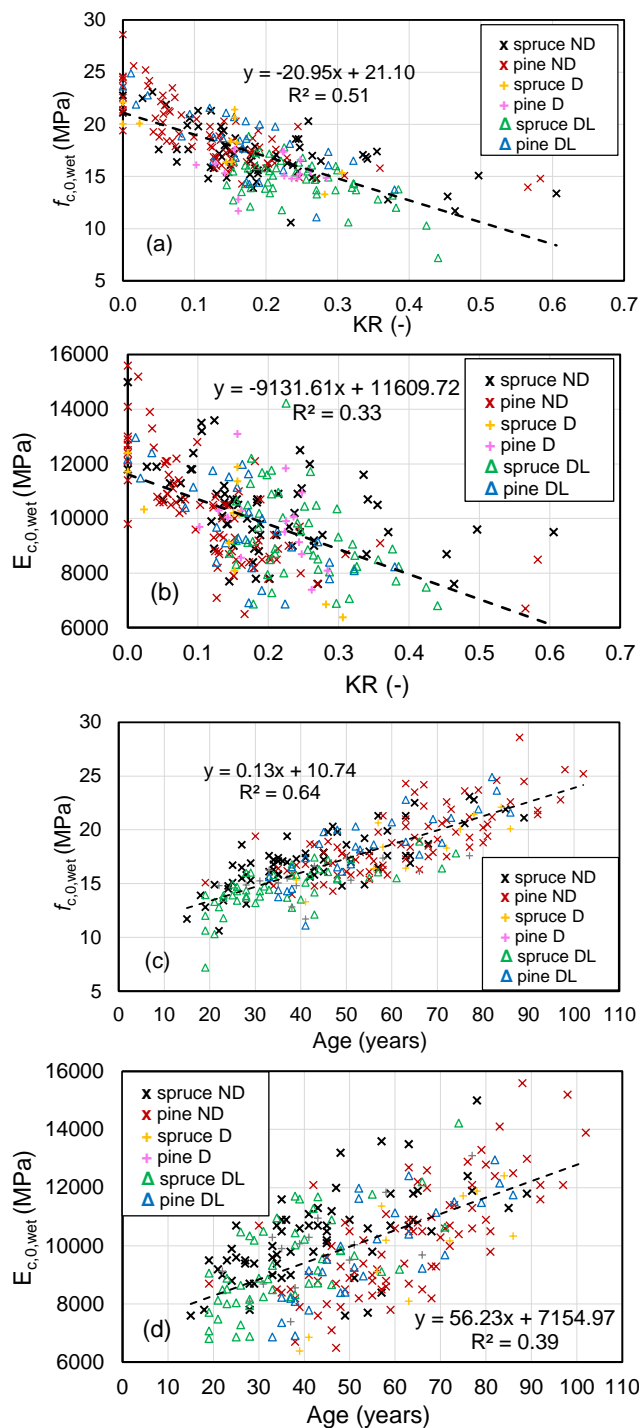
The visual relationships between $f_{c,0,wet}$, $E_{c,0,wet}$ and the visually-determined growth characteristics for both spruce and pine piles, were presented in Figure 4.8, based on the results in Table 4.4. The majority of the piles exhibited $0 \leq KR \leq 0.4$ (Figure 4.8a), where spruce and pine tips revealed a $KR_{mean} > 0.2$, while middle-parts and heads had a $KR_{mean} < 0.2$ (Table 4.4).

The linear regression in Figure 4.8a gives almost a zero strength value for $KR = 1$ (i.e. pile section completely full of knots), suggesting that a zero strength zone is associated to a knot, where the fibers in the longitudinal direction deviate.

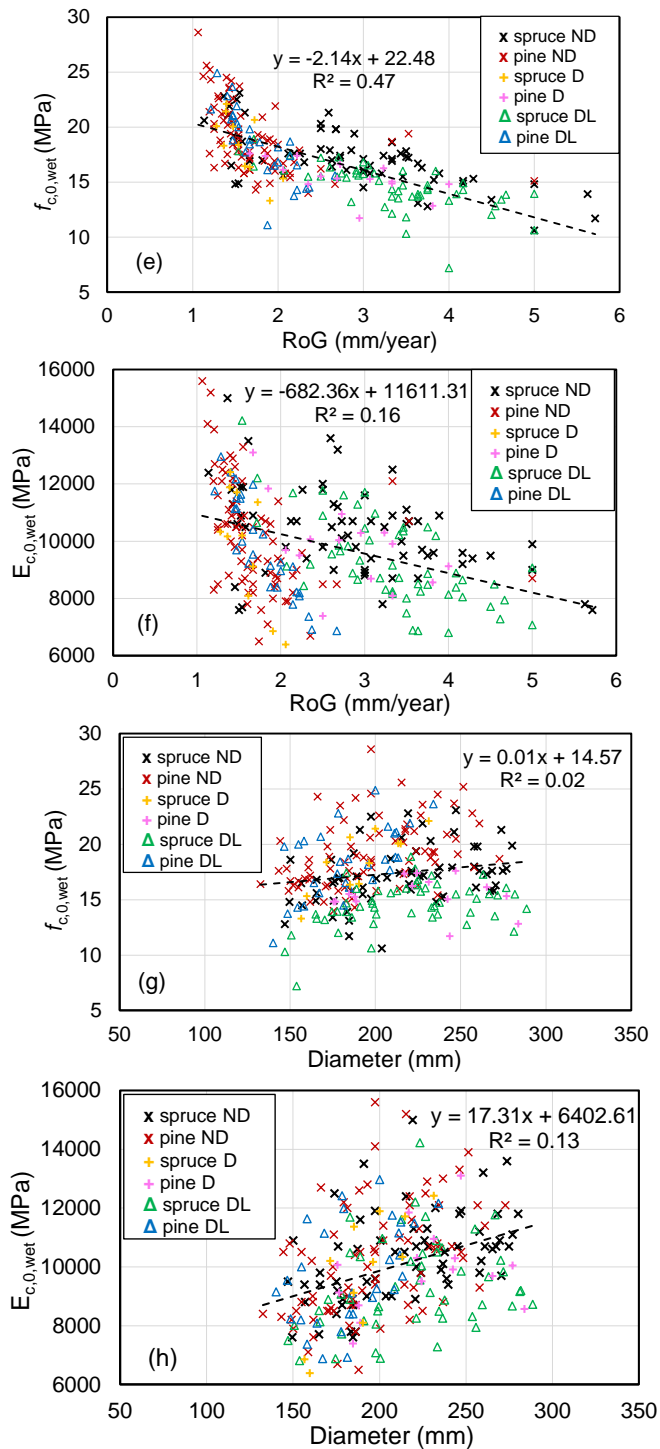
The relationship between $f_{c,0,wet}$ and Age (Figure 4.8c) showed that all the pile segments were ranging between 15 years and 100 years, where the spruce piles were on average 20 years younger than the pine piles. On average, an incremental number of annual rings was measured from tips to heads, with a difference of 10-15 years among each part: tip, middle-part and head (Table 4.4).

Pine piles showed an average low RoG (ranging from 1 mm/year to 2.5 mm/year), while spruce pile segments were more spread from 1 mm/year to almost 6 mm/year (Table 4.4). Figure 11e revealed variations of roughly 10 MPa in the $f_{c,0,wet}$ for the same values of RoG, in particular for spruce and pine heads with RoG = 1.5. A very low correlation was found between the $f_{c,0,wet}$, $E_{c,0,wet}$ and diameter (Figure 4.8g; Figure 4.8h), confirming that the diameter is not an influencing parameter for the wet compressive strength and stiffness of spruce and pine piles.

For almost all the segments, the taper was less than 15 mm/m, which corresponds to the maximum taper for wooden foundation piles according to prEN 1995-1-1/NB:2023. However, Figure 4.8i and Figure 4.8j confirmed that the tapering of the pile segments resulted in almost no correlation with the mechanical properties.



4.3 Correlations between strength and visually- and experimentally-determined parameters



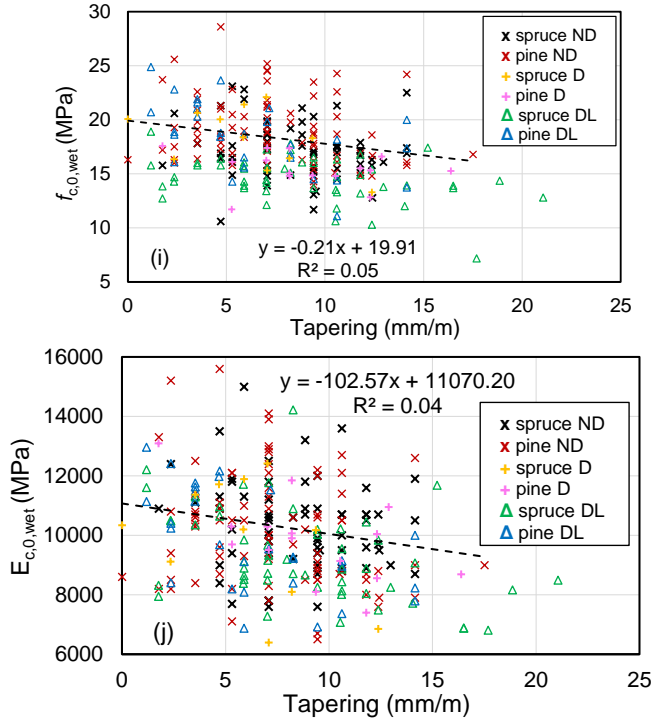


Figure 4.8: Compressive strength $f_{c,0,wet}$ and modulus of elasticity $E_{c,0,wet}$ parallel to the fiber versus visually-determined material properties: KR (a, b), Age (c, d), RoG (e, f), diameter (g, h), and tapering (i, j) of all the tested categories of spruce and pine pile segments.

4.3.1 Relationships among strength, stiffness and density

The wet compressive strength for all the category of tested piles was correlated with the density adjusted to MC = 12% (ρ_{12}).

The revealed moderate correlation between $f_{c,0,wet}$ and ρ_{12} (Figure 4.9a) and between $E_{c,0,wet}$ and ρ_{12} (Figure 4.9b), is possibly attributed to the fact that the ρ_{12} is significantly influenced by KR, age and RoG, as presented in the correlation analysis in Section 4.3.

The relationship between $f_{c,0,wet}$ and $E_{c,0,wet}$ (Figure 4.10a) exhibited an $R^2 = 0.59$, indicating that the stiffness is a good indicator for the wet compressive strength. A very similar correlation was also found between the $f_{c,0,wet}$ and $E_{c,0,wet,dyn}$ (Figure 4.10b), determined through frequency response measurements.

This implies that the $E_{c,0,wet}$ and $E_{c,0,dyn,wet}$ are strongly correlated, as shown in Figure 4.11, with a $R^2 = 0.93$ between these two parameters, suggesting that frequency response measurements can be used to efficiently estimate the modulus of elasticity of wooden piles.

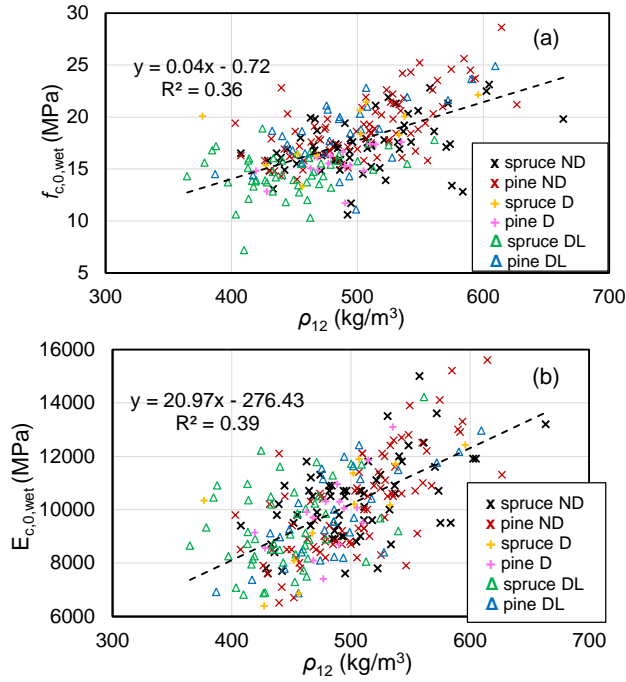


Figure 4.9: Relationship between $f_{c,0,wet}$ and density ρ_{12} (a) and $E_{c,0,wet}$ and density ρ_{12} (b) for all the categories of tested pile segments.

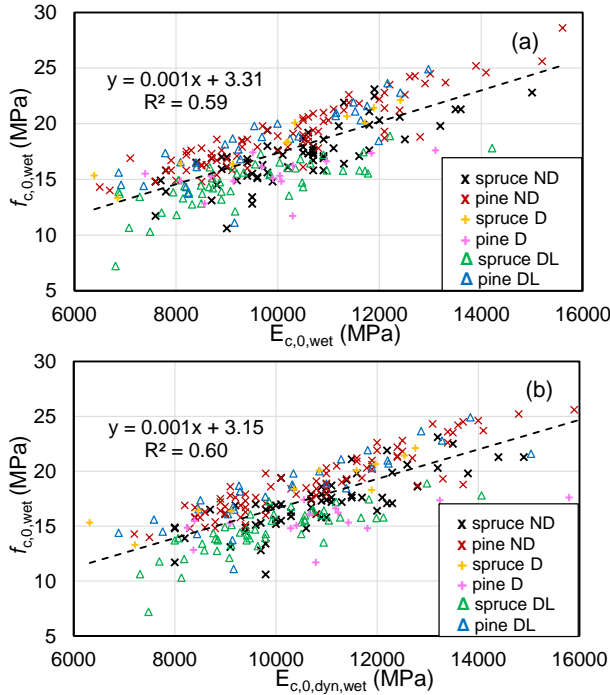


Figure 4.10: Relationship between $f_{c,0,wet}$ and $E_{c,0,wet}$ (a) and $f_{c,0,wet}$ and $E_{c,0,dyn,wet}$ (b) for all the categories of tested pile segments.

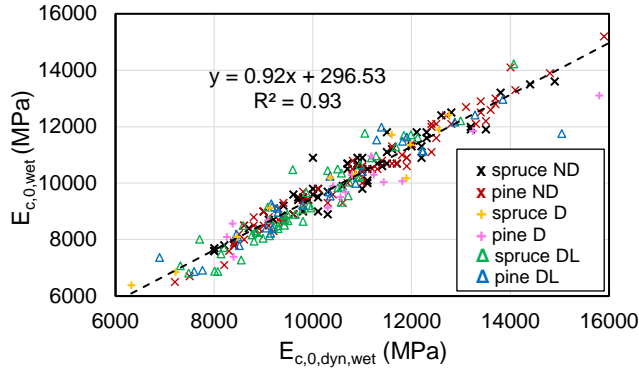


Figure 4.11: Relationship between $E_{c,0,wet}$ and $E_{c,0,dyn,wet}$ for all the categories of tested pile segments.

4.3.2 Influencing parameters on the compressive strength of the piles

$E_{c,0,dyn,wet}$, density ρ_{12} , age, KR, and RoG resulted to be the parameters that had a significant influence on the wet compressive strength of the pile, as presented in Section 4.3. The age was positively correlated with the density. An age difference of 10-15 years was measured among heads, middle-parts, and tips (see Table 4 4). Older segments, such as heads, revealed a higher portion of mature wood in the cross section, corresponding to higher densities [71]. Younger segments, such as tips, presented a higher portion of juvenile wood, characterized by a lower density than mature wood [72]. The KR was negatively correlated with the density, since higher KRs were present, especially in spruce and pine tips, characterized by lower density than middle-parts and heads, that were instead associated with lower KRs. However, the density of a pile could increase with a large presence and size of knots, since the density of a knot is roughly twice the density of a free-knot area [168],[110]. For example, between two piles that exhibit the same ratio of mature to juvenile wood and the same RoG, the one with a larger amount and size of knots could have a higher density. The RoG was also negatively correlated with the density, since faster growing softwood trees exhibit higher RoG values associated with lower density [106]. This relationship among ρ_{12} , age and KR can be observed in Table 4 4, where both spruce and pine ND had equal mean density ($\rho_{12,mean}$), but pine piles ND had a 30% lower KR_{mean} and were on average 20 years older than spruce ND, resulting into a RoG_{mean} approximately halved in comparison to spruce ND. This contributed to a difference of 2 MPa between $f_{c,0,mean,wet}$ of pine ND and spruce ND. This scatter reached 3 MPa in the heads, where pine heads ND were characterized by very low $KR_{mean} = 0.05$ and $RoG_{mean} = 1.5$ mm/year. Spruce exhibited a larger presence of knots compared to pine, especially for heads and middle-parts. This is due to the fact that the crown of pine trees develops on the upper part, resulting in fewer and smaller branches on the bottom part compared to spruce trees, where the crown already starts from the bottom part of the stem.

4.4 Effect of pile driving and in-situ loading on the strength properties

The effect of the pile driving on piles D and the in-situ loading on piles DL, with stress levels on the pile heads up to 6.9 MPa, had no significant influence on the mechanical properties of spruce and pine piles. The difference in the wet compressive strength measured among the pile categories ND, D and DL (see Table 4.3), was associated to the variation of the knot-ratio, age and RoG in heads, middle-parts, and tips, which significantly influenced the wet compressive strength of the piles (see Table 4.4). It should be noted that, in this study, the effect of the soil environment was not taken into account, since the research focused on the mechanical properties of spruce and pine piles.

The maximum stress measured on the pile head during the in-situ loading (carried out within 1 day) was 6.9 MPa for category DL, below the maximum design strength for short-term loading $f_{c,0,d,short} = 11.5$ MPa provided in the current NEN-EN 1995-1-1/NB:2013 [19]. Therefore, the piles DL were not loaded to failure. This is because the applied short-term in-situ loading had the goal of assessing the maximum geotechnical failure load (the failure with respect to the soil settlement) correspondent to a maximum displacement of the head of the pile equal to 10% of the head diameter, in accordance with NEN 9997-1+C2:2017 [147].

For the two piles belonging to category DL-1, the maximum stress on the head reached 4.5 MPa and then 80% of this stress (c.a. 3.6 MPa) was kept for 22 days. The constant load applied to DL-1 was representing a possible real service condition of the piles, with stresses below the maximum design strength for long-term loading $f_{c,0,d,long} = 9.8$ MPa provided in [19]. Based on the average wet compressive strength determined for spruce and pine heads ND (see Table 4.3), the stress applied in situ was approximately 1/3 of the maximum wet compressive strength.

However, all the spruce segments D and DL exhibited approximately 10-15% lower $f_{c,0,wet,mean}$ compared to all the spruce segments ND (see Table 4.3). The decrease in strength among the 3 categories was not present in pine pile segments, where approximately the same $f_{c,0,wet,mean}$ was determined for both segments ND, D, and DL.

The lower strength of spruce D and DL could be attributed to the effect of driving and preloading on the piles. However, by observing Figure 4.12 and Figure 4.13, it is possible to distinguish how the physical properties of spruce ND and spruce D + DL exhibit differences particularly for KR (Figure 4.12a) and RoG (Figure 4.13a), where the data clouds of spruce piles shows observable scatters between ND and D + DL.

On the other hand, the physical properties of pine piles resulted to be more uniform among the three categories ND, D, and DL, exhibiting no major differences in the correlation between $f_{c,0,wet}$ vs KR and RoG. KR and RoG represented the growth characteristics with the highest influence on the compressive strength. A very weak correlation was found between $f_{c,0,wet}$ vs diameter and between $f_{c,0,wet}$ vs tapering, which were not considered as influencing parameters for the compressive strength.

Based on these assumptions, all the categories ND, D, and DL can be considered together, with the only distinction between spruce and pine, where the variations of the $f_{c,0,wet,mean}$

among the categories are attributed to the different physical properties of timber, in particular the KR and the RoG.

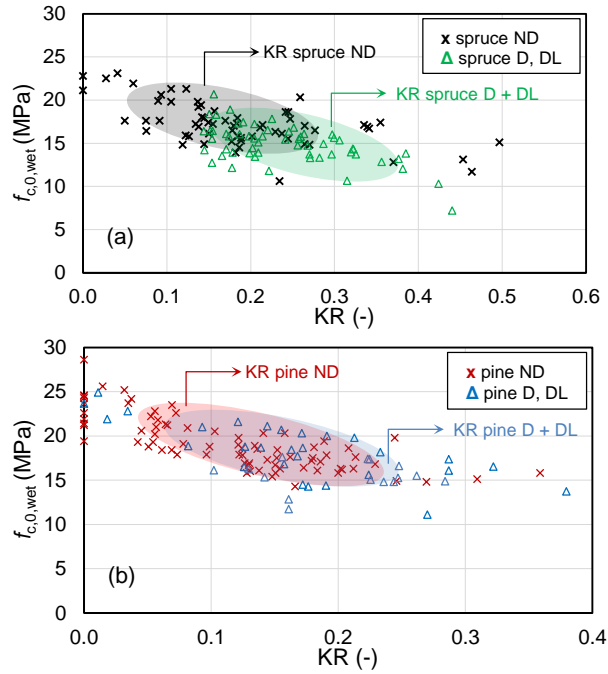


Figure 4.12: Correlation between $f_{c,0,wet}$ and KR for: a) spruce ND vs spruce D + DL; b) pine ND vs pine D + DL.

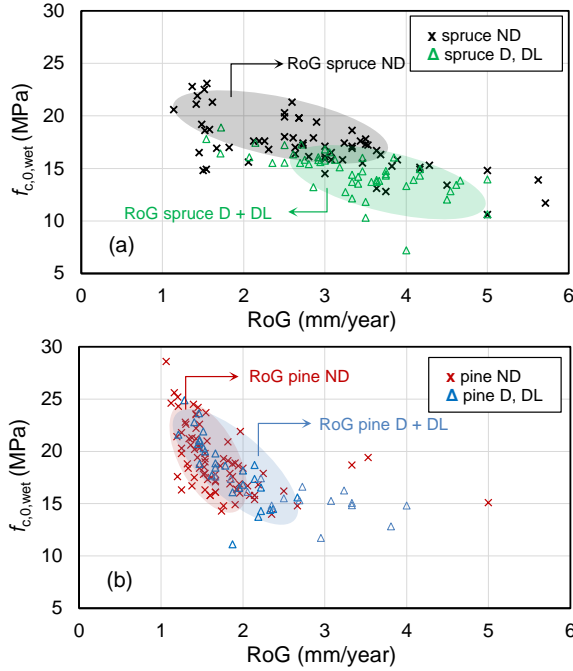


Figure 4.13: Correlation between $f_{c,0,wet}$ and RoG for: a) spruce ND vs spruce D + DL; b) pine ND vs pine D + DL.

More specifically, the middle-parts and tips of spruce D and ND had comparable mean density ($\rho_{12,mean}$), KR_{mean} , mean age and RoG_{mean} (see Table 4 4), with no significant differences in $f_{c,0,wet,mean}$ among the pile segments, also due to the limited number of spruce segments D (Appendix B3). However, spruce heads D exhibited roughly 20% lower $f_{c,0,wet,mean}$ in relation to spruce pile heads ND. This could be explained by the lower $\rho_{12,mean}$ of spruce heads D, although no significant differences in terms of KR, age and RoG were observed from the results in Table 4 4.

The spruce piles DL, that were loaded in-situ, presented lower $f_{c,0,wet,mean}$ than spruce D, possibly related to lower values of $\rho_{12,mean}$, especially for middle-parts and tips. All the spruce segments DL were characterized by higher KRs than spruce D, and lower age related to a larger presence of juvenile wood [106], with RoG_{mean} up to 3.8 mm/year in tips. Hence, the lower $f_{c,0,wet,mean}$ of spruce piles DL in comparison to spruce D, could be attributed to a lower quality of the piles, confirming the assumption that the load, applied in situ to the piles, did not have a significant effect on the wet compressive strength of the pile. Finally, the effect of the loading for 22 days on spruce DL-1 showed no significant influence on the $f_{c,0,wet,mean}$ of the piles, which is in line with spruce DL and D (Appendix B3).

Among all the groups of segments of pine piles ND, D and DL, no significant difference in the $f_{c,0,wet,mean}$ was measured. In particular, no effect of pile driving was observed in the $f_{c,0,wet,mean}$ among pine heads D/DL and ND. The quality of all pine heads (ND, D and DL) resulted to be higher compared to spruce heads, with maximum KRs below 0.09, mean

age of 80 years and $RoG_{mean} = 1.4$ mm/year, even if variations in $\rho_{12,mean}$ were measured (see). Therefore, both the effect of pile driving and the in-situ loading applied to the piles resulted to have no significant influence on the wet mean compressive strength of the piles, that revealed to be governed by the density, the KR, the age of the specimen and the rate of growth, as outlined in [35],[106].

As mentioned at the beginning of this paragraph, during in-situ testing the highest load applied to the piles DL corresponded to the geotechnical failure of the pile, which did not correspond to the material failure. In this context, it is important to mention that after driving piles D and DL, residual loads could develop in the pile [170],[171] influencing the maximum stress recorded on the pile head. Upon driving a pile for installation, residual loads are to fully develop after the driving force is removed. Residual compressive stresses could be present, especially at the pile base and balanced by the negative skin friction of the shaft [170]. These residual stresses were not considered during in-situ preloading and thus neglected during the stress measurement on the pile. In addition, the confining pressure applied to the timber pile shaft was neglected, since the modulus of elasticity perpendicular to the grain of the pile is 30 times smaller than that parallel to the grain ($E_{c,90} = 1/30 E_{c,0}$) as outlined in EN 338 (2016). The effect of the soil environment was not specifically studied in this research work. Thus, possible minimal residual loads could have occurred in the pile.

4.5 Characteristics values for visual grading

Characteristic values for $f_{c,0,wet}$ and $E_{c,0,wet}$, and $\rho_{12,k}$ of all spruce (*Picea abies*) and pine (*Pinus sylvestris*) pile segments are reported in Table 4.7 in accordance with NEN-EN 14358 (2016), on the basis of the mean values listed in Table 4.3. The characteristic values were calculated for visual grading boundaries (according to the Dutch grading standard for timber foundation piles NEN 5491 2010 and prEN 1995-1-1 2023), related to three IPs (See Appendix A2):

- **IP 1:** Knot ratio (KR): lower than 0.5;
- **IP 2:** Age between 20 and 100 years;
- **IP 3:** Rate of growth (RoG) lower than 5 mm/year.

The values were derived from an extensive experimental campaign involving 253 pile segments, and are applicable to the whole pile and/or its parts – head, middle-part, and tip. It should be noted that among the segments, multiple segments retrieved from the same pile are present, belonging to pile parts that were subdivided in multiple sub-segments.

All spruce and pine segments had a diameter between 150 mm and 290 mm, assigned to size 13-16 according to Annex Q of prEN 1995-1-1 2023. The wet strength and stiffness values can be applied to spruce and pine either separately, or to both species combined. No significant difference was measured between the spruce head and middle-part, which were considered as one class (Appendix B3). All the values reported for head, middle-part, and tip resulted in a significant difference in the $f_{c,0,k,wet}$, $E_{c,0,k,wet}$ and $\rho_{12,k}$. For pine and spruce, a significant difference was measured in the mechanical properties along the piles.

4.5 Characteristics values for visual grading

Possible strength classes for timber piles are defined in accordance with the indications in prEN 1995-1-1 (2023), with the goal of defining a new strength classification for timber foundation piles that could be implemented in the prEN 1995-1-1 (2023).

Table 4.7: Characteristic wet compressive strength and modulus of elasticity determined in accordance with the parametric calculation in NEN-EN 14358 (2016) along spruce and pine foundation piles.

Wood species (All categories ND, D, DL - no distinction)	Segment	Sample size (No.)	$E_{c,0,k,wet}$	$f_{c,0,k,wet}$	$\rho_{12,k}$
			(MPa) mean	(MPa) X05	(kg/m ³) X05
Spruce (<i>Picea abies</i>)	All	132	9800	11.3	390
	Head + Middle	81	10800	12.0	400
	Tip	51	8800	10.6	380
Pine (<i>Pinus sylvestris</i>)	All	121	10000	13.4	410
	Head	35	11800	17.1	440
	Middle	37	10300	14.8	420
	Tip	49	8600	12.9	400

4.5.1 Derivation of characteristic values based on combined visually-graded properties

Knot-ratio (KR) at the failure section of the pile, growth rate (RoG), and number of annual rings (Age) were selected according to the correlation analysis in Section 4.3, as the most influencing strength-reducing characteristic for visual grading of the pile segments.

The grading was done in accordance with prEN 1995-1-1 2023, NEN 5491 2010 and NEN-EN 384, first separating spruce and pine piles, and then exploring the possibility of considering one strength grading for spruce and pine together.

All the mechanical properties ($f_{c,0,wet}$, $E_{c,0,wet}$, and ρ_{12}) were determined according to EN 408 2010.

The cumulative distribution of the 3 visually-graded parameters are shown in Figure 4.14 and Figure 4.15 for pine and spruce, respectively.

All the parameters were normally distributed. It is possible to observe how head, middle-part and tip present a distinction in terms of KR, Age, and RoG. Tips are always presenting the highest KR and RoG and the lowest Age. This suggests that the overall behaviour of the pile could be governed by the visual grade of the tips (further discussed in paragraph 4.5.3).

In the following sub-sections, the characteristic values of compressive strength of the spruce and pine pile segments are predicted on the basis of indicating properties (IPs), derived with the combination of the 3 IPs (KR, Age and RoG).

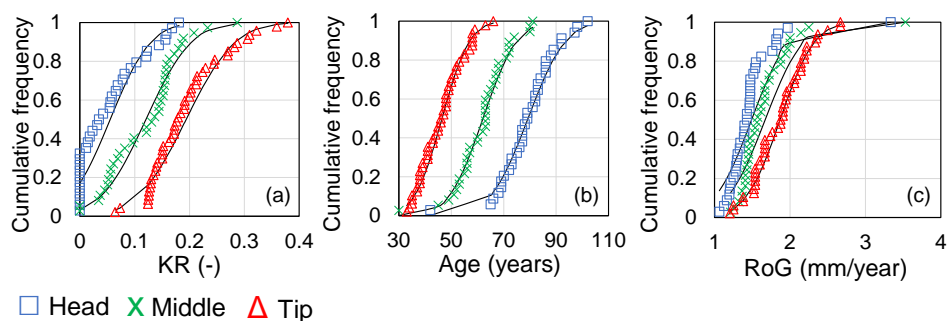


Figure 4.14: Cumulative distribution of visually-graded parameters: (a) KR; (b) Age; (c) RoG, for pine head, middle-part and tip of all the “new” piles. The lines show the normal distribution fitted to the data.

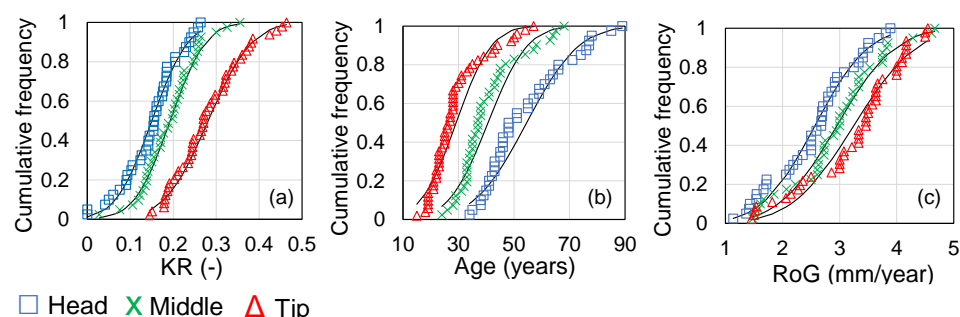


Figure 4.15: Cumulative distribution of visually-graded parameters: (a) KR; (b) Age; (c) RoG, for spruce head, middle-part and tip of all the “new” piles. The lines show the normal distribution fitted to the data.

Characteristic values based on combined IPs separately for spruce and pine

For spruce pile segments, IPs (where s stands for spruce) was based on visually-graded independent variables: KR, RoG and annual rings (Age) listed Table 4.8. For spruce piles, diameter, tapering and moisture content were not included as relevant parameters (p -value > 0.05). Equation 4.1 represents the IPs ($f_{c,0,wet}$) for spruce, with a F-value = 54.4 ($n = 132$), a multiple coefficient of determination (adjusted R^2) of 0.55 and a standard error of 1.73.

$$IP_S(f_{c,0,wet}) = 17.429 + 0.052 \text{ Age} - 6.516 \text{ KR} - 0.718 \text{ RoG} \quad (4.1)$$

Table 4.8: Multipliers and statistical parameters for 95% confidence interval in regression IP for spruce.

Variables	Coefficients	Standard Error	t-stat	p-value	Lower 95%	Upper 95%
Intercept	17.429	1.906	9.143	1.19E-15	13.657	21.201
Age	0.052	0.021	2.459	0.0153	0.010	0.094
KR	-6.516	2.029	-3.211	0.0017	-10.531	-2.501
RoG	-0.718	0.315	-2.282	0.024	-1.340	-0.095

4.5 Characteristics values for visual grading

The multiple regression model also works without considering RoG as independent variable (Table 4.9), making it easier in practice, where only the annual rings can be calculated. Equation 4.2 represents the $IP_s^* (f_{c,0,wet,pred})$ for spruce, with a F-value = 76.5 ($n = 132$), a multiple coefficient of determination (adjusted R^2) of 0.54 and a standard error of 1.76. Figure 4.16 shows the relationship between the two regression models IP_s and IP_s^* . All multipliers were significant and the residuals had relatively equal variances.

$$IP_s^* (f_{c,0,wet}) = 13.568 + 0.091 Age - 6.06 KR \quad (4.2)$$

Table 4.9: Multipliers and statistical parameters for 95% confidence interval in regression IP_s^* for spruce.

Variables	Coefficients	Standard Error	t-stat	p-value	Lower 95%	Upper 95%
Intercept	13.568	0.892	15.209	1E-30	11.803	15.333
Age	0.0914	0.012	7.1343	6E-11	0.066	0.116
KR	-6.063	2.052	-2.955	0.0037	-10.123	-2.003

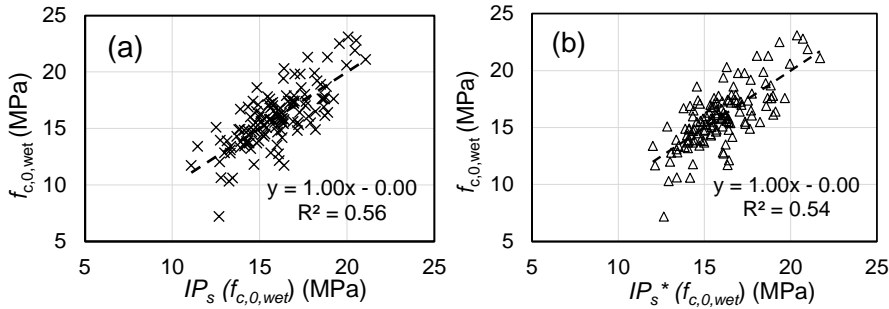


Figure 4.16: (a) Multiple regression model IP_s for spruce with relationship between IP_s ($f_{c,0,wet}$) and $f_{c,0,wet}$ calculated with Age, RoG and KR; (b) Multiple regression model IP_s^* for spruce with relationship between IP_s^* ($f_{c,0,wet}$) and $f_{c,0,wet}$ calculated with Age and KR;

For pine pile segments, IP_P (where P stands for pine) was based only on visually-graded independent variables: KR and annual rings (Age). RoG, diameter, tapering and moisture content were not included as relevant parameters (p -value > 0.05).

Equation 4.3 represents the $IP_P (f_{c,0,wet})$ for pine, with a F-value = 107.6 ($n = 121$), a multiple coefficient of determination (adjusted R^2) of 0.64 and a standard error of 1.83. Figure 4.17 shows the model IP_P . All multipliers were significant and the residuals had relatively equal variances.

The results of the characteristic values for two possible grades A and B for spruce and pine are presented in Table 4.11 and Figure 4.18. The IP were chosen on the basis of the minimum samples for each grading class (≥ 40) according to EN 338 2016.

$$IP_P (f_{c,0,wet}) = 14.862 + 0.09 Age - 10.79 KR \quad (4.3)$$

Table 4.10: Multipliers and statistical parameters for 95% confidence interval in regression IP_P for pine.

Variables	Coefficients	Standard Error	t-stat	p-value	Lower 95%	Upper 95%
Intercept	14.862	1.111	13.379	2.10E-25	12.662	17.062
Age	0.090	0.014	6.460	2.44E-09	0.063	0.118
KR	-10.792	2.319	-4.653	8.63E-06	-15.385	-6.199

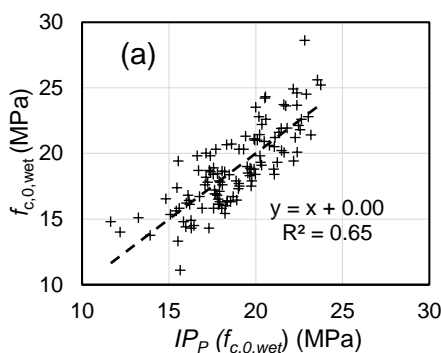


Figure 4.17: Multiple regression model IP_P for pine with relationship between $IP_P (f_{c,0,wet})$ and $f_{c,0,wet}$ calculated with Age and KR.

Table 4.11: Grading classes A and B for visual grading of pine and spruce pile segments according to prEN 1995-1-1 2023 and the parametric calculation in NEN-EN 14358: 2016

Species	Grading category	No. of segme nts (N ≥ 40)	IP limit (MPa)	$f_{c,0,wet}$ (MPa)			$E_{c,0,wet}$ (MPa)		ρ_{12} (kg/m ³)		
				mean	COV	x05	mean	COV	mean	COV	x05
Spruce	Grade A	87	15.0	16.9	13%	12.8	9400	17%	480	11%	400
	Grade B	45	12.0	14.1	14%	10.3	8800	16%	460	10%	380
Pine	Grade A	72	18.0	20.4	13%	15.5	10500	18%	505	11%	420
	Grade B	49	12.0	16.6	12%	13.1	8700	19%	475	12%	400

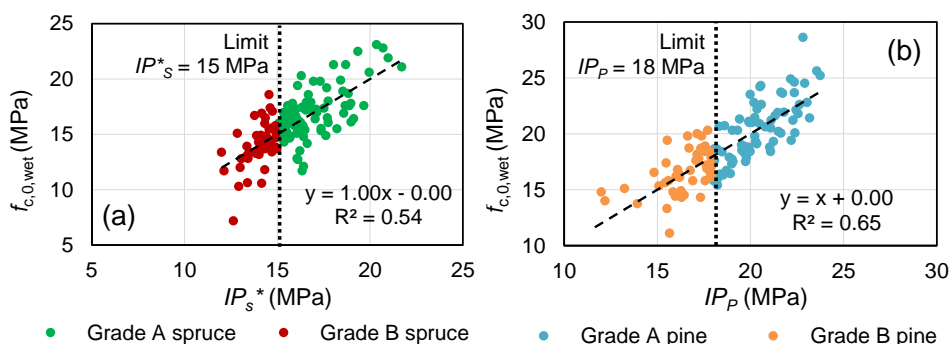


Figure 4.18: Grades A and B based on IP_P s for (a) spruce pile segments; (b) pine pile segments.

Characteristic values based on combined IPs for all pile segments (spruce + pine)

The possibility of combining spruce and pine for visual grading is studied with Equation 4.4, where IP_{SP} (SP stands for spruce and pine together) is calculated based on common visually-graded independent variables for spruce and pine: KR and Age in Table 4.12. Only KR and Age were statistically significant (p -value < 0.05 in Table 4.12). Thus, RoG was not taken into account in the regression model. Equation 4.4 represents the IP_{SP} ($f_{c,0,wet}$) for spruce/pine, with a F-value = 261.3 ($n = 252$), a multiple coefficient of determination (adjusted R^2) of 0.68 and a standard error of 1.8. All multipliers were significant and the residuals had relatively equal variances. The feasibility of combining spruce and pine is supported by Figure 4.19, where spruce and pine trendlines are superimposable and exhibit a similar trend. The individual grading approach for spruce and pine could still be adopted. However, more data are needed to understand the trends of spruce and pine.

The results of the characteristic values for 4 possible grades A, B, C, D for spruce and pine are presented in Table 4.13. The IPs were chosen on the basis of the minimum samples for each grading class (≥ 40) according to EN 338 2016. The characteristic values provided in Table 4.13 match well with those derived separately for spruce and pine in Table 4.11. This means that the characteristic strength values for grading can be determined for both spruce and pine.

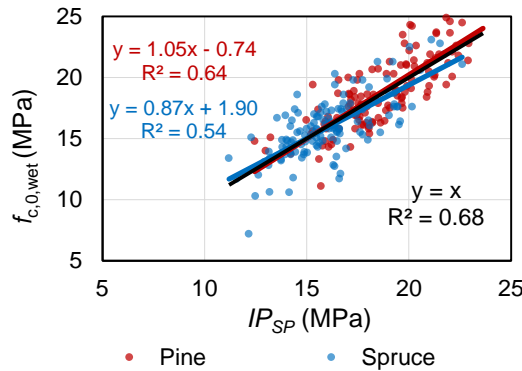


Figure 4.19: Multiple regression model IP_{SP} (combined spruce and pine) with relationship between IP_{SP} ($f_{c,0,wet}$) and $f_{c,0,wet}$ calculated with Age and KR.

$$IP_{SP} (f_{c,0,wet}) = 13.92 + 0.097 \text{ Age} - 8.22 \text{ KR} \quad (4.4)$$

Table 4.12: Multipliers and statistical parameters for 95% confidence interval in regression IP_{SP} for combined spruce and pine.

Variables	Coefficients	Standard Error	t-stat	p-value	Lower 95%	Upper 95%
Intercept	13.925	0.678	20.536	1.4E-55	12.589	15.26
Age	0.097	0.008	11.184	8.18E-24	0.08	0.114
KR	-8.22	1.548	-5.309	2.43E-07	-11.274	-5.172

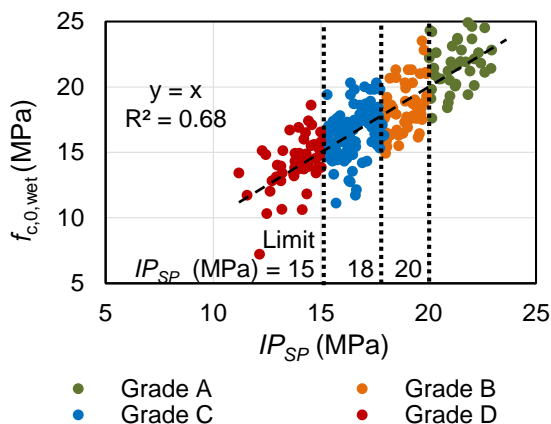


Figure 4.20: Grades A, B, C, D based on IP_{SP} for combined spruce and pile segments.

Table 4.13: Grading classes A and B for visual grading of combined pine and spruce pile segments according to prEN 1995-1-1 2023 and the parametric calculation in NEN-EN 14358: 2016

Species	Grading category	No. of segments (N ≥ 40)	IP limit (MPa)	$f_{c,0,wet}$ (MPa)			$E_{c,0,wet}$ (MPa)			ρ_{12} (kg/m ³)		
				mean	COV	x ₀₅	mean	COV		mean	COV	x ₀₅
Spruce + Pine	Grade A	43	20.0	22.0	10%	18.0	11200	15%		510	11%	430
	Grade B	54	18.0	18.4	11%	14.8	10200	15%		490	11%	410
	Grade C	106	15.0	16.4	11%	13.2	9000	17%		480	11%	400
	Grade D	50	11.0	14.1	14%	10.5	8700	14%		460	10%	380

4.5.2 Derivation of characteristic values based on individual visual grades

Visual grades were defined in relation to two strength classes of characteristic compressive strength of the piles, for a minimum number of 40 samples per grading category, as outlined in the NEN-EN 384. For pine, Table 4.14, Table 4.15, and Table 4.16 describe the visual grades for IP1 (KR), IP2 (Age) and IP3 (RoG), respectively. The derivation of characteristic values for the mechanical properties ($f_{c,0,wet}$, $E_{c,0,wet}$ and ρ_{12}), calculated with the parametric calculation in NEN-EN 14358 2016, are associated with possible grades (A and B) according to prEN 1995-1-1 2023. The distribution of $f_{c,0,wet}$ for the possible grades A and B for pine segments is reported in Figure 4.21, where the data are overlapping for the two grades, since the $f_{c,0,wet}$ of the piles is more uniform compared to spruce.

For spruce, Table 4.17, Table 4.18, and Table 4.19 describe the visual grades for IP1 (KR), IP2 (Age) and IP3 (RoG), respectively. The same procedure conducted for pine is carried out for spruce for the derivation of characteristic values. The distribution of $f_{c,0,wet}$ for the possible grades A and B for spruce segments is reported in Figure 4.22, where a distinction between the 2 classes is more evident in comparison to pine.

4.5 Characteristics values for visual grading

Table 4.14: Grading classes A and B for IP1 (KR) of pine segments according to prEN 1995-1-1 2023 and with the parametric calculation in NEN-EN 14358: 2016.

Category	Grade	IP1: KR (-)	$f_{c,0,wet}$ (MPa)			$E_{c,0,wet}$ (MPa)		ρ_{12} (kg/m ³)		
	No. of segments (N ≥ 40)	limits	mean	COV	x05	mean	COV	mean	COV	x05
Pine A 145 < d < 260	A (72)	0.15	20.1	14%	15.2	9700	14%	490	7%	425
Pine B 135 < d < 275	B (46)	0.4	17.0	13%	13.0	10000	14%	480	8%	410
Rejected	R (2)	> 0.4	14.3	-	-	7300	-	440	-	-

Table 4.15: Grading classes A and B for IP2 (Age) of pine segments according to prEN 1995-1-1 2023 and with the parametric calculation in NEN-EN 14358: 2016

Category	Grade	IP2: Age (year)	$f_{c,0,wet}$ (MPa)			$E_{c,0,wet}$ (MPa)		ρ_{12} (kg/m ³)		
	No. of segments (N ≥ 40)	limits	mean	COV	x05	mean	COV	mean	COV	x05
Pine A 145 < d < 260	A (79)	55	20.1	14%	15.2	10900	15%	510	10%	420
Pine B 135 < d < 275	B (40)	30	16.4	12%	12.9	8600	16%	475	8%	400
Rejected	R (1)	< 30	15.1	-	-	8700	-	490	-	-

Table 4.16: Grading classes A and B for IP3 (RoG) of pine segments according to prEN 1995-1-1 2023 and with the parametric calculation in NEN-EN 14358: 2016

Category	Grade	IP3: RoG (mm/year)	$f_{c,0,wet}$ (MPa)			$E_{c,0,wet}$ (MPa)		ρ_{12} (kg/m ³)		
	No. of segments (N ≥ 40)	limits	mean	COV	x05	mean	COV	mean	COV	x05
Pine A 140 < d < 260	A (72)	1.7	20.2	14%	15.2	10900	15%	520	10%	425
Pine B 135 < d < 275	B (47)	3.5	16.8	13%	12.9	8800	15%	470	10%	400
Rejected	R (1)	> 3.5	15.1	-	-	8700	-	490	-	-

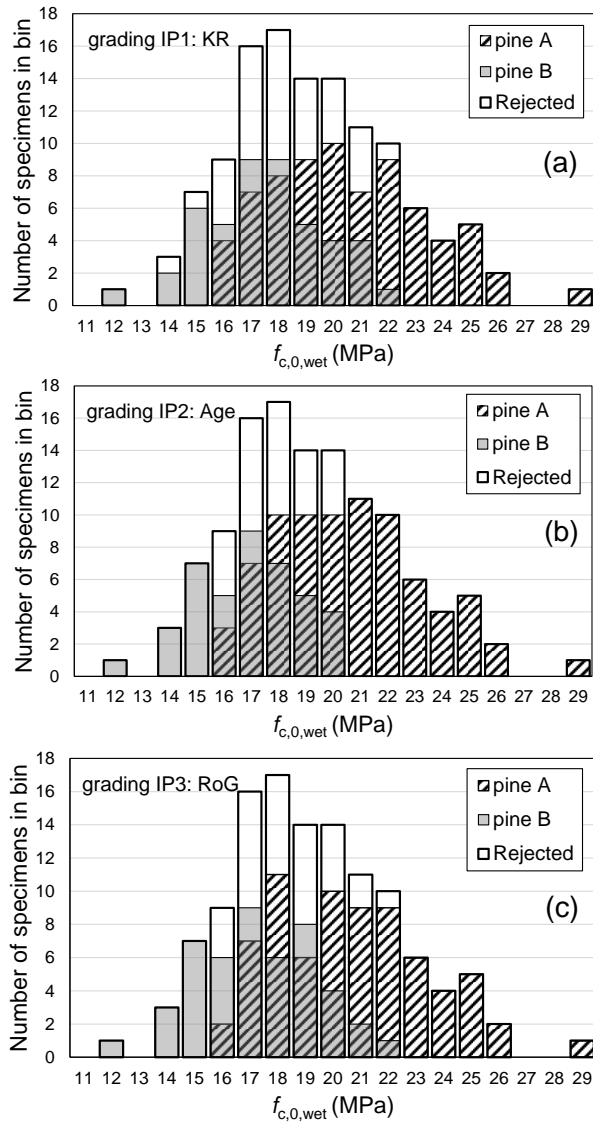


Figure 4.21: Distributions of $f_{c,0,wet}$ based on the number of pile segments in different bins, for saturated pine grade A and B for (a) IP1; (b) IP2; (c) IP3.

4.5 Characteristics values for visual grading

Table 4.17: Grading classes A and B for IP1 (KR) of spruce segments according to prEN 1995-1-1 2023 and with the parametric calculation in NEN-EN 14358: 2016.

Category	Grade	IP1: KR (-)	$f_{c,0,wet}$ (MPa)			$E_{c,0,wet}$ (MPa)			ρ_{12} (kg/m ³)		
	No. of segments (N ≥ 40)	limits	mean	COV	χ_{05}	mean	COV		mean	COV	χ_{05}
Spruce A 170 < d < 290	A (35)	0.15	18.0	15%	13.2	10800	14%		480	10%	390
Spruce B 150 < d < 290	B (95)	0.5	15.2	14%	11.4	10000	14%		470	10%	390
Rejected	R (2)	>0.5	14.2	-	-	9500	-		490	-	-

Table 4.18: Grading classes A and B for IP2 (Age) of spruce segments according to prEN 1995-1-1 2023 and with the parametric calculation in NEN-EN 14358: 2016

Category	Grade	IP2: Age (year)	$f_{c,0,wet}$ (MPa)			$E_{c,0,wet}$ (MPa)			ρ_{12} (kg/m ³)		
	No. of segments (N ≥ 40)	limits	mean	COV	χ_{05}	mean	COV		mean	COV	χ_{05}
Spruce A 170 < d < 290	A (54)	42	17.6	13%	13.2	10800	15%		495	10%	400
Spruce B 150 < d < 290	B (71)	20	15.0	12%	11.9	9400	13%		470	9%	390
Rejected	R (7)	< 20	11.0	-	-	7900	-		475	-	-

Table 4.19: Grading classes A and B for IP3 (RoG) of spruce segments according to prEN 1995-1-1 2023 and with the parametric calculation in NEN-EN 14358: 2016

Category	Grade	IP3: RoG (mm/ year)	$f_{c,0,wet}$ (MPa)			$E_{c,0,wet}$ (MPa)			ρ_{12} (kg/m ³)		
	No. of segments (N ≥ 40)	limits	mean	COV	χ_{05}	mean	CO V		mean	COV	χ_{05}
Spruce A 150 < d < 290	A (67)	3.0	17.3	13%	13.2	10600	15%		495	10%	410
Spruce B 150 < d < 290	B (65)	5.0	14.8	13%	11.4	9300	13%		465	10%	380
Rejected	R (6)	> 5.0	12.0	-	-	8400	-		470	-	-

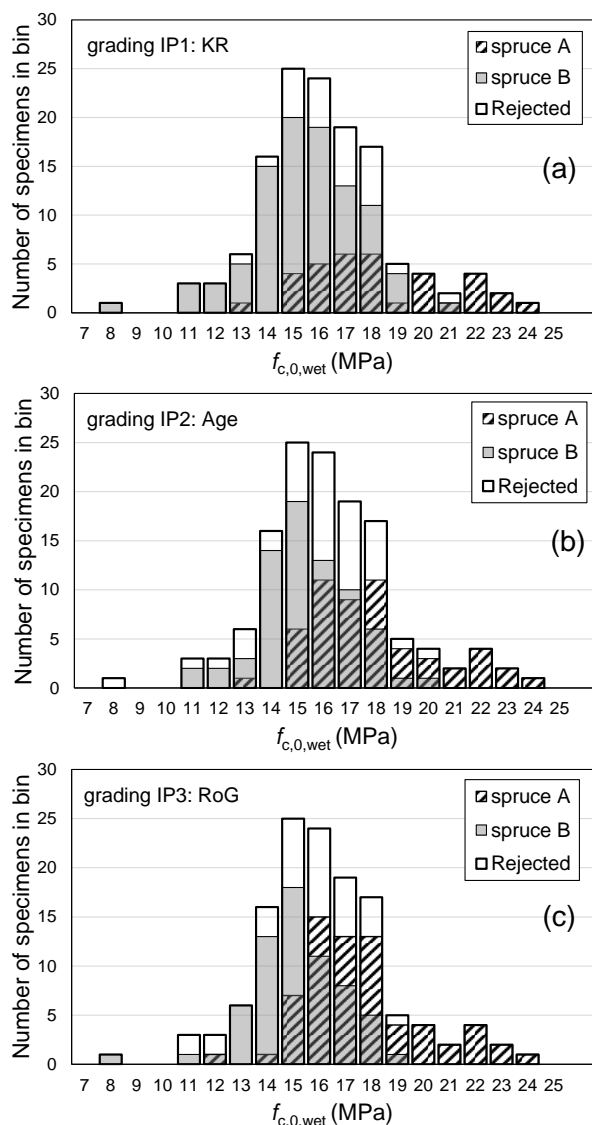


Figure 4.22: Distributions of $f_{c,0,wet}$ based on the number of pile segments in different bins, for saturated spruce grade A and B for (a) IP1; (b) IP2; (c) IP3.

4.5.3 Derivation of characteristic values for visual grade of pile tips

The cumulative distributions of the visually-graded parameters (Figure 4.14 and Figure 4.15) show how tips featured the highest KR and RoG, and the lowest Age, related to the lowest mechanical properties within the pile.

This can be visually observed for pine piles (Figure 4.24; Figure 4.25; Figure 4.26) and for spruce piles (Figure 4.27; Figure 4.28; Figure 4.29), with the relationships between KR, Age, RoG, and the mechanical properties ($f_{c,0,wet}$, $E_{c,0,wet}$ and ρ_{12}) of the piles.

4.5 Characteristics values for visual grading

In the light of this, the tip should be considered as the critical part of a tapered pile since:

- The tip features the lowest mechanical properties of the pile;
- Depending on soil conditions, the tip corresponds to the critical cross section of the pile during service, primarily due to the high stresses associated with its smaller cross section.

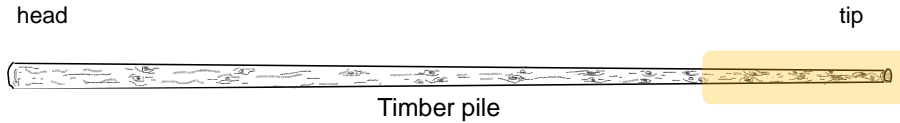


Figure 4.23: Critical part of a tapered timber pile: tip.

Thus, the tip represents the governing part of the pile in terms of mechanical properties, and the strength grading of the pile is mainly governed by the strength of the tip.

Table 4.20 shows the visual grades associated to spruce tips ($150 \text{ mm} < d < 200$) and pine tips ($140 \text{ mm} < d < 190$) according to prEN 1995-1-1 2023 (related to minimum size = 13). Table 4.20 shows the derivation of characteristic values for the mechanical properties of spruce and pine tips ($f_{c,0,wet}$, $E_{c,0,wet}$ and ρ_{12}) in accordance with the parametric calculation in NEN-EN 14358 (2016).

Therefore, the selection of the tip from a log, used as foundation pile, can imply different material properties related to visually-graded parameters varying with the wood species, growing conditions and areas, and required size (pile length and tip diameter) of the timber piles employed in a foundation.

Table 4.20: Grading classes A and B for IP1 (KR) of spruce segments according to prEN 1995-1-1 2023 and with the parametric calculation in NEN-EN 14358: 2016.

Category	Grade	IP1:	IP2:	IP3:	$f_{c,0,wet}$ (MPa)			$E_{c,0,wet}$ (MPa)		ρ_{12} (kg/m ³)		
		KR (-)	Age (year)	RoG (mm/year)								
	No. of segments (N ≥ 40)	limit	limit	limit	mean	COV	x05	mean	COV	mean	COV	x05
Spruce tips 150 < d < 220	ST (41)	0.45	20	4.5	14.2	12%	11.2	8900	14%	460	10%	380
Pine tips 135 < d < 200	PT (46)	0.4	35	2.7	16.8	12%	13.0	8700	14%	475	8%	405
Spruce Rejected	R (10)	>0.4 5	<20	>4.5	11.0	-	-	8300	-	490	-	-
Pine Rejected	R (3)	>0.4	<35	>4.5	14.6	-	-	8000	-	455	-	-

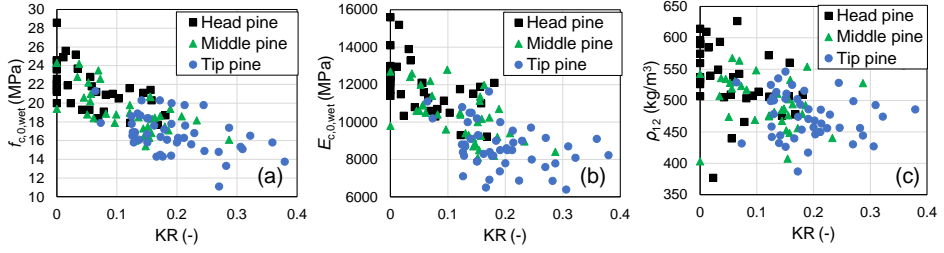


Figure 4.24: Correlation between mechanical properties of “new” pine segments and knot-ratio (KR) at failure section: (a) $f_{c,0,wet}$ vs KR; (b) $E_{c,0,wet}$ vs KR; (c) ρ_{12} vs KR.

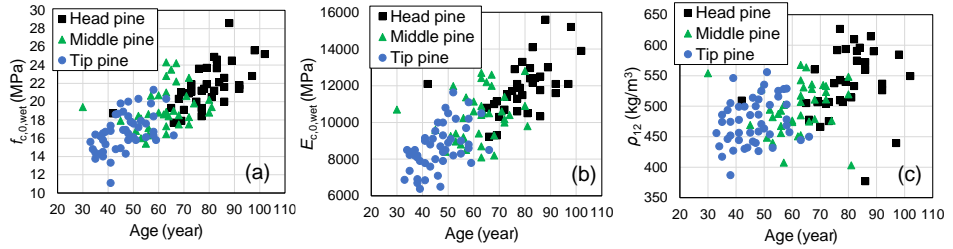


Figure 4.25: Correlation between mechanical properties of “new” pine segments and number of annual rings (Age): (a) $f_{c,0,wet}$ vs Age; (b) $E_{c,0,wet}$ vs Age; (c) ρ_{12} vs Age.

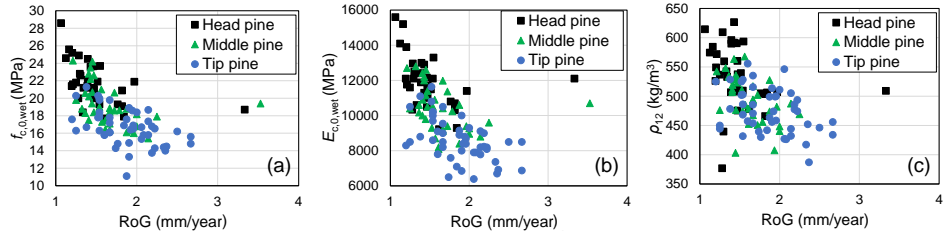


Figure 4.26: Correlation between mechanical properties of “new” pine segments and rate of growth (RoG): (a) $f_{c,0,wet}$ vs RoG; (b) $E_{c,0,wet}$ vs RoG; (c) ρ_{12} vs RoG.

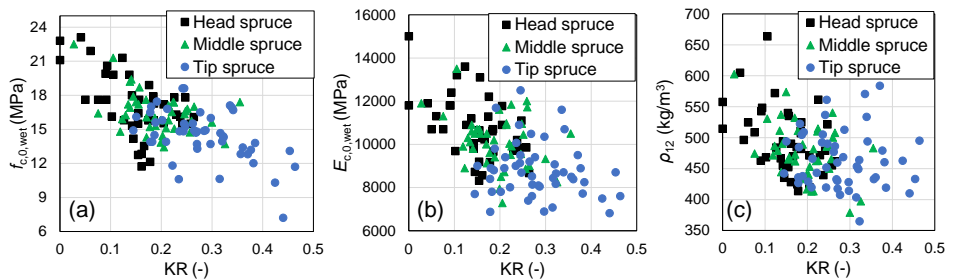


Figure 4.27: Correlation between mechanical properties of “new” spruce segments and knot-ratio (KR) at failure section: (a) $f_{c,0,wet}$ vs KR; (b) $E_{c,0,wet}$ vs KR; (c) ρ_{12} vs KR.

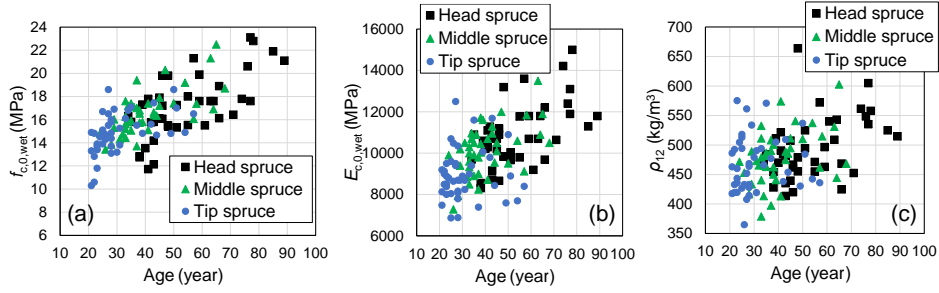


Figure 4.28: Correlation between mechanical properties of “new” spruce segments and annual rings (Age) at failure section: (a) $f_{c,0,wet}$ vs Age; (b) $E_{c,0,wet}$ vs Age; (c) ρ_{12} vs Age.

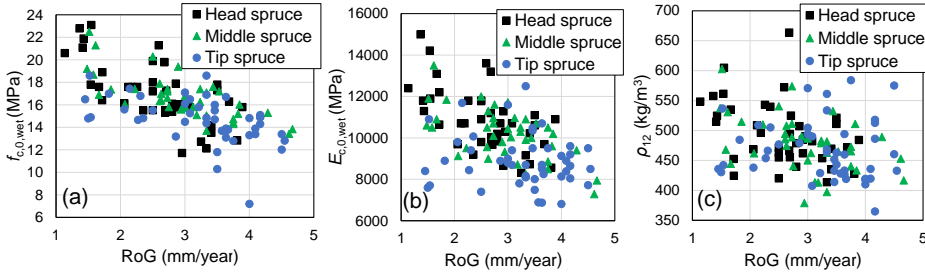


Figure 4.29: Correlation between mechanical properties of “new” spruce segments and rate of growth (RoG) at failure section: (a) $f_{c,0,wet}$ vs RoG; (b) $E_{c,0,wet}$ vs RoG; (c) ρ_{12} vs RoG.

4.5.4 Case study: application of visual grading on wooden pile

In engineering practice, when a wooden pile is sourced from a tree, a visual grading of the pile tip can be conducted in order to classify the compressive strength for its application in foundations. As demonstrated in Paragraph 4.5.3, the pile strength grading is governed by the tip. Thus, for the application of piles in foundations, tip diameter and length are selected on the basis of the design project of the foundation (called sizes from 8 to 16 in the prEN 1995-1-1 2023). The size selection can depend on multiple factors related to the design, such as geotechnical parameters (soil stratigraphy, resistance of the soil, water table, etc.), number of piles employed in the foundation and magnitude of the load acting on the piles. However, the influencing visually-graded properties on the compressive strength of the pile are not related to the size (diameter and length) but to the KR_s, Age and RoG of the pile. Therefore, independently from the pile size, a visual grading of the tip should be conducted in order to assign the pile to specific strength classes (presented in Paragraph 4.5.3).

The visual grading for the determination of strength classes for spruce and pine piles (developed in Paragraph 4.5.1 and 4.5.2), is exemplified in spruce pile OAM P2.1 and validated in the case study in Figure 4.30. The pile was subdivided into head middle-part, and tip, and the mechanical properties of all the segments were characterized. The visual grading was applied to 2 different sections along the length of the pile: the tip, considering the full-length pile of 12.7 m (size 15); hypothetical “section 2”, considering that the pile has a length of 9 m (size 16 and above). This might be useful in case a pile is to be cut in

smaller lengths to adapt it to different engineering project needs or re-use it for other applications. Figure 4.30, shows the visual grading with 3 different approaches:

- Grade based on combined IP^*_s for spruce piles (See Paragraph 4.5.1).
- Grade based on combined IPs and combined spruce and pine IP_{SP} (See Paragraph 4.5.1);
- Tips grading according to Paragraph 4.5.3.

The results show differences below 10% between the assigned compressive strength of the visual classes and the actual $f_{c,0,wet}$ determined with the compression test on the pile segment above the selected section. In this context, the visual grading classes are effectively applicable not only to the pile tip, but also to different sections along the pile.

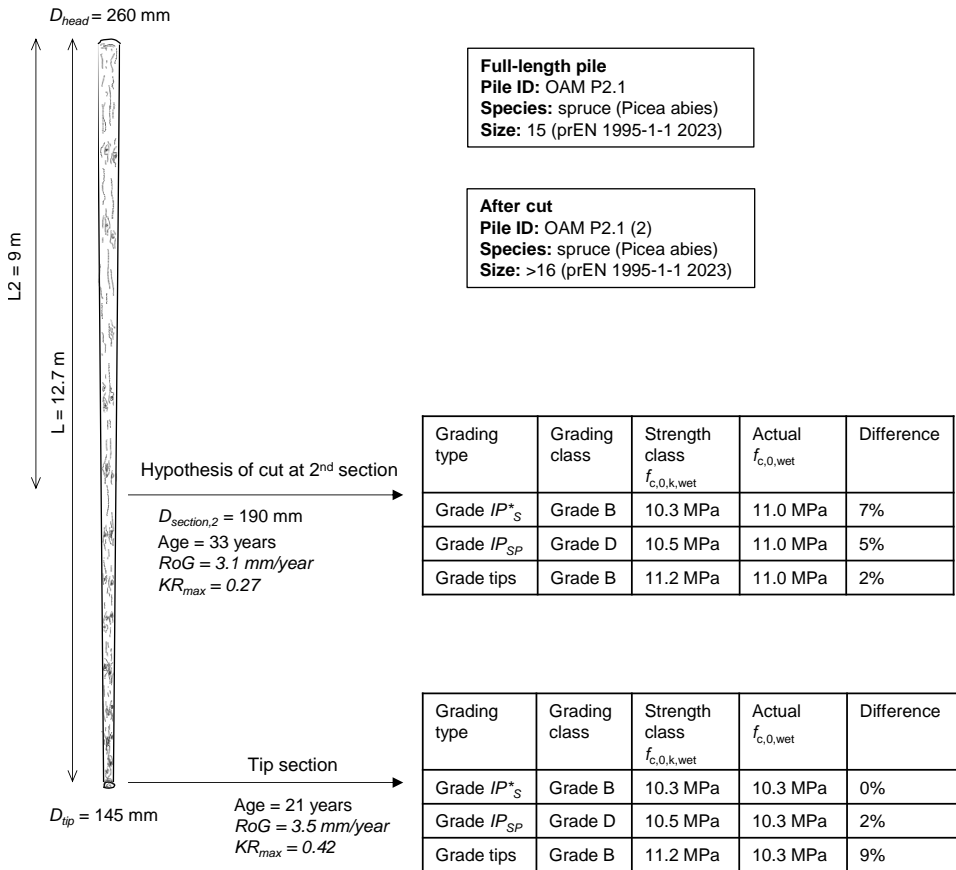


Figure 4.30: Case study for the applicability of visual grading on a spruce pile

4.6 Proposal for compressive strength design values according to draft EC5 2023

Given the good applicability of the model based on combined spruce and pine piles, the values of $f_{c,0,k,wet}$ correspondent to 4 different strength classes (See Table 4.13) were used to calculate the design values for the engineering design of wooden piles according to the indications provided in the draft EC5 2023 [21], outlined in detail in Paragraph 2.5.5.

Design values are calculated for European spruce and pine in Table 4.21, by applying modification factors for long-term loading ($k_{mod,sat} = 0.6$) and short-term loading ($k_{mod,sat} = 0.9$), together with partial factors for resistances of timber piles $\gamma_M = 1.3$ (Ultimate Limit State, ULS) to $f_{c,0,k,wet}$. These values do not consider the system strength factor ($k_{sys} = 1.1$), applicable when the load is shared by a minimum of three piles. Table 4.21 includes also the calculation of design values according to the Dutch National Annex to EC5 2013 (EC5 NB 2013) [19], obtained by applying to the dry characteristic strength value ($f_{c,0,rep} = 19.8$ MPa) the k_{mod} (0.7 for short- and 0.6 long-term loading corresponding to service class 3 for high moisture contents) and $\gamma_M = 1.2$ (Reported in detail in Paragraph 2.5.5).

The design values (Table 4.21) calculated according to the draft EC5 2023, based on spruce and pine piles characterized in this study, resulted to be up to 50% lower in long-term loading situations compared to the design values calculated with EC5 NB 2013.

This highlights that the current approach in EC5 NB 2013 based on one single dry compressive strength value, might not be adequate for the calculation of design values of wooden foundation piles.

A more accurate design can be conducted using the provisions in the draft EC5 2023, by adopting directly $f_{c,0,k,wet}$ and applying $k_{mod,sat}$ only accounting for the effect of the duration of load in a timber pile, since the effect of moisture is already accounted in $f_{c,0,k,wet}$ of spruce and pine piles tested in fully-saturated conditions.

Furthermore, this research underlines the importance of considering the different strength distribution from the pile head to the tip when calculating the design strength values for tapered timber foundation piles.

Experimental results of “new” wooden foundation piles

Table 4.21: Design strength values for spruce and pine piles calculated according to the draft EC5 2023 and differences (Diff.) with those according to EC5 NB 2013.

Norm	Species	Grad ing class	$f_{c,0,rep}$ (MPa)	$f_{c,0,k,wet}$ (MPa)	$f_{c,0,d,short}$ (MPa)	$f_{c,0,d,long}$ (MPa)	Diff. $f_{c,0,d,short}$ draft EC5 2023 vs EC5 NB 2013 (%)	Diff. $f_{c,0,d,long}$ draft EC5 2023 vs EC5 NB 2013 (%)	k_{mod}	k_{mod}	γ_M
			Dry: MC =12%	wet MC \geq 50%	Short term	Long term			Short term	Long term	ULS
Draft EC5 2023	EU spruce and pine	A	-	18.0	12.5	8.3	8	-15			
		B	-	14.8	10.2	6.8	-11	-30			
		C	-	13.2	9.1	6.1	-21	-38	$k_{mod,sat}$ = 0.9	$k_{mod,sat}$ = 0.6	1.3
		D	-	10.5	7.3	4.8	-37	-51			
EC5 NB 2013	EU spruce	None	19.8	-	11.5	9.8	-	-	k_{mod} = 0.7	k_{mod} = 0.6	1.2

4.7 Summary of the test results

The mechanical properties of 38 spruce (*Picea abies*) and 32 pine (*Pinus sylvestris*) full-sized tapered round piles, averaging 12 m in total length, were tested in line with prEN 1995-1-1 2023. The mechanical properties were investigated in saturated conditions ($MC_{\text{mean}} = 70\% \pm 20\%$), by performing axial compression tests on pile segments extracted from head, middle-part and tip of each full-length pile in order to study different pile diameters ranging from 130 mm to 300 mm (size 13-16 according to Annex Q of prEN 1995-1-1 2023). The wooden piles were subdivided in 3 categories: piles never driven into the soil (ND); piles driven into the soil (D); piles driven into the soil and subjected to in-situ loading (DL). The determined mechanical properties were studied in relation to visually-graded parameters of timber that could possibly affect the saturated compressive strength.

The conclusions drawn from this experimental study can be summarized as follows:

- The effect of the pile driving on piles D and the in-situ loading on piles DL, with stress levels on the pile heads up to 6.9 MPa, revealed to have no significant influence on the mechanical properties of spruce and pine piles. The difference in the wet compressive strength measured among the pile categories ND, D and DL (Section 4.4), was associated to the variation of the knot-ratio (KR), annual rings (Age) and rate of growth (RoG) in heads, middle-parts and tips, that significantly influenced the wet compressive strength of the piles. It should be noted that, in this study, the effect of the soil environment was not taken into account, since the research focused on the material and mechanical properties of spruce and pine piles.
- Characteristic wet values for compressive strength and modulus of elasticity of spruce (*Picea abies*) and pine (*Pinus sylvestris*) piles were derived in Section 4.5, for $KR < 0.5$, age between 20 and 100 years and rate of growth lower than 5 mm/year. This opened up the opportunity for grading of multiple strength classes for combined visual grades (IP1, IP2, IP3), distinctively for spruce and pine and for spruce and pine combined (Section 4.5.1). In addition, the characteristic compressive strength values were derived on the basis of individual visual grades (IP1, IP2, IP3, separately). The derived strength classes are applicable to the whole pile and/or its parts: head, middle-part and tip.
- Based on the possible strength classes determined in this Chapter, design values for spruce and pine foundation piles were calculated in accordance with the provisions outlined in the draft of the new Eurocode 5 (2023). These design values resulted to be up to 50% lower than those calculated according to the current Dutch National Annex to EC5 (2013) based on one single dry compressive strength value. This highlighted that more accurate and reliable design values of timber piles can be obtained according to the approach in the draft EC5 2023, by using saturated characteristic compressive strength values ($f_{c,0,k,wet}$) and the modification factor ($k_{mod,sat}$) applied in the new defined service class 4. Differently from the approach in the Dutch National annex to EC5 (2013), $k_{mod,sat}$ only accounts for the effect of load duration in the piles, since the effect of moisture is already accounted in $f_{c,0,k,wet}$ determined in fully-saturated conditions.
- The pile tip resulted to be the critical section of the pile, featuring the lowest saturated compressive strength and stiffness. Therefore, the mechanical

properties of the spruce and pine piles revealed to be governed by the tips, whose characteristic strength properties were presented in paragraph 4.5.3, in relation to their visual grades.

- The number of annual rings (Age) in a pile, and its relation with the diameter (rate of growth, RoG) had a significant influence on the density and wet compressive strength. Age and RoG decreased from the head to the tip of the pile, resulting in consequent decreasing density and $f_{c,0,wet}$. This was related to the proportion between mature wood and juvenile wood (See Section 2.4) in the pile: heads presented higher portions of mature wood featuring higher densities and compressive strength; tips exhibited larger portions of juvenile wood, with lower densities and compressive strength. Thus, higher Age and lower RoG were associated to higher $f_{c,0,wet}$ values. In general, pine piles exhibited higher $f_{c,0,wet}$ values than spruce, which were on average 20-years younger than pine piles and featured higher RoG values.
- The wood species and the location in the stem affect the knot-ratio, with consequent influence on the wet compressive strength distribution along the pile. Pine pile heads were characterized by a very low $KR_{mean} = 0.05$, since the branches of pine trees are mainly located on the upper part of the tree (See Figure 2.18), resulting in increasing dimension and number of the knots in middle-part and tip of the pile. The larger and more frequent knots, in combination with the decreasing diameter along the tapered pile, result in higher KRs in pine middle-parts and tips. This factor contributes to having a decreasing compressive strength along the pile, from head to tip. Whereas, for spruce trees, where the crown already starts from the bottom part of the log, the branches are more regularly distributed along the tree (See Figure 2.18). This means that larger and more frequent knots were measured in spruce heads and middle-parts compared to pine. As a consequence, spruce heads and middle-parts had similar KRs ($KR_{mean} = 0.15$ for heads and $KR_{mean} = 0.20$ for middle-parts), revealing no significant difference in $f_{c,0,k,wet}$, differently from pine, where the strength difference between heads and middle-parts was significant. For spruce piles, KR gradually increases from heads to middle-parts, characterized by a larger distinction between middle-part and tip, both in terms of KR and compressive strength.

5

Experimental results of historical wooden foundation piles

5.1 Introduction

Chapter 5 presents the results of the characterization of historical timber piles and the influence of bacterial decay on their material and mechanical properties. Section 5.2 outlined the characterization of the remaining mechanical properties of the piles through large-scale compression tests on the head, middle-part, and tip, establishing correlations with their physical and material properties.

Decay assessment using micro-drilling is presented in Section 5.3, where the micro-drilling methodology is calibrated and validated (on the assumptions in Section 3.9) based on the experimental tests on all the historical pile segments. The influence of moisture content on micro-drilling is examined in Section 5.4, revealing that moisture content has no effect on the assessment of decay with micro-drilling. In Section 5.5, the applicability of micro-drilling for determining the extent of decay at different moisture contents is demonstrated.

The influence of physical and material properties, as well as the extent of decay—quantified through micro-drilling—on the remaining short-term compressive strength of the piles is analysed on a large scale. This assessment is conducted with respect to different sections of the piles, specifically the head, middle, and tip, to provide a comprehensive understanding of strength variation along their length. In Section 5.6, the effect of decay on the material properties at the cross-sectional level is investigated.

Finally, Section 5.7 explores the extent of decay within the cross-section (in sapwood and heartwood) and along the pile (from head to tip), supported by CT-scanning and light microscopy results (see methodology in Sections 3.12 and 3.13).

The summary of the results is reported in Section 5.8.

5.2 Results of material and mechanical characterization of historic spruce and fir piles

5.2.1 Preliminary results on full-length piles

The results of the preliminary tests conducted on 55 spruce and 5 fir full-length historical piles are presented in Table 5.1 (building year 1727) and Table 5.2 (1886 and 1922). The 5 fir piles were all driven in 1886. Spruce piles were driven in 1727, 1886, and 1922.

$E_{c,0,dyn,wet}$ of piles from 1727 was in some cases very low, related to large amount of decay within the pile. This topic is discussed in Paragraph 5.5.

Table 5.1: Preliminary material properties of full-length historical spruce piles from 1727 retrieved from bridge 30 (BRU0030) and bridge 41 (BRU0041) in Amsterdam.

File ID	species	year	L (mm)	D_{head} (mm)	D_{tip} (mm)	D_{avg} (mm)	Taper (mm/m)	ρ_{wet} (kg/m ³)	$E_{c,0,dyn,wet}$ (MPa)
BRU0030 PL1 P1.6	spruce	1727	9940	181	115	157	6.7	760	8800
BRU0030 PL1 P2.13	spruce	1727	10400	181	111	153	6.7	815	10500
BRU0030 PL2 P2.19	spruce	1727	9470	202	123	170	8.4	920	7000
BRU0030 PL2 P2.21	spruce	1727	10031	212	102	173	10.9	775	5900
BRU0030 PL1 P2.9	spruce	1727	11700	150	92	138	4.9	1020	4400
BRU0030 PL2 P1.18	spruce	1727	14600	185	121	158	4.4	820	4600
BRU0030 PL1 P2.7	spruce	1727	9760	204	108	162	9.8	920	6100
BRU0030 PL1 P1.9	spruce	1727	9460	210	100	150	11.8	890	4800
BRU0030 PL1 P1.10	spruce	1727	10110	220	156	190	6.3	865	8200
BRU0030 PL2 P2.22	spruce	1727	12003	196	169	185	2.3	885	7700
BRU0030 PL2 P1.17	spruce	1727	12000	185	80	145	9.0	880	6400
BRU0030 PL1 P1.7	spruce	1727	9760	196	92	148	10.6	945	6400
BRU0030 PL1 P1.13	spruce	1727	9460	181	124	159	6.1	800	3600
BRU0030 PL1 P2.10	spruce	1727	10110	181	92	144	8.8	860	7500
BRU0030 PL2 P2.25	spruce	1727	10012	140	98	135	4.2	800	5600
BRU0041-PL1-P1.5	spruce	1727	11800	277	127	195	12.7	980	8100
BRU0041-PL1-P1.6	spruce	1727	9200	274	156	217	12.8	675	7800
BRU0041-PL1-P1.8	spruce	1727	10200	245	130	190	11.3	-	-
BRU0041-PL1-P1.10	spruce	1727	10540	236	146	205	8.5	880	4500
BRU0041-PL1-P1.11	spruce	1727	11100	293	156	235	12.3	880	4200
BRU0041-PL1-P1.12	spruce	1727	11340	277	159	224	10.4	795	4700
BRU0041-PL1-P1.13	spruce	1727	11500	274	115	199	13.8	795	4400
BRU0041-PL1-P1.14	spruce	1727	9800	242	150	201	9.4	755	-
BRU0041-PL2-P1.28	spruce	1727	11150	271	201	243	6.3	700	8400
BRU0041-PL2-P1.29	spruce	1727	11160	229	162	208	6.0	705	7100
BRU0041-PL2-P1.30	spruce	1727	11050	245	140	205	9.5	860	9000
BRU0041-PL2-P1.31	spruce	1727	9650	232	142	224	9.4	690	3200
BRU0041-PL2-P1.32	spruce	1727	11200	229	118	185	9.9	710	8700
BRU0041-PL2-P1.33	spruce	1727	11380	216	137	188	7.0	870	5700
BRU0041-PL2-P1.37	spruce	1727	11320	220	162	205	5.1	860	9400

Experimental results of historical wooden foundation piles

Table 5.2: Preliminary material properties of full-length historical spruce and fir piles from 1886 and 1922 retrieved from bridge 30 (BRU0030) and bridge 41 (BRU0041) in Amsterdam.

File ID	species	year	L (mm)	D_{head} (mm)	D_{tip} (mm)	D_{avg} (mm)	Taper (mm/m)	ρ_{wet} (kg/m ³)	$E_{c,0,dyn,wet}$ (MPa)
BRU0030 PL1 P3.2	fir	1886	11270	255	175	221	7.1	870	10100
BRU0030 PL1 P1.20	spruce	1886	10580	229	181	212	4.5	665	13800
BRU0041 PL2 P1.24	fir	1886	13580	242	146	197	7.0	680	10100
BRU0041 PL2 P1.25	spruce	1886	12560	236	143	200	7.3	660	8900
BRU0030 PL1 P1.1	fir	1886	9760	248	166	216	8.5	760	16500
BRU0030 PL1 P5.1	spruce	1886	9460	255	172	225	8.7	910	11600
BRU0030 PL1 P1.2	fir	1886	10110	239	206	230	3.3	700	9200
BRU0030 PL1 P1.19	spruce	1886	10012	236	185	214	5.1	700	10400
BRU0030 PL1 P1.17	spruce	1886	11700	261	166	219	8.2	740	8900
BRU0030 PL1 P3.18	spruce	1886	10012	244	175	212	6.8	650	11600
BRU0030 PL2 P1.13	spruce	1886	14600	255	204	236	3.5	660	9400
BRU0030 PL1 P3.14	spruce	1886	14030	253	162	210	6.5	720	8200
BRU0030 PL2 P1.30	spruce	1886	13650	251	204	230	3.5	845	11500
BRU0030 PL1 P3.1	spruce	1886	11700	245	169	215	6.5	650	11600
BRU0030 PL2 P5.30	spruce	1886	14600	271	181	231	6.1	740	10200
BRU0041 PL1 P1.17	fir	1886	14030	258	120	202	10.0	800	13500
BRU0041 PL1 P1.33	spruce	1922	13460	271	172	236	7.3	620	11600
BRU0041 PL1 P3.36	spruce	1922	13270	251	162	208	6.7	655	9800
BRU0041 PL2 P3.12	spruce	1922	11960	242	169	213	6.1	700	7500
BRU0041 PL2 P1.9	spruce	1922	11420	261	156	226	9.2	695	11200
BRU0041 PL1 P1.23	spruce	1922	14030	271	166	236	7.5	610	10900
BRU0041 PL1 P3.24	spruce	1922	12003	271	207	244	5.3	570	10700
BRU0041 PL1 P1.29	spruce	1922	13650	261	172	228	6.5	560	9600
BRU0041 PL1 P5.41	spruce	1922	12000	267	150	228	9.8	600	12900
BRU0041 PL2 P1.13	spruce	1922	12330	271	181	232	7.2	640	10900
BRU0041 PL1 P1.21	spruce	1922	12003	248	175	216	6.1	660	13100
BRU0041 PL1 P1.39	spruce	1922	13650	255	146	216	7.9	505	11000
BRU0041 PL2 P1.1	spruce	1922	12000	239	188	217	4.2	690	11000
BRU0041 PL2 P1.3	spruce	1922	12330	251	159	217	7.5	725	8900
BRU0041 PL2 P3.2	spruce	1922	12100	239	175	210	5.3	645	11700

5.2.2 Compression test results of pile segments from different historical periods

The results of large-scale mechanical testing are presented in Table 5.3, including a total of 201 pile segments extracted from 60 full-length spruce and fir piles, subdivided in head, middle-part, and tip. No significant difference in the mechanical properties was found between the building year 1922 and 1886, and between head and middle-part of spruce

and fir piles from 1922, 1886, and 1727 (See statistics in Appendix C3). This can be observed in the distribution of the data for $f_{c,0,wet}$ and $E_{c,0,wet}$ in Figure 5.1, as well as in Figure 5.2, where the piles from 1886/1992 are grouped together. Piles from 1727 are clearly distinguished from 1886 and 1992, exhibiting significantly lower $f_{c,0,wet}$ and $E_{c,0,wet}$. The head and middle-part of the piles exhibited no significant difference in terms of $f_{c,0,wet}$ and $E_{c,0,wet}$ (Table 5.3), while for tips a significant difference was measured (Appendix C3).

The box plot in Figure 5.3 shows the distribution of the data for head, middle-part, and tip. The results in Table 5.3 showed that the remaining $f_{c,0,wet}$ of wooden piles that have been in service for a long time was lower than that provided for “new” spruce, determined in Chapter 4.2, and lower than $f_{c,0,wet}$ determined for spruce in literature ($f_{c,0,wet,mean} = 20 \pm 2.2$ MPa, Van de Kuilen 1994 [33]). The lower remaining $f_{c,0,wet}$ is attributable to the presence of decay in the piles, which is discussed in Paragraph 5.5.

Pile segments from 1727 had large average moisture contents (up to 200%), low densities ρ_{12} (360-380 kg/m³) and mechanical properties. Thus, compared to reference values for “new” spruce piles (Table 5.3), the piles from 1727 exhibited more than twice the moisture content and only half of the remaining $f_{c,0,wet}$ and $E_{c,0,wet}$. The piles from 1886 and 1922 had approximately 10-15% lower $f_{c,0,wet}$ compared to “new” spruce piles in Table 5.3. This difference could be related to the physical properties of the piles, natural variability of the mechanical properties, or the possible presence of decay. These aspects are further elaborated in Section 5.2.3 and Paragraph 5.5.

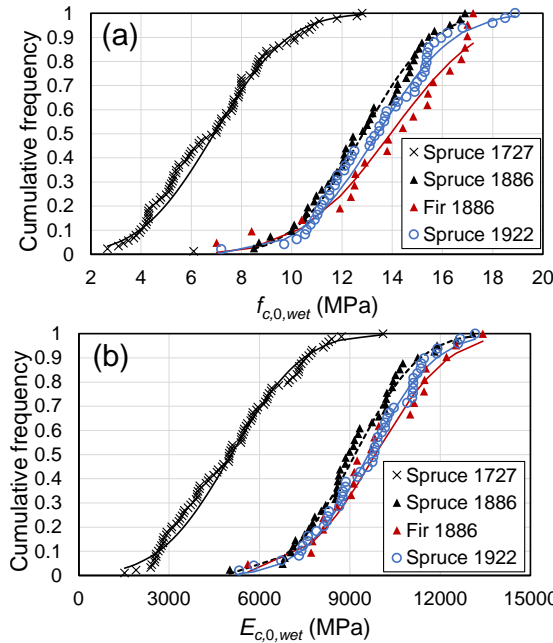


Figure 5.1: Cumulative distributions of $f_{c,0,wet}$ (a) and $E_{c,0,wet}$ (b) for spruce and fir pile segments from 1727, 1886 and 1922 tested according to EN 408 (2010) in wet status ($MC_{mean} > 70\%$). The lines show the normal distribution fitted to the data.

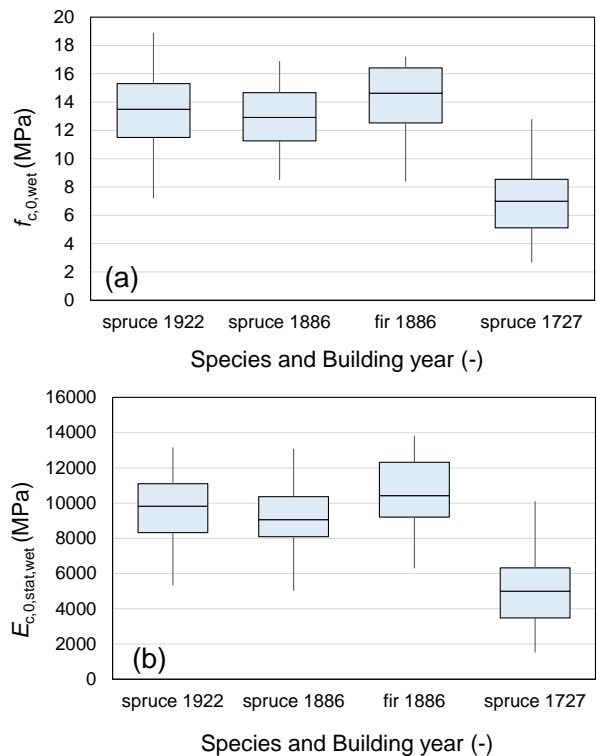


Figure 5.2: Box plots with data distribution for (a) $f_{c,0,wet}$ and (b) $E_{c,0,stat,wet}$ of spruce and fir pile segments divided in 3 building years (1922, 1886, 1727).

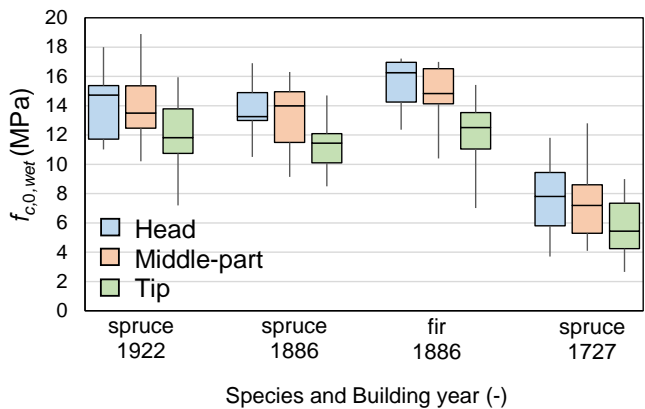


Figure 5.3: Box plot with data distribution of $f_{c,0,wet}$ of head, middle-part and tip of spruce and fir pile segments divided in 3 building years (1922, 1886, 1727).

5.2 Results of material and mechanical characterization of historic spruce and fir piles

Table 5.3: Results for spruce and fir pile segments tested in compression parallel to the fiber in water saturated state according to EN 408. Mean values and standard deviation (SD) are reported.

Wood species	Building year	Part (No. segments)	$f_{c,0,wet}$ (MPa)		$E_{c,0,wet}$ (MPa)		ρ^{12} (kg/m ³)		D (mm)		MC (%)	
			mean	SD	mean	SD	mean	SD	mean	SD	mean	SD
Spruce	"New piles" (Van de Kuilen 1994)	- (57)	20.0	2.2	-	-	-	-	142	12	115	28
		Head/Middle (81)	16.8	2.2	10500	1400	485	44	240	20	85	15
	(Section 4.2.2)	Tip (51)	14.4	2.1	8800	1500	465	39	180	15	85	15
		Head/Middle (59)	13.8	2.1	9900	1580	480	42	240	18	80	21
	1922/1886	Tip (32)	11.8	2.1	8400	1610	450	48	190	15	95	24
		Head/Middle (60)	7.5	2.4	5500	1890	380	54	200	34	160	48
	1727	Tip (30)	5.8	1.8	4200	1590	360	47	150	27	195	54
		Head/Middle (13)	15.1	2.1	11100	1770	490	43	220	30	100	24
Fir	1886	Tip (7)	12.0	3.0	9500	2420	460	70	160	29	100	19

5.2.3 Results from the characterization of the material properties of the historical piles

The material properties of the historical pile segments are presented in Table 5.4, characterized according to Section 3.5, in order to find their correlations with their remaining short-term compressive strength.

The results in Table 5.4 showed no significant difference between spruce piles from 1922 and 1886, which were grouped in one category (See statistics in Appendix C3).

The spruce piles from 1727 were 10-15 years younger but resulted in similar RoG, due to average smaller diameters compared to piles from 1922 and 1886. Spruce piles from 1727 exhibited larger KRs, possibly associated with their smaller diameters, which could influence the remaining short-term compressive strength.

For all piles, the proportions of area (%) of sapwood (SW), heartwood (HW), and juvenile wood (JW), were calculated according to Section 3.12.1.

The values refer to the total cross-sectional area of the pile. The results showed that:

- The percentage of SW area slightly increases from head to tip, especially in spruce and fir piles from 1922/1886.

- The heartwood area increases from tip to head.
- Juvenile wood area decreases to from pile tip to head.
- The average portion of juvenile wood in the tips reaches approximately 85-95% of the heartwood.

Since juvenile wood features lower density (See Section 2.4), this can explain the lower ρ_{12} of the tips, which present a large portion of JW in their cross section, and the consequent lower strength properties associated with it. However, for piles from 1727, the significantly lower density was possibly caused by a large amount of decay (Section 5.5).

Table 5.4. Physical properties of head, middle-part and tip spruce and fir piles. The Area (%) of sapwood (SW), heartwood (HW) and juvenile wood (JW) refers to the total cross-sectional area of the pile.

Wood species	Building year	Part (No. segments)	Diameter (mm)		Age (year)		RoG (mm/year)		KR (-)		ρ_{12} (kg/m ³)		SW Area (%)		HW Area (%)		JW Area (%)	
			mean	SD	mean	SD	mean	SD	mean	SD	mean	SD	mean	SD	mean	SD	mean	SD
Spruce	1922/ 1886	Head (29)	249	15	68	16	1.7	0.4	0.11	0.07	475	38	65	8	35	8	13	5
		Middle (30)	226	13	58	16	1.8	0.5	0.16	0.06	465	44	69	7	31	7	15	3
		Tip (32)	193	15	45	13	2.0	0.7	0.26	0.09	450	48	74	5	26	5	22	2
	1727	Head (30)	212	33	55	11	1.7	0.5	0.20	0.1	385	50	71	5	29	5	15	3
		Middle (30)	189	31	45	10	1.9	0.6	0.28	0.1	375	55	74	4	26	4	20	3
		Tip (30)	150	27	38	10	1.8	0.7	0.36	0.1	360	47	75	3	25	3	23	2
Fir	1886	Head (6)	235	30	72	19	1.5	0.4	0.09	0.04	500	44	63	9	37	9	12	3
		Middle (7)	208	25	57	16	1.6	0.4	0.16	0.07	485	38	69	7	31	7	16	5
		Tip (7)	162	29	46	11	1.5	0.3	0.28	0.1	460	70	72	4	28	4	22	5

5.2.4 Relationship among the mechanical properties

The remaining short-term $f_{c,0,wet}$ for all the categories of tested piles was correlated to the density adjusted to MC = 12% (ρ_{12}). Both $f_{c,0,wet}$ and ρ_{12} (Figure 5.4a), and $E_{c,0,wet}$ and ρ_{12} (Figure 5.4b) were strongly correlated.

In spruce piles from 1727, ρ_{12} was significantly lower compared to 1922/1886, possibly due to large decay (See paragraph 5.5). The strong correlation between $f_{c,0,wet}$ and $E_{c,0,wet}$ (Figure 5.5a), indicates that the stiffness is a good indicator for the remaining short-term compressive strength.

A very similar correlation was also found between $f_{c,0,wet}$ and $E_{c,0,wet,dyn}$ (Figure 5.5b), determined through frequency response measurements. This suggests that frequency response measurements can be used to estimate the modulus of elasticity of historical timber piles efficiently.

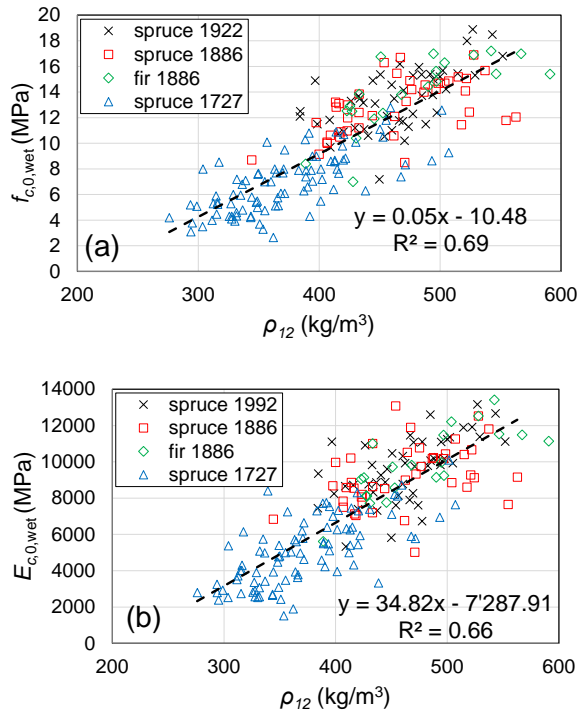


Figure 5.4: Relationship between (a) $f_{c,0,wet}$ and density ρ_{12} ; (b) $E_{c,0,wet}$ and density ρ_{12} for all the categories of tested pile segments.

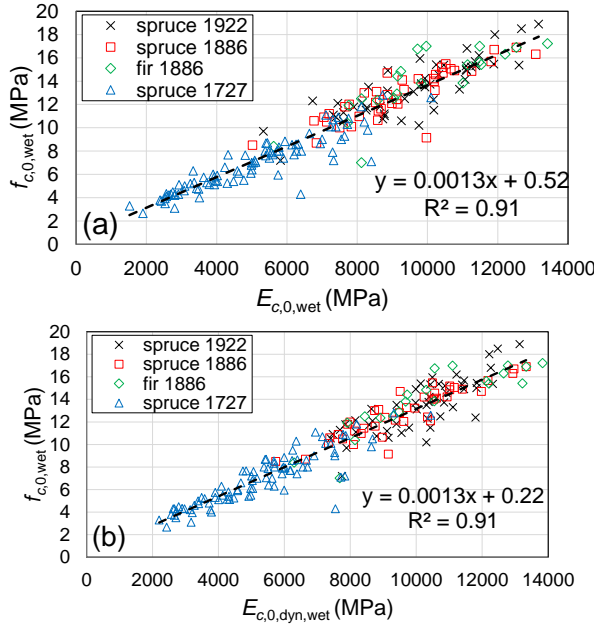


Figure 5.5: Relationship between (a) $f_{c,0,wet}$ and $E_{c,0,wet}$; (b) $f_{c,0,wet}$ and $E_{c,0,dyn,wet}$ for all the categories of tested pile segments.

5.2.5 Correlation analysis between the remaining short-term compressive strength and material properties

The correlation analysis was conducted for all the material and mechanical properties at the test moisture content ($MC > 70\%$), well above fiber saturation, determined according to Paragraph 3.5 and 3.6. This was done to analyse the parameters that have a significant influence on the remaining short-term $f_{c,0,wet}$ of the pile. The correlation matrixes were presented for spruce piles from 1727 (Table 5.5), 1886 (Table 5.6), and 1922 (Table 5.7), and for fir piles from 1886 (Table 5.8).

The remaining $f_{c,0,wet}$ of all the spruce and fir piles exhibited a strong correlation with ρ_{12} , $E_{c,0,wet}$ and $E_{c,0,dyn,wet}$ as presented in Paragraph 5.2.4. In addition, a strong correlation was found between $f_{c,0,wet}$ and MC in spruce piles from 1727, slowly decreasing in more recent piles from 1886 and 1922, where a moderate correlation was found. $f_{c,0,wet}$ of fir piles from 1886 was weakly correlated with MC. This suggests that high moisture contents were associated with the oldest piles, possibly due to a large amount of decay (Section 5.6)

Diameter (D), KR, and RoG, showed weak correlations with $f_{c,0,wet}$ in spruce piles from 1727, while Age showed a moderate correlation with $f_{c,0,wet}$. In spruce piles from 1886, $f_{c,0,wet}$ was strongly correlated with the Age, and moderately correlated with D , KR, and RoG. In more recent spruce piles from 1922, the correlation between these four growth characteristics and $f_{c,0,wet}$ does not follow the same trend for 1886, where $f_{c,0,wet}$ was weakly correlated with Age and RoG, and moderately with KR and D . Finally, in fir piles from 1886, $f_{c,0,wet}$ exhibited a strong correlation with KR and D , and a weak correlation with Age

Experimental results of historical wooden foundation piles

and RoG. However, the analysis comprised only 5 fir piles from 1886. More data is needed to make a solid correlation analysis for this category.

These correlations will be further discussed in Section 5.5, where the remaining short-term $f_{c,0,wet}$ of the piles is studied in relation to the amount of decay and its effect on the material properties of the piles.

Table 5.5. Correlation matrix for spruce piles from 1727

	$f_{c,0,wet}$	$E_{c,0,wet}$	$E_{c,0,dyn,wet}$	D	ρ_{12}	MC	KR	RoG	Age
$f_{c,0,wet}$	1								
$E_{c,0,wet}$	0.91	1							
$E_{c,0,dyn,wet}$	0.89	0.98	1						
D	0.26	0.25	0.21	1					
ρ_{12}	0.71	0.69	0.70	0.01	1				
MC	-0.69	-0.66	-0.66	-0.25	-0.74	1			
KR	-0.17	-0.14	-0.12	-0.78	-0.05	0.15	1		
RoG	-0.33	-0.28	-0.27	0.46	-0.32	0.09	-0.40	1	
Age	0.51	0.45	0.41	0.18	0.29	-0.18	-0.15	-0.72	1

Table 5.6. Correlation matrix for spruce piles from 1886

	$f_{c,0,wet}$	$E_{c,0,wet}$	$E_{c,0,dyn,wet}$	D	ρ_{12}	MC	KR	RoG	Age
$f_{c,0,wet}$	1								
$E_{c,0,wet}$	0.87	1							
$E_{c,0,dyn,wet}$	0.91	0.96	1						
D	0.38	0.24	0.17	1					
ρ_{12}	0.56	0.42	0.51	0.04	1				
MC	-0.62	-0.47	-0.54	-0.12	-0.64	1			
KR	-0.54	-0.45	-0.40	-0.67	-0.18	0.25	1		
RoG	-0.48	-0.39	-0.40	-0.12	-0.56	0.51	0.22	1	
Age	0.68	0.53	0.54	0.46	0.58	-0.53	-0.50	-0.85	1

Table 5.7. Correlation matrix for spruce piles from 1922

	$f_{c,0,wet}$	$E_{c,0,wet}$	$E_{c,0,dyn,wet}$	D	ρ_{12}	MC	KR	RoG	Age
$f_{c,0,wet}$	1								
$E_{c,0,wet}$	0.84	1							
$E_{c,0,dyn,wet}$	0.81	0.89	1						
D	0.42	0.48	0.46	1					
ρ_{12}	0.61	0.60	0.57	0.23	1				
MC	-0.57	-0.60	-0.71	-0.49	-0.63	1			
KR	-0.51	-0.53	-0.57	-0.73	-0.24	0.43	1		
RoG	-0.21	-0.19	-0.09	-0.35	-0.26	0.27	0.02	1	
Age	0.36	0.35	0.25	0.66	0.26	-0.33	-0.34	-0.87	1

Table 5.8. Correlation matrix for fir piles from 1886

	$f_{c,0,wet}$	$E_{c,0,wet}$	$E_{c,0,dyn,wet}$	D	ρ_{12}	MC	KR	RoG	Age
$f_{c,0,wet}$	1								
$E_{c,0,wet}$	0.82	1							
$E_{c,0,dyn,wet}$	0.88	0.97	1						
D	0.71	0.60	0.60	1					
ρ_{12}	0.74	0.78	0.86	0.41	1				
MC	-0.25	-0.55	-0.54	-0.17	-0.62	1			
KR	-0.78	-0.60	-0.60	-0.77	-0.34	0.14	1		
RoG	0.34	0.13	0.25	0.15	0.26	0.16	-0.10	1	
Age	0.27	0.35	0.27	0.63	0.12	-0.25	-0.50	-0.66	1

5.3 Decay assessment with micro-drilling approach

In this paragraph, the micro-drilling approach is presented. The procedure for the determination of the “soft shell” (the degraded outer portion of the cross section) with micro-drilling is explained in Paragraph 5.3.1. The approach is calibrated and validated in Paragraph 5.3.2 and Paragraph 5.3.3, respectively.

5.3.1 Determination of the soft shell and relative zero-strength zones

For each tested segment, the lengths of zones 1, 2, 3, and 4 on both sides of the micro-drilling signal were determined. The representation of the zones and the micro-drilling signal is showcased in Figure 5.6.

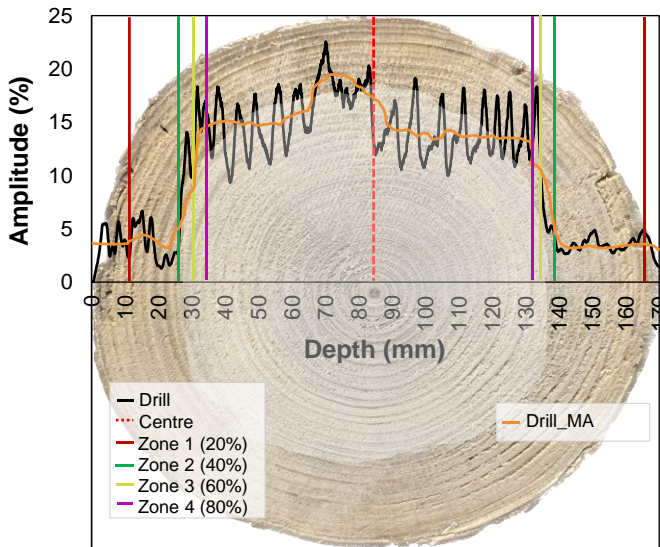


Figure 5.6: Example of calculation of zone 1-2-3-4 for a spruce pile from 1727.

After this, the sound short-term compressive strength ($f_{c,0,wet,sound}$) was determined from 62 spruce and fir pile segments with a cross-sectional area (A_{sound}) between 95-100% of the full cross-sectional area (A_{tot}). This means that the sum of zones 1+2+3 of both sides of the

micro-drilling signal was less than 5% of the diameter of the pile (exemplified in Figure 5.7). The values of $f_{c,0,wet,sound}$ of these piles were taken as a reference for sound material.

The average values of $f_{c,0,wet,sound}$ of the 62 segments are shown in Table 5.9 for head, middle-part and tip. No significant difference was found between 1922 and 1886 (Appendix C3).

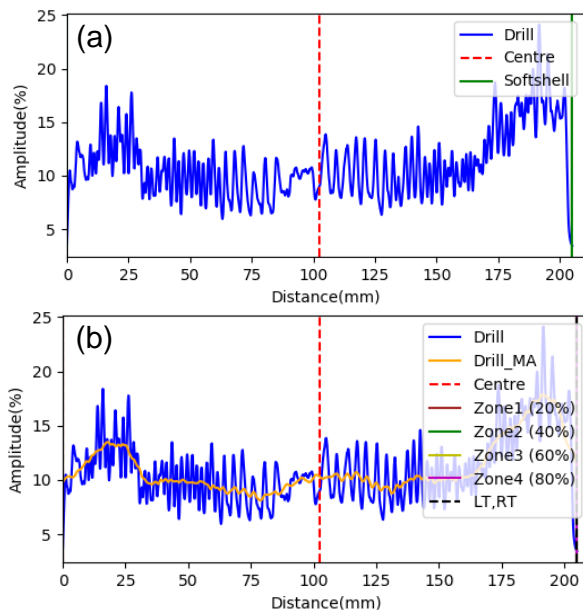


Figure 5.7: Example of sound spruce pile from 1922, where the zones 1-2-3 of both sides of the signal are less than 5% of the diameter of the pile. In this case, 100% of the cross section is sound.

Table 5.9. Reference for short-term sound compressive strength $f_{c,0,wet,sound}$ for 62 sound piles from 1922/1886.

Material status	Building year	Part (No. segments)	$f_{c,0,wet,sound}$ (MPa)	
			mean	SD
Sound ($A_{sound} > 95\%$)	1922/1886	Segments head (21)	15.4	1.5
		Segments middle (30)	14.9	2.2
		Segments tip (11)	13.7	2.2

The correlation analysis between the maximum force measured with compression tests of the pile segments ($F_{c,0,test}$) and the force ($F_{c,0,mod}$) calculated with Zone 1, Zone 1+2, and Zone 1+2+3 (Section 5.3) of the micro-drilling signal, is shown in Figure 5.8. $F_{c,0,mod}$ was determined with $f_{c,0,wet,sound}$ values in Table 5.9.

Zones 1+2 represented the best correlation in terms of R^2 and slope of the line that is closer to the bisector. Based on this, zones 1+2 of the micro-drilling signal were chosen to determine the soft shell. The approach assumes $f_{c,0,wet} = 0$ MPa in zones 1+2.

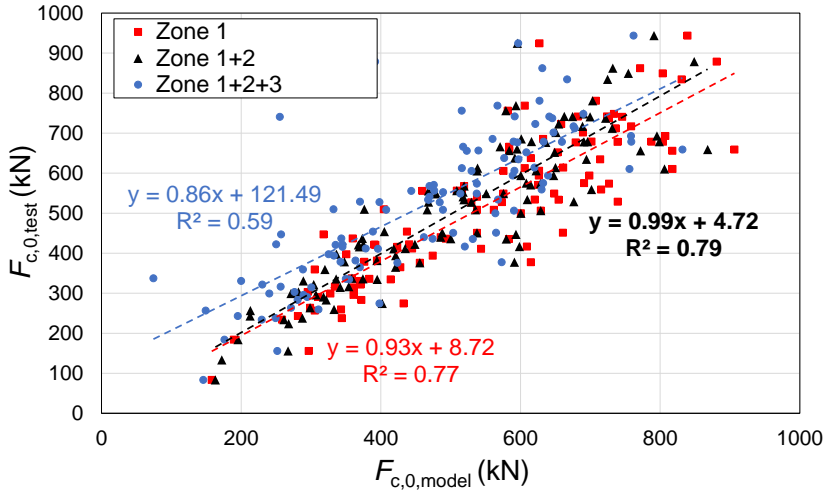


Figure 5.8: Correlation between $F_{c,0,test}$ and $F_{c,0,model}$, calculated with $f_{c,0,sound}$ assuming zero strength associated with zone 1, zone 1+2 and zone 1+2+3 of the micro-drilling signal.

5.3.2 Equivalent sound compressive strength values

The zones 1+2 are now designated as the “soft shell” as shown in Figure 5.9. The mean equivalent sound compressive strength (EQ $f_{c,0,wet,sound}$) related to A_{sound} , assuming zero strength associated with the soft shell, is presented in Table 5.10.

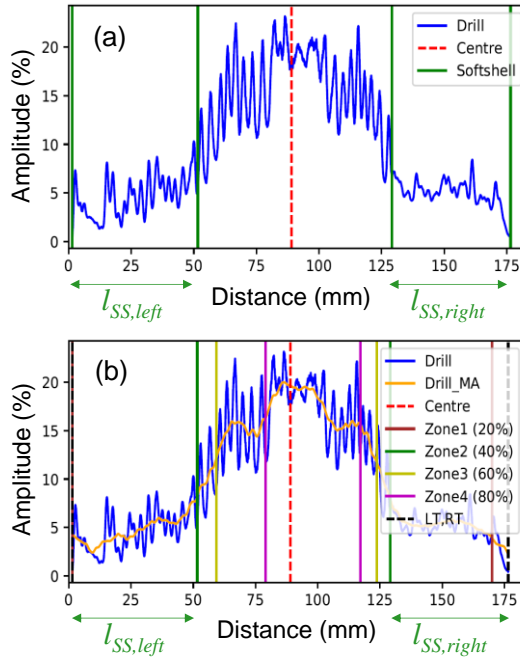


Figure 5.9: Example of estimation of the soft shell length l_{ss} (left and right) of a spruce pile from 1727 with the TU-Delft developed algorithm (Appendix E).

The results show an EQ $f_{c,0,wet,sound}$ for all piles from 1922/1886 in line with the reference $f_{c,0,wet,sound}$ in Table 5.9, and a lower EQ $f_{c,0,wet,sound} = 12.0$ MPa for all segments from 1727. For the segments from 1727, no significant difference was found between head, middle, and tip for the EQ $f_{c,0,wet,sound}$ values.

The lower EQ $f_{c,0,wet,sound}$ of the piles from 1727 compared to piles from 1886/1922, was not attributed to a lower quality of the material since no clear difference in the basic quality of the material was found between year 1727 and 1886/1922 in Section 5.2.3. The difference could be caused by long-term loading effects, since the piles from 1727 were loaded for approximately 300 years in comparison to piles from 1886 (ca. 135 years) and 1922 (ca. 100 years). In this context, the stress level in piles from 1727 could have been potentially higher than for the piles from 1922/1886, since the load was taken up by a smaller remaining sound cross section due to a larger amount of decay in the cross section.

Table 5.10. Equivalent sound compressive strength (EQ $f_{c,0,wet,sound}$) calculated with zone 1+2 for piles from 1922, 1886, and 1727.

Material status	Building year	Part (No. segments)	EQ $f_{c,0,wet,sound}$ (MPa)	
			mean	SD
Sound cross section	1922/1886	Head/Middle (72)	15.0	2.3
		Tip (39)	13.7	2.4
	1727	All segments (90)	12.0	2.8

5.3.3 Validation of the soft shell for all piles based on the equivalent sound compressive strength

The applicability of the presented TU-Delft-developed algorithm (appendix E) to determine the zones (and from that a soft shell) of a micro-drilling signal was validated in Figure 5.10.

The good correlation between $F_{c,0,test}$ and $F_{c,0,mod}$ calculated with zone 1+2 of the micro-drilling signal is shown, comprising all the pile segments from 1922, 1886, and 1727. The difference with Figure 5.8, lies in the application of the TU-Delft-developed algorithm to determine the soft shell of all pile segments, including the 62 non-decayed segments from 1922/1886, initially designated as sound (for which no soft shell at all was assumed in the first calibration step).

Furthermore, Figure 5.10 includes the pile segments from 1727, initially not considered in the calibration. However, the allocation of zones 1+2 (calibrated on $f_{c,0,wet,sound}$ of 62 piles from 1886/1922) to the soft shell resulted in a good fitting also for the piles from 1727.

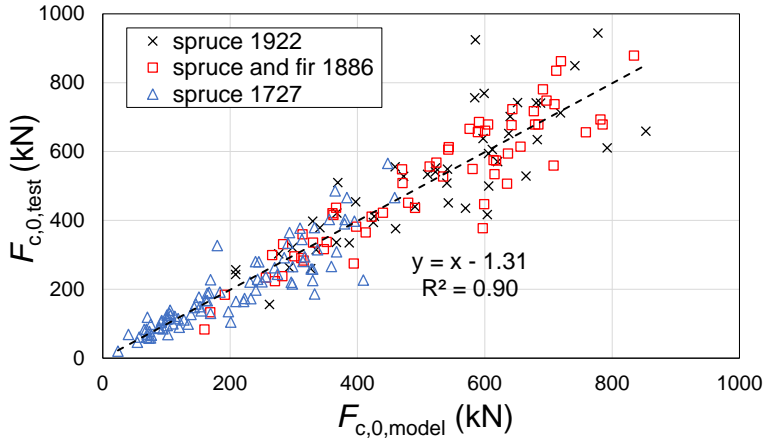


Figure 5.10: Relationship between $F_{c,0,test}$ and $F_{c,0,model}$ calculated from $EQ f_{c,0,sound}$ and A_{sound} based on the soft shell related to zone 1+2 of the micro-drilling signal of pile segments from 1922, 1886, 1727.

5.4 Influence of moisture content on decay assessment with micro-drilling

Micro-drilling was applied to 24 pile segments at different moisture content levels according to Section 3.10 (Special thanks to my colleague Dr. Ing. Michele Mirra for collaborating on this project [31] and for providing the images and research data essential to this study). Representative results from the 240 conducted measurements are shown in Figure 5.11 in terms of micro-drilling signals at different MC levels and time in service. Progressively lower drilling resistance was obtained when MC increased. However, this does not influence the detection of specific features of a pile segment, such as denser sapwood for sound samples (Figure 5.11a), presence of an internal knot (Figure 5.11b), very low drilling amplitude when crossing outer beyond the soft shell length (l_{ss}) for the oldest pile segments (Figure 5.11e).

The soft shell was characterised by much lower drilling resistance compared to the sound part of the pile, independently of the MC. This outcome, visible in Figure 5.11d for sample 1727 1-middle and Figure 5.11e for 1727- 2-head, was also obtained for all other segments from 1727, as shown in Table 5.11, reporting the detected l_{ss} as a function of the global MC of the segments. As observed, the outer degraded portions of the cross section only show small variations for different MC values (in Table 5.11). This very limited scatter is unavoidable, as the micro-drilling measurements were conducted close to each other, but local variations along the drilling depth are very likely to be present. Based on the obtained results, micro-drilling signals can reliably identify decayed portions and their extent along the drilling depth independently of the MC. This outcome is relevant since the determination of the actual MC of a large number of piles on site would not be practically feasible. Furthermore, the distinction between sound and decayed parts of the cross section is also possible when comparing micro-drilling signals with the MC gradients determined in submerged conditions.

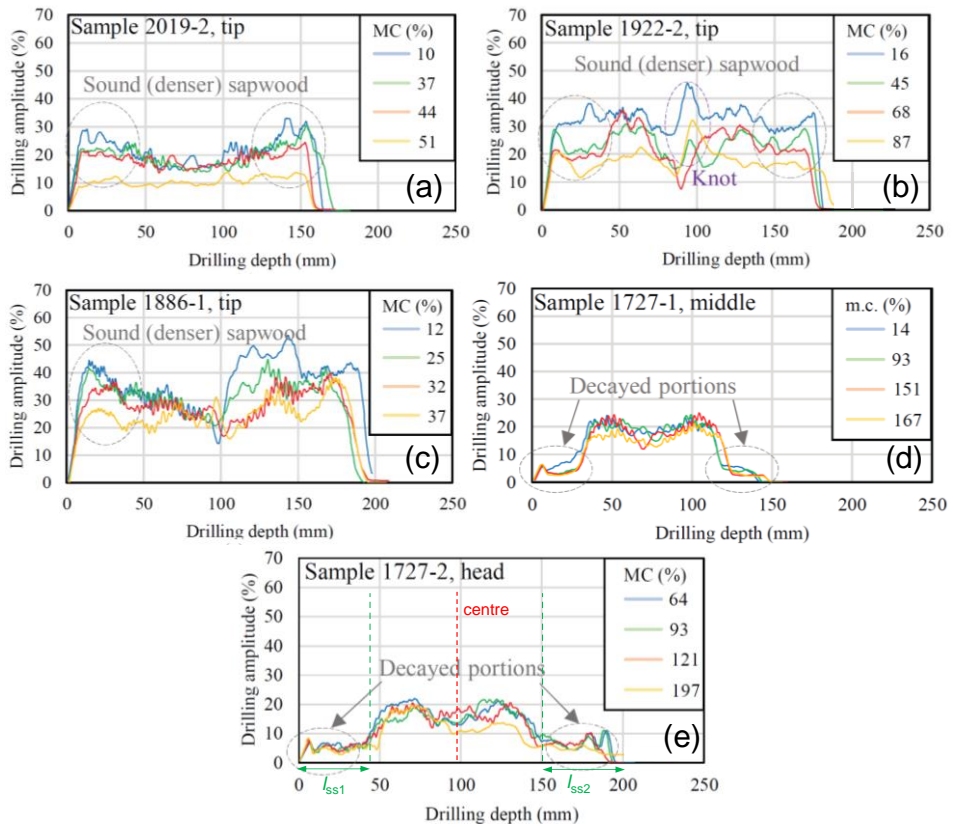


Figure 5.11: Micro-drilling signals (displayed in terms of a 100-mm moving average) ordered from lowest to highest MC for representative pile segments with TS = 2 years (a), 99 years (b), 135 years (c), and 294 years (d-e).

Table 5.11: Overview of the soft shell length (*alss*), determined with micro-drilling as a function of MC for the piles from 1727.

Piles (year and part)	<i>alss</i> (mm)	MC (%)
1727-1-head	12	13
	10	94
	10	129
	9	153
	10	182
1727-1-middle	23	14
	25	93
	24	151
	24	167
	23	170
1727-1-tip	16	13
	17	88
	17	153
	17	188
	16	212
1727-2-head	40	64
	35	93
	36	107
	37	121
	36	197
1727-2-middle	34	105
	33	145
	36	164
	34	179
	35	184
1727-2-tip	24	84
	25	125
	26	139
	22	146
	26	175

The previous results, which referred to the MC of global segments, are also confirmed when analysing local MC gradients along the drilling depth at the cross-sectional level. (Figure 5.13). These MC gradients, determined with the five prisms retrieved from the cross sections of the segments (According to Section 3.10), show a typical profile with larger MCs pertaining to the outer prisms (1 and 5 in Figure 5.13) containing sapwood.

However, for sound cross sections of a pile from 2019 (Figure 5.13a-c) the MCs range of prisms containing sapwood was 70–150%, whereas in decayed samples (Figure 5.13d-e), values up to 350% were determined. On the contrary, when considering MCs of the heartwood and juvenile wood portions, these always fall in the range of 40–60%, also in the case of the decayed samples.

This outcome is confirmed by the micro-drilling signals as well: the drilling resistance in the inner part of the cross section is in all cases close to 20%; for sound sapwood, the larger

amplitude correctly corresponds to its larger density, whereas in the presence of decay, a large drop in the drilling resistance is observed.

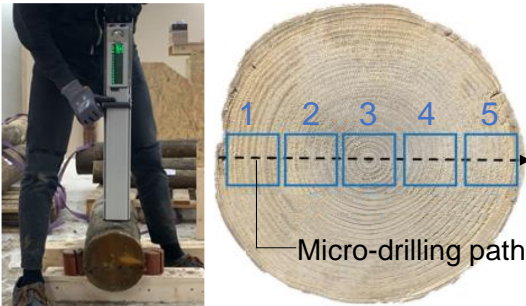
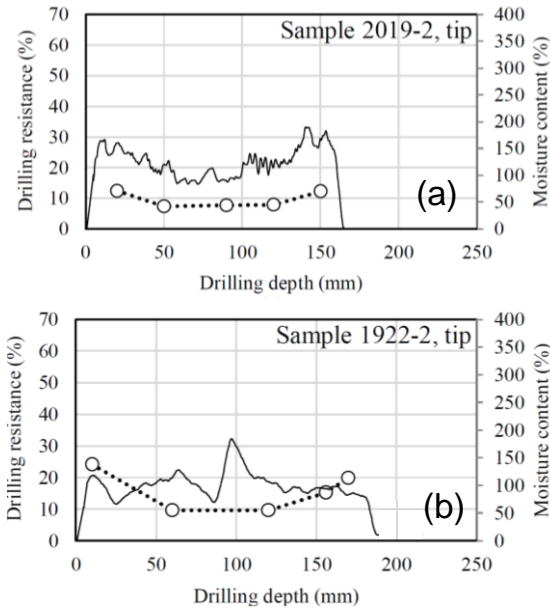


Figure 5.12: Wood prisms 1-5 extracted from the cross-section after micro-drilling.



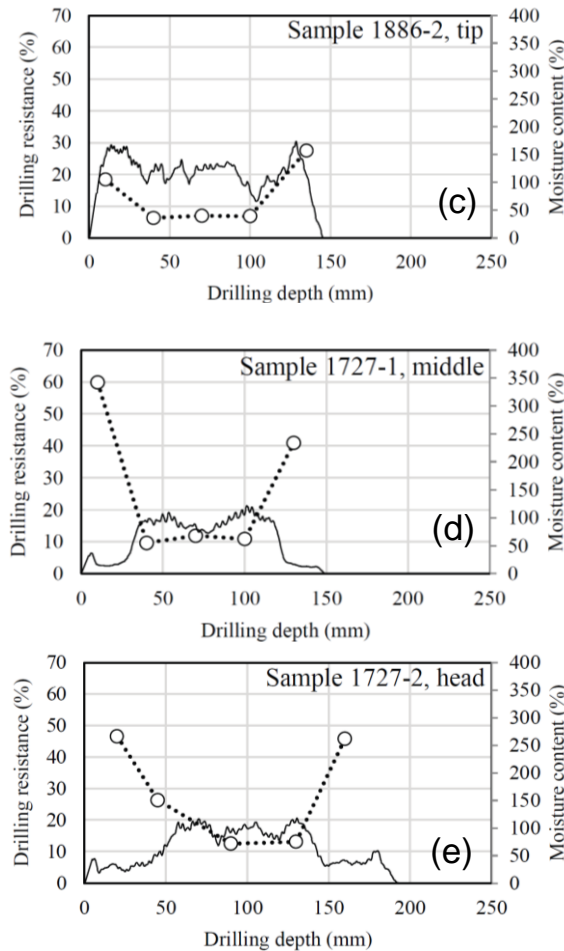


Figure 5.13: Example of drilling resistance profile and MC gradient (dashed) for representative pile segments with time in service = 2 years (a), 99 years (b), 135 years (c), and 294 years (d-e) in submerged conditions. For d-e, very large MC is observable in the decayed portions, which is not the case in sound samples.

5.5 Effect of decay and physical properties on the remaining short-term compressive strength

The average soft shell length (al_{ss}) and the remaining sound cross-sectional area (A_{sound}) are presented for all historical pile segments in Table 5. 12, based on the micro-drilling approach presented in Section 5.3.

A larger amount of decay was determined for piles from 1727 compared to 1886/1922, where al_{ss} ranged at 20-22 mm, with approximately the same soft shell lengths across head, middle and tip of the pile. This highlights that bacterial decay is potentially uniform along the pile length, useful information for the assessment of in-situ historical wooden foundation piles, where micro-drilling can be conducted only on the pile head, which comes out of the soil. To this end, the extension of decay within the cross section in sapwood and heartwood and the degradation pattern along the pile are further discussed in Sections 5.6 and 5.7.

Although al_{ss} resulted to be constant along the piles, the pile geometry is tapered, meaning that the diameter decreases from head to tip, resulting in a lower average A_{sound} in the tips, compared to head and middle-part, for the same values of al_{ss} as shown in Figure 5.14. This is showcased in Table 5. 12, especially in tips from 1727, where A_{sound} values are 15-20 % lower compared to head/middle which exhibit approximately the same A_{sound} . The pile segments from 1922/1886 exhibited a small amount of decay, with al_{ss} below 7 mm, approximately constant along the pile. A_{sound} resulted to be approximately constant in head and middle-part, with a slight decrease in the tips, due to their inherent smaller cross-sectional area. In fir piles the average al_{ss} remains always below 2 mm, indicating a very low amount of decay for this wood species, in line with [145],[14].

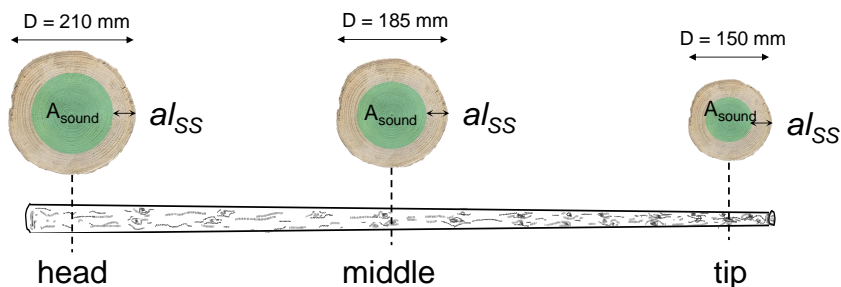


Figure 5.14: A_{sound} decreasing along the pile for the same value of soft shell length al_{ss} in head, middle-part and tip.

The larger amount of decay (higher al_{ss} values) found in piles from 1727, had a significant effect on the remaining $f_{c,0,wet}$, highlighted by a strong correlation between al_{ss} and $f_{c,0,wet}$ represented in Figure 5.15. Decay also had a direct effect on the density (ρ_{12}) and MC, since when bacterial decay progresses to the extent that most of the cell walls are eroded, a strong reduction of density and compressive strength occurs, linked to an increase in moisture content as well (as explained in Section 2.6). This was confirmed by the strong correlation between $f_{c,0,wet}$, ρ_{12} and MC of piles from 1727 in Table 5.5. However, the

5.5 Effect of decay and physical properties on the remaining short-term compressive strength

remaining $f_{c,0,wet}$ in piles from 1727 was poorly correlated with their growth characteristics (KR, RoG, Age, and diameter), possibly due to the large amount of decay. On the other hand, piles from 1886/1922 exhibited a moderate/low correlation with $alss$, and a moderate/good correlation with the most relevant growth characteristics.

The remaining short-term compressive strength resulted to be well correlated with A_{sound} (Figure 5.16), especially for the piles from 1727, which exhibit a large range of A_{sound} roughly between 25% and 85% of the full cross-sectional area. Figure 5.16 highlighted the presence of bacterial decay also in piles from 1922/1886; however, limited to a lower range $65\% < A_{sound} < 100\%$ of the full cross-sectional area.

The remaining short-term strength of a pile can be estimated with Equation 5.1, from the average reference $f_{c,0,wet,sound} = 14.74$ MPa (see Figure 5.16), and the A_{sound} (%), determined with micro-drilling. This experimental equation is based only on micro-drilling measurements and pile diameter, in order to determine A_{sound} . This gives the possibility to have a direct estimation of the remaining short-term compressive strength directly from the micro-drilling.

$$f_{c,0,wet} = 14.74 e^{0.0182 (A_{sound}-100)} \quad (5.1)$$

Table 5. 12. Remaining short-term strength properties in relation to ρ_{12} , A_{sound} and the percentage of decayed sapwood.

Wood species	Building year	Part (No. segments)	$f_{c,0,wet}$ (MPa)		EQ $f_{c,0,wet,sound}$ (MPa)		ρ_{12} (kg/m ³)		A_{sound} (%)		$alss$ (mm)	
			mean	SD	mean	SD	mean	SD	mean	SD	mean	SD
Spruce	"New" piles (Section 4.2.2)	Head/ Middle (81)	16.8	2.2	-	-	485	45	100	-	0	-
		Tip (51)	14.4	2.1	-	-	470	40	100	-	0	-
	1922/ 1886	Head (29)	13.9	2.0	15.3	2.5	465	42	91	8	6	5
		Middle (30)	13.7	2.3	14.7	2.3	470	45	94	7	4	4
		Tip (32)	11.8	2.1	13.7	2.4	450	48	87	10	7	5
	1727	Head (30)	7.5	2.3	12.2	3.3	385	55	63	14	22	11
		Middle (30)	7.3	2.4	12.3	2.9	375	48	62	20	20	11
		Tip (30)	5.8	1.8	11.6	2.4	360	47	50	15	22	9
	Fir	Head (6)	15.2	2.0	16.0	1.8	495	34	97	4	2	2
		Middle (7)	14.8	2.3	15.2	1.7	485	48	97	6	1	3
		Tip (7)	12.0	3.0	12.5	2.8	460	70	96	7	2	3

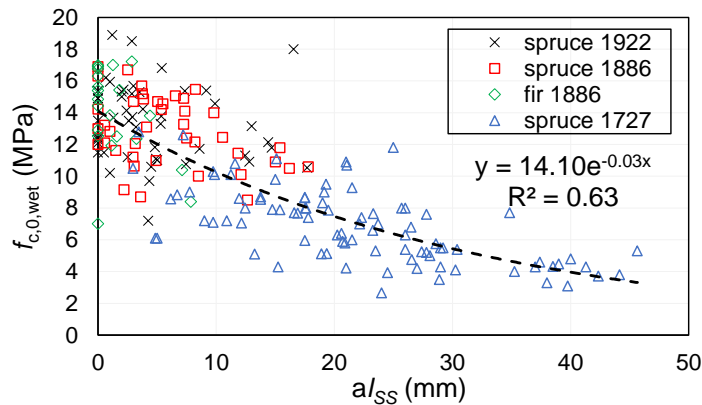


Figure 5.15: Relationship between $f_{c,0,wet}$ and average soft shell length ($a/_{ss}$) of all the historical timber piles

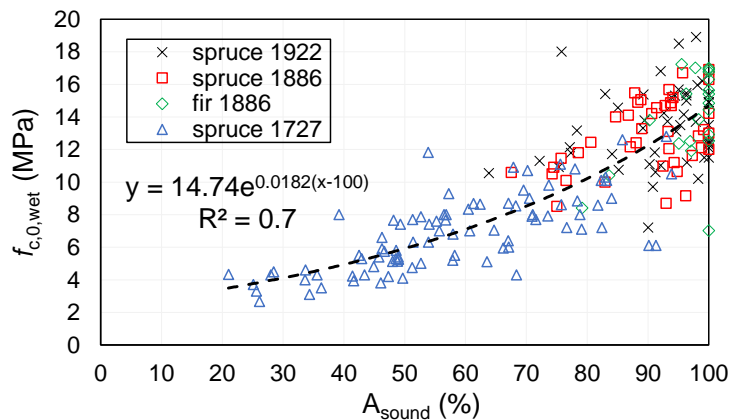


Figure 5.16: Relationship between $f_{c,0,wet}$ and the percentage of sound cross-sectional area A_{sound} of all the historical timber piles

5.6 Effect of decay on the material properties within the cross section

To comprehensively assess the impact of bacterial decay on the material properties of the piles, the properties of small-scale prismatic samples extracted from various locations along the pile cross-section were studied. This analysis was correlated with micro-drilling signals, CT scanning, and light microscopy observations.

Special thanks to my colleagues, Dr. Ing. Michele Mirra and Ir. Michael Lee, for their collaboration on this project [184] and for providing the invaluable images and data that significantly contributed to this study.

5.6.1 Material and mechanical properties within the cross section of the pile

The outcomes from the small-scale compression tests on prisms retrieved from the cross sections of the 15 pile segments (according to Section 3.11) belonging to group 1 are reported in Figure 5.17 for samples from 1727, 1886, and 1922, respectively. The graphical distributions of moisture content, dry density, compressive strength, and modulus of elasticity (the latter measured only for the 120-mm-high prisms) are shown in Figure 5.17a-d. The tabular results of the individual tests can be found in Appendix C4.

The results exhibited very small differences (10% on average) in all parameters for the two prism sizes ($40 \times 40 \times 120 \text{ mm}^3$ and $40 \times 40 \times 60 \text{ mm}^3$), suggesting that the size effect did not influence the results.

These findings indicate the presence of decay for all segments from 1727, even though limited to the outer prisms (1 and 5): these show high moisture contents (up to 300%), as well as low dry density, compressive strength ($f_{c,0,wet,prism}$), and modulus of elasticity ($E_{c,0,wet,prism}$), whereas the other prisms (2, 3, 4) show values in line with those from piles 1922/1886. Thus, a drop in load-bearing capacity of the most ancient piles can be expected, because of the poor material and mechanical properties of the outer portion of their cross section, the inner part remaining sound.

However, although biological decay was absent in this inner portion, the presence of mechanical degradation cannot be a priori excluded, given the observable difference in properties between older (1886 and 1727) and more recent segments (1922).

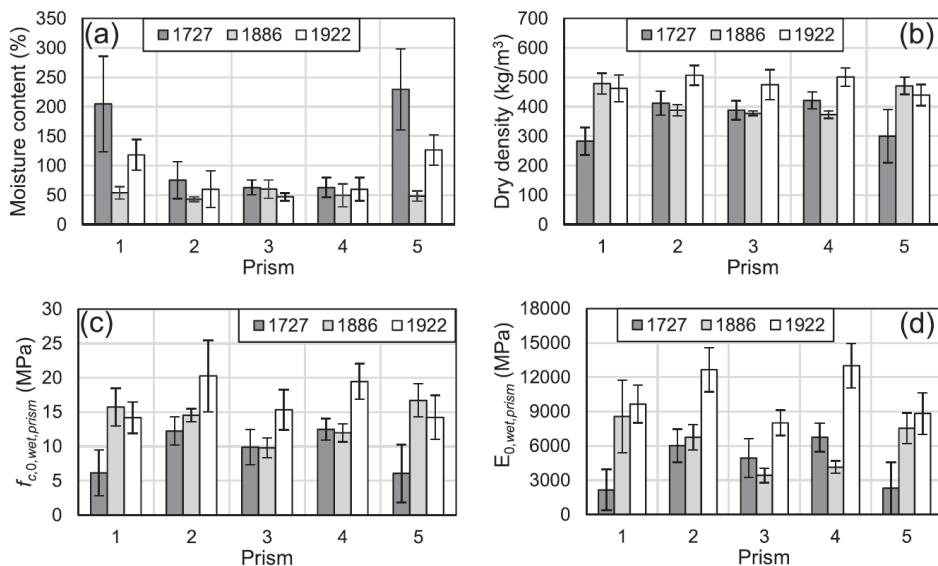


Figure 5.17: Results from the small-scale compression tests on prisms retrieved along the cross sections of pile segments of group 1 (Section 2.2.3): (a) moisture content gradient; (b) dry density distribution; (c) wet compressive strength distribution; (d) wet modulus of elasticity distribution; average values and standard deviations are shown.

5.6.2 Correlations between micro-drilling and material properties of the prisms

The signals from the executed micro-drilling measurements were then compared with the variation of mechanical properties along the cross section of the piles: four representative examples are provided in Figure 5.18 for two decayed and two sound segments.

For the decayed segments from 1727 (Figure 5.18a-b), a comparison is provided between head and tip of the same pile: it is interesting to notice how the micro-drilling signal is able to capture the decrease in mechanical properties within the cross section of the pile tip, mainly due to more extensive bacterial decay in prisms 1 and 5, and larger presence of juvenile wood in prisms 2 and 4, as compared to the head. In general, the drilling resistance profiles provide a reliable representation of the characteristics of the cross section, with the compressive strength of the single prisms following the same pattern as the measured amplitude. In particular, a clear identification of decayed portions was possible, and this was well in line with the results obtained from the tests on the prisms in Paragraph 5.6.1.

The latter statement is also supported by Figure 5.19, showing the correlations between the average drilling amplitude measured within the width of the prisms, and their material and mechanical properties. In general, the low or very low drilling amplitudes found in the outer prisms (1 and 5 in Figure 5.17) are linked to low dry densities, compressive strength, and modulus of elasticity, and to large moisture contents, all features imputable to the effects of bacterial decay in the outer portion of the cross section. It should be noticed that the obtained correlations between the drilling amplitude and the

5.6 Effect of decay on the material properties within the cross section

strength and stiffness of the prismatic samples refer to clear wood, while the compressive failure of full piles may also be influenced by the presence of defects such as knots.

The correlation with the dry density can instead be employed to reconstruct the density profile of a cross section along the drilling depth, and will be therefore validated in the following using the micro-drilling measurements conducted on the segments from group 2 (Paragraph 5.6.2)

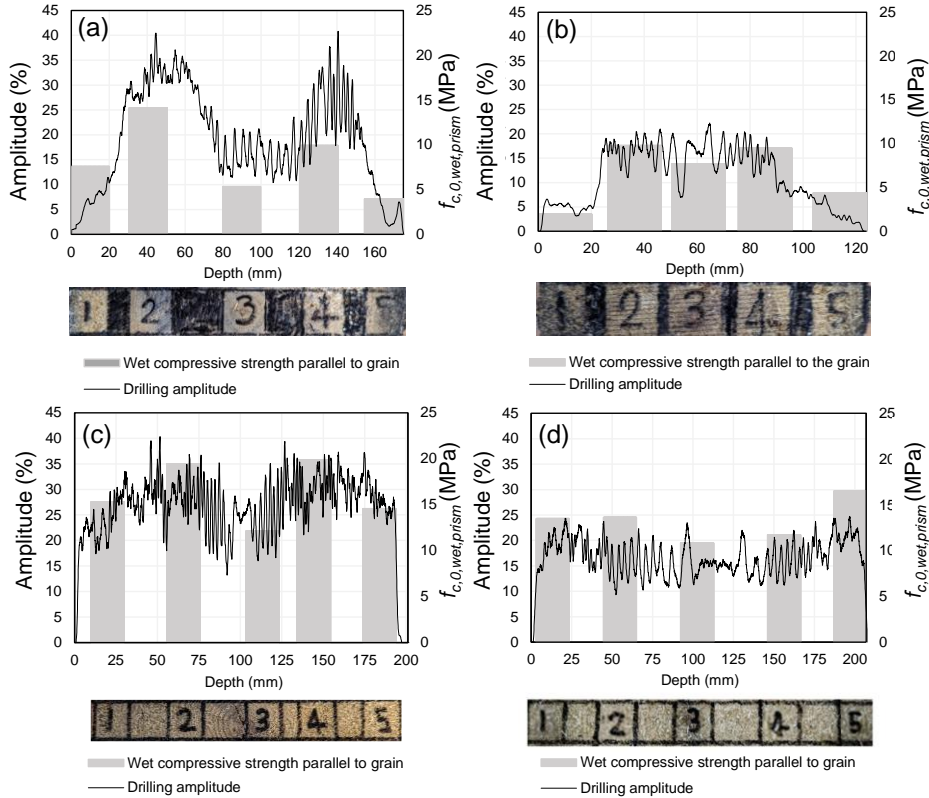


Figure 5.18: Comparison between micro-drilling signals and wet compressive strength profiles of the prisms along the cross section for two representative decayed segments – 1727–1–head (a) and 1727–1–tip (b), and two sound ones – 1922–1–middle (c) and 1886–3–middle (d).

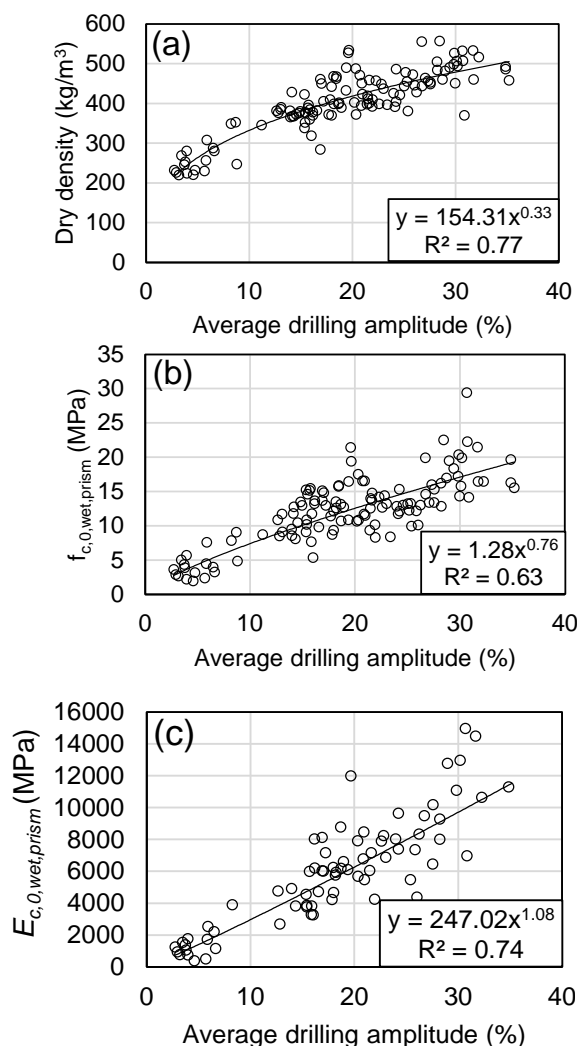


Figure 5.19: Correlations derived from the small-scale tests on prisms retrieved along the cross sections of the pile segments of group 1: relationship between average drilling amplitude over the width $B = 20$ mm of each prism and their (a) dry density; (b) $f_{c,0,wet,prism}$ (c) $E_{c,0,wet,prism}$.

5.6.3 CT scans and light microscopy observations

CT scans, light microscopy observations, and micro-drilling measurements performed on the 18 segments of group 2 (according to paragraph 3.11), are compared in this section. Among these pile segments, six from 1727 were also part of group 1, to fully characterise their state.

The more recent pile segments from 1922 did not show biodegradation phenomena (Figure 5.20); in few cases, incipient decay was found in 1886 segments (Figure 5.21); both drilling resistance and density distribution from CT scans exhibited lower values on a very

limited outer portion of the segment, where light microscopy observations revealed the presence of moderate decay as defined in Paragraph 3.13. Most of the cells in the radial sections taken from the surface of the segments still showed birefringence (Figure 5.21-A1), but several darker areas with the typical degradation pattern of erosion bacteria [1,4,6], were visible. The radial sections taken from the inner of the segments were intact, with smooth cell walls and intense birefringence (Figure 5.21-A2). A more critical situation was found in the segments from 1727 (Figure 5.22 and Figure 5.23), all featuring moderate to severe decay (Section 3.13) extending from their surface up to a depth of approximately 50 mm, as also confirmed by the very low drilling resistance and density distribution from CT scans.

The corresponding radial sections observed under the microscope, featured erosion channels due to bacterial action, and almost no birefringence under the microscope's polarized light, with only few sound cells left, indicating severe decay (Figure 5.22-A1 and Figure 5.23- A1).

On the contrary, no evidence of decay was found in the radial sections taken from the inner of the segments (Figure 5.22-A2 and Figure 5.23-A2). This underpins the outcomes presented in Paragraph 5.6.1, where the inner prisms (2, 3, 4) had properties in line with sound wood even in the oldest samples from 1727.

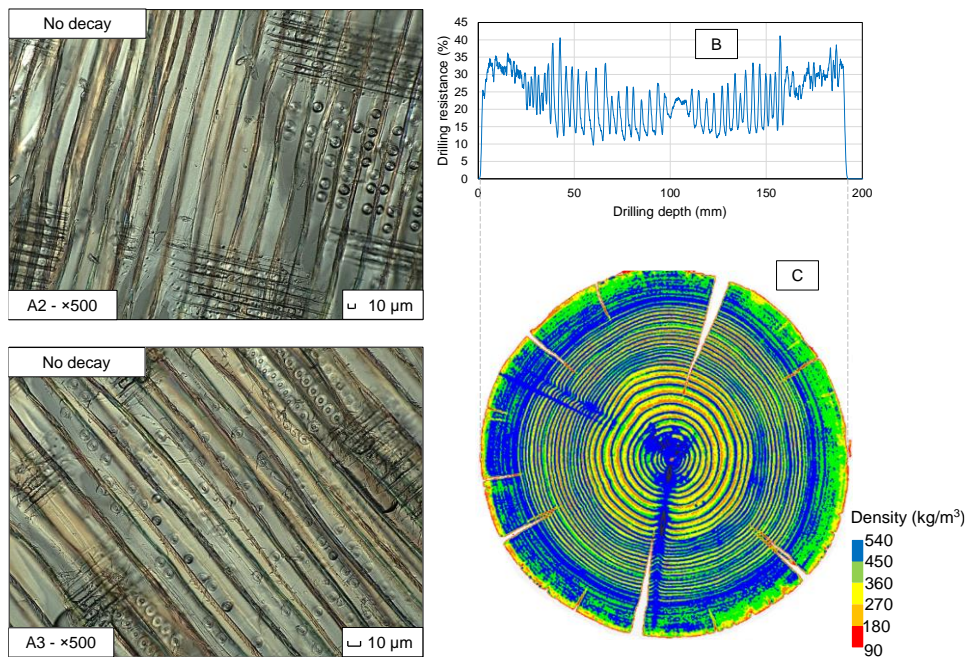


Figure 5.20: [184] Comparison between light microscopy observations (A1-A2, with reported magnification and scale) and micro-drilling signal (B) along the cross section of sample 1922-2-tip (sound spruce segment), and its corresponding CT scan (C). Smooth cell walls and intensive birefringence were observed, corresponding to the absence of decay (Paragraph 3.13) in the examined radial sections (A1-A2), a result confirmed by micro-drilling and CT scan.

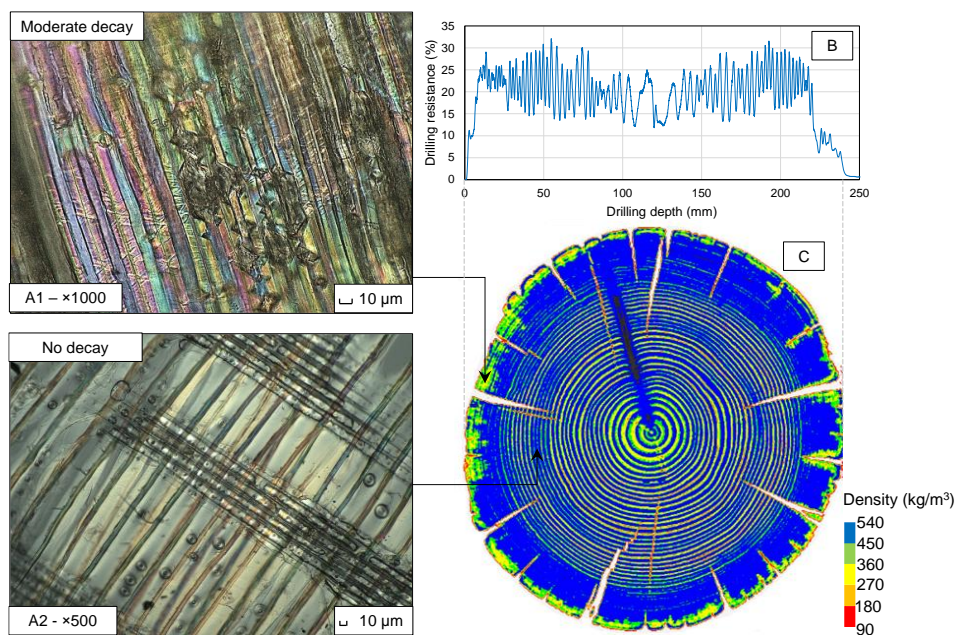
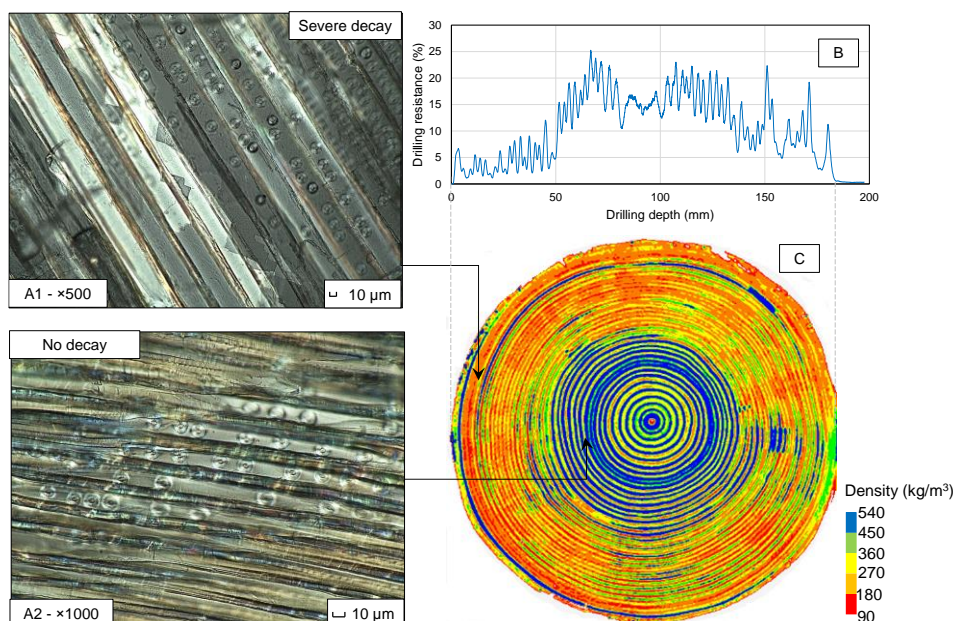


Figure 5.21: [184] Comparison between light microscopy observations (A1-A2, with reported magnification and scale) and micro-drilling signal (B) along the cross section of sample 1886-2-head (fir segment, incipient moderate decay in the very outer portion), and its corresponding CT scan (C). In radial section A1, a matrix of sound cells showing birefringence is observed, but with some tracheids showing darker triangular-shaped notches caused by bacterial degradation, corresponding to moderate decay (Paragraph 3.13); radial section A2 featured no signs of decay: both results are confirmed by micro-drilling and CT scans.



5.6 Effect of decay on the material properties within the cross section

Figure 5.22: [184] Comparison between light microscopy observations (A1-A2, with reported magnification and scale) and micro-drilling signal (B) along the cross section of sample 1727-2-tip (spruce segment, severely decayed in the outer portion), and its corresponding CT scan (C). In radial section A1, only few sound cells showing birefringence are present, whereas the other tracheids are fully degraded and do not exhibit birefringence, corresponding to severe decay (Paragraph 3.13); radial section A2 featured no signs of decay: both results are confirmed by micro-drilling and CT scans.

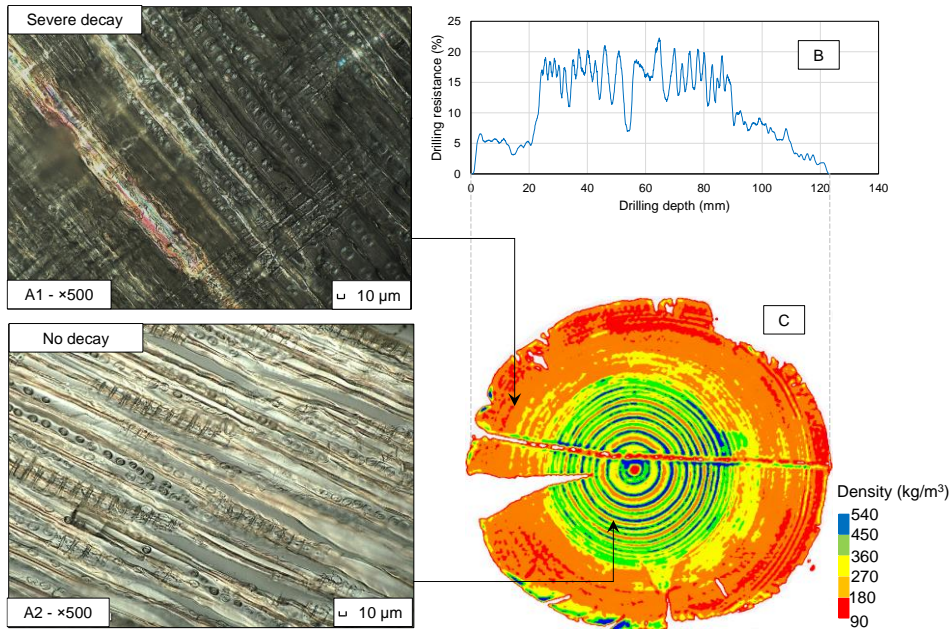


Figure 5.23: [184] Comparison between light microscopy observations (A1-A2, with reported magnification and scale) and micro-drilling signal (B) along the cross section of sample 1727-1-tip (spruce segment, severely decayed in the outer portion), and its corresponding CT scan (C). In radial section A1, only few sound cells showing birefringence are present, whereas the other tracheids are fully degraded and do not exhibit birefringence, corresponding to severe decay (Paragraph 3.13); radial section A2 featured no signs of decay: both results are confirmed by micro-drilling and CT scans.

5.6.4 Reconstruction of the density profile of the cross section from micro-drilling signals

Since the effects of decay could be well captured with micro-drilling measurements (in Paragraphs 5.6.1 and 5.6.2), a reconstruction of the cross section of the pile segments in terms of dry density is possible, because of the good relationship between this parameter and the drilling amplitude established with the small-scale tests on group 1 prisms (showcased in Figure 5.19).

The obtained regression equation 5.2 in Figure 5.19 was applied to the micro-drilling measurements conducted on the segments of group 2, and the resulting density profiles were compared to those retrieved from the CT scans along the path followed by the drill.

$$y = 154.31 x^{0.33} \quad (5.2)$$

The outcomes of this analysis are shown in Figure 5.24: the density profiles could be successfully reconstructed for both decayed (Figure 5.24a,b) and sound segments (Figure 5.24c,d). Furthermore, for sample 1886-1-head (Figure 5.24c), the presence of compression wood was observed in the left part of the cross section, and this specific feature could be accurately captured with the micro-drilling signal as well, showing a larger amplitude in that area.

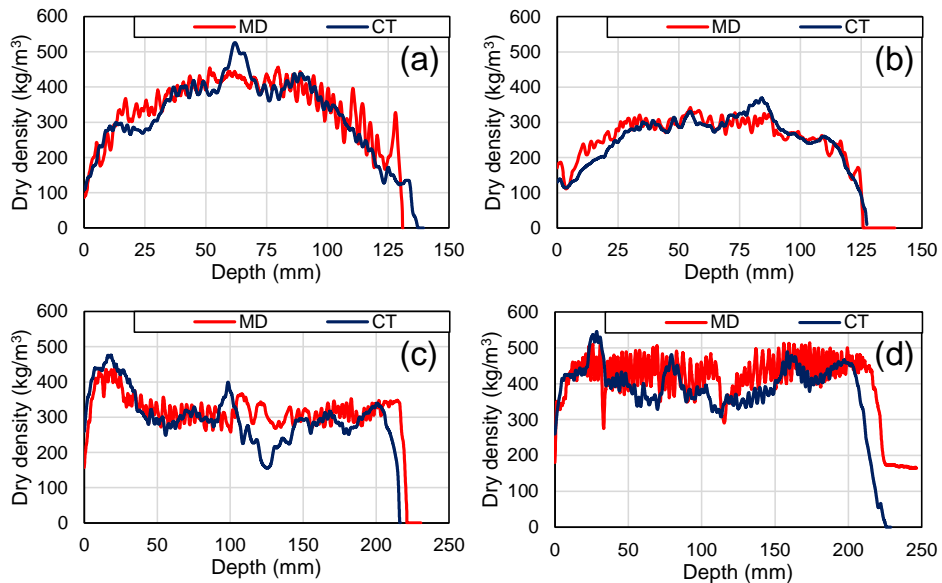


Figure 5.24: Reconstruction of density profiles from micro-drilling (MD) measurements compared to those retrieved from CT scans for: two spruce decayed segments 1727-2-tip (a) and 1727-1-tip (b); sound spruce segment 1886-1-head featuring compression wood on the left side (c); sound fir segment 1886-2-head (d).

5.7 Extent of decay within the cross section and along the piles

Section 5.6 illustrates how the material and mechanical properties vary within the cross section in relation to bacterial decay. The next step, outlined in Paragraph 5.7.1, involves determining the extent of decay in the sapwood and heartwood of the piles studied, which include specimens of various ages. Additionally, Paragraph 5.7.2 presents a case study that estimates the distribution of decay and the remaining short-term compressive strength along the pile, starting from the head of the pile.

5.7.1 Extent of decay in spruce and fir sapwood

The degradation pattern along the pile, for all the historical spruce and fir piles tested in this research, resulted in an approximately constant soft shell length (al_{ss}) across head, middle-part and tip (Section 5.5). The CT scans and the light microscopy observations in Paragraph 5.6.3 allowed to inspect the extent of decay at cross-sectional level in 18 segments (6 full-piles), showing that bacterial decay was only present in the sapwood. No degradation was detected in the heartwood. However, it cannot be ruled out that decay may also be present in other sections of the heartwood that were not investigated, or in piles that have been exposed to degrading agents for a longer period.

In this Paragraph, the sapwood of all 60 spruce and fir historical piles was calculated according to Paragraph 3.12.1, and reported in Table 5.13.

The results show that al_{ss} remains always below the sapwood width (W_s), in line with the research reported in the literature [5],[11],[145], where the bacterial decay seems to stop at the sapwood–heartwood boundary of spruce and pine, highlighting the very good durability of heartwood against bacterial decay.

On average, the percentage of decayed sapwood area reached 66 % in spruce pile tips from 1727, with extreme cases in which 90% of the sapwood was degraded (Table 5.13). This suggests that the remaining sound material comprises a larger portion of sound heartwood than sapwood. A larger portion of heartwood would result in an intrinsic lower density (ρ_{12}), at similar RoG and Age, as observable in piles from 1727 where ρ_{12} ranged at 360-385 kg/m³. This had also a considerable influence on $EQ f_{c,0,wet,sound}$, since the remaining short-term strength of the A_{sound} comprised a large portion of less dense heartwood. Furthermore, an even lower ρ_{12} and $EQ f_{c,0,wet,sound}$ were determined for tips from 1727, attributable to the proportion of juvenile wood, which closely aligned with the entirety of the heartwood portion (see Table 5.13).

On the other hand, in piles from 1922/1886, the maximum average decayed sapwood remained within 20%, resulting in a larger contribution of sound available sapwood (above 80%). In this case, only little variations in the density (ρ_{12}) were measured, $EQ f_{c,0,wet,sound}$, especially in head and middle-parts. For tips, approximately 10% lower ρ_{12} and $EQ f_{c,0,wet,sound}$ were determined for tips from 1727, explained by the fact that the portion of juvenile wood corresponded approximately to the whole heartwood (see Table 5.13).

Table 5.13: Remaining short-term compressive strength in relation to: A_{sound} , sapwood width (W_s), soft shell length (a_{ss}) and percentage of decayed sapwood (Decayed SW) for head, middle-part and tip of all historical piles from 1922/1886/1727.

Wood species	Building year	Part (No. segments)	$f_{c,0,\text{wet}}$ (MPa)		EQ $f_{c,0,\text{wet,sound}}$ (MPa)		ρ_{12} (kg/m ³)		A_{sound} (%)		W_s^a (mm)		a_{ss} (mm)		Decayed SW (%)	
			mean	SD	mean	SD	mean	SD	mean	SD	mean	SD	mean	SD	mean	SD
Spruce	1922/1886	Head (29)	13.9	2.0	15.3	2.5	465	42	91	8	52	8	6	5	14	14
		Middle (30)	13.7	2.3	14.7	2.3	470	45	94	7	50	7	4	4	9	10
		Tip (32)	11.8	2.1	13.7	2.4	450	48	87	10	47	5	7	5	18	13
	1727	Head (30)	7.5	2.3	12.2	3.3	385	55	63	14	49	10	22	11	53	20
		Middle (30)	7.3	2.4	12.3	2.9	375	48	62	20	46	9	20	11	52	28
		Tip (30)	5.8	1.8	11.6	2.4	360	47	50	15	38	7	22	9	66	20
Fir	1886	Head (6)	15.2	2.0	16.0	1.8	495	34	97	4	47	11	2	2	5	6
		Middle (7)	14.8	2.3	15.2	1.7	485	48	97	6	46	8	1	3	4	9
		Tip (7)	12.0	3.0	12.5	2.8	460	70	96	7	38	6	2	3	5	10

^a calculated according to Sellin 1996 (Section 3.12.1).

5.7.2 Decay distribution along the piles

The decay along the pile was analysed in relation to the soft shell length, sapwood width, and the remaining short-term strength of the pile head. This approach was chosen because, during in-situ assessments of historical timber foundation piles, the pile head can be examined using micro-drilling, allowing its remaining short-term compressive strength to be estimated based on the experimental equation presented in Section 5.5.

Based on this information, and the data collected along the length of the 60 spruce and fir historical foundation piles, the distribution between $f_{c,0,wet}$ of the pile head and the tip is shown in Figure 5.25. On average, the pile tip exhibited on average a decrease in $f_{c,0,wet}$ of 2 MPa. However, this is variable in some cases, as shown in Figure 5.25, where the scatter can be up to 5 MPa.

The regression Equation 5.3 can be used to predict the short-term compressive strength of the tip ($Pred. f_{c,0,wet,tip}$) from $f_{c,0,wet,head}$ of the pile head. The correlation between $Pred. f_{c,0,wet,tip}$ and the actual $f_{c,0,wet,tip}$ determined for the tips with compression tests (Paragraph 5.2.2) is shown in Figure 5.26, showing a strong relationship between the two parameters.

$$Pred. f_{c,0,wet,tip} = -0.76 + 0.88 f_{c,0,wet,head} \quad (5.3)$$

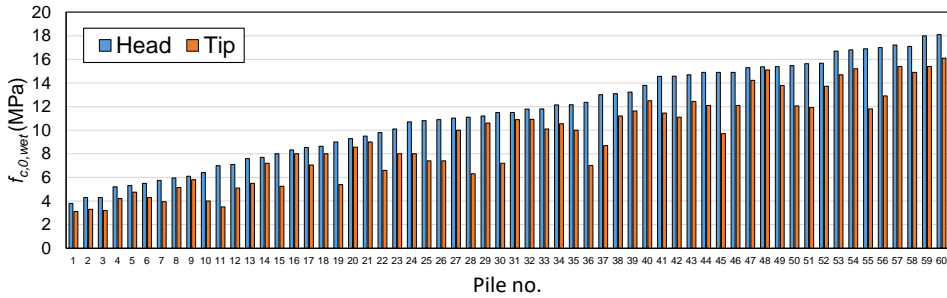


Figure 5.25: Correlation between $f_{c,0,wet}$ of the pile head and the tip of all the 60 piles studied in this work

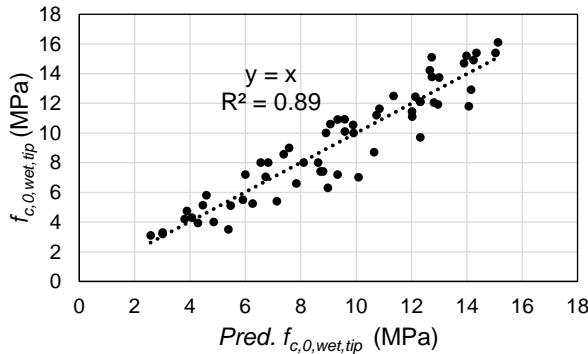


Figure 5.26: Relationship between $Pred. f_{c,0,wet,tip}$ and $f_{c,0,wet,tip}$ based on the regression Equation 5.3.

5.7.3 Overview of the decay distribution in the foundation plan of bridge 30 and 41

The distribution of decay in the foundation plan of the two bridges, from which the wooden foundation piles were extracted, is illustrated in Figure 5.27 (Bridge 30) and Figure 5.28 (Bridge 41). Only the soft shell length (al_{ss}) and the sapwood width (W_s) of the pile heads are reported, as outlined in Paragraph 5.7.1.

For the section of the bridges built in 1727, it can be observed that al_{ss} in the piles generally exceeds 10 mm, reaching lengths of up to 45 mm. However, al_{ss} never exceeds W_s .

It is important to note that a significant difference was observed between al_{ss} measured in the spruce pile heads (1727) retrieved from the external and internal rows of the bridges (Figure 5. 29).

Pile heads from 1727 located in the internal rows showed a lower amount of decay compared to the external rows, suggesting that the direct contact of the pile head with the water flow in the canals could have increased the speed of bacterial decay in the sapwood as found in previous research [5],[11],[14],[1].

However, since only 8 segments were part of the internal rows, uncertainties are related to the average al_{ss} measured in the pile heads, which is a topic for further investigation.

5.7 Extent of decay within the cross section and along the piles

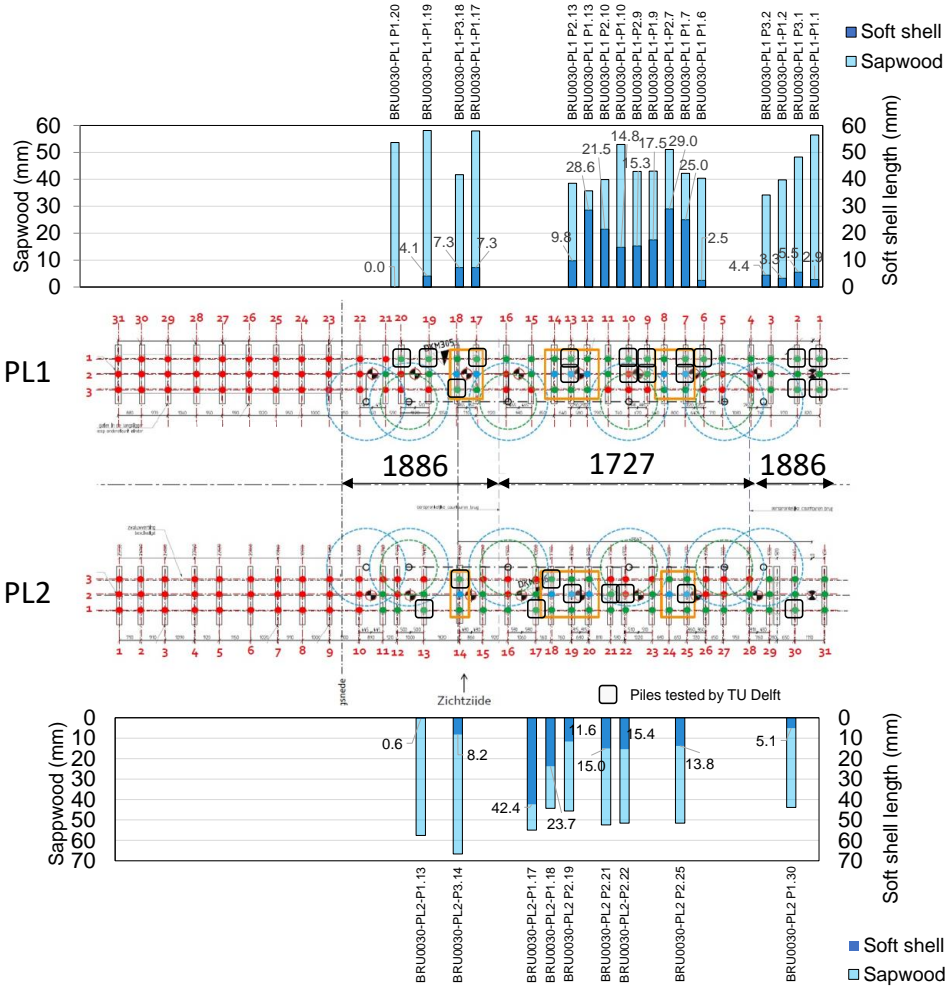


Figure 5.27: Bridge 30: overview of soft shell and sapwood of the head of the piles in the foundation plan.

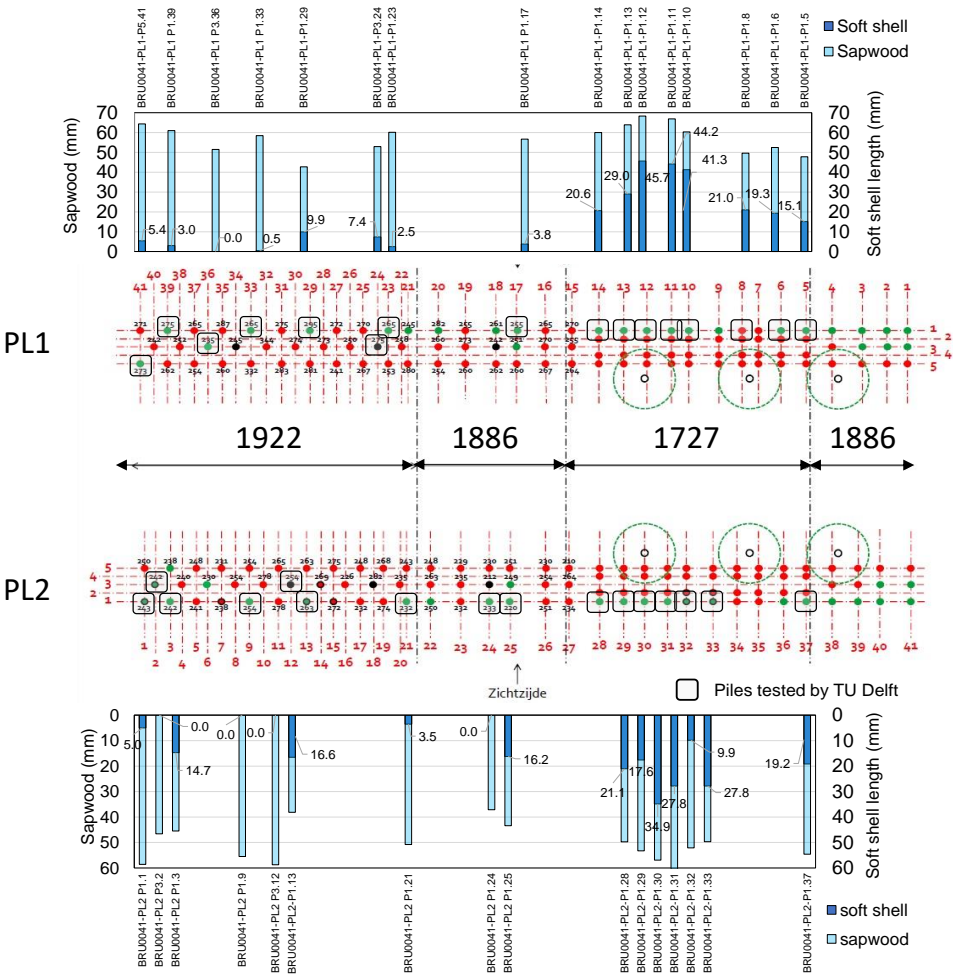


Figure 5.28: Bridge 41: overview of soft shell and sapwood of the head of the piles in the foundation plan.

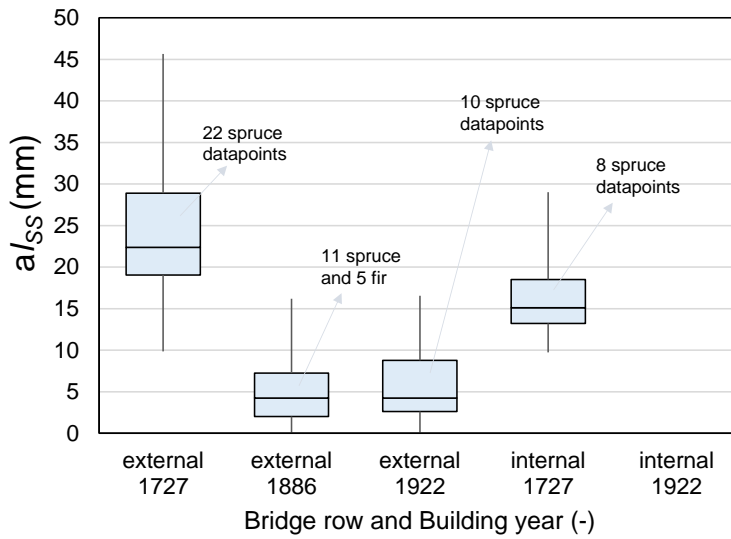


Figure 5. 29: Soft shell length (a_{ss}) of the pile heads in the external and internal rows of the foundation plan of bridge 30 and 41.

5.8 Summary of the test results

Chapter 5 presented the results of the experimental campaign aimed at characterizing the effects of bacterial decay on wooden foundation piles supporting bridges in the historic city centre of Amsterdam (NL), from both material and mechanical perspectives.

The primary objectives of Chapter 5 were to characterize the material and mechanical properties of historical spruce and fir foundation piles that have been in service for approximately 100 to 300 years, and to validate the TU-Delft developed algorithm (Appendix E) for analysing the decayed portion of the piles (*soft shell*) from the signals obtained through micro-drilling measurements. The aim was to study the effects and distribution of decay within the pile cross-sections. Bacterial decay was characterized using micro-drilling measurements, small-scale material and compressive tests on prismatic samples extracted from the piles' cross-sections, computed tomography scans of pile segments, and light microscopy observations. Finally, the correlation between strength properties and decay, as measured through micro-drilling, was explored to assess the impact of decay on strength and to develop experimental equations for predicting the remaining strength of the piles.

Piles from 1922 and 1886 showed minimal degradation, with a soft shell of 4–7 mm. In contrast, moderate to severe decay was observed in piles from 1727, affecting the outer 20–50 mm of their cross-section, causing a reduction of their remaining short-term compressive strength by up to 50–60% compared to new piles. This significant strength loss was primarily due to decay, particularly in the 1727 piles, which had a service life of approximately 300 years. The exposure of these older piles to bacterial decay for approximately 300 years also resulted in higher moisture contents, reduced densities and stiffness. However, also the more recent piles from 1922 and 1886 exhibited a 10–20% reduction in short-term compressive strength despite their lower levels of decay. Regardless of soft shell depth, all pile tips showed an average decrease of 2 MPa in remaining short-term compressive strength compared to the pile heads.

The results showed that the remaining short-term compression strength of wooden piles that have been in service for a long time is lower than the strength values provided for “new” piles. This is partly due to the presence of decay, especially for older piles from 1727. However, lower short-term compressive strength values were also determined for more recent piles from 1922/1886, which exhibited a low amount of decay. These strength values have to be taken into account in future assessments of wooden foundation piles.

Micro-drilling allowed to estimate the “soft shell” of each pile: the degraded outer layer of the cross section to which zero strength is assigned. A TU-Delft developed algorithm (Appendix E) was used and validated to determine the degraded parts of the cross section based on the micro-drilling signal, calibrated on the full-size compression test results of sound piles from 1922/1886, from which the length of the soft shell could be determined.

Based on the determined soft shell, the equivalent sound compressive strength for piles of all time periods could be determined. For the piles from 1727, the equivalent sound strength values were lower than for the piles from 1922/1886, which might be caused by the fact that the stress level during the service life of piles from 1727 was higher, due to a

larger presence of decay and thus a smaller sound load-bearing cross section. This was verified by applying an average equivalent sound compressive strength to the sound remaining cross section of all piles, assuming zero strength of the soft shell layer: with this, the short-term compression strength could be accurately predicted for all the pile parts from all the time periods.

It was demonstrated that micro-drilling signals were well correlated with the material properties throughout the cross section of the piles, providing both qualitative and quantitative information on the degradation state of the piles. In particular, from the correlation established with the dry density and the remaining short-term compressive strength it was possible to:

- Accurately predict the dry density profiles of the piles' cross sections, which were successfully validated against those obtained with the CT scans (Section 5.6).
- Predict the remaining short-term compressive strength of the piles on the basis of the remaining sound cross-sectional area (A_{sound}), determined through the analysis of the micro-drilling signals with the TU-Delft developed algorithm (Section 5.5). The algorithm is explained in Appendix E.

Based on small-scale testing, computed tomography scans, and light microscopy observations, it was possible to assess that the decay extent within the cross-section of the piles was only limited to the sapwood and never present in the heartwood. This was confirmed in the results from micro-drilling of all the piles, where the soft shell length never exceeded the sapwood width. The same findings are also reported in literature [5],[11],[145], where the bacterial decay seemed to stop at the sapwood–heartwood boundary of spruce and pine, highlighting the very good durability of heartwood against bacterial decay. The degradation of the piles was attributed to bacterial decay, confirming that the piles extracted from bridge 30 and 41 in Amsterdam remained submerged in anoxic conditions throughout their service life. However, it should be noticed that it cannot be excluded a priori that other degradation types such as soft rot fungi (in low-oxygen conditions) might be present in isolated spot of the piles or in other timber piles in Amsterdam.

The soft shell length was found to be on average constant along the pile, from the head to the tip. A useful information for the assessment of in-situ historical wooden foundation piles, where the soft shell length can be measured with micro-drilling on the pile head, and therefore assumed as constant along the whole pile. Although the soft shell length proved to be constant along the piles, the pile geometry is tapered, meaning that the diameter decreases from head to tip, resulting in a lower average sound core (A_{sound}) in the pile tip, compared to head and middle-part. Based on this, a regression equation was proposed (Equation 5.3 in Section 5.7) to predict the short-term compressive strength of the tip from $f_{c,0,wet,head}$ of the pile head.

It should be noted that the results presented in this study are based on micro drilling measurements conducted in the laboratory. After the test phase of micro-drilling, the micro drilling technique is now applied on a large scale in the city of Amsterdam. Analyses of in-situ micro-drilling measurements show the same quality as the laboratory

measurements, and thus they can be used for the analysis of the soft shell of the wooden foundation piles. To this end, it has been proved that the detection of specific features or decayed portions of the cross section through the drilling profiles is not influenced either by the global moisture content of a segment or by the moisture content gradient within its cross section. Thus, based on the obtained results, biological degradation phenomena can be reliably identified with micro-drilling signals also in underwater conditions, where it is not necessary to know the exact moisture content.

However the micro-drilling in-situ applicability, with measurements performed underwater on timber foundation piles, could have measurement errors associated with the difficulties of conducting underwater measurements, and the accuracy and precision of the operator. For a correct analysis of the signal, it is recommended not to change the settings for drilling speed (2500 r/min) and feed speed (150 cm/min) reported in Paragraph 3.9. In addition, an accurate measurement of the diameter of the pile section where micro-drilling is conducted is of importance for an adequate estimation of the remaining sound cross-sectional area, for the prediction of the remaining short-term compressive strength.

The analysis of the signal is also sensitive to the location where micro-drilling is performed: the presence of wood knots, cracks, dirt, or other irregularities could influence the signal and the estimation of the soft shell. To overcome these issues, the divers who conduct the measurements need clear instructions. When an underwater micro-drilling measurement is taken, the signal has to be simultaneously checked by a technician above water in order to decide whether the measurement was adequately performed, or whether a new measurement has to be conducted.

Promising results were obtained in relation to the use of underwater micro-drilling measurements for in-situ monitoring of historical wooden foundation piles. These outcomes have been supported by the unique opportunity to examine in detail samples dated back to different construction years and from the same location, adopting an integrated approach at different scales for their characterisation. The results of this study contribute to the research framework supporting testing and modelling methods for estimating decay, (residual) load-bearing capacity, and the remaining service life of wooden foundation structures.

6

Prediction equations for the short-term compressive strength

6.1 Introduction

Chapter 6 presents prediction equations for the short-term compressive strength of “new” spruce and pine piles, based on machine grading of the dynamic modulus of elasticity (Section 6.2), as well as experimental equations to predict the remaining short-term compressive strength of historical timber piles, based on micro drilling measurements (Section 6.3).

In Section 6.2, two regression models for predicting the short-term compressive strength of “new” saturated timber foundation piles are reported – one for spruce and one for pine piles – based on machine-graded dynamic modulus of elasticity. These models complement the characteristic strength classes defined for visual grading in Chapter 4, providing an additional tool for the determination of the short-term saturated compressive strength of the piles.

Section 6.3 outlines the direct predictive equation for the remaining short-term compressive strength of historical timber foundation piles, based on the remaining sound cross-sectional area of the pile head, determined with micro-drilling. This allows for the prediction of remaining short-term compressive strength along the pile, from the head to the tip, based on the experimental analyses conducted on the historical piles in Chapter 5.

6.2 Regression models for “new” spruce and pine foundation piles

Three regression models were developed: two for spruce and pine piles, separately; and one model for spruce and pine piles together. From the models, the saturated compressive strength could be predicted based on the machine-graded dynamic modulus of elasticity ($E_{c,0,dyn,wet}$ in MPa), resulting to be the most influencing parameter on the compressive strength (See Section 4.3).

Influencing visually-graded parameters such as knot ratio (KR), rate of growth (RoG), and Age (number of annual rings) of the piles were also used to predict the saturated compressive strength, as already reported in Section 4.5, and therefore not included in this Chapter. In this way, for each wood species, the models can be used for visual or machine grading.

6.2.1 Regression model for spruce piles

Model S considered $E_{c,0,dyn,wet}$ as independent variable (Table 6.1). The prediction Equation 6.1 represents the $f_{c,0,wet,pred}$ for Model S. Model S presented a F-value = 208.9, ($n = 132$), a multiple coefficient of determination (adjusted R^2) of 0.61 and a standard error of 1.6. Figure 6.1 shows the relationship between $f_{c,0,wet}$ and $f_{c,0,wet,pred}$, the normal probability plot, and the residuals. All multipliers in Model S were significant and the residuals had relatively equal variances.

$$f_{c,0,wet,pred} = 2.71 + 0.0127 E_{c,0,dyn,wet} \quad (6.1)$$

Table 6.1: Multipliers and statistical parameters for 95% confidence interval in regression Model S for “new” spruce.

Variables	Coefficients	Standard Error	t-stat	p-value	Lower 95%	Upper 95%
Intercept	2.710	0.926	2.924	0.004	0.876	4.544
$E_{c,0,dyn,wet}$	0.00127	8.8E-05	14.453	9.4E-29	0.001	0.001

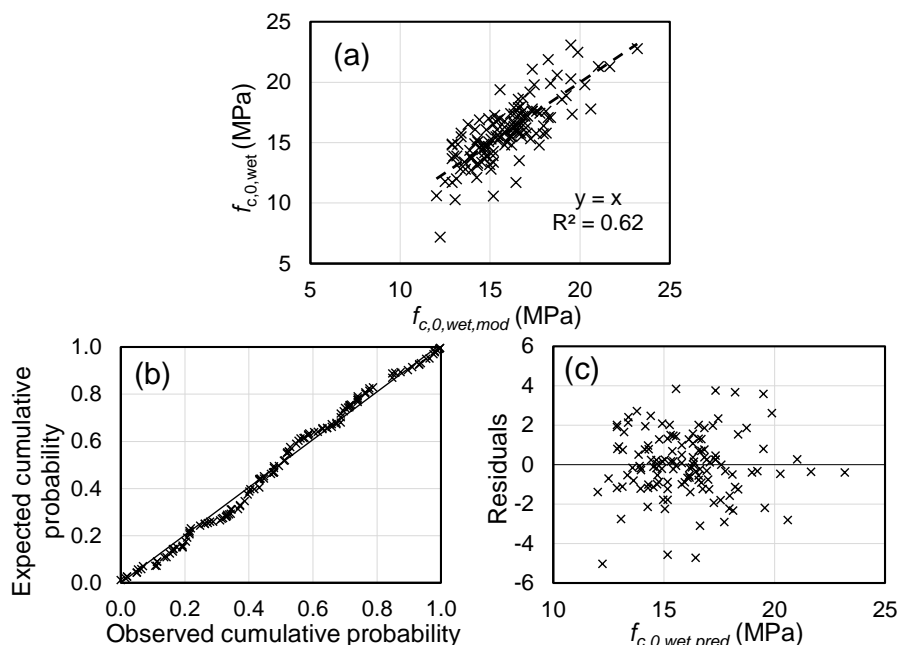


Figure 6.1: Regression Model S with relationship between $f_{c,0,wet}$ and $f_{c,0,wet,pred}$ (a), normal probability plot (b), and residuals (c).

6.2.2 Regression model for pine piles

Model *P* considered $E_{c,0,dyn,wet}$ as independent variable (Table 6.2). The prediction Equation 6.2 represents the $f_{c,0,wet,pred}$ for Model *P*. Model *P* presented a F-value = 515.5 ($n = 120$), a multiple coefficient of determination (adjusted R^2) of 0.81 and a standard error of 1.32. Figure 6.2 shows the relationship between $f_{c,0,wet}$ and $f_{c,0,wet,pred}$, the normal probability plot and the residuals. All multipliers in Model *P* were significant and the residuals had relatively equal variances.

$$f_{c,0,wet,pred} = 4.144 + 0.0138 E_{c,0,dyn,wet} \quad (6.2)$$

Table 6.2: Multipliers and statistical parameters for 95% confidence interval in regression Model *P* for “new” pine.

Variables	Coefficients	Standard Error	t-stat	p-value	Lower 95%	Upper 95%
Intercept	4.144	0.658	6.294	5.34E-09	2.840	5.447
$E_{c,0,dyn,wet}$	0.00138	6.07E-05	22.705	4.52E-45	0.001	0.001

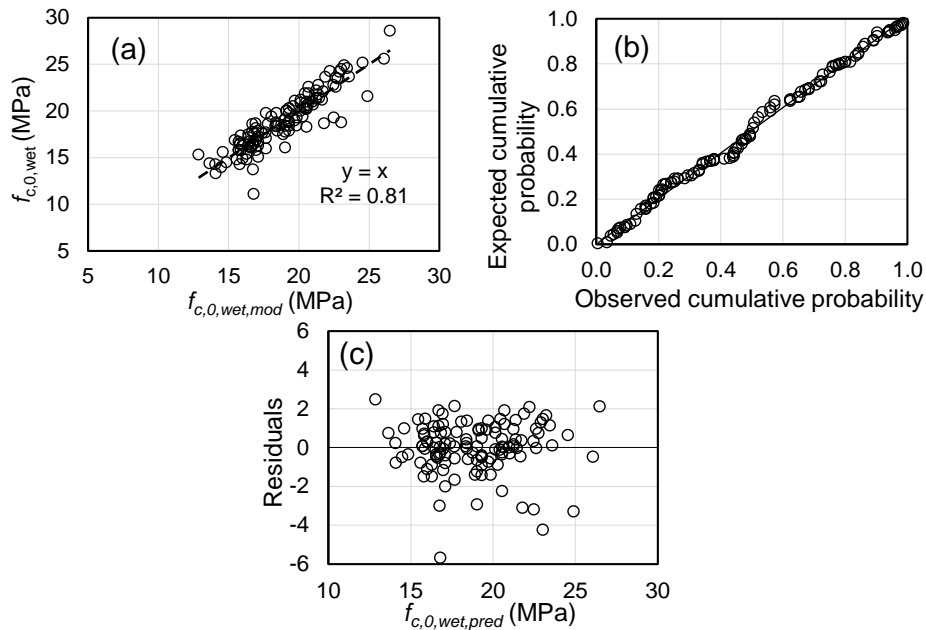


Figure 6.2: Regression Model P with relationship between $f_{c,0,wet}$ and $f_{c,0,wet,mod}$ (a), normal probability plot (b), and residuals (c).

6.2.3 Regression model for “new” spruce and pine piles

The two individual models for spruce (S) and pine (P), presented in Sections 6.2.1 and 6.2.2, respectively, exhibited similar trends (Figure 6.3). Spruce piles were more distributed in the lower part of the graph, due to their lower wet compressive strength values compared to pine. Nevertheless, the models show a strong correlation with each other.

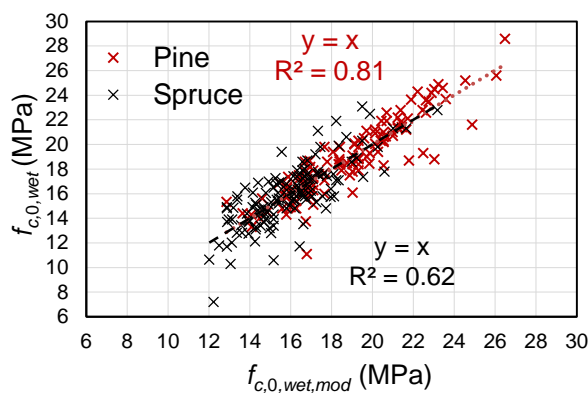


Figure 6.3: Comparison between Model S and Model P for spruce and pine piles respectively.

Hence, a regression model (Model S+P) for both spruce and pine was constructed, based on $E_{c,0,dyn,wet}$ (Table 6.3). The regression analysis for Model S+P resulted in the multiple

Prediction equations for the short-term compressive strength

regression equation 6.3 for predicted wet compressive strength ($f_{c,0,wet,pred}$). Model S+P presented a F-value = 407.9 (n = 253), a multiple coefficient of determination (adjusted R^2) of 0.62 and a standard error of 1.95. All multipliers were significant and the residuals had relatively equal variances. Figure 6.4 shows the relationship between $f_{c,0,wet}$ and $f_{c,0,wet,pred}$, the normal probability plot, and the residuals. All multipliers in Model S+P were significant and the residuals had relatively equal variances.

$$f_{c,0,wet,pred} = 2.771 + 0.00138 E_{c,0,dyn,wet} \quad (6.3)$$

Table 6.3: Multipliers and statistical parameters for 95% confidence interval in regression Model S+P for “new” spruce and pine.

Variables	Coefficients	Standard Error	t-stat	p-value	Lower 95%	Upper 95%
Intercept	2.771	0.731	3.788	0.00019	1.330	4.212
$E_{c,0,dyn,wet}$	0.00138	6.85E-05	20.195	1.91E-54	0.00124	0.001

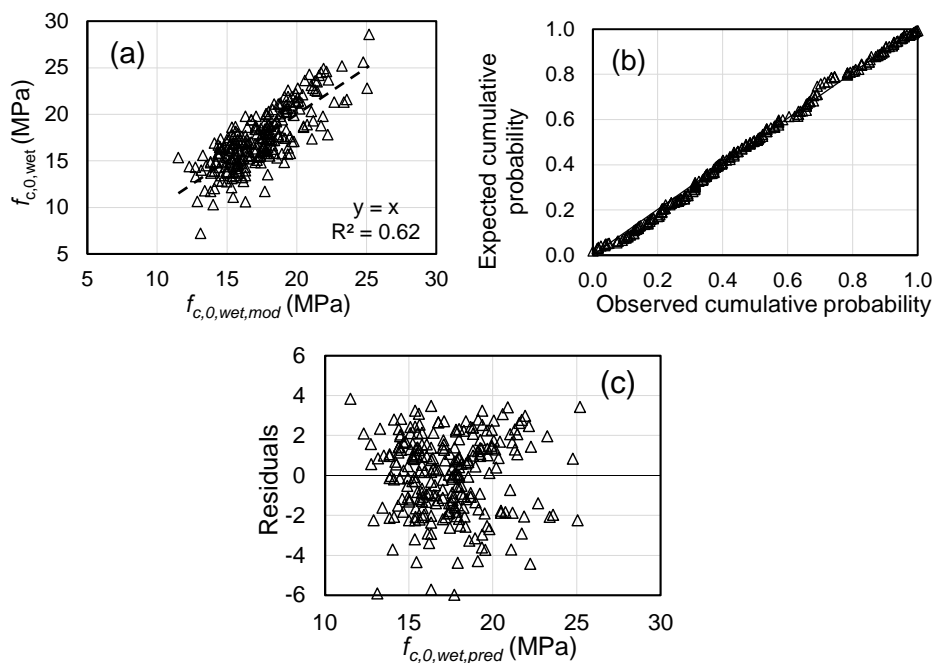


Figure 6.4: Regression Model S+P with relationship between $f_{c,0,wet}$ and $f_{c,0,wet,pred}$ (a), normal probability plot (b) and residuals (c).

6.3 Experimental equations for predicting the remaining short-term strength of historical piles

6.3.1 Micro-drilling assessment

In order to estimate the remaining short-term compressive strength of a wooden foundation pile, the first step involves:

- Underwater micro-drilling measurements (A and B) on the head of the pile (Figure 6.5).
- Measurement of the pile diameter.

The signals retrieved from micro-drilling measurements A-B are analysed with the TU-Delft developed algorithm, explained in appendix E. The soft shell calculation is shown in Figure 6. 6) and the results of the analysis of the signals are presented in Section 5.3, with the goal of determining the soft shell length (a/ss).

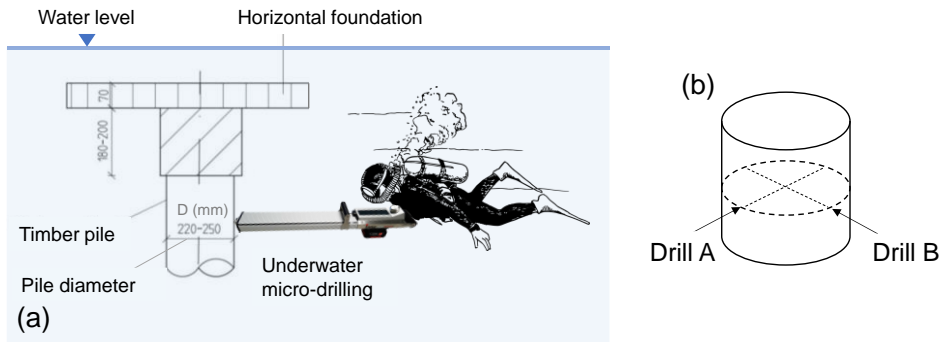
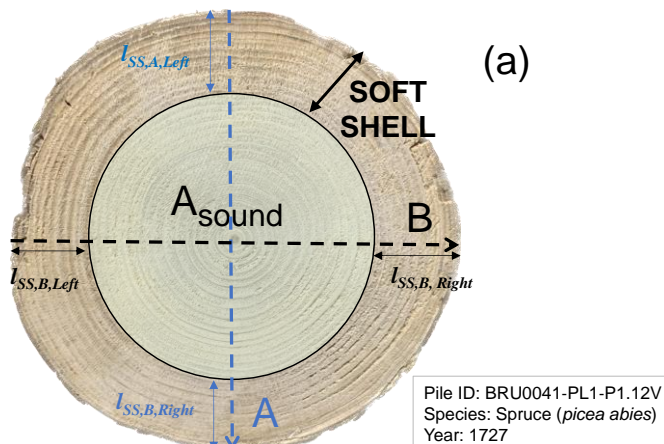


Figure 6.5: (a) Example of underwater micro-drilling on a timber pile; (b) micro-drilling measurements A+B.



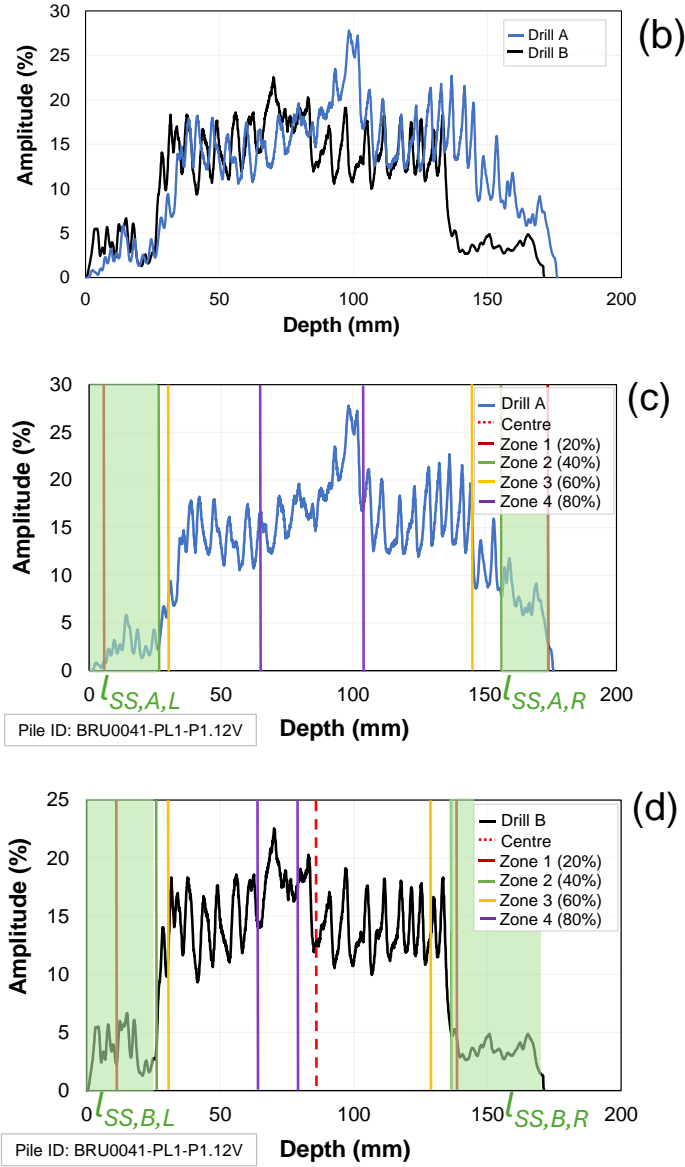


Figure 6. 6: (a) Example of analysis of A and B signals from micro-drilling on spruce pile P1.12V from 1727 and determination of A_{sound} from al_{ss} , averaged from soft shell right and left of signal A and B. (b) two superimposed micro drilling signals A and B. (c) Calculation of soft shell left ($l_{SS,A,L}$) and right ($l_{SS,A,R}$) of micro drilling measurement A. (d) Calculation of soft shell left ($l_{SS,B,L}$) and right ($l_{SS,B,R}$) of micro drilling measurement B.

6.3.2 Prediction of the remaining short-term strength along the pile

The experimental Equation 6.4 (Section 5.5) can be directly applied to predict the remaining short-term compressive strength of the pile head ($f_{c,0,wet,head}$).

$$f_{c,0,wet,head} = 14.74 e^{0.0182 (A_{sound}-100)} \quad (6.4)$$

The same strength value can be taken for middle-parts ($f_{c,0,wet,middle}$) – See Figure 6.7 – since no relevant difference was measured in the remaining short-term strength (See Paragraph 5.2.2.).

From $f_{c,0,wet,head}$, the remaining short-term compressive strength of the tip ($Pred. f_{c,0,wet,tip}$) can be estimated with Equation 6.5, derived from the correlation between head and tip of individual pile segments in Paragraph 5.7.2. This is based on the assumption supported by the results in Paragraph 5.7.1, where the amount of decay remains constant along the length of the pile.

$$Pred. f_{c,0,wet,tip} = 0.88 f_{c,0,wet,head} - 0.76 \quad (6.5)$$

For in-situ assessment of historical wooden foundation piles (Figure 6.7), it is important to derive $f_{c,0,wet,tip}$ since the pile tip corresponds to the critical section of the pile, featuring the lowest mechanical properties (Paragraph 5.2.2). This could have an influence on the load-bearing capacity of the pile, where depending on soil conditions, the tip could be subjected to high stresses during service, primarily due to its smaller cross section.

The presented model for the direct prediction of the remaining short-term compressive strength on the basis of the micro-drilling signals is derived from the experimental analysis of the wooden piles presented in Chapter 5.

Therefore, the experimental prediction equations can be adopted in practice for an estimation of the remaining compressive strength of the piles, keeping in mind that the mechanical properties of the piles could be different depending on the load levels acting on the foundation piles for centuries.

Further research is envisaged to investigate the remaining short-term compression tests of other wood species, in particular pine, very diffused in Amsterdam (Paragraph 2.6.3).

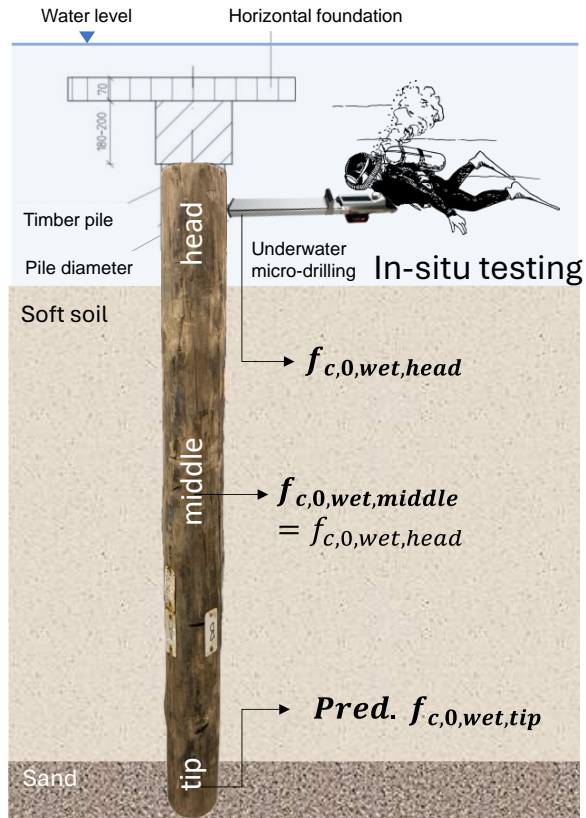


Figure 6. 7: Example of short-term strength prediction along an in-situ timber pile starting from micro-drilling analysis on the pile head.

Conclusions and outlook

7.1 Main outcomes of the dissertation and concluding remarks

The objectives of this dissertation have been the characterization of the mechanical properties along the length of “new” saturated spruce (*Picea abies*) and pine (*Pinus sylvestris*) piles, providing reliable saturated compressive strength values, and grading specifications that can enable engineers to adequately design timber foundation piles. These values can be used together with the provisions in the new Eurocode 5 2023. Moreover, the remaining material and mechanical properties of historical spruce (*Picea abies*) and fir (*Abies*) piles were characterized. An innovative application of micro-drilling measurements was introduced, for the assessment of their biological decay and the remaining short-term compressive strength. Based on these endeavours, the main research question is addressed and discussed:

How can the mechanical properties along wooden foundation piles be methodically characterized through mechanical testing, in relation to biodegradation and quality variables that could possibly influence their compressive strength?

A large testing campaign was conducted, aimed at characterizing 70 newly harvested, full-size saturated spruce (*Picea abies*) and pine (*Pinus sylvestris*) piles, sourced from forests in Holterberg (NL) and Nuremberg (DE), respectively. Additionally, 60 historic, full-size saturated spruce (*Picea abies*) and fir (*Abies alba*) piles, aged between 100 and 300 years and exhibiting varying decay levels, retrieved from two bridges in Amsterdam. The three most common wood species for timber piles were investigated.

“New” timber piles

The compression tests conducted on 132 spruce (*Picea abies*) and 121 pine (*Pinus sylvestris*) pile segments—extracted from the head, middle section, and tip of full-sized tapered piles—enabled a comprehensive characterization of the saturated material and mechanical properties along the length of the piles. These tests provided valuable insights into the grading of the piles for engineering applications and the potential integration of their design strength and stiffness values into industry standards.

- a. The mechanical properties of both spruce and pine piles were found to be governed by the tips, as the distribution of saturated compressive strength decreased from the head to the tip in both species. This was associated with the variation of the most influencing parameters: knot-ratio (KR), annual rings (Age), rate of growth (RoG), and the increasing portion of juvenile wood from head to tip. More specifically, large KR values were associated with lower saturated compressive strength of the piles, due to the grain deviation around the knots. This trend was particularly evident at the tips, where a larger number and size of knots, combined with the reduced diameter, resulted in higher KR values. From the head to the tip of the pile, both decreasing Age and increasing RoG were observed, which correlated with reductions in density and saturated compressive strength. This was also related to the larger portions of juvenile wood in younger pile sections (such as tips). In particular, middle-parts and heads presented higher portions of mature wood featuring higher densities and compressive strength; tips exhibited larger portions of juvenile wood, with lower densities and compressive strength. Pile tips exhibited the lowest strength properties, characterized by the larger number and size of knots and smaller diameters, resulting in higher KR values, lower Age and higher RoG compared to the pile's middle-part and head.
- b. The good correlation with visually-graded parameters opened up the opportunity for grading of multiple strength classes for combined visual grades, distinctively for spruce and pine and for spruce and pine combined. The derived strength classes are applicable to the whole pile and/or its parts: head, middle-part and tip. This is important especially for tips, since depending on soil conditions, they correspond to the critical cross section of the pile during service, primarily due to the high stresses associated with its smaller cross section. In addition, the strength classes are also applicable in case where a pile needs to be cut in a shorter part to be used for different design purposes; the shorter part can be re-graded to be assigned to a possible different strength class.
- c. Based on the possible determined strength classes, design values for (combined) spruce and pine foundation piles were calculated in accordance with the provisions outlined in the draft of the new Eurocode 5 (2023). These design values resulted to be up to 50% lower than those calculated according to the current National Annex to Eurocode 5 (2013) based on one single dry compressive strength value. This highlighted that more accurate and reliable design values of timber piles can be obtained according to the approach in the draft EC5 2023, by using saturated characteristic compressive strength values ($f_{c,0,k,wet}$) and the modification factor ($k_{mod,sat}$) applied in the new defined service class 4. Differently from the approach in the EC5 (2013), $k_{mod,sat}$ only accounts for the effect of load duration in the piles, since the effect of moisture is already accounted for $f_{c,0,k,wet}$ determined in fully-saturated conditions.
- d. Two regression models were developed for the prediction of the short-term compressive strength of "new" saturated timber foundation piles, both for spruce and pine. These were based on machine grading of the dynamic modulus of elasticity. These models add to the characteristic strength classes defined with

visual grading, providing an useful tool to be used in practice for the determination of the saturated compressive strength of the piles.

The saturated compressive strength values and grading boundaries presented in this study contribute to the engineering design of European softwood foundation piles in the context of a new circular construction ecosystem, and support the integration of reliable design values into future versions of Eurocode 5.

Historic timber piles

The large-scale compression tests carried out on segments extracted from head, middle-part and tip of historical spruce (*Picea abies*) and fir (*Abies*) foundation piles allowed to characterize their remaining mechanical properties along their length. A total of 201 pile segments were characterized in relation to different times in service.

- a. The extent of biological decay along the pile could be accurately assessed using an innovative methodology based on micro-drilling measurements, even in underwater conditions and regardless of the moisture content of the piles. Utilizing a database of approximately 500 micro-drilling measurements, a TU Delft algorithm (appendix E) was used to analyse micro-drilling signals. This algorithm enables the precise quantification of the soft shell length, representing the depth of decayed wood in the outer layer of the cross-section.
- b. The degradation of the piles was attributed to bacterial decay, confirming that the piles extracted from bridge 30 and 41 in Amsterdam remained submerged in anoxic conditions throughout their service life. However, it should be noticed that it cannot be excluded a priori that other degradation types such as soft rot fungi (in low-oxygen conditions) might be present in isolated spot of the piles or in other timber piles in Amsterdam.
- c. The extent of decay (soft shell) was found to be consistent along the entire length of the pile, from the head to the tip. This is a significant finding, as it allows for the assumption that the soft shell remains uniform throughout the pile when conducting micro-drilling investigations on the pile head—the only accessible part underwater. Although the soft shell length remains constant along the piles, the tapered geometry causes the diameter to decrease from head to tip. As a result, the average remaining sound cross-sectional area is smaller at the tip compared to the head and middle section. These insights enhance the reliability of structural assessments based on limited access points.
- d. Based on small-scale testing, computed tomography scans, and light microscopy observations, it was possible to assess that the decay extent within the cross-section of the piles was only limited to the sapwood and not detected in the heartwood. These findings align with existing literature, which indicates that bacterial decay consistently slows as it approaches the sapwood–heartwood boundary in spruce piles, highlighting the excellent durability of heartwood against bacterial deterioration. However, it cannot be ruled out that in older piles or those exposed to different environmental conditions, the inner heartwood may remain entirely intact. For engineering assessment of timber foundation piles in Amsterdam, in the absence of precise data, it can be reasonably assumed

that in spruce piles up to 300 years old, like those tested in this study, the heartwood remains structurally sound.

- e. Piles from 1922 and 1886 showed minimal degradation, with a soft shell of 4–7 mm. In contrast, moderate to severe decay was observed in piles from 1727, affecting the outer 20–50 mm of their cross-section, causing a reduction of their remaining short-term compressive strength by up to 50–60% compared to new piles. This significant strength loss was primarily due to decay, particularly in the 1727 piles, which had a service life of approximately 300 years. However, even the more recent piles from 1922 and 1886 exhibited a 10–20% reduction in short-term compressive strength despite their lower levels of decay. Regardless of soft shell depth, all pile tips showed an average decrease of 2 MPa in remaining short-term compressive strength compared to the pile heads.
- f. The equivalent sound compressive strength associated with the remaining sound cross section of historical piles (A_{sound} – sound core) from all time periods could be determined. This gave useful information about the remaining mechanical properties of the non-decayed part of the piles. The equivalent sound compressive strength of piles from 1727 was lower than those from 1922 and 1886, due to a larger decayed portion of sapwood, resulting in a remaining sound core with poorer mechanical properties, associated with the intrinsic lower compressive strength of heartwood and juvenile wood. However, this might also be partly attributed to the mechanical degradation due to higher stress levels during the service life of piles from 1727, associated with their larger presence of decay and thus a smaller sound load-bearing cross section. It should be noted that the effect of long-term loading was not investigated in this dissertation. However, the data determined in this study can be useful to support the analysis of mechanical damage on historic piles.
- g. Experimental prediction equations were developed for practical application in estimating the density and remaining short-term compressive strength along the pile. These equations are based on the strong correlation between micro-drilling signals and the mechanical properties of the piles. In particular, the underwater micro-drilling analysis of the pile head allows for the experimental prediction of the remaining short-term compressive strength along the whole pile, from the head to the tip. This represents a significant advancement in assessing the remaining load-carrying capacity of historic wooden piles, where evaluations can only be performed on the accessible pile head (underwater) by divers or drones. This assessment can be integrated with soil and load analyses to determine stress levels in the piles, considering load distribution and soil stratigraphy. In particular, the possibility to predict the strength of the pile tip is important, given that the pile tip typically corresponds to the critical section with the lowest mechanical properties, and it may experience high stresses during service due to its reduced cross-section, depending on soil conditions. It should also be noted that the mechanical properties of the piles could be different depending on the load levels acting on the foundation piles for centuries.
- h. Underwater micro-drilling measurements are currently widely used in Amsterdam for the assessment of timber foundation piles. It should be noted, that micro-drilling could have measurement errors associated with the

difficulties of conducting underwater measurements, and the accuracy and precision of the operator. For an accurate analysis of the signal, it is recommended to use the drilling and feed speed settings specified in Section 3.9. Additionally, precise measurement of the pile section diameter at the micro-drilling location is crucial for accurately estimating the remaining sound cross-sectional area and predicting the remaining short-term compressive strength. The signal analysis is also sensitive to the specific drilling location, as factors such as wood knots, cracks, dirt, or other irregularities may affect the signal and influence the estimation of the soft shell. To address these challenges, divers conducting the measurements must receive clear and precise instructions. During underwater micro-drilling, a technician above water should simultaneously monitor the signal in real time to determine whether the measurement is valid or if a new measurement is required. This ensures data accuracy and minimizes errors caused by irregularities in the material.

In conclusion, promising results were obtained regarding the use of micro-drilling measurements for in-situ monitoring of historic wooden foundation piles. The research provided a unique opportunity to characterize the material and mechanical properties of piles from different construction periods and varying levels of decay. The micro-drilling technique is now widely applied in Amsterdam to obtain signals that help determine the soft shell, enabling the estimation of the remaining load-carrying capacity of wooden foundation piles. The findings from this research support the city of Amsterdam in planning timely maintenance interventions and contribute to the broader research framework for developing deterministic models and reliability-based assessments. This includes predicting the remaining service life of timber pile foundations, ensuring their long-term structural integrity.

7.2 Recommendations for further research

Besides the knowledge gaps addressed by this dissertation, some other open research lines are presented for future research:

- The variability in the mechanical properties along the length of timber piles is of importance when considering the stress distribution in an axially-loaded pile and its interaction with the soil. Pile-soil interaction has not been addressed in this study. However, it is an important issue for separate studies on the estimation of the load-bearing capacity of wooden pile foundations, supported by their material and mechanical properties characterized in this dissertation. In this context, distributed optic fiber sensors (DFOSs) could be employed on timber piles to efficiently assess the stress distribution along their length and the pile-soil interaction.
- The saturated compressive strength of the piles was found to be correlated with visual growth characteristics that could be measured in practice utilizing wood optical/digital scanners allowing a proper utilization of timber piles in the design.

- The experimental investigations on historical piles involved spruce and fir, two of the most diffused wood species for foundation piles in Amsterdam. However, further research is envisaged to investigate the effects of biological decay on the remaining short-term mechanical properties of pine foundation piles, very diffused in Amsterdam, and might have different effects depending on the wood species.
- Although biological decay was absent in this inner portion of historical spruce and fir piles, the presence of mechanical degradation cannot be a priori excluded, given the difference in short-term compressive strength between older (1886 and 1727) and more recent segments (1922), and between historical piles and “new” piles. Long-term loading for decades may have affected the remaining short-term compressive strength of “sound wood” with respect to time. To this end, the material history over extended periods of time, and the load history (or stress conditions) need to be investigated to better understand the effects of mechanical degradation on timber piles.
- The remaining strength properties and decay levels of long-term loaded historical timber piles can serve as a foundation for developing predictive models to estimate the mechanical damage and remaining service life of timber pile foundations. By analysing the effects of sustained stresses over time in conjunction with the gradual reduction of the sound core due to decay, these models can provide valuable insights into the time to failure of piles under continuous loading. This approach enables a more accurate assessment of structural integrity, considering both the impact of prolonged mechanical stresses and the progressive deterioration of material strength, supporting maintenance, retrofitting, and risk mitigation strategies for aging timber foundations.
- The use of timber foundation piles in bridges primarily subjects them to compressive loads. However, to extend this study to other infrastructure in Amsterdam, such as quay walls, further research is needed on the behaviour of piles subjected to a combination of compression and bending. This requires mechanical testing of saturated historic piles under bending loads to better understand their structural response in such conditions.

References

1. Van de Kuilen, J.W.G. (2007). Service life modelling of timber structures. *Materials and Structures* 40(1), 151–161 (2007) <https://doi.org/10.1617/s11527-006-9158-0>
2. Izzo, F.C., Biscontin, G., Rinaldi, E. (2009). Il sistema delle fondazioni lignee a Venezia, CORILA, Venezia (2009) (in Italian).
3. Klaassen, R.K.W.M., Creemers, J.G.M. (2012). Wooden foundation piles and its underestimated relevance for cultural heritage. *Journal of Cultural Heritage* 13(3), 123–128, <https://doi.org/10.1016/j.culher.2012.02.014>
4. Pagella, G., Ravenshorst, G.J.P., Wolfgang, G., van de Kuilen, J.W.G. (2022). Characterization and assessment of the mechanical properties of spruce foundation piles retrieved from bridges in Amsterdam. *International Conference on Timber Bridges ICTB2021plus*, Biel, Switzerland. <https://doi.org/10.24451/cmcs-1s31>
5. Klaassen, R.K.W.M. (2008) Bacterial decay in wooden foundation piles — Patterns and causes: A study of historical pile foundations in the Netherlands, *International Biodeterioration & Biodegradation*, Volume 61, Issue 1, Pages 45–60, ISSN 0964-8305. <https://doi.org/10.1016/j.ibiod.2007.07.006>.
6. Gard, W., Ravenshorst, G., van de Kuilen, JW. (2024). Historical Wooden Pile Foundations in Amsterdam: An Integrated Approach for the Estimation of Structural Performance and Residual Service Life. In: Endo, Y., Hanazato, T. (eds) *Structural Analysis of Historical Constructions. SAHC 2023. RILEM Bookseries*, vol 47. Springer, Cham. https://doi.org/10.1007/978-3-031-39603-8_110
7. Macchioni, N., Pizzo, B., Capretti, C. (2013). Grading the decay of waterlogged archaeological wood according to anatomical characterisation. *International biodeterioration & Biodegradation* 84 54–64, 2013.
8. Singh, A.P., Kim, Y.S., Singh, T. (2016). Bacterial degradation of wood. *Secondary Xylem Biology*, Chapter 9, 2016.
9. Wang, C., Leicester, R.H., Nguyen M. (2008). Probabilistic procedure for design of untreated timber poles in-ground under attack of decay fungi, *Reliability Engineering and System Safety* 93, 476–481
10. Irbe, I., Bikovens, O., Fridrihsone, V., Dzenis, M. (2019). Impact of biodeterioration on structure and composition of waterlogged foundation piles from Riga Cathedral (1211 CE), Latvia. *Journal of archaeological science: reports* 23, 196, 2019.
11. Björdal, C.G., Elam, J. (2021). Bacterial degradation of nine wooden foundation piles from Gothenburg historic city center and correlation to wood quality, environment and time in service. *International Biodeterioration & Biodegradation* 164, 2021.
12. Pedersen, N.B., Björdal, C.G., Jensen, P., Felby, C. (2013). *Bacterial Degradation of Archaeological Wood in Anoxic Waterlogged Environments*. RSC Publishing, The royal chemical Society, Cambridge, 2013.
13. Grinda, M. (1997). Some experience with attack of microorganisms on wooden constructions supporting foundations of houses and bridges. *IRG/WP 97-10232*, The international research group on wood preservation, 1997.
14. Klaassen, R.K.W.M., van Overeem, B.S. (2012). Factors that influence the speed of bacterial wood degradation. *Journal of cultural heritage* 13S, S129–S134, 2012

15. Björdal, C.G. (2012). Microbial degradation of waterlogged archaeological wood. *Journal of cultural heritage* 13 (3), 118-122, 2012.
16. Van de Kuilen, J.W.G., Beketova-Hummel, O., Pagella, G., Ravenshorst, G.J.P., Wolfgang G. (2021). An integral approach for the assessment of timber pile foundations. In: *World Conference on Timber Engineering 2021, WCTE 2021*, pp. 2–8, Santiago, Chile (2021)
17. Nieuwe Richtlijn Funderingen onder gebouwen (New Guideline for Foundations under Buildings), 2023. Kennis Centrum Aanpak Funderingsproblematiek – KCAF. in Dutch.
18. EN 1995-1-1 (2010)+AC (2006)+A1 (2008) Eurocode 5: design of timber structures–part 1-1: General–common rules and rules for buildings. European Committee for Standardization (CEN), Brussels, Belgium (2012)
19. NEN-EN 1995-1-1/NB:2013. National annex to NEN-EN 1995-1-1, Eurocode 5: design of timber structures–part 1-1: General–common rules and rules for buildings (includes C1:2006 and A1:2008). Netherlands Standardisation Institute (NEN), Delft, The Netherlands (2011)
20. NEN 5491: Quality requirements for wood (KVH 2010) - Piles - European softwood. Netherlands Standardisation Institute (NEN), Delft, The Netherlands (2010) (in Dutch)
21. prEN 1995-1-1:2023. Draft of the new Eurocode 5 2023. NEN-EN 1995-1-1 (2023) Eurocode 5: Design of timber structures – Common rules and rules for buildings – Part 1-1: General. Netherlands Standardisation Institute (NEN), Delft, The Netherlands (2023)
22. F3O (2011) F3O Richtlijn: Onderzoek en beoordeling van houten paalfunderingen onder gebouwen. Rapportnummer: 978-90-816732-1-1 (in Dutch).
23. NEN 8707 (2018)+C2 (2023). Assessment of the structural safety of an existing structure during renovation and rejection - Geotechnical constructions, Nederlands Normalisatie-instituut (NEN).
24. Ruwan Rajapakse (2008). *Pile Design in Sandy Soils*, Editor(s): Ruwan Rajapakse, *Pile Design and Construction Rules of Thumb*, Butterworth-Heinemann, Pages 41-73, ISBN 9780750687638, <https://doi.org/10.1016/B978-0-7506-8763-8.00004-0>.
25. Singh, A.P.; Kim, Y.S.; Chavan, R.R. Advances in Understanding Microbial Deterioration of Buried and Waterlogged Archaeological Woods: A Review. *Forests* 2022, 13, 394. <https://doi.org/10.3390/f13030394>
26. Gao S., Wang X., Brashaw B.K., Ross R.J., Wang L., (2012) Rapid assessment of wood density of standing tree with nondestructive methods – A review. *Proceedings of 2012 International Conference on Bio-based Material Science and Engineering*. IEEE.
27. Gard W.F., Van de Kuilen, J.W.G. (2018) Micro-drilling resistance measurements of dense hardwoods for hydraulic structures. *WCTE - World Conference on Timber Engineering*, Seoul, South-Korea.
28. Sharapov E., Wang X., Smirnova E., Wacker J.P. (2018) Wear behavior of drill bits in wood drilling resistance measurements, *Wood Fiber Sci* 50:154 –166.
29. Humar, M., Balzano, A., Kržišnik, D., Lesar, B. (2021). Assessment of Wooden Foundation Piles after 125 Years of Service. *Forests* 12, 143, 2021.

30. Nowak, T.P., Jasieńko, J., Hamrol-Bielecka, K. (2016). In situ assessment of structural timber using the resistance drilling method – Evaluation of usefulness. *Construction and Building Materials* 102, 403-415, 2016.
31. Mirra, M., Pagella, G., Gard, W.F., Ravenshorst, G.J.P., van de Kuilen, J.W.G. (2023). Influence of moisture content on the assessment of decay levels by micro-drilling measurements in wooden foundation piles. *World Conference on Timber Engineering*, Oslo, Norway, 2023.
32. Buiten H, Rijdsdijk JF (1982) Compressive strength of larch, Douglas fir and spruce piles (in dutch). Rapport HI 82.1140, Houtinstituut TNO, Postbus 151, 2600 AD Delft, order Nr.: 30.01.1.0002
33. Van de Kuilen, J.W.G.: Bepaling van de karakteristieke druksterkte van houten heipalen. Toegepast-Natuurwetenschappelijk Onderzoek (TNO), order Nr. 94-con-RO271. Delft, The Netherlands. (1994) (in Dutch)
34. Ranta-Maunus, A. (2000). Bending and compression properties of small diameter round timber. In: *World Conference of Timber Engineering WCTE 2000*, Whistler, Canada, pp. 1-8.
35. Boren, H.: Factors affecting properties of round wood sawn Finnish pine (*Pinus sylvestris*) and spruce (*Picea abies*). Manuscript for doctoral thesis, University of Joensuu, Finland (2000)
36. Aicher, S., Stapf, G.: Compressive strength parallel to the fiber of spruce with high moisture content. *Eur. J. Wood Prod.* 74, 527-542 (2016) <https://doi.org/10.1007/s00107-015-1004-z>
37. Kollmann F.: *Technology of wood and wood-based materials*. Springer, Berlin, Germany (1955)
38. Blaß, H., Sandhaas, C. (2017). *Timber Engineering - Principles for Design*, Karlsruhe: KIT Scientific Publishing, 2017.
39. Mattheck C, Kubler H. (1997). *Wood—The Internal Optimization of Trees*. Berlin, Germany: Springer-Verlag.
40. Ansell, M.P. (2015). 1 - Wood microstructure – A cellular composite, Editor(s): Martin P. Ansell, *Wood Composites*, Woodhead Publishing, 2015, Pages 3-26, ISBN 9781782424543, <https://doi.org/10.1016/B978-1-78242-454-3.00001-9>.
41. Sørensen, J.D., Stang, B.F.D., Svensson, S. (2002). Calibration of Load Duration Factor k_{mod} . Dept. of Building Technology and Structural Engineering. *Structural Reliability Theory* Vol. R0223 No. 222
42. Hoffmeyer P. Strength under long-term loading. Chapter of textbook in Swedish Ph.D.-course on Timber Engineering. Wiley; 2001. p. 25.
43. Barret, J.D., Foschi, R.O. (1978). Duration of load and probability of failure in wood. Part 2: constant, ramp and cyclic loadings. *Canadian J. of Civil Eng.*, Vol. 5, No. 4, 1978, pp. 515-532.
44. Roß M (1936) Wood as a building material (in German). 1. Schweiz. Kongress zur Förderung der Holzverwertung, Bern, Switzerland.
45. Kühne, H., Fischer, H., Vodoz, J., Wagner, T. (1955). Influence of water content, bulk density, fiber position and tree ring position on the strength and ductility of swiss spruce, fir, larch, red beech and oak (in German). Report 183, Swiss Federal Laboratories for Materials Science and Technology (EMPA), Zurich, Switzerland

46. Glos, P. (1978). Determination of the strength behavior of glulam under compressive stress from material and action parameters (in German). PhD thesis, Technische Universität München, Fachbereich Bauingenieur-und Vermessungswesen.
47. Cherkasova, L.: (2016) Wooden foundations history and prospects MATEC Web Conf. 86 04021 (2016). <https://doi.org/10.1051/mateconf/20168604021>
48. Humar, M.; Balzano, A.; Kržišnik, D.; Lesar, B. Assessment of Wooden Foundation Piles after 125 Years of Service. *Forests* 2021, 12, 143. <https://doi.org/10.3390/f12020143>
49. Lamé, F., Maring, L., Swartjes, F. (2014). Booklet: Into Dutch Soils (2014). Rijkswaterstaat – Dutch Ministry of Infrastructure and the Environment.
50. Spruit, R., & Hutcheson, E. (2019). Draaiboek proefopstelling houten palen (tech. rep.). IB Gemeente Amsterdam (in Dutch).
51. Janse, H. (2000). Amsterdam gebouwd op palen, Ploegsma, Amsterdam (in Dutch)
52. Korff, M. (2012). Response of piled buildings to the construction of deep excavations (Doctoral dissertation). University of Cambridge. IOS Press BV.
53. Kumar, S. (2010). Geotechnical engineering handbook. In B. Das (Ed.). J. Ross Publishing, Inc.
54. Latinga, C. (2015). De resterende (geotechnische) draagkracht van bestaande houten funderingspalen (in Dutch), TU Eindhoven.
55. Zantkuijl, H. J. (1993). Bouwen in Amsterdam - het woonhuis in de stad (in Dutch). Architectura & Natura.
56. Elam, J., Björdal, C.G. (2022). Long-term study on wood degradation in urban soil-water systems - implications for service life of historic foundation piles, *International Biodeterioration & Biodegradation*, Volume 167, 2022, 105356, ISSN 0964-8305, <https://doi.org/10.1016/j.ibiod.2021.105356>.
57. Macchioni, N., Pizzo, B., Capretti, C., (2016). An investigation into preservation of wood from Venice foundations, *Construction and Building Materials*, Volume 111, 2016, Pages 652-661, ISSN 0950-0618, <https://doi.org/10.1016/j.conbuildmat.2016.02.144>.
58. Boren, H.: Factors affecting properties of round wood sawn Finnish pine (*Pinus sylvestris*) and spruce (*Picea abies*). Manuscript for doctoral thesis, University of Joensuu, Finland (2000)
59. Wilkinson, T.L. (1968). Strength evaluation of round timber piles. Forest products laboratory, U.S.D.A. forest service, U.S. Department of Agriculture. Madison Wisconsin U.S.A. Research paper FPL 101, 1968.
60. ASTM Standard D 198-67 (1967). Static tests of timbers in structural size. Amer. SOC. Testing Mater., Philadelphia, Pa.
61. Beck, H. E., Zimmermann, N. E., McVicar, T. R., Vergopolan, N., Berg, A., Wood, E. F. (2018). Present and future Köppen-Geiger climate classification maps at 1-km resolution. *Scientific Data*, 5(1), Article 180214. <https://doi.org/10.1038/sdata.2018.214>
62. Resch, H., Parker, R. (1981). Strength and stiffness of preservative treated marine piles. *Wood and Fiber* 14(4), 1982, pp. 310-319. Society of Wood Science and Technology.
63. Ibach, R.E. (2003). Wood preservation. McGraw-Hill yearbook of science & technology 2003. New York : McGraw-Hill, c2003: pages 469-471.

64. Michael Barnes. Managing Treated Wood in Aquatic Environments. Chapter 2, Basic Treating Processes, pp. 9-24. Western Wood Preservers Institute.
65. American Wood-Preservers' Association. 1964. Preservative treatment of piles by pressure processes. AWPASpecif. C3-64.
66. American Wood Preservers Institute. 1961. Pressure treated timber foundation piles for permanent structures. American Wood Preservative Institute, Chicago, Ill.
67. American Society for Testing and Materials. 1964. Standard specifications for round timber piles. ASTM Specif. D 25-58, Amer. Soc. Testing Mater., Philadelphia, Pa.
68. De Vries, P., Gard, W.G.: The development of a strength grading system for small diameter roundwood. *HERON*, 43 (4), 1998. 43. (1998).
69. Pagella, G., Mirra, M., Ravenshorst, G.J.P., van de Kuilen, J.W.G.: Influence of knots and density distribution on compressive strength of wooden foundation piles. In: Current Perspectives and New Directions in Mechanics, Modelling and Design of Structural Systems, 1st edition CRC Press, London. Proceedings of The Eighth International Conference on Structural Engineering, Mechanics and Computation, Cape Town, South Africa, (2022) <https://doi.org/10.1201/9781003348450-277>
70. Zobel, B.J., van Buijtenen, J.P.: The Effect of Growth Rate on Wood Properties. In: Wood Variation. Springer Series in Wood Science. Springer, Berlin, Heidelberg (1989). https://doi.org/10.1007/978-3-642-74069-5_5
71. Gryc, V., Vavřík, H., & Horn, K.: Density of juvenile and mature wood of selected coniferous species. *Journal of Forest Science*, 57(3), (2011), 123-130. doi: 10.17221/18/2010-JFS
72. Zobel, B.J., Sprague, J.R.: Characteristics of Juvenile Wood. In: Juvenile Wood in Forest Trees. Springer Series in Wood Science. Springer, Berlin, Heidelberg (1998). https://doi.org/10.1007/978-3-642-72126-7_2
73. Vieira Rocha, M.F., et al. (2018). Wood knots influence the modulus of elasticity and resistance to compression, *Floresta e Ambiente*. 25. 10.1590/2179-8087.090617.
74. Ravenshorst, G.J.P., (2015). Species independent strength grading of structural timber, Doctoral Thesis.
75. Mutz, R., Guilley, E., Sauter, U.H., Nepveu, G., (2004). Modelling juvenile-mature wood transition in Scots pine (*Pinus sylvestris* L.) using nonlinear mixed-effects models. <http://dx.doi.org/10.1051/forest:2004084>. 61. 10.1051/forest:2004084.
76. Hautamäki, S., Kilpeläinen, H., Kannisto, K., Wall, T., Verkasalo, E. (2010). Factors Affecting the Appearance Quality and Visual Strength Grade Distributions of Scots Pine and Norway Spruce Sawn Timber in Finland and North-Western Russia. *Baltic Forestry* 16 (2): 217-234.
77. Ranta-Maunus, A. (2007). Strength of Finnish grown timber. VTT Publications 668. VTT, Espoo, 60pp. + App. 3p. Available: <http://www.vtt.fi/inf/pdf/publications/2007/P668.pdf>
78. Sass-Klaassen, U., Vernimmen, T., Baittinger, C. (2008). Dendrochronological dating and provenancing of timber used as foundation piles under historic buildings in The Netherlands. *International Biodeterioration & Biodegradation* 61 (1). - p. 96 - 105.
79. Ramage, M.H. et al. (2017). The wood from the trees: The use of timber in construction, *Renewable and Sustainable Energy Reviews*, Volume 68, Part 1, 2017, Pages 333-359, ISSN 1364-0321, <https://doi.org/10.1016/j.rser.2016.09.107>.

80. Bažant, Z.P. (1979). Chapter 15 - Piles, Developments in Geotechnical Engineering, Elsevier, Volume 24, 1979, Pages 327-406, ISSN 0165-1250, ISBN 9780444997890, <https://doi.org/10.1016/B978-0-444-99789-0.50021-2>
81. Gunnvard, P.; Mattsson, H.; Laue, J. (2022). Evaluating the Design Criteria for Light Embankment Piling: Timber Piles in Road and Railway Foundations. Appl. Sci. 2022, 12, 166. <https://doi.org/10.3390/app12010166>
82. Lindström, J. (2023). The effect of taper on pile shaft bearing capacity – Finite element analysis of a tapered wooden pile in sulfate soil. Master thesis, Luleå University of Technology Department of Civil, Environmental and Natural Resources Engineering.
83. Björklund, L.; Hesselman, J.; Lundgren, C.; Nylinder, M. (2009). Jämförelser Mellan Metoder för Fastvolymbestämning av Stockar; Institutionen för Skoglig Resurshållning (Department of Forest Resource Management) Report 15; Swedish University of Agricultural Sciences: Uppsala, Sweden, 2009. (In Swedish)
84. Brüchert F, Becker G, Speck T. (2000). The mechanics of Norway spruce [*Picea abies* (L.) Karst]: mechanical properties of standing trees from different thinning regimes. For Ecol Manag. 135:45–62.
85. Cajander AK. (1949). Forest types and their significance. Helsinki: Suomalaisen Kirjallisuuden Seuran Kirjapainon Oy.
86. Cameron AD. 2002. Importance of early selective thinning in the development of long-term stand stability and improved log quality: a review. Forestry. 75:25–35.
87. Cremer KW, Borough CJ, McKINNELL FH. 1982. Effects on stocking and thinning on wind damage in plantations. N Z J For Sci. 12:624–668.
88. Bouillon, A. M. (1935). Wooden Foundation Piles. The Military Engineer, 27(151), 22–28. <http://www.jstor.org/stable/44566590>
89. Mohren, G.M.J., Vodde, F. (2006). Forests and Forestry in the Netherlands. Forests and forestry in European Union Countries / Arkuszewska, A., Warsaw : The State Forest Information Centre and the For. Research Ins - ISBN 9788389744425 - p. 334 - 352.
90. Spathelf, P., Ammer, C. (2015). Forest management of scots pine (*Pinus sylvestris* L.) in northern Germany-a brief review of the history and current trends. Forstarchiv. 86. 59-66. 10.4432/0300-4112-86-59.
91. Krasnodebski, Marcin. (2019). The Social Construction of Pine Forest Wastes in Southwestern France During the Nineteenth and Twentieth Centuries. Environment and History. 28.
92. Pretzsch, H., Biber, P., Schütze, G., Uhl, E., Rötzer, T. (2014). Forest stand growth dynamics in Central Europe have accelerated since 1870. Nat Commun 5, 4967 (2014).
93. Anders S., Beck W., Hornschuh F., Müller J., Steiner A. (2004). Vom Kiefern-Reinbestand zum Kiefern-Buchen-Mischbestand – Ökologische Veränderungen, waldwachstums-kundliche und landschaftsökologische Folgen so-wie waldbaulich-praktische Empfehlungen. Beiträge für Forstwirtschaft und Landschaftsökologie 38, 55–67 (in German).
94. W. Marchand, A. Buechling, M. Rydval, V. Čada, A.I. Stegehuis, A. Fruleux, M. Poláček, J. Hofmeister, J. Pavlin, D. Ralhan, M. Dušátko, P. Janda, M. Mikoláš, O. Vostarek, R. Bače, M. Frankovič, D. Kozák, C-C. Roibu, O. Chaskovskyy, S. Mikac, T. Zlatanov, M. Panayotov, A. Diku, E. Toromani, M. Svoboda, (2023). Accelerated growth rates of Norway spruce and European beech saplings from Europe's

95. temperate primary forests are related to warmer conditions, *Agricultural and Forest Meteorology*, Volume 329, 2023, 109280, ISSN 0168-1923.
96. Ross, R.J.: Wood handbook wood as an engineering material. Forest Products Laboratory. General Technical Report FPL-GTR-282. Madison, WI: U.S. Department of Agriculture, Forest Service, Forest Products Laboratory. 543 p (2021)
97. Polman, J.E., Militz, H. (1996). Wood quality of Douglas fir (*Pseudotsuga menziesii* (Mirb) Franco) from trees stands in the Netherlands.. *Annales des Sciences Forestières* 53 (1996) 1127-1136.
98. Blohm, J. H., Evans, R., Koch, G., and Schmitt, U. (2016). "Identification and characterisation of Douglas-fir (*Pseudotsuga menziesii* (Mirb.) Franco) juvenile and adult wood grown in southern Germany," *Drewno* 59(197), 41-47. DOI: 10.12841/wood.1644-3985.c01.05
99. Gagli, K., Timko, L., Gryc, V., Vavřík, H. (2019). Is the quality of the non-native Douglas-fir wood produced in the Czech forests comparable to native softwoods?. *BioResources*. 14. 10.15376/biores.14.2.2931-2945.
100. Zeidler, A., Borůvka, V., Černý, J., Baláš, M. (2022). Douglas-fir outperforms most commercial European softwoods, *Industrial Crops and Products*, Volume 181, 2022, 114828, ISSN 0926-6690, <https://doi.org/10.1016/j.indcrop.2022.114828>.
101. Kollmann F., Côté, W.A. (1968). *Principles of Wood Science and Technology*. Springer-Verlag, Berlin · Heidelberg 1968, Ed. 1, 1968, 592 p, ISBN 978-3-642-87930-2. <https://doi.org/10.1007/978-3-642-87928-9>
102. Millers, M. (2013). The proportion of heartwood in conifer (*Pinus sylvestris* L., *Picea abies* [L.] H. Karst.) trunks and its influence on trunk wood moisture. *Journal of Forest Science*, 59, 2013 (8): 295-300
103. Gjerdrum P. (2003): Heartwood in relation to age and growth rate in *Pinus sylvestris* L. in Scandinavia. *Forestry*, 76: 413–424.
104. Whitehead D. (1978): The estimation of foliage area from sapwood basal area in Scots pine. *Forestry*, 51: 137–149
105. Albrektson A. (1984): Sapwood basal area and needle mass of Scots Pine (*Pinus sylvestris* L.) trees in central Sweden. *Forestry*, 57: 35–43. Bamber R.K. (1976): Heartwood, its function and formation. *Wood Science and Technology*, 10: 1–8.
106. Zobel, B.J., Van Buijtenen, J.P. (1989). *Wood variation: its causes and control*. Springer, Berlin, p 363
107. Hoffmeyer, P. (1987). The role of grain angle, knots, tension wood, compression wood, and other anomalies on the mechanical properties of wood. Technical University of Denmark.
108. Chauhan, S., Donnelly, R., Huang, Cl., Nakada, R., Yafang, Y., Walker, J.C.F. (2006). Wood quality: in context. In: *Primary Wood Processing*. Springer, Dordrecht. https://doi.org/10.1007/1-4020-4393-7_5
109. Cown, D.J., McConchie, D.L. (1980). Wood property variations in an old-crop stand of radiata pine. *New Zealand Journal of Forestry Science* 10, 508–520 (1980).
110. Oh, J.-K., Shim, K., Kim, K.-M., Lee, J.-J.: Quantification of knots in dimension lumber using a single-pass X-ray radiation. *J Wood Sci* 55, 264–272 (2009). <https://doi.org/10.1007/s10086-009-1031-7>

111. Zobel, B.J., van Buijtenen, J.P.: The Effect of Growth Rate on Wood Properties. In: Wood Variation. Springer Series in Wood Science. Springer, Berlin, Heidelberg (1989). https://doi.org/10.1007/978-3-642-74069-5_5
112. ISO 24294 2021. Timber - Round and sawn timber - Vocabulary, International Organization for Standardization (ISO).
113. Briggert, A. (2020). Modelling and strength grading of structural timber and glulam lamellae on the basis of optical scanning and dynamic excitation. Doctoral Dissertation, Department of Building Technology, Linnaeus University, Växjö, 2020.
114. Qu, H., Ming, C., Yuan, H., Jianhua, L. (2020). Effect of trees knot defects on wood quality: a review. IOP Conference Series: Material Science and Engineering. 738. 012027. <https://doi.org/10.1088/1757-899x/738/1/012027>
115. Bano, V., Arriaga, F., Soilán, A., Guaita, M. (2010). F.E.M. analysis of the strength loss in timber due to the presence of knots. World Conference on Timber Engineering. WCTE 2010.
116. Hoffmeyer, P. (1987). The role of grain angle, knots, tension wood, compression wood, and other anomalies on the mechanical properties of wood. Technical University of Denmark. Byg Rapport No. TR-183.
117. Namari, S., Drosky, L., Pudlitz, B., Haller, P., Sotayo, A., Bradley, D., Mehra, S., O'Ceallaigh, C., Harte, A.M., El-Houjeiri, I., Oudjene, M., Guan, Z. (2021). Mechanical properties of compressed wood, Construction and Building Materials, Volume 301, 2021, 124269, ISSN 0950-0618, <https://doi.org/10.1016/j.conbuildmat.2021.124269>
118. Gardiner, B., Macdonald, E. (2005). Compression wood in conifers – the characterisation of its formation and its relevance to timber quality. European Union-Framework Programme FP5-Quality of Life and Management of Living Resources, QLRT-2000-00177, 376.
119. Schulgasser, K., Witztum, A. The mechanism of spiral grain formation in trees. Wood Sci Technol 41, 133–156 (2007). <https://doi.org/10.1007/s00226-006-0100-y>
120. Włoch, W., Mazur, E. & Beltowski, M. Formation of spiral grain in the wood of *Pinus sylvestris* L.. Trees 16, 306–312 (2002). <https://doi.org/10.1007/s00468-002-0174-6>
121. Bodig, J., Jayne, B.A. (1982). Mechanics of Wood and Wood Composites. University of Michigan. Van Nostrand Reinhold, 1982. ISBN 0442008228.
122. Wilson, T.R. (1921). The Effect of Spiral Grain on the Strength of Wood. Journal of Forestry, 19, 740-747.
123. NEN-EN 408 (2010) + A1 (2012): Timber structures–structural timber and glued laminated timber–determination of some physical and mechanical properties. European Committee for Standardization (CEN), Brussels, Belgium (2012)
124. EN 14251 (2003) Structural round timber - Test methods. European Committee for Standardization (CEN), Brussels, Belgium (2012)
125. EN 338 (2016). Structural Timber- Strength classes. Brussels. CEN.
126. NEN-EN 350 (2016). Durability of wood and wood-based products - Testing and classification of the durability to biological agents of wood and wood-based materials. European Committee for Standardization (CEN), Brussels, Belgium (2012)
127. NEN 6760-(1997) nl: Technische grondslagen voor bouwconstructies - TGB 1990 - Houtconstructies - Basiseisen en bepalingmethoden (in Dutch) Netherlands Standardisation Institute (NEN), Delft, The Netherlands (2011)

128. Ranta-Maunus, A. and Korttesmaa, M. (2000). Creep of timber during eight years in natural environments. World Conference on Timber Engineering, 2000, Canada.
129. Porteous, J., Kermani, A. (2009). EC5 - Deformation and creep of timber structures. 87. 25-29.
130. Granello, G., Palermo, A. (2019). Creep in Timber: Research Overview and Comparison between Code Provisions. 27. 6-22.
131. Findley, W.N., Davis, F.A. (2013). Creep and Relaxation of Nonlinear Viscoelastic Materials. Dover Civil and Mechanical Engineering, Courier Corporation, 2013, ISBN 9780486145174.
132. Molier, P. (1994). Creep in Timber Structures. Report of RILEM Technical Committee 112-TSC. RILEM 1944 (The International Union of Testing and Research Laboratories for Materials and Structures). Taylor and Francis, London and New York, 1994, ISBN 0419188304.
133. Wanninger, F., Frangi, A., Fragiaco, M. (2014). Long-Term Behavior of Post-tensioned Timber Connections. *Journal of Structural Engineering*. 141(6): 04014155.
134. Dinwoodie, J.M., Robson, D.J., Paxton, B.H., Higgins, J.S. (1991). Creep in chipboard. *Wood Science and Technology*. 25, 225–238 (1991). <https://doi.org/10.1007/BF00223473>
135. Olsson, A-M., Salmén, L., Eder, M., Burgert, I. (2007). Mechano-sorptive creep in wood fibres. *Wood Science and Technology*. 41. 59-67. <https://doi.org/10.1007/s00226-006-0086-5>
136. van de Kuilen, J.W. (1999). The residual load carrying capacity of timber joints. *HERON*, 44 (3), 1999.
137. Yu, T., Khaloian-Sarnaghi, A., van de Kuilen, J.W. (2022). An improved model for the time-dependent material response of wood under mechanical loading and varying humidity conditions. *Engineering Structures*. 259. 114116. <https://doi.org/10.1016/j.engstruct.2022.114116>
138. van de Kuilen, J.W. (2007). Service life modelling of timber structures. *Materials and Structures*. 40. 151-161. <https://doi.org/10.1617/s11527-006-9158-0>
139. Holt, D.M., Jones, E.B. Bacterial degradation of lignified wood cell walls in anaerobic aquatic habitats. *Applied and environmental microbiology* 46 (3), 722-727, 1983.
140. Daniel, G.F., Nilsson, T. Ultrastructural Observations on Wood Degrading Erosion bacteria. IRG/WP/1283 the International Research Group on Wood Preservation, 1986.
141. Schwarze, F. W. (2007). Wood decay under the microscope. *Fungal biology reviews*, 21(4), 133-170.
142. Kim, Y.S., Singh, A.P. (2016). Wood as Cultural Heritage Material and its Deterioration by Biotic and Abiotic Agents. <https://doi.org/10.1016/B978-0-12-802185-9.00012-7>
143. Varossieau, W.W. (1949). Opgegraven en aangetast hout uit biologisch oogpunt gezien. W. Boerhave Beekman (Ed.) 1949 (In Dutch).
144. Kurstjens, P.B.J. (1988). De druksterkte van enkele heipaal – Monsters uit een 113 jaar oude sluis. Rapport 25-88-35/04-HE-17. Stevin Laboratorium. Delft University of Technology. Delft, The Netherlands.
145. Klaassen, R.K.W.M. et al. (2005). Preserving cultural heritage by preventing bacterial decay of wood in foundation poles and archaeological sites. Final report EVK4-CT-2001-00043. Wageningen 2005.

146. Clarke, R. W., & Squirrell, J. P. (1985). The Pilodyn: An Instrument for Assessing the Condition of Waterlogged Wooden Objects. *Studies in Conservation*, 30(4), 177–183. <https://doi.org/10.2307/1506040>
147. NEN 6760-(1997) nl: Technische grondslagen voor bouwconstructies - TGB 1990 - Houtconstructies - Basiseisen en bepalingmethoden (in Dutch) Netherlands Standardisation Institute (NEN), Delft, The Netherlands (2011)
148. NEN-EN 13183-1 (2002): Moisture content of a piece of sawn timber - Part 1: Determination by oven dry method. Netherlands Standardisation Institute (NEN), Delft, The Netherlands (2011)
149. NEN-EN 1309-3 (2018): Round and sawn timber - Methods of measurements - Part 3: Features and biological degradations. Netherlands Standardisation Institute (NEN), Delft, The Netherlands (2011)
150. EN 14358 (2016) Timber structures – Calculation and verification of characteristic values. European Committee for Standardization (CEN), Brussels, Belgium
151. Dharmaraja, S., Dipayan, D.: Introduction to Statistical Methods, Design of Experiments and Statistical Quality Control, Springer Nature Singapore Pte Ltd. (2018) <https://doi.org/10.1007/978-981-13-1736-1>
152. Lindgren, O. (1992). Medical CT-scanners for nondestructive wood density and moisture content measurements. Diss. Luleå tekniska universitet, 1992.
153. Gard, W. F., Van de Kuilen, J.W.G. (2018). Micro-drilling resistance measurements of dense hardwoods for hydraulic structures. WCTE -World Conference on Timber Engineering, Seoul, South-Korea, 2018.
154. Roy, A., Ravenshorst, G.J.P., Gard, W.F., van de Kuilen, J.W.G. (2021). Handleiding Soft Shell Calculator TU Delft versie 0.1. Report (in Dutch). Delft University of Technology
155. VROM (Dutch ministry of building), "Protocol Voor het uit Voeren van een Inspectie aan Houten Paalfundering. Directoraat-Generaal Wonen, Directie Strategie, Den Haag (in Dutch). Dutch ministry of building, 2003.
156. Heinz, I. (2004). Systematische Erfassung und Dokumentation der mikroanatomischen Merkmale der Nadelhölzer aus der Klasse der Pinatae. Diss., Technischen Universität München
157. Schweingruber, F.H. (1990). Anatomy of European woods. Verlag Paul Haupt, Stuttgart.
158. Broder, J., Preston, R. (2015). Imaging the head and brain, *Diagnostic Imaging for the Emergency Physician*, pages 1–45, 2015.
159. Lin, C.-J., Wang, S.-Y., Lin, F.-C., Chiu, C.-M. (2003). Effect of moisture content on the drill resistance value in Taiwan plantation wood. *Wood Fiber Sci.* 35:234-238, 2003.
160. Jaskowska-Lemańska, J., Przesmycka, E. (2021). Semi-Destructive and Non-Destructive Tests of Timber Structure of Various Moisture Contents. *Materials* 14, 2021.
161. Ravenshorst, G.J.P., Van de Kuilen, J.W.G. (2009). Relationships between local, global and dynamic modulus of elasticity for soft- and hardwoods. CIB W18, proceedings paper 42-10-1, Dubendorf, Switzerland, 2009
162. F. Longuetaud, F. Mothe, J.-M. Lebsan, A. Makela (2007). *Picea abies* sapwood width: variations within and between trees, *Scand. J. For. Res.* 21 (1), 41–53.

163. C. Freyburger, F. Longuetaud, F. Mothe, T. Constant, J.-M. Leban (2009). Measuring wood density by means of X-ray computer tomography, *Ann. For. Sci.* 66 (8), 804.
164. Scheiding, W., Direske, M., Zauer, M., Water absorption of untreated and thermally modified sapwood and heartwood of *Pinus sylvestris* L. *European Journal of Wood and Wood Products* 74, 585-589, 2016.
165. Fredriksson, M., Lindgren, O., End grain water absorption and redistribution in slow-grown and fast-grown Norway spruce (*Picea abies* (L.) Karst.) heartwood and sapwood. *Wood Material Science and Engineering* 8(4), 245–252, 2013.
166. Sjökvist, T., Wålinder, M. E. P., Blom, Å., Liquid sorption characterisation of Norway spruce heartwood and sapwood using a multicycle Wilhelmy plate method, *International Wood Products Journal*, 9:2, 58-65, 2018.
167. Wagenführ, R., *Holzatlas* (2006). Timber atlas, Fachbuchverlag Leipzig, 2006 (in German).
168. Caceres, C.B., Uliana, L., Henrandez, R.E.: Orthogonal cutting study of wood and knots of white spruce, *Wood and Fiber Science*, vol. 50 (1), (2018), pp. 55-65. <https://doi.org/10.22382/wfs-2018-006>
169. EN 12699:2015. Execution of special geotechnical works – Displacement piles. European Committee for Standardization (CEN), Brussels, Belgium (2015)
170. Fellenius, B: Static tests on instrumented piles affected by residual load. *DFI Journal: The Journal of the Deep Foundations Institute*, Vol. 9 (1), (2015). <https://doi.org/10.1179/1937525515Y.0000000001>.
171. Bengt, H., Fellenius, B.: Determining the true distributions of load in instrumented piles. *Deep Foundations*, (2002), 1455-1470. [https://doi.org/10.1061/40601\(256\)104](https://doi.org/10.1061/40601(256)104).
172. Green, D.W.; Gorman, T.M.; Evans, J.W.; Murphy, J.F. Mechanical Grading of Round Timber Beams. *J. Mater. Civ. Eng.* 2006, 18, 1–10.
173. Fernández-Golfín, J.I.; Díez Barra, M.R.; Hermoso, E.; Mier, R. Mechanical Characterization of Visually Classified, Small-Diameter Laricio Pine Round Timber. *Span. J. Agric. Res.* 2007, 5, 304–311.
174. Vestøl, G.I.; Høibø, O. Bending Strength and Modulus of Elasticity of *Pinus Sylvestris* Round Timber from Southern Norway. *Scand. J. For. Res.* 2010, 25, 185–195.
175. Morgado, T.F.; Dias, A.M.; Machado, J.S.; Negrão, J.H.; Marques, A.F. Grading of Portuguese Maritime Pine Small-Diameter Roundwood. *J. Mater. Civ. Eng.* 2017, 29, 04016209.
176. Aira, J.R.; Villanueva, J.L.; Lafuente, E. Visual and Machine Grading of Small Diameter Machined Round *Pinus Sylvestris* and *Pinus Nigra* Subsp. *Salzmannii* Wood from Mature Spanish Forests. *Mater. Struct.* 2019, 52, 32.
177. Vega, A.; González, L.; Fernández, I.; González, P. Grading and Mechanical Characterization of Small-Diameter Round Chestnut (*Castanea Sativa* Mill.) Timber from Thinning Operations. *Wood Mater. Sci. Eng.* 2019, 14, 81–87.
178. Green, D.W.; Gorman, T.M.; Evans, J.W.; Murphy, J.F. Improved Grading System for Structural Logs for Log Homes. *For. Prod. J.* 2004, 54, 52–62.
179. Vries de, P., Gard, W., (1998). The Development of a Strength Grading System for Small Diameter Roundwood. *Heron* 1998, 43, 183–198.
180. Johnson, R. A. & Wichern, D. W. (2013). *Applied multivariate statistical analysis: Pearson new international edition*. Pearson Education Limited, London, England. ISBN: 978-1-292-02494-3.

181. Sellin, A., Sapwood amount in *Picea Abies* (L.) Karst. Determined by tree age and radial growth rate. *Holzforschung* 50, 291-296, 1996.
182. Kolmogorov, A.N. (1933) *Foundations of Probability Theory*. Julius Springer, Berlin.
183. Milliken J.S., Johnson D.E., (1984) *The t-test: A Statistical Method for Testing the Significance of Differences*. Journal of Educational and Behavioral Statistics, 1984.
184. Mirra, M., Pagella, G., Lee, M., Gard, W., Ravenshorst, G., van de Kuilen, G.J.W. (2024). Characterisation of bacterial decay effects on wooden foundation piles across various historical periods, ISSN 0950-0618, *Constr. Build. Mater.* Volume 421 2024, 135670, <https://doi.org/10.1016/j.conbuildmat.2024.135670>.
185. Pagella, G., Ravenshorst, G., Mirra, M., Gard, W., van de Kuilen, J. W. (2024). Innovative application of micro-drilling for the assessment of decay and remaining mechanical properties of historic wooden foundation piles in Amsterdam, ISSN 2666-1659, *Dev. Built Environ.* Volume 19 2024, 100514, <https://doi.org/10.1016/j.dibe.2024.100514>.
186. Beketova-Hummel, Olga; Beketova-Hummel, <https://orcid.org/> (2021): MicroDrill (.rgp) file processing / Version 1. Version 1. 4TU.ResearchData. software. <https://doi.org/10.4121/16896394.v1>
187. Ravenshorst, G.J.P. (2023). Overdracht brief broncode Softshell Calculator TU Delft aan gemeente Amsterdam. (in Dutch). Report TUD-20230303-GR
188. Roy, A. Ravenshorst, G.J.P. Gard, W.F., van de Kuilen, J.W.G. (2021). Handleiding Soft Shell Calculator TU Delft versie 0.1. (in Dutch). Report TUD-F.RPD.4-20211208-AR-v1
189. Mirra, M., Ravenshorst, G.J.P., Gard, W.F., van de Kuilen, J.W.G. (2022). Investigation into the application of micro-drilling (RPD) measurements as replacements of drill cores extractions in determining the soft shell according to the Amsterdam method. Report TUD-FRPD.5-20230308-MM-v4. Delft University of Technology

Appendix A

Regression analysis for visual grading

A1 Introduction to regression analysis

The most influencing visually-graded properties on the saturated compressive strength ($f_{c,0,wet}$) of “new” spruce and pine piles were used to calculate one or several Indicating Properties “IP” (see A2) by means of multiple linear regression defined in Equation A 1.1. A set of known dependent variables (i.e. a set of values of $f_{c,0,wet}$) and predictor variables (i.e. determined visually-graded properties) z_1, z_2, \dots, z_m , were then used to estimate the regression coefficients ($\hat{\beta}_m$). Regression analysis was adopted to evaluate the statistical relationship between a set of known dependent and independent variables. When only one predictor variable is applied, a single regression analysis in Equation A1.2 (or simple regression analysis) is carried out in the regression model. When multiple predictor variable are used, a multiple regression analysis is used.

$$\hat{y}_j = \hat{\beta}_0 + \hat{\beta}_1 z_{j1} + \hat{\beta}_2 z_{j2} + \dots + \hat{\beta}_m z_{jm} \quad (A\ 1.1)$$

$$\hat{y}_j = \hat{\beta}_0 + \hat{\beta}_1 z_{j1} \quad (A\ 1.2)$$

The quality of a linear regression model is evaluated with coefficient of determination in Equation A1.2, as the explained variation (or difference between the sum of square regression, SSR), and the total variation (sum of squares total, SST).

$$R^2 = \frac{SSR}{SST} = \frac{\sum_{i=1}^n (\hat{y}_j - \bar{y})^2}{\sum_{i=1}^n (y_j - \bar{y})^2} \quad (A\ 1.3)$$

Where:

\bar{y} = the arithmetic mean of the set of known dependent variables.

R^2 = the proportion of the variance in the dependent variable explained by means of the predictor variable(s) between 0 and 1. $R^2 = 0$ means no linear relationship between predictor and dependent variables).

Since R^2 tends to increase as the number of predictor variables in a model increases, even when the additional variables do not actually enhance the accuracy of the model, an adjusted coefficient of determination (R^2_{adj}) is always reported, calculated in Equation A1.4.

$$R^2_{adj} = \frac{(1-R^2)(n-1)}{n-m-1} \quad (A\ 1.4)$$

Where :

n = number of observation.

m = number of predictor variables.

The accuracy of the prediction model is defined by the standard error of estimate (*SEE*), which is calculated in Equation A1.5 as:

$$SEE = \sqrt{\frac{\sum_{i=1}^n (y_i - \hat{y}_i)^2}{n-2}} \quad (\text{A } 1.5)$$

Finally, the F-value (Eq. A1.6) was used to test the null hypothesis that the model has no statistical significance in explaining the dependent variable. Meaning that a higher F-value indicates a greater likelihood that the model is statistically useful. A general rule is that if $F > 2.5$, the null hypothesis can be rejected, suggesting that at least one parameter value is not zero.

$$F = \frac{R^2 / (m-1)}{(1-R^2) / (n-m)} \quad (\text{A } 1.6)$$

A2 Indicating Properties (IPs)

An IP can be visually-graded property of a spruce or pine pile such as: Knot-Ratio (KR), number of annual rings (Age) or rate of growth (RoG). Determined visual grade properties, such as those just mentioned, can also be applied as predictor variables in multiple linear regression to define an IP.

Each grade has its Grade Determining Properties (GDPs), which for timber piles studied in this work include only saturated compressive strength parallel to the grain ($f_{c,0,wet}$). A set of known dependent variables (i.e. a set of values of $f_{c,0,wet}$) and predictor variables (i.e. determined visually-graded properties) are then used to estimate the regression coefficients by, for example, the least square method (Section A1).

Using the obtained regression equation and a pile set of visually-graded properties, it is possible to predict the compressive strength value of the pile as in Equation A1.4. A multiple linear regression can be used to combine different IPs (such as KR, Age and RoG), where the IP is calculated using the regression equation based on the estimated regression coefficients (carried out in Section 4.5.1).

In alternative, a linear regression can be used with only one IP, which is directly correlated to $f_{c,0,wet}$. In this case the grading is based on individual IPs and their direct correlation with $f_{c,0,wet}$ (Section 4.5.2).

A3 Determination of characteristic values based on IP limits

The strength grading of saturated spruce and pine piles is carried out by choosing IP limits such that minimum requirements of characteristic values of the GDP ($f_{c,0,wet}$) are fulfilled when piles with IPs exceeding the determined limits are assigned to a graded class.

Once an IP limit is chosen (Figure A1.1) the characteristic compressive strength below that limit is calculated with the parametric method according to EN 14358 2016. The calculation is based on Parametric Tolerance Limit (PTL) approach. PTL is defined as the value for which, with a probability of α (confidence level), the $p\%$ fractile of the underlying population is higher than this value. The approach works with the assumption that the population of data is normally distributed, denoted as m_1, m_2, \dots, m_n . The n test values constitute the sample. For the calculation of the saturated characteristic compressive strength of the piles PTL ($f_{c,0,k,wet}$), a confidence level $p = 5\%$ is considered, resulting in

Appendix A

Equation A1.10. For calculation, the standard deviation S_y (Eq. A1.12) has to be multiplied by a factor $k(n)$ in Equation A1.13 (the confidence level factor) and subtracted from the mean value \bar{y} (Eq. A1.11).

$$PTL(f_{c,0,k}) = \bar{y} - k(n) * s_y \quad (A.1.7)$$

$$\bar{y} = \frac{1}{n} \sum_{i=1}^n m_i \quad (A.1.8)$$

$$s_y = \sqrt{\frac{1}{n-1} \sum_{i=1}^n (m_i - \bar{y})^2} \quad (A.1.9)$$

$$k(n) = u_{1-p} + \frac{u_\alpha}{\sqrt{n}} \quad (A.1.10)$$

Where:

u_{1-p} is the $(1 - p)$ percentile of the standardised normal distribution function ($p = 5\%$ shall be assumed).

u_α is the α -percentile of the standardised normal distribution function ($\alpha = 75\%$ shall be assumed).

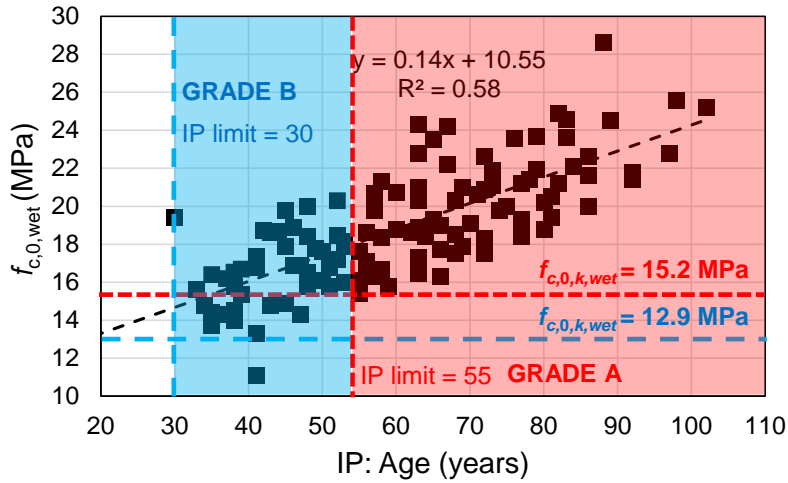


Figure A1.1: Example of determination of two characteristic compressive strength values for visual grading (Age) and possible two grading classes A and B.

A4 Regression analysis statistics

In this section, an overview is provided of the important statistics for performing regression analysis. This is not intended to be a complete listing of the required analysis and evaluate metrics, but these will serve as an appropriate starting place for the analyses.

K-S Test for normality

The Kolmogorov-Smirnov test (K-S test) [182] is used to test the null hypothesis that a set of data comes from a normal distribution, as one of the most widely used methods to test the normality of homogeneous data. The K-S test produces test statistics that are used (along with a degrees of freedom parameter) to test for normality, i.e. to test the null hypothesis that a set of data comes from a normal distribution. It is based on the empirical distribution function (ECDF). Given n -ordered data points Y_1, Y_2, \dots, Y_N , the ECD is define in Equation A 1.14.

$$E_N = n(i)/N \quad (\text{A 1.11})$$

where $n(i)$ is the number of points less than Y_i and the Y_i are ordered from smallest to largest value. This is a step function that increases by $1/N$ at the value of each ordered data point.

The graph below (Figure A.1) is an example of a plot of the empirical distribution function with a normal cumulative distribution function for 100 normal random numbers. The K-S test is based on the maximum distance between these two curves.

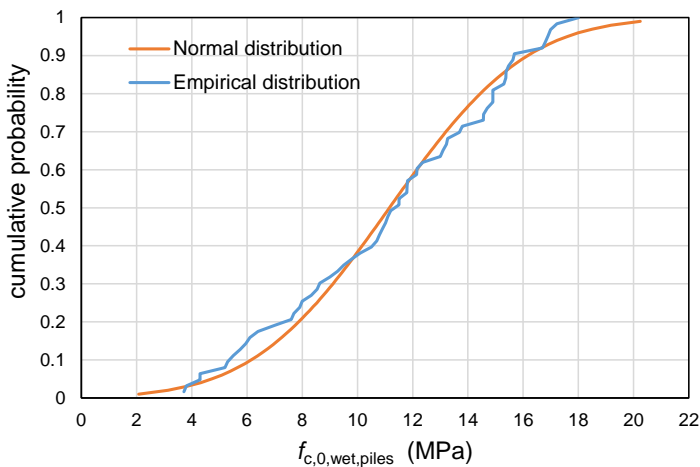


Figure A.1: examples of cumulative distribution for the $f_{c,0,wet}$ of 65 historical spruce pile segments

The K-S test is defined by:

Null hypothesis (H_0): The data follow a specified distribution.

Alternative hypothesis (H_a): The data do not follow the specified distribution.

The K-S test statistic is defined in Equation A1.15.

$$D = \max_{1 \leq i \leq N} \left(F(Y_i) - \frac{i-1}{N}, \frac{i}{N} - F(Y_i) \right) \quad (\text{A } 1.12)$$

where F is the theoretical cumulative distribution of the distribution being tested which must be a continuous and homogeneous distribution. The hypothesis regarding the distributional form is rejected if the test statistic (D) is greater than the critical value obtained from the K-S table [182]. The critical values vary depending on the chosen significance level α . For the datasets studied in this work, a significance level $\alpha = 0.05$ was always chosen.

In order to validate whether the datasets are normally distributed the K-S test was conducted on the mean wet compressive strength ($f_{c,0,wet,mean}$) of the pile segments. The K-S test was applied to the all datasets. The results obtained from the mechanical testing were subdivided depending on the categories:

- ND, D, DL and DL-1 for “new” piles, the two different populations (spruce and pine) and the different pile parts (head, middle-part and tip).
- 1922, 1886 and 1727 for historical piles, the two different populations (spruce and fir) and the different pile parts (head, middle-part and tip).

t-Test

On this basis of the mean wet compressive strength ($f_{c,0,wet,mean}$), each category of pile was compared, in order to test that the difference among mean values of different groups was significant. To this end, a t-test was conducted, a statistical test that is used to compare the means of two groups, to understand if the difference between the means is significant or due to chance [182],[183]. When more than two groups are compared (multiple comparisons), an ANOVA test or a post-hoc test are needed.

The t-test assumes that the data:

- are independent;
- are normally distributed;
- have a similar amount of variance (the square of standard deviation of a mean value) within each group being compared (i.e. homogeneity of variance).

If the dataset does not match with the aforementioned assumptions, a nonparametric test has to be adopted, such as the Wilcoxon Signed-Rank test for data with unequal variances [182].

In this report two-sample t-test (independent test) was conducted, to compare groups (e.g., two different building years) and to investigate if the groups could be associated to one population. For that, a one-tailed t-test was adopted, searching whether one population mean is significant greater than or less than the other to be regarded coming from the same population.

The following formula A1.16 was used for the two-sample *t*-test (a.k.a. the Student’s *t*-test) for equal variances to calculate the *t*-value.

$$t = \frac{\bar{x}_1 - \bar{x}_2}{s \sqrt{\frac{1}{n_1} + \frac{1}{n_2}}} \quad (\text{A } 1.13)$$

where: t is the t -value; \bar{x}_1 and \bar{x}_2 are the means of the two groups; s is the pooled standard deviation of the two groups; n_1 and n_2 are the number of observations in each group.

The calculated t -value was compared to the t -critical value, in the one-tailed critical value chart (Student's t table) [183], for a significance level $\alpha = 0.05$, to determine whether the t -value is greater than what would be expected by chance. If so, it means that the difference between the means of the two samples is significant.

p -value

The p -value was also calculated, as the statistical measure that determines the level of significance of the difference between the means of two samples, describing the probability of obtaining a t -value as large as, or larger than, the one calculated from the samples data, assuming that the null hypothesis is true. The p -value was calculated for significance level $\alpha = 0.05$. This is the range of numbers within which the true difference in means will fall 95% of the time.

Appendix B

Results of the material and mechanical characterization of “new” wooden piles

B1 Results from the compression tests

The results from the compression tests of representative “new” wooden piles are presented for 3 spruce (*Picea abies*) – Figures B1-3 – and 3 pine (*Pinus sylvestris*) piles – Figures B4-6. Head, middle-part and tip of the piles were tested according to Section 3.6. The following Figures B1-6 represent the tested segment, the force-displacement curves measured by S-sensors attached to the compression machine, and by P-sensors attached to the pile.

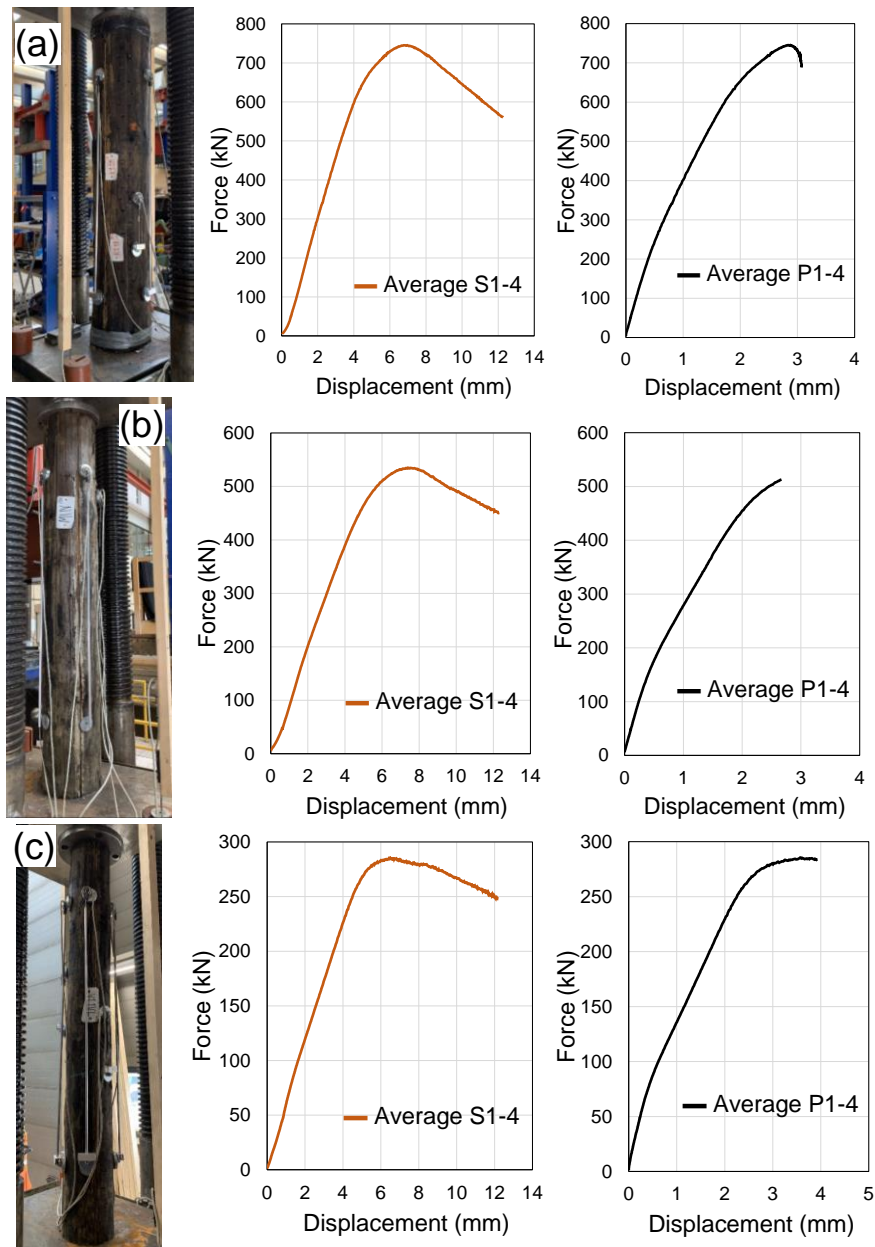


Figure B.1: Results from the compression test of "new" spruce (*Picea abies*) pile OAM P1.1: (a) head; (b) middle-part; (c) tip.

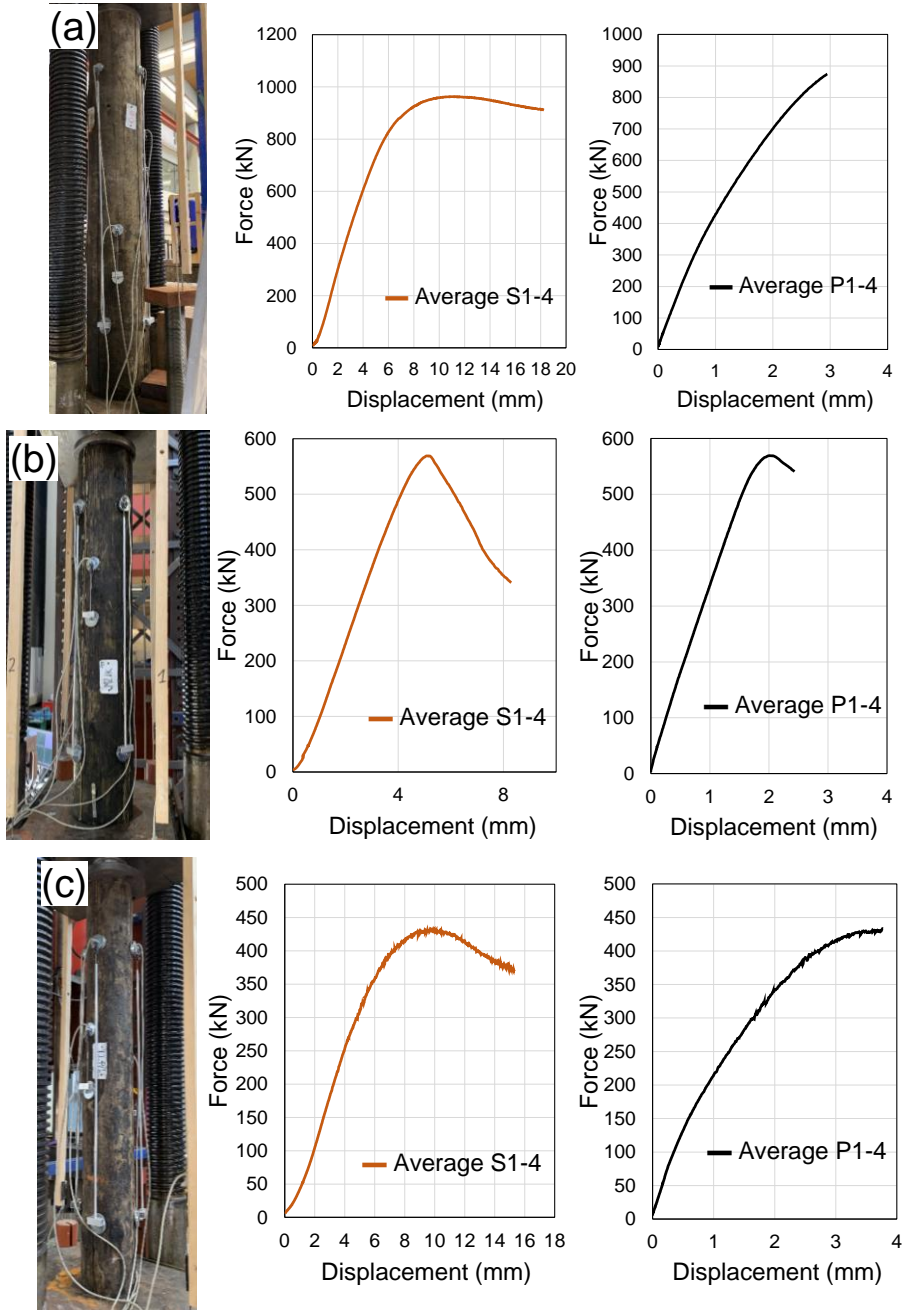


Figure B. 2: Results from the compression test of "new" spruce (*Picea abies*) pile OAM P1.4: (a) head; (b) middle-part; (c) tip.

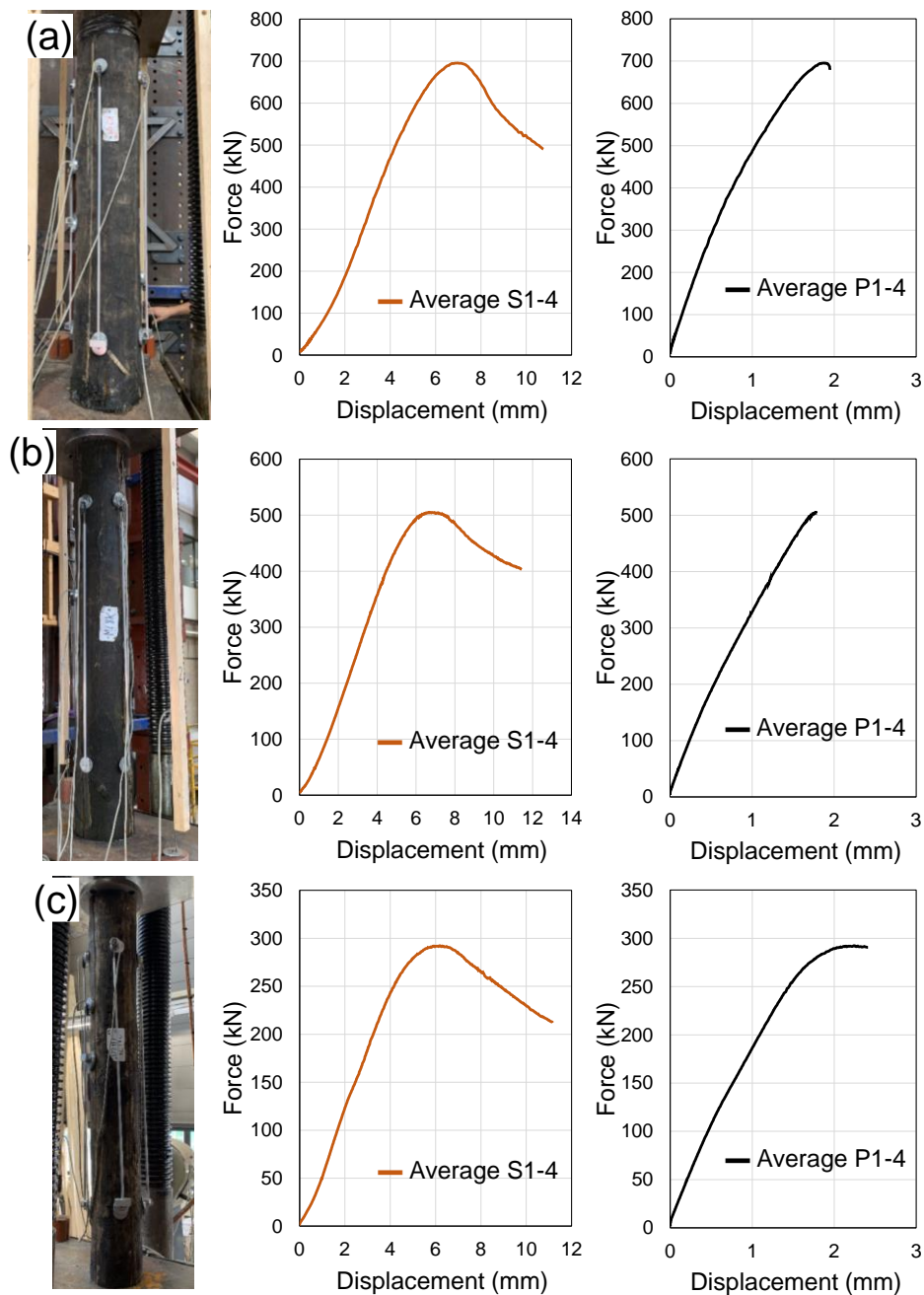


Figure B. 3: Results from the compression test of "new" spruce (*Picea abies*) pile OAMP2.1: (a) head; (b) middle-part; (c) tip.

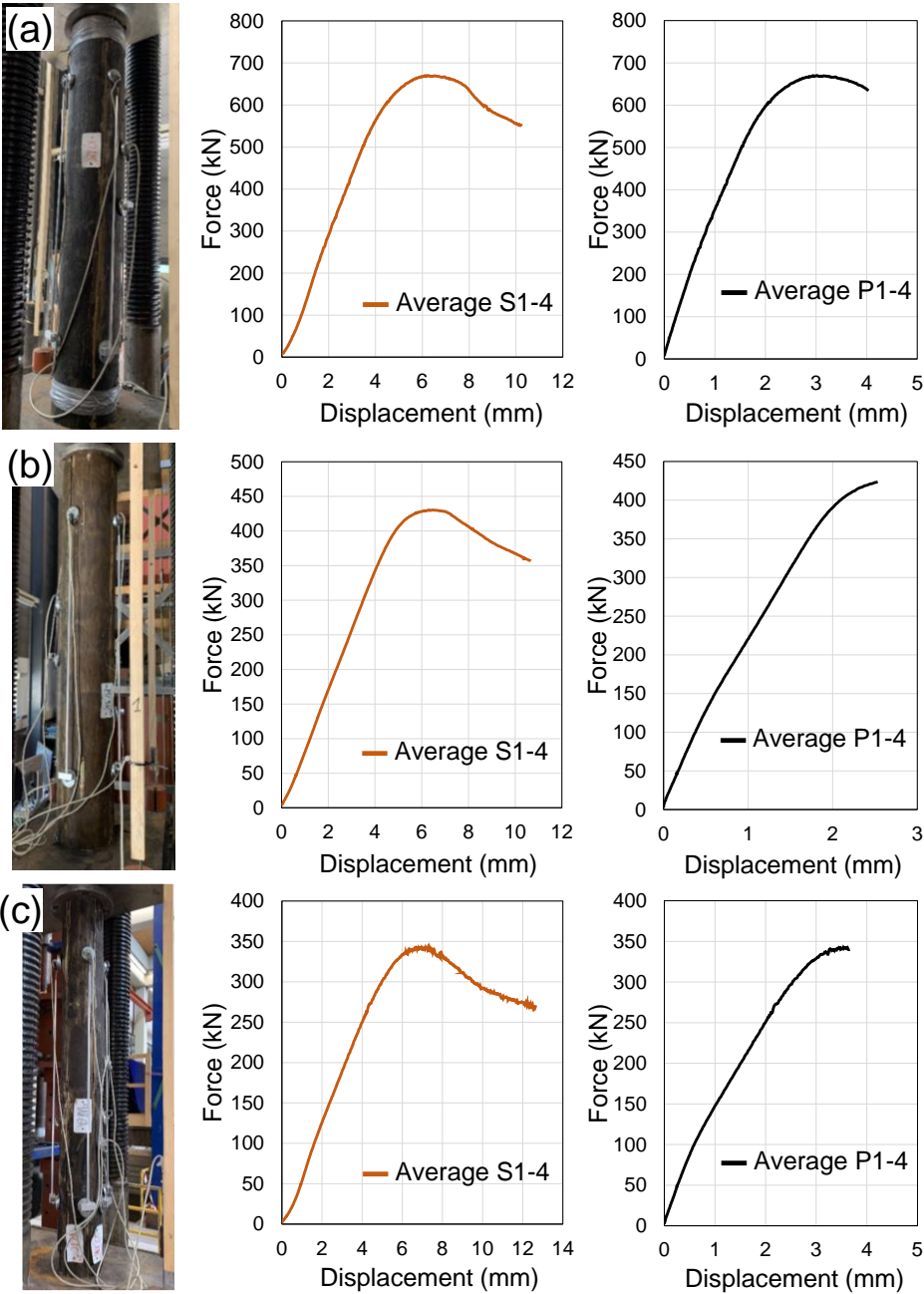


Figure B. 4: Results from the compression test of "new" pine (*Pinus sylvestris*) pile OAM P2.8: (a) head; (b) middle-part; (c) tip.

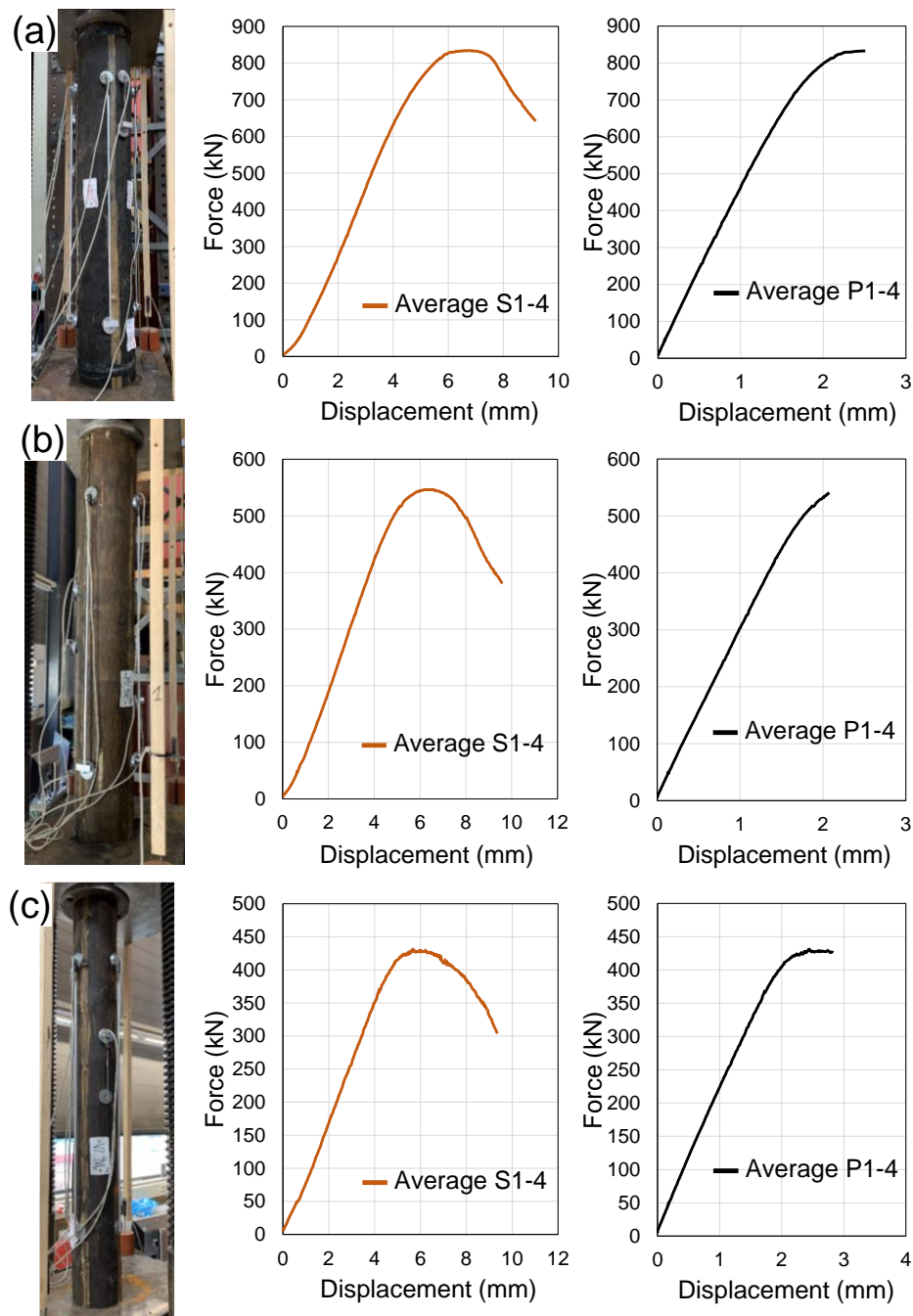


Figure B. 5: Results from the compression test of "new" pine (*Pinus sylvestris*) pile OAM P2.9: (a) head; (b) middle-part; (c) tip.

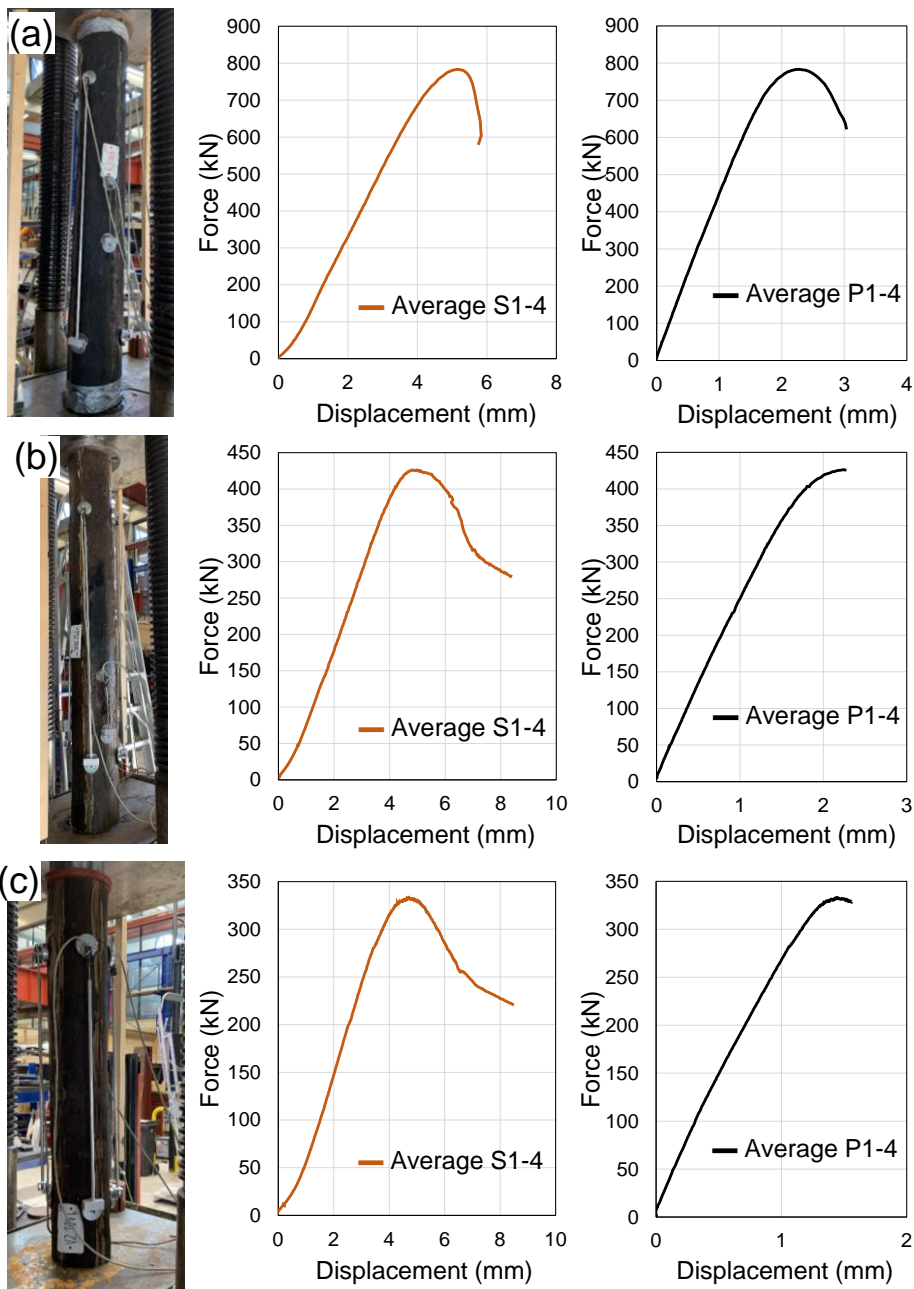


Figure B. 6: Results from the compression test of "new" pine (*Pinus sylvestris*) pile OAM P2.10: (a) head; (b) middle-part; (c) tip.

B2 Test for normality of all categories of “new” spruce and pine piles

The normality of all the categories (ND, D, DL, DL-1) of “new” spruce and pine piles was validated and presented in Table B. 1. All the categories were normally distributed according to Section A4.

Table B. 2 reports the normality test for all piles grouped in 1 category. All the groups were normally distributed according to Section A4.

Table B. 1: K-S test for normality applied to the $f_{c,0,wet,mean}$ of all categories: a division in spruce and pine, and relative head, middle-part and tip of the full pile.

Categories	number of observations	$f_{c,0,wet,mean}$	SD	Variance	K-S test		
		MPa	MPa	(MPa) ²	max value	critical value	normality
All segments spruce + pine ND	145	18.3	3.0	8.93	0.063	0.113	yes
All segments spruce + pine D	26	16.7	2.6	6.78	0.121	0.266	yes
All segments spruce + pine DL	82	16.0	3.1	9.61	0.095	0.141	yes
All segments spruce DL-1	6	14.8	1.3	1.60	0.187	0.519	yes
All segments spruce ND	64	17.2	2.6	6.67	0.096	0.170	yes
All segments pine ND	81	19.1	3.0	9.28	0.084	0.151	yes
All segments spruce D	15	15.5	1.6	2.63	0.219	0.338	yes
All segments pine D	11	18.5	2.8	7.67	0.178	0.391	yes
All segments spruce DL	53	14.6	2.0	4.10	0.097	0.187	yes
All segments pine DL	40	18.5	3.2	10.13	0.075	0.215	yes
Spruce head ND	20	18.9	2.3	5.39	0.152	0.304	yes
Spruce middle ND	20	17.8	2.0	4.02	0.127	0.304	yes
Spruce tip ND	24	15.4	2.0	3.98	0.108	0.277	yes
Pine head ND	23	21.9	2.7	7.16	0.069	0.283	yes
Pine middle ND	25	19.4	2.5	6.10	0.095	0.264	yes
Pine tip ND	33	16.9	1.7	2.84	0.092	0.391	yes
Spruce head D	5	14.8	2.4	5.83	0.199	0.563	yes
Spruce middle D	5	16.6	1.0	0.93	0.206	0.563	yes
Spruce tip D	5	15.1	0.3	0.10	0.229	0.563	yes
Pine head D	4	21.0	1.0	1.04	0.198	0.624	yes
Pine middle D	4	18.0	2.0	4.06	0.218	0.624	yes
Pine tip D	3	15.7	2.6	6.51	0.189	0.708	yes
Spruce head DL	15	15.6	1.9	3.47	0.191	0.351	yes
Spruce middle DL	16	15.3	1.1	1.13	0.187	0.391	yes
Spruce tip DL	22	13.4	2.1	4.39	0.194	0.391	yes
Pine head DL	8	21.4	2.3	5.47	0.193	0.454	yes
Pine middle DL	8	18.9	2.1	4.49	0.129	0.454	yes
Pine tip DL	13	16.3	2.8	7.81	0.121	0.361	yes

Table B. 2: K-S test for normality applied to the $f_{c,0,wet,mean}$ of spruce and pine segments considering all in 1 category: a division in spruce and pine.

Categories	number of observations	$f_{c,0,wet,mean}$	SD	VarianceK-S test			
		MPa	MPa	(MPa) ²	max value	critical value	normality
<i>All categories: all segments spruce</i>	132	15.9	2.6	6.67	0.078	0.118	yes
<i>All categories: all segments pine</i>	121	18.8	3.1	9.31	0.062	0.123	yes
<i>All categories: spruce heads</i>	40	17.1	2.8	7.74	0.106	0.210	yes
<i>All categories: spruce middle-parts</i>	41	16.6	1.9	3.79	0.124	0.212	yes
<i>All categories: spruce tips</i>	51	14.4	2.1	4.59	0.090	0.190	yes
<i>All categories: pine heads</i>	35	21.6	2.4	5.97	0.085	0.230	yes
<i>All categories: pine middle-parts</i>	37	19.1	2.3	5.50	0.111	0.223	yes
<i>All categories: pine tips</i>	49	16.6	2.1	4.22	0.063	0.194	yes

B3 t-Test for significant difference in mean $f_{c,0,wet}$

Once the normality of the data is assumed (Table B.2), the t-test for the comparison of the $f_{c,0,wet,mean}$ was conducted for “new” spruce and pine piles divided in head, middle, and tip (Table B. 3). All the means were significantly different except for spruce heads and middle-parts, which were grouped in one category.

Table B. 3: t-Test for unequal variances ($\alpha = 0.05$) conducted on $f_{c,0,wet,mean}$

$f_{c,0,wet,mean}$ comparison	mean difference	t-test: one tail - unequal variances $\alpha = 0.05$					significance
	MPa	std err	t-stat	d.f.	p-value	t-crit	
<i>All categories spruce - pine</i>	-2.90	0.354	-8.126	236	1.25E-14	1.651	yes
<i>All categories spruce Head - Middle</i>	0.52	0.532	0.966	70	1.69E-01	1.667	no
<i>All categories spruce Head - Tip</i>	2.70	0.516	5.065	72	1.52E-06	1.666	yes
<i>All categories spruce Middle - Tip</i>	2.18	0.432	5.104	89	9.37E-07	1.662	yes
<i>All categories spruce Head - Middle</i>	2.54	0.564	4.503	69	1.33E-05	1.667	yes
<i>All categories spruce Head - Tip</i>	5.00	0.492	9.859	65	7.80E-15	1.669	yes
<i>All categories spruce Middle - Tip</i>	2.45	0.476	5.061	72	1.54E-06	1.666	yes
<i>All categories Head spruce - pine</i>	-4.50	0.609	-7.458	73	7.32E-11	1.666	yes
<i>All categories Middle spruce - pine</i>	-2.47	0.486	-5.036	70	1.78E-06	1.667	yes
<i>All categories Tip spruce - pine</i>	-2.20	0.420	-5.241	98	4.58E-07	1.661	yes

Appendix C

Results of mechanical characterization of historical wooden piles

C1 Results from the compression tests

The results from the compression tests of representative historical wooden piles are presented: 3 spruce piles from 1922 (Figure C.1-3); 2 fir from 1886 (Figure C.4-5); 2 spruce from 1886 (Figure C.6-7); 4 spruce from 1727 (Figure C.8-11). Head, middle-part and tip of the piles were tested according to Section 3.6, with different amount of decay (reported in the figure description).

The following Figures represent the picture of the tested segment, the force-displacement curves measured by the S-sensors attached to the compression machine, and by the P-sensors attached to the pile.

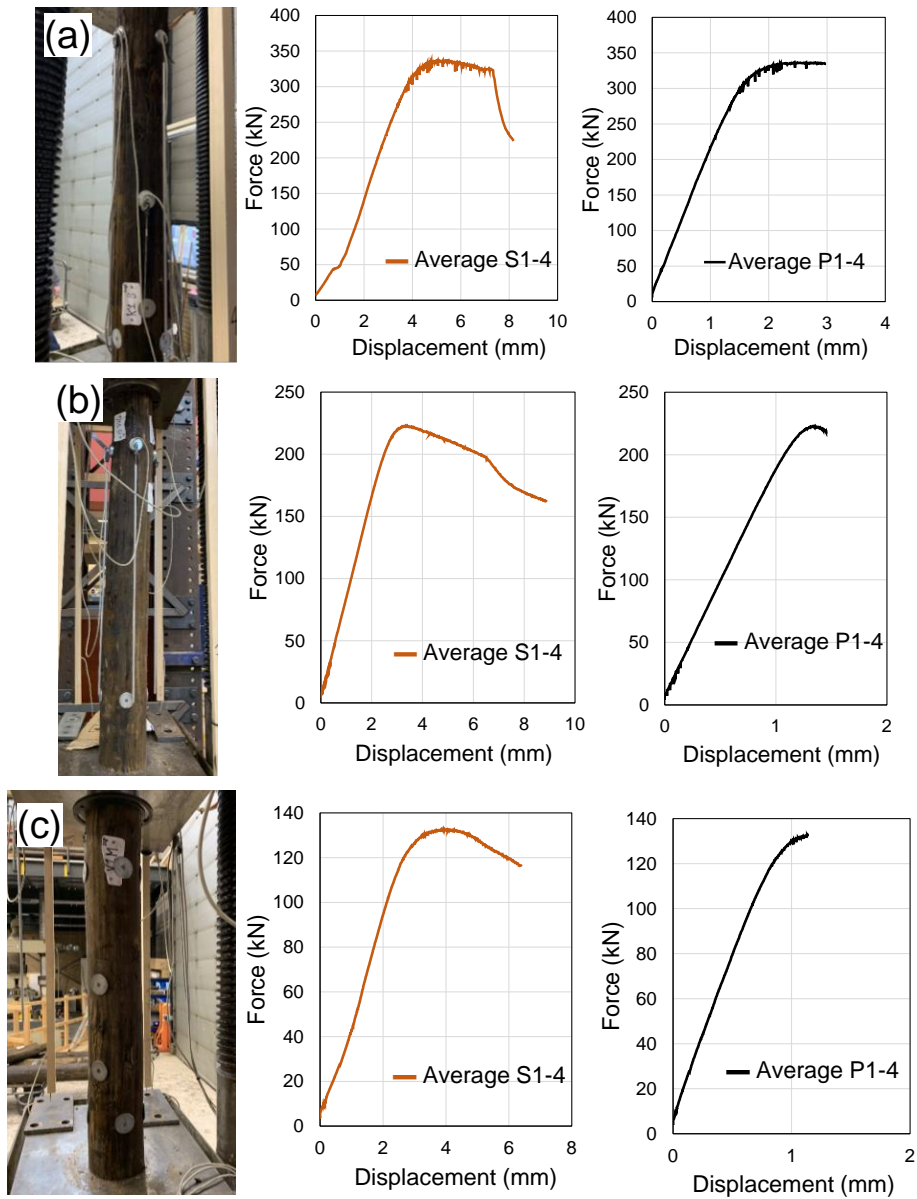


Figure C.1: Results from the compression test of spruce (Picea abies) pile BRU0041-PL1 P1.33 from 1922: (a) head, with $a_{ss} = 0$ mm, $A_{sound} = 100\%$; (b) middle-part with $a_{ss} = 0$ mm, $A_{sound} = 100\%$; (c) tip with $a_{ss} = 5.3$ mm, $A_{sound} = 89\%$.

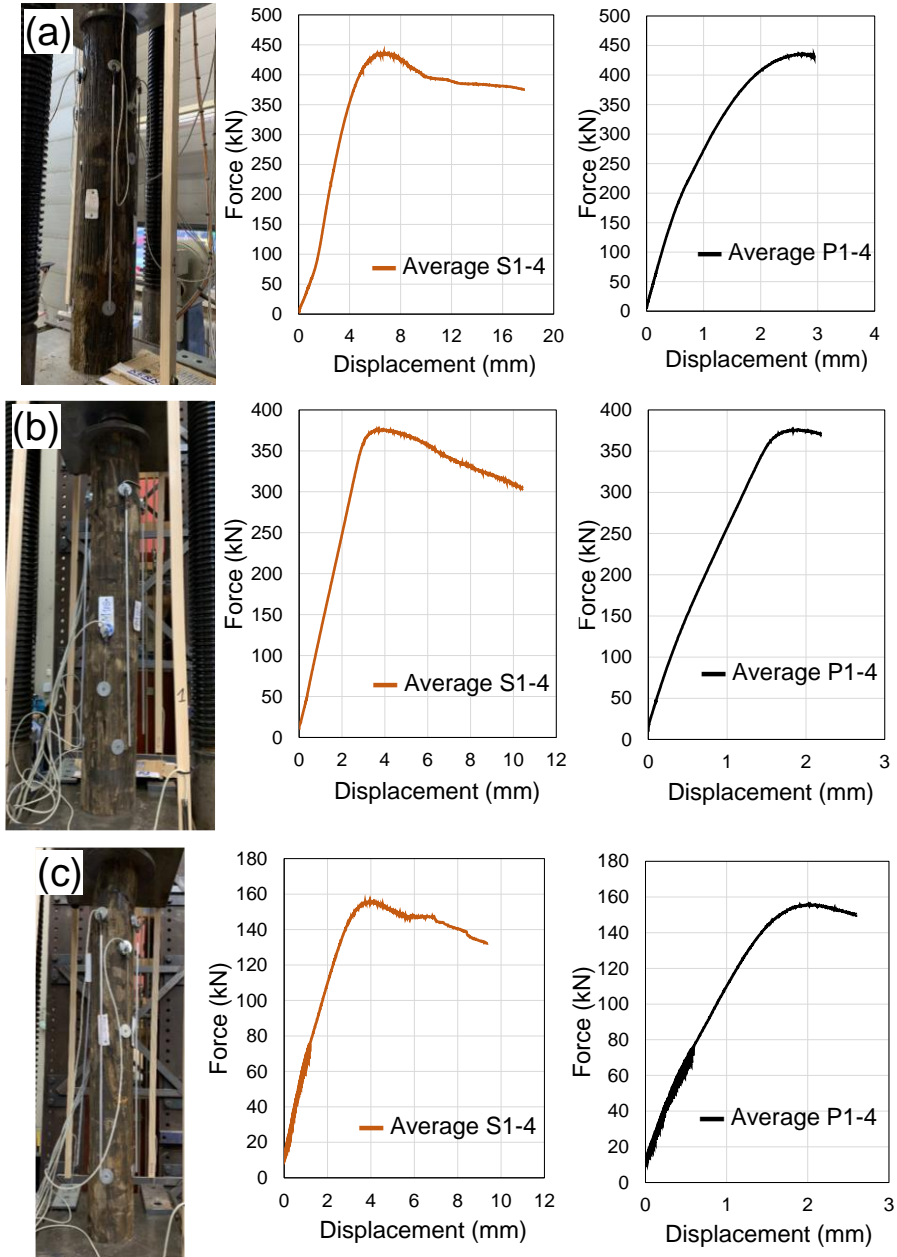


Figure C.2: Results from the compression test of spruce (*Picea abies*) pile BRU0041-PL2 P1.9 from 1922: (a) head, with $a_{SS} = 0$ mm, $A_{\text{sound}} = 100\%$; (b) middle-part with $a_{SS} = 0$ mm, $A_{\text{sound}} = 100\%$; (c) tip with $a_{SS} = 4.3$ mm, $A_{\text{sound}} = 90\%$.

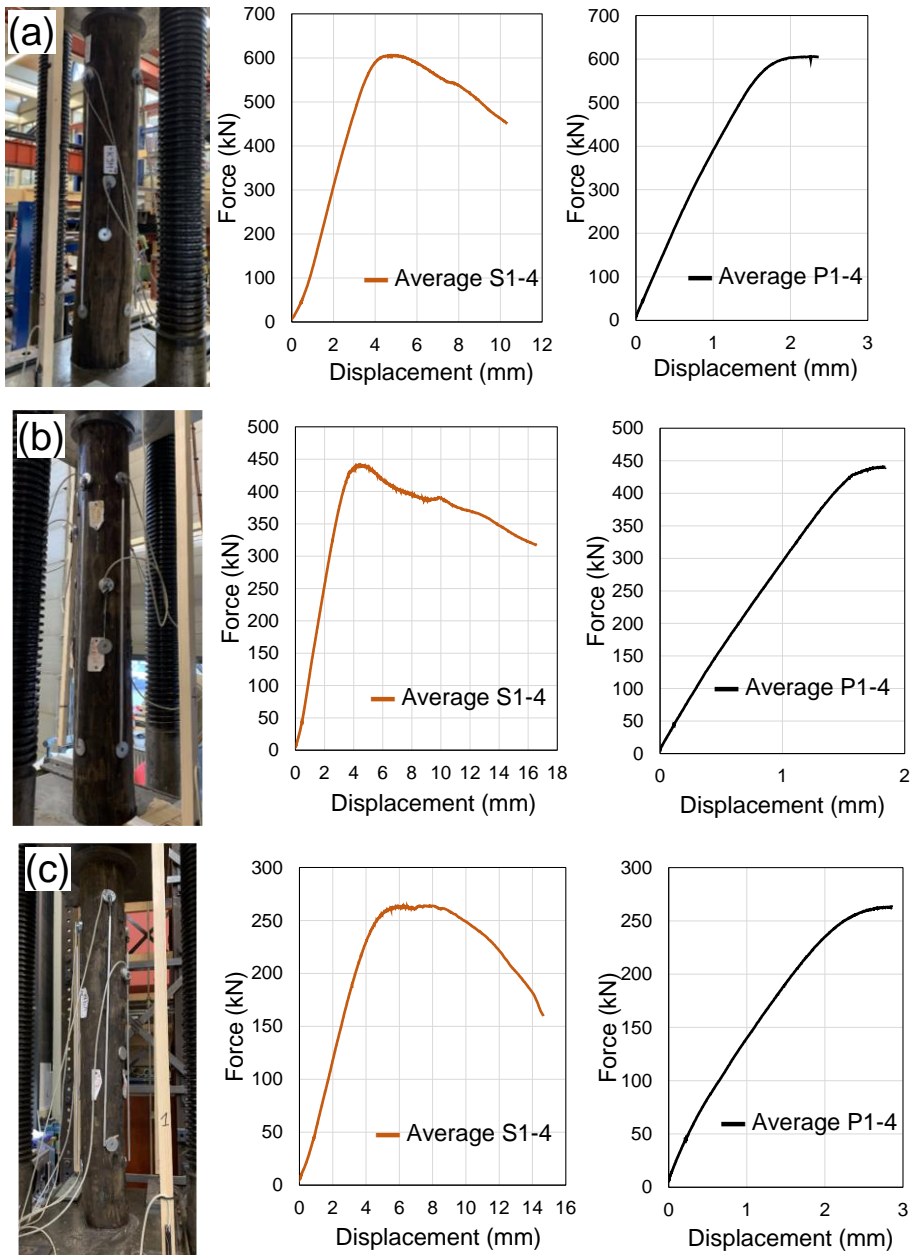


Figure C.3: Results from the compression test of spruce (*Picea abies*) pile BRU0041-PL2 P3.12 from 1922: (a) head, with $a_{SS} = 0$ mm, $A_{\text{sound}} = 100\%$; (b) middle-part with $a_{SS} = 0$ mm, $A_{\text{sound}} = 100\%$; (c) tip with $a_{SS} = 0$ mm, $A_{\text{sound}} = 100\%$.

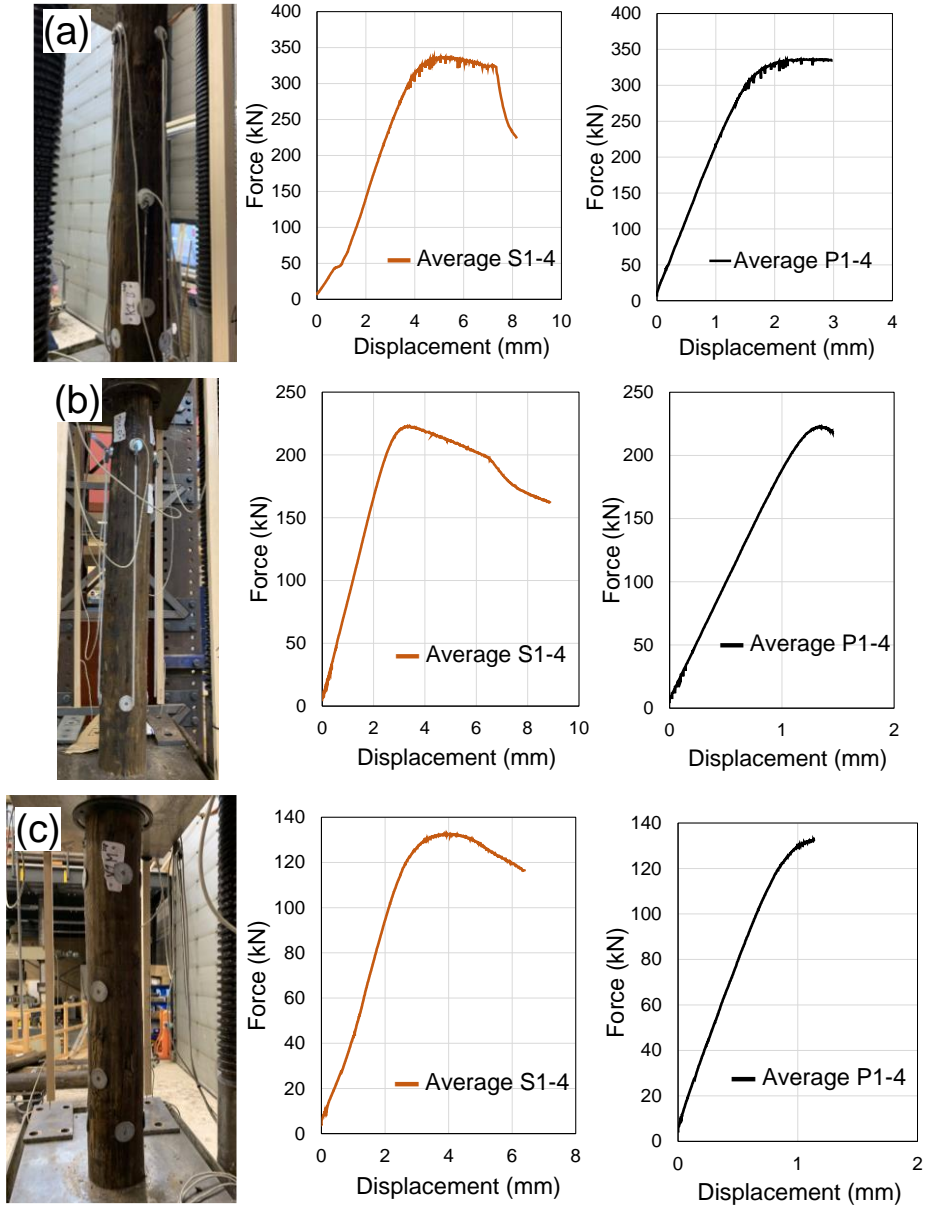


Figure C.4: Results from the compression test of fir (*Abies*) pile BRU0030-PL1 P3.2 from 1886: (a) head, with $a_{ss} = 3.0$ mm, $A_{sound} = 95\%$; (b) middle-part with $a_{ss} = 1.2$ mm, $A_{sound} = 97\%$; (c) tip with $a_{ss} = 1.1$ mm, $A_{sound} = 97\%$.

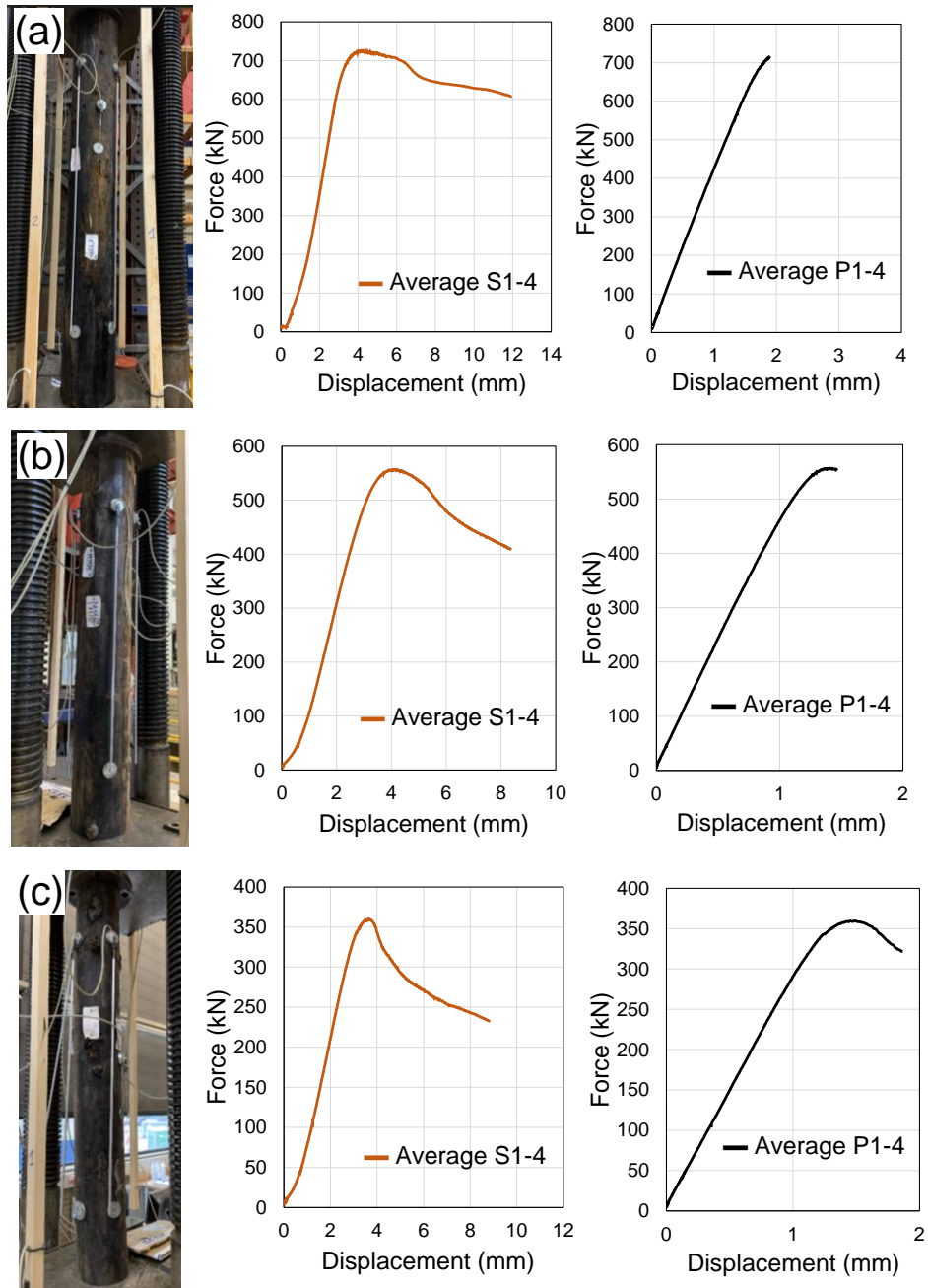


Figure C.5: Results from the compression test of fir (*Abies*) pile BRU0041-PL2 P1.24 from 1886: (a) head, with $a_{SS} = 0$ mm, $A_{sound} = 100\%$; (b) middle-part with $a_{SS} = 0$ mm, $A_{sound} = 100\%$; (c) tip with $a_{SS} = 7.0$ mm, $A_{sound} = 80\%$.

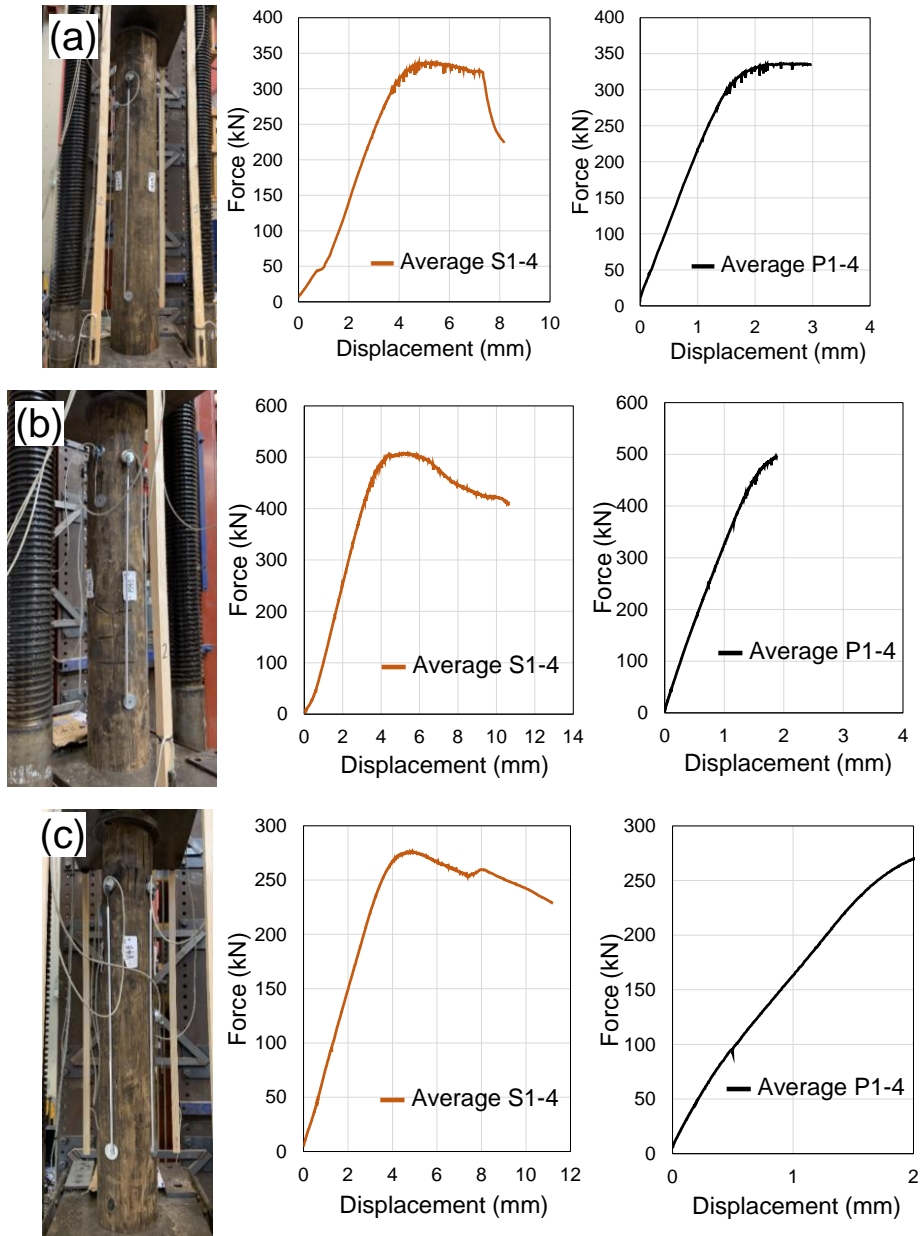


Figure C.6: Results from the compression test of spruce (*Picea abies*) pile BRU0030-PL1 P1.20 from 1886: (a) head, with $a_{SS} = 0$ mm, $A_{\text{sound}} = 100\%$; (b) middle-part with $a_{SS} = 0$ mm, $A_{\text{sound}} = 100\%$; (c) tip with $a_{SS} = 3.6$ mm, $A_{\text{sound}} = 93\%$.

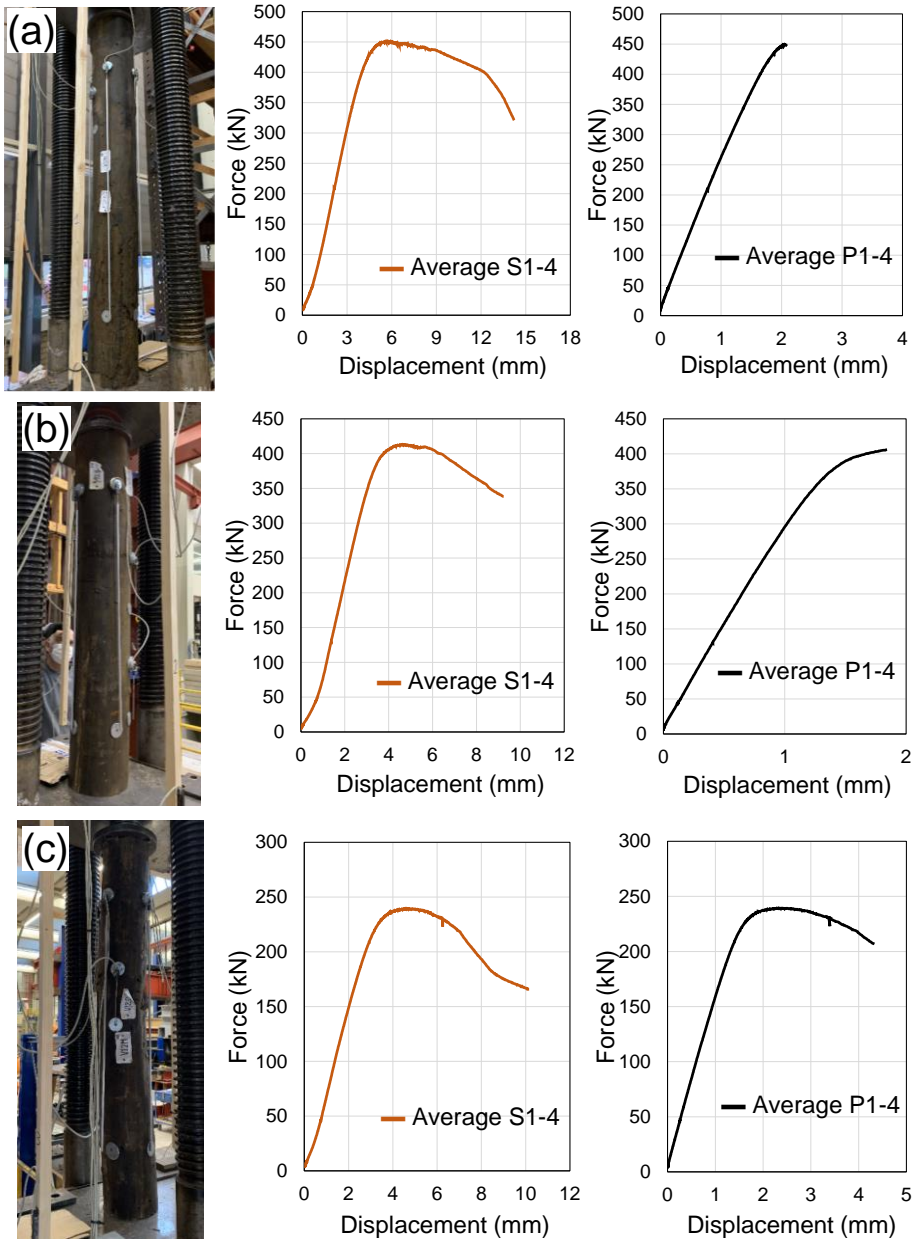


Figure C.7: Results from the compression test of spruce (*Picea abies*) pile BRU0030-PL1 P1.20 from 1886: (a) head, with $a_{SS} = 16.2$ mm, $A_{sound} = 74\%$; (b) middle-part with $a_{SS} = 15$ mm, $A_{sound} = 74\%$; (c) tip with $a_{SS} = 12.7$ mm, $A_{sound} = 75\%$.

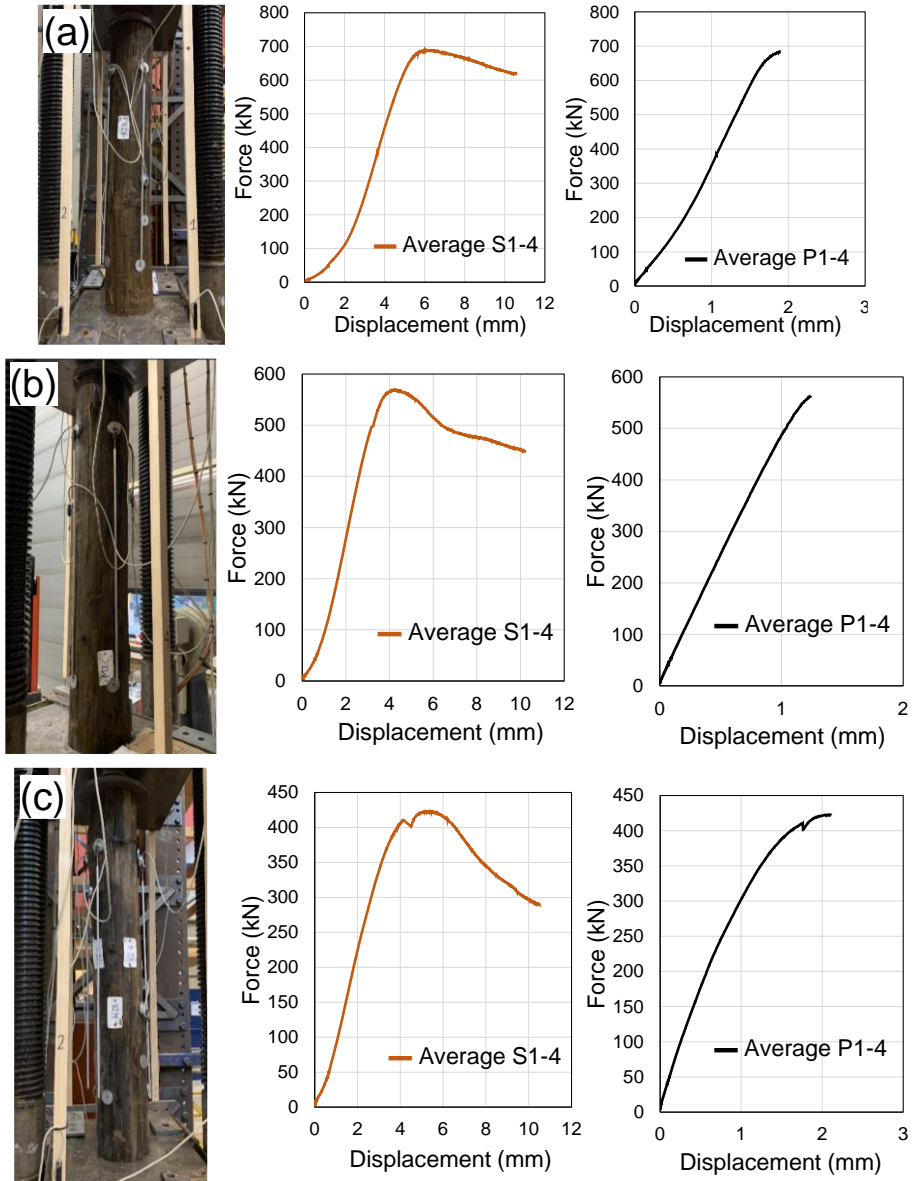


Figure C.8: Results from the compression test of spruce (*Picea abies*) pile BRU0030-PL1 P1.6 from 1727: (a) head, with $a_{SS} = 2.5$ mm, $A_{sound} = 97\%$; (b) middle-part with $a_{SS} = 0$ mm, $A_{sound} = 100\%$; (c) tip with $a_{SS} = 3$ mm, $A_{sound} = 94\%$.

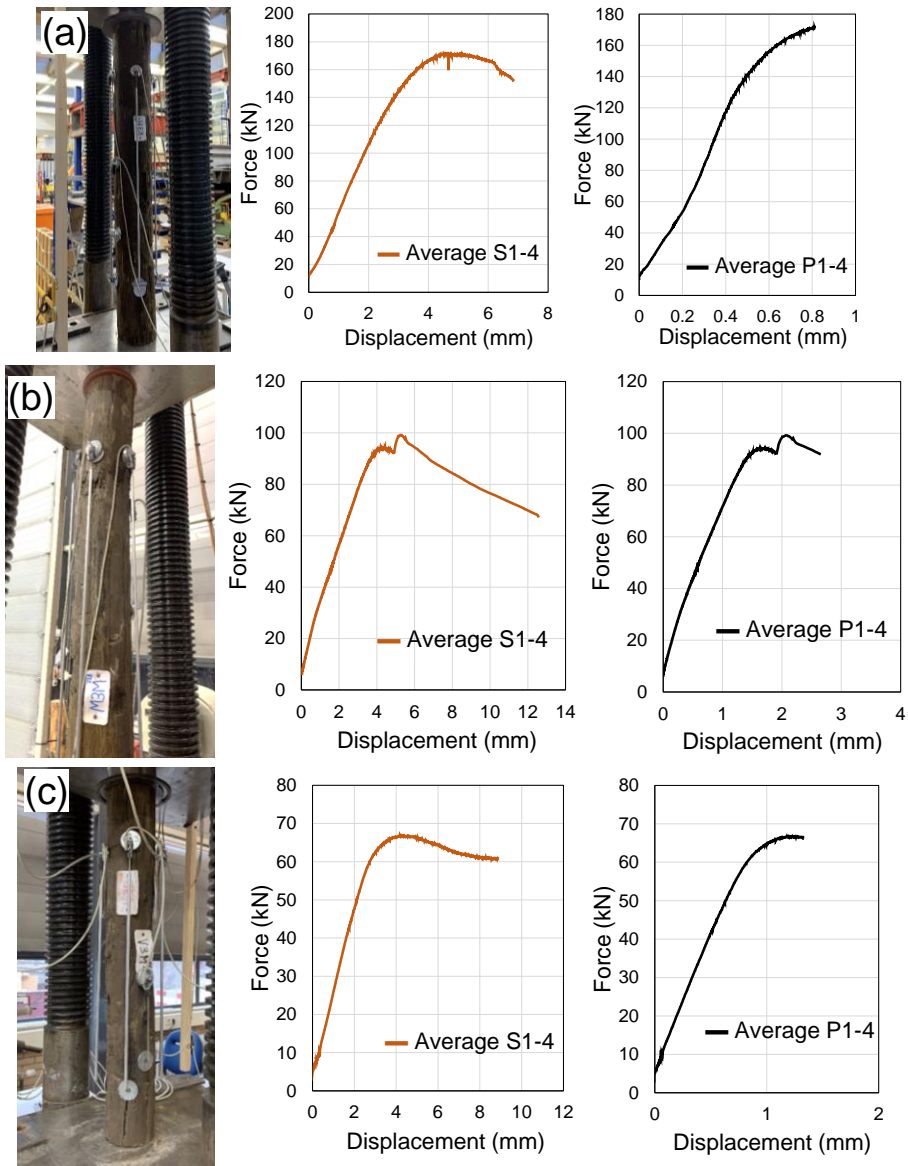


Figure C.9: Results from the compression test of spruce (*Picea abies*) pile BRU0030-PL1 P1.6 from 1727: (a) head, with $a_{ss} = 9.8$ mm, $A_{sound} = 79\%$; (b) middle-part with $a_{ss} = 23.5$ mm, $A_{sound} = 49\%$; (c) tip with $a_{ss} = 13.3$ mm, $A_{sound} = 64\%$.

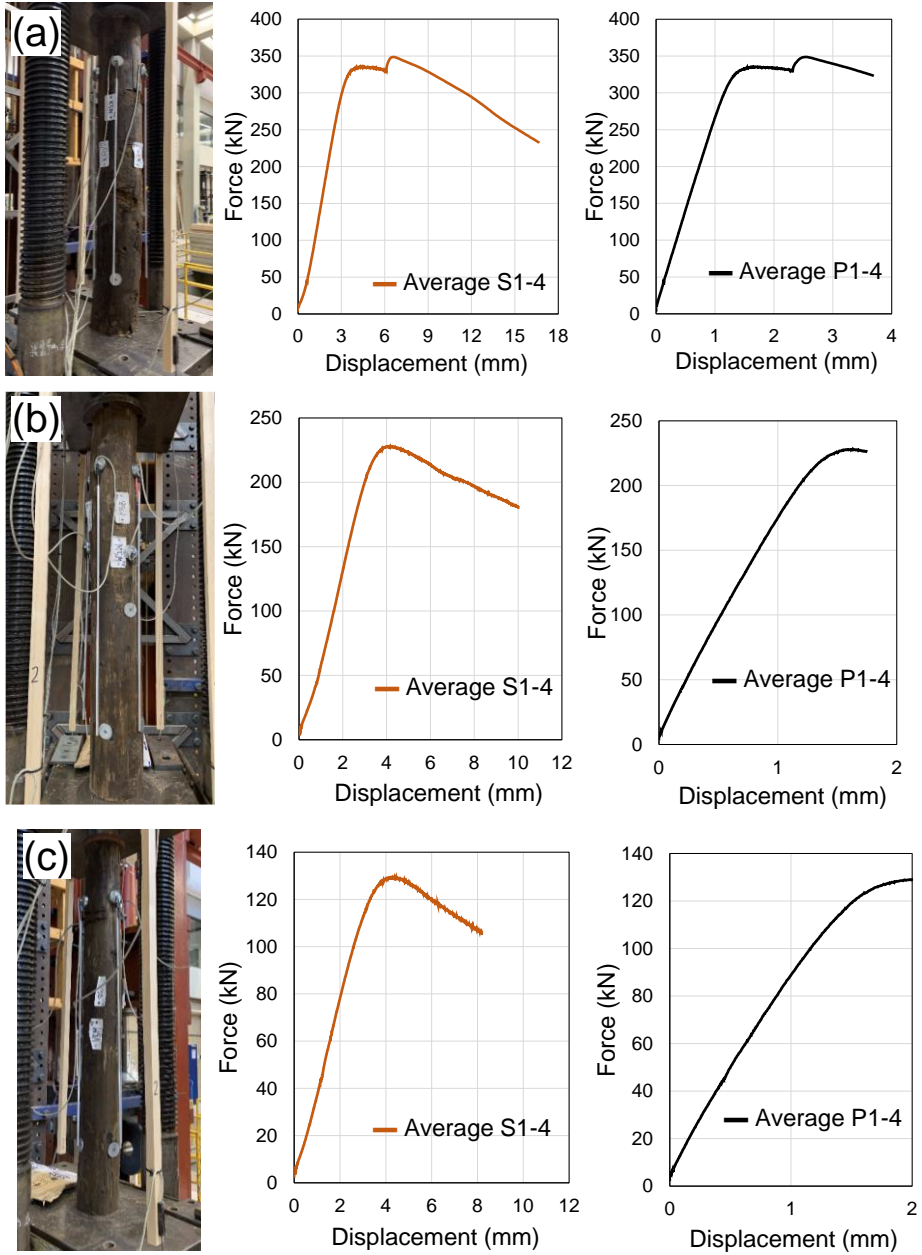


Figure C.10: Results from the compression test of spruce (*Picea abies*) pile BRU0030-PL2 P2.19 from 1727: (a) head, with $a_{ss} = 11.6$ mm, $A_{sound} = 78\%$; (b) middle-part with $a_{ss} = 12.0$ mm, $A_{sound} = 76\%$; (c) tip with $a_{ss} = 22.3$ mm, $A_{sound} = 49\%$.

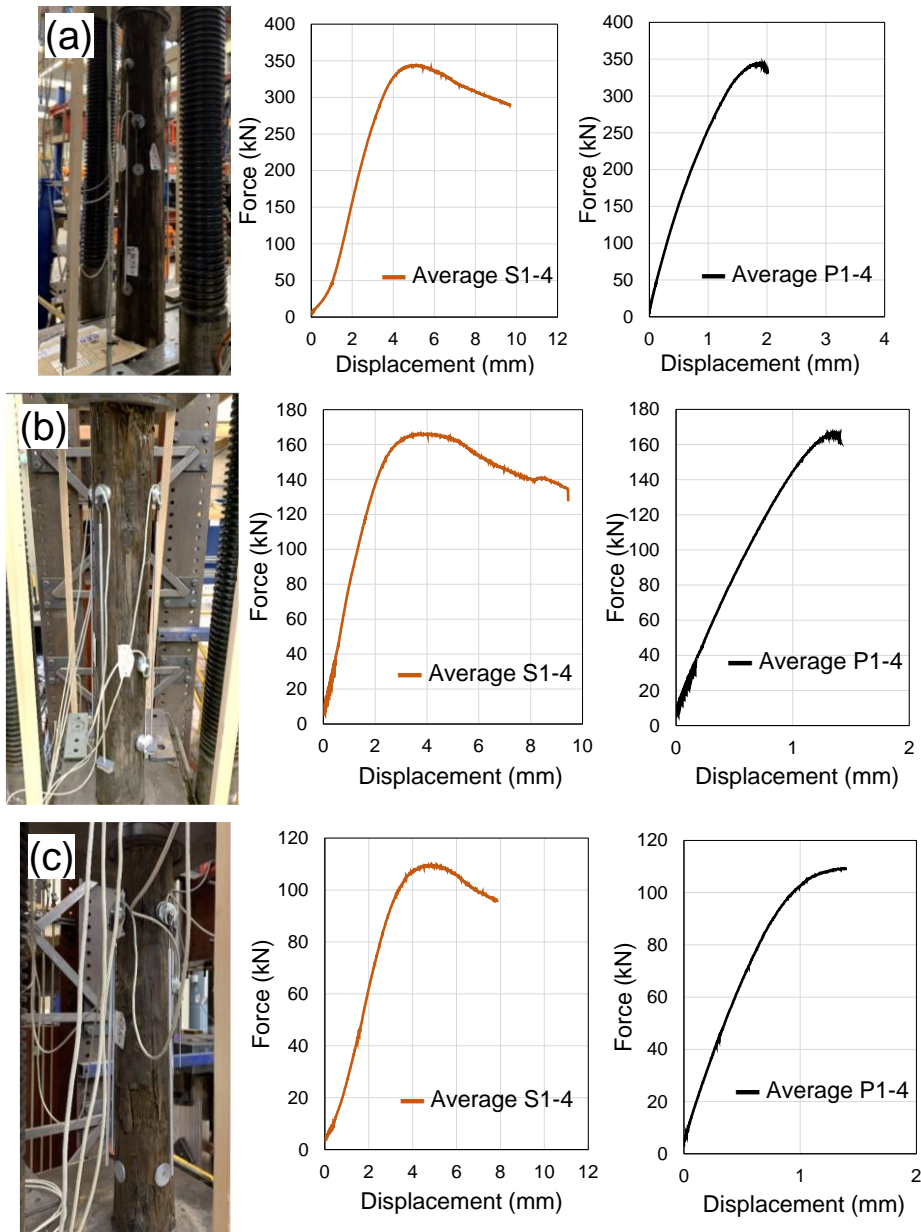


Figure C.11: Results from the compression test of spruce (*Picea abies*) pile BRU0030-PL2 P2.21 from 1727: (a) head, with $a_{ss} = 19.0$ mm, $A_{sound} = 65\%$; (b) middle-part with $a_{ss} = 26.0$ mm, $A_{sound} = 51\%$; (c) tip with $a_{ss} = 23.3$ mm, $A_{sound} = 46\%$.

C2 Test for normality of the pile categories

The normality of all the categories of historical spruce and fir piles was tested and presented in Table C.1. All the groups were normally distributed according to the K-S test (Section A4).

Table C.1: K-S test for normality applied to the $f_{c,0,wet,mean}$ Of all categories: a division in spruce and pine, and relative head, middle-part and tip of the full pile.

Categories	number of observations	$f_{c,0,wet,mean}$	SD	Variance	K-S test		Normality
		MPa	MPa	(MPa) ²	max value	critical value	
All segments	201	10.4	3.95	15.64	0.061	0.096	yes
Spruce	180	10.0	3.92	15.37	0.064	0.101	yes
Fir	21	13.6	2.56	6.54	0.161	0.296	yes
Spruce 1922	49	13.6	2.45	5.99	0.096	0.194	yes
Spruce 1886	56	13.1	2.34	5.45	0.074	0.181	yes
Spruce 1727	96	7.2	2.64	6.95	0.075	0.139	yes
Fir 1886	21	13.6	2.56	6.54	0.161	0.296	yes
Head 1727	30	7.5	3.82	14.62	0.092	0.241	yes
Middle-part 1727	30	7.3	4.00	16.00	0.103	0.241	yes
Tip 1727	30	5.8	3.68	13.57	0.085	0.241	yes
Head spruce 1886	13	13.9	1.90	3.61	0.110	0.361	yes
Middle-part spruce 1886	15	13.5	2.10	4.41	0.180	0.337	yes
Tip spruce 1886	16	11.6	1.80	3.24	0.243	0.327	yes
Head spruce 1922	16	14.0	2.20	4.84	0.170	0.327	yes
Middle-part spruce 1922	16	13.9	2.40	5.76	0.162	0.327	yes
Tip spruce 1922	17	12.0	2.30	5.29	0.111	0.318	yes
Head fir 1886	6	15.2	2.00	4.00	0.280	0.519	yes
Middle-part fir 1886	7	14.9	2.30	5.29	0.190	0.483	yes
Tip fir 1886	7	12.0	3.00	9.00	0.236	0.483	yes
Bridge 30	92	9.9	3.87	14.97	0.082	0.142	yes
Bridge 41	109	10.8	3.97	15.76	0.075	0.130	yes
External rows	162	10.5	3.99	15.92	0.070	0.107	yes
Internal rows	34	8.7	3.22	10.37	0.127	0.221	yes

C3 t-Test for significant difference in mean $f_{c,0,wet}$

Once the normality of the data is assumed (Table C.1), the t-test for the comparison of the remaining short-term $f_{c,0,wet,mean}$ was conducted for historical spruce and fir piles divided in head, middle and tip (Table C.2). Piles from 1922-1886 were not significantly different.

All the head-middle of spruce piles from 1922, 1886, and 1727 were not significantly different.

C4 Results of small-scale compression tests on prismatic samples across the cross-section

Table C.2: Test for unequal variances ($\alpha = 0.05$) conducted on $f_{c,0,wet,mean}$

$f_{c,0,wet,mean}$ comparison	$f_{c,0,wet,mean}$ difference	t-test: one tail - equal variances $\alpha = 0.05$					significance
	MPa	std err	t-stat	d.f.	p-value	t-crit	
1922 - 1886 all spruce	0.4	0.472	0.948	10 3	0.173	1.660	no
1922 - 1727 all spruce	6.3	0.446	13.159	14 3	1.03E-26	1.656	yes
1886-1727 all spruce	5.9	0.428	13.786	15 0	9.51E-29	1.655	yes
Head - middle 1922 (spruce)	0.1	0.803	-0.166	30	0.434	1.697	no
Head- tip 1922 (spruce)	2.0	0.763	2.334	31	0.013	1.694	yes
Middle - Tip 1922 (spruce)	1.9	0.790	2.413	31	0.011	1.696	yes
Head - middle 1886 (spruce)	0.4	0.767	0.851	26	0.201	1.706	no
Head- tip 1886 (spruce)	2.3	0.732	3.430	24	0.001	1.711	yes
Middle - Tip 1886 (spruce)	1.9	0.760	2.478	26	0.010	1.706	yes
Head - middle 1727 (spruce)	0.2	0.617	0.652	58	0.258	1.672	no
Head- tip 1727 (spruce)	1.7	0.544	3.470	58	0.001	1.673	yes
Middle - Tip 1727 (spruce)	1.5	0.552	2.674	58	0.005	1.675	yes
Head - middle 1886 (fir)	0.3	1.201	0.579	11	0.287	1.796	no
Head- tip 1886 (fir)	3.2	1.415	2.603	12	0.012	1.782	yes
Middle - Tip 1886 (fir)	2.9	1.390	2.040	13	0.031	1.771	yes

C4 Results of small-scale compression tests on prismatic samples across the cross-section

The outcomes from the small-scale compression tests on prisms retrieved from the cross sections of the 15 pile segments (according to Section 3.11) are reported in Table C.3-5 for samples from 1727, 1886, and 1922, respectively.

Table C.3: Results from small-scale compression tests on prisms retrieved from 9 pile segments (3 head, 3 middle, 3 tip parts) from 1727.

Prism number	Sample size	Presence of decay	Prism height (mm)	MC at testing		Dry density (MC = 0%)		$f_{c,0,wet}$	
				mean (%)	COV	mean (kg/m ³)	COV	mean (MPa)	COV
1	9	Yes	120	216	0.37	304	0.13	8.2	0.64
2	9	No	120	89	0.23	439	0.03	12.0	0.18
3	9	No	120	62	0.23	402	0.02	10.1	0.31
4	9	No	120	63	0.39	439	0.03	13.2	0.01
5	9	Yes	120	212	0.50	358	0.32	8.4	0.63
1	3	Yes	60	146	0.57	315	0.19	7.5	0.31
2	3	No	60	52	0.34	436	0.14	13.8	0.15
3	3	No	60	60	0.10	403	0.04	10.8	0.18
4	3	No	60	58	0.37	452	0.02	13.7	0.06
5	3	Yes	60	189	0.43	351	0.32	8.6	0.64

Appendix C

Table C.4: Results from small-scale compression tests on prisms retrieved from 3 pile segments (head, middle, tip) from 1886.

Prism number	Sample size	Presence of decay	Prism height (mm)	MC at testing		Dry density (MC = 0%)		$f_{c,0,wet}$	
				mean (%)	COV	mean (kg/m ³)	COV	mean (MPa)	COV
1	3	No	120	52	0.32	496	0.07	16.8	0.18
2	3	No	120	44	0.05	378	0.03	14.0	0.07
3	3	No	120	55	0.13	373	0.01	9.1	0.16
4	3	No	120	58	0.48	372	0.05	10.9	0.07
5	3	No	120	51	0.11	453	0.01	15.5	0.06
1	3	No	60	55	0.04	460	0.07	14.6	0.17
2	3	No	60	41	0.12	398	0.06	15.1	0.03
3	3	No	60	65	0.34	382	0.02	10.4	0.13
4	3	No	60	41	0.04	374	0.02	13.0	0.03
5	3	No	60	45	0.27	488	0.07	17.9	0.17

Table C.5: Results from small-scale compression tests on prisms retrieved from 3 pile segments (head, middle, tip) from 1922.

Prism number	Sample size	Presence of decay	Prism height (mm)	MC at testing		Dry density (MC = 0%)		$f_{c,0,wet}$	
				mean (%)	COV	mean (kg/m ³)	COV	mean (MPa)	COV
1	3	No	120	120	0.19	487	0.01	14.8	0.12
2	3	No	120	46	0.20	510	0.05	19.1	0.13
3	3	No	120	49	0.17	460	0.11	13.5	0.17
4	3	No	120	59	0.43	499	0.01	19.8	0.13
5	3	No	120	143	0.17	428	0.07	13.9	0.14
1	3	No	60	117	0.29	436	0.13	13.5	0.22
2	3	No	60	74	0.57	503	0.09	21.4	0.36
3	3	No	60	44	0.10	489	0.12	17.1	0.14
4	3	No	60	61	0.30	502	0.10	19.1	0.16
5	3	No	60	111	0.15	450	0.10	14.5	0.32

Appendix D

Validation of experimentally-determined sapwood with CT scanning

D1 Results from validation of sapwood with CT scanning

In order to validate the experimentally-determined sapwood with CT scanning (Paragraph 3.12.1), a total of 45 wooden discs were scanned according to Table D.1.

The results of the validation are shown in Figure D.1, where in average the sapwood width measured with CT scans was similar to that measured with experimental Equation 3.15 in Paragraph 3.12.1.

In addition, a good correlation was found (Figure D.2) between all the datapoints of measured and predicted sapwood width.

Table D.1: Wooden discs selected for the validation of sapwood width

Sample	Building year	Time in service (years)
OAM-P2.7		
OAM-P2.8		
OAM-P2.9		
OAM-P2.10		
010892K-423		
010586K-423		
03855K-423		
010575K-423		
10642K-423		
10597V-423		
03805V-419	"new"	-
010587K-423		
03886K-423		
03824K-423		
010584K-423		
OAM-P2.3		
OAM-P2.5		
OAM-P1.1		
OAM-P2.1		
03823-427		
BRU0041-PL2-P1.9	1922	100
BRU0041 PL1 P1.23	1922	100
BRU0041-PL1-P3.24	1922	100
BRU0041-PL1-P1.29	1922	100
BRU0041-PL1-P5.41	1922	100
BRU0030-PL1-P1.2	1886	135
BRU0030-PL1-P5.1	1886	135
BRU0030-PL1-P5.1	1886	135
BRU0041-PL2-P1.25	1886	135
BRU0030-PL2-P1.13	1886	135
BRU0030-PL1-P1.20	1886	135
BRU0030-PL1-P1.6	1886	135
BRU0030-PL1-P1.1	1886	135
BRU0030-PL1-P2.9	1727	295
BRU0030-PL1-P2.13	1727	295
BRU0030-PL1-P2.7	1727	295
BRU0041-PL1-P1.6	1727	295
BRU0041-PL1-P1.14	1727	295
BRU0041-PL1-P1.10	1727	295
BRU0041-PL1-P1.11	1727	295
BRU0030-PL2-P1.18	1727	295
BRU0030-PL2-P2.21	1727	295
BRU0030-PL1-P2.9	1727	295
BRU0030-PL1-P2.7	1727	295
BRU0041-PL1-P1.13	1727	295

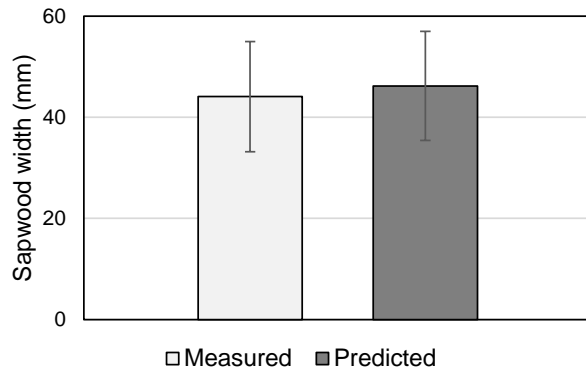


Figure D.1: measured sapwood width with CT scanning and predicted sapwood width with experimental Equation 3.15 in Paragraph 3.12.1. The bars represent the average values, the lines the standard deviation.

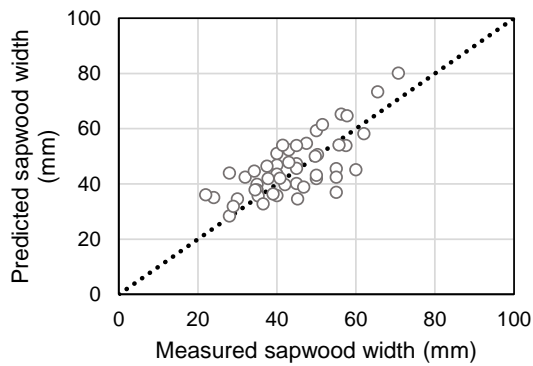


Figure D.2: correlation between measured sapwood width with CT scanning and predicted sapwood width with experimental Equation 3.15 in Paragraph 3.12.1.

Appendix E

Micro-drilling signal analysis

E1 TU-Delft developed algorithm for micro-drilling signal analysis

The TU-Delft developed algorithm to analyse micro-drilling signals used in this dissertation and its development are explained in this Section.

The algorithm was developed in 2021 and implemented in Excel by dr. G. Ravenshorst from the biobased structures and materials group (BSM group) at Delft University of Technology, containing the theory and principles behind the analysis of the micro-drilling signals, as analysed in [27].

The algorithm was subsequently programmed in Python by Olga Beketova-Hummel in 2021 (who was a PhD student at BSM group at the time), and finalised in 2021 [186]. O. Beketova-Hummel created the version 1 of the software (*MicroDrill (.rgp) file processing / Version 1*), allowing for faster analysis and visualisation of the micro-drilling signal measured in a timber pile.

A new software was subsequently programmed by dr. Anindya Roy in 2021 [188], who was a Postdoc at BSM group during 2021-2022, based on the original algorithm developed by dr. G. Ravenshorst. The steps describing how this software works are listed in detail from step 1 to 4 in Appendix E2, and reported in [189]. This software is referred in this dissertation as *TU-Delft developed algorithm*. The software has been made available to the city of Amsterdam in [187] (under the name of *Soft Shell Calculator TU Delft versie 0.1.*). The source code is fully listed in Appendix E3. The *TU-Delft developed algorithm* was validated by G. Pagella in this dissertation (Section 3.9.2), based on the characterised mechanical properties of historic timber piles retrieved in Amsterdam (Paragraph 5.3), using the software developed by dr. A. Roy.

The TU-Delft developed algorithm was further delivered to the municipality of Amsterdam [187], including the validated software developed by dr. A. Roy, under the name of *Soft Shell Calculator TU Delft versie 0.1.* in 2023 after calibration and validation. The algorithm is currently used by the TU Delft and the municipality of Amsterdam to analyse micro-drilling signals.

A special acknowledgment to all the people who contributed to the analysis and processing of micro-drilling signals:

- G.J.P. Ravenshorst, the creator of the algorithm and developer of the theory and principles behind the analysis and processing of the micro-drilling signals.

- O. Beketova-Hummel, for the creating the first version of the software based on the algorithm, and for contributing to the research work leading to a better understanding of micro- and core-drilling data and analysis, decay processes in timber foundation piles, and possible measuring techniques and solutions to better assess their state of conservation.
- A. Roy, for the development of the final version of the software (*Soft Shell Calculator TU Delft versie 0.1.*) currently in use by the TU Delft and the municipality of Amsterdam.
- M. Mirra, for the research contributions and interaction during the development of the analysis and processing of micro-drilling signals, and decay assessment of timber foundation piles.
- W.F. Gard, for the research contribution on the biological decay of timber piles, interpretation and analysis of micro-drilling signals, and the influence of decay on the mechanical properties of the piles.
- J.W.G. van de Kuilen, for the supervision of the project and software development, research knowledge contribution to timber behaviour, decay process, and micro-drilling signal assessment.

E2 Steps outlining the functioning of the TU-Delft developed algorithm.

Step 1: the user provides the following input data:

- Micro-drilling signal file (*.rgp), with name, depth (mm), drill amplitude (%), feed amplitude (%);
- Optional: diameter of pile measured by divers;

Step 2: calculation of moving average of feed amplitude (MA_{fA}):

- The signal is cut off at the beginning and at the end (left and right in the graph) to obtain measurements in wood only. No adjustment of the signals is done before cut off procedure (no assumption of friction phenomena yet);
- Creation of moving average of the feed amplitude as an average of 100 measurement point (10 mm):
 - From $n = 1$ (1 to 50), $n = 2$ (1 to 51), $n = 3$ (1 to 52), ..., $n = 51$ (1 to 101), $n = 52$ (2 to 102), $n = 53$ (3 to 103), $n = n$ ($n-50$ to $n+50$), ..., $n = N-51$ ($n-50$ to $n+50$), $n = N-50$ ($n=N-100$ to N), $n = N-49$ ($N-99$ to N), ..., $n = N-2$ ($N-52$ to N), $n = N-1$ ($N-51$ to N), $n = N$ ($n-50$ to N);
 - Cut off signal on the left: exclude from $n = 1$ the signal values $<$ threshold left (TL) until a value n_{TL} is found $>$ TL. From then on all data points are included. When further on for $n > n_{TL}$ a value higher than TL is found it is still included in the signal;
 - Cut off signal on the right: exclude from $n = N$ all values that are both lower for :
 - MA_{fA} = moving average value of feed amplitude. Search for $n = n_{TR,A}$ for the first time when $MA_{fA} > TR_A$ (threshold right A);
 - MA_{fB} = difference between moving average of n and $n-1$. So start with $n=N$: difference between N and $n-1$ etc. Search for $n=n_{TR,B}$ for the first time which $MA_{fB} > TR_B$ (threshold right B);

- Then the threshold is the highest value for $n_{TR,A}$ and $n_{TR,B}$, which is $n_{TR,T}$. All values below $n_{TR,T}$ are included;
- Creation of a graph with drilling amplitude and feed amplitude against distance from left of original micro-drilling signal with centre and display of TL and TR;

Step 3: calculation of moving average of drill amplitude and IOMA:

- Rename cut-off values between $n = n_{TL}$ to $n_{TR,T}$. as $n=1$ to $N = n_{TR,T}$ and go on with this data set;
- Determine centre n_C of the signal as $N/2$;
- Calculate moving average MA_{DA} of the drilling amplitudes for the cut-off signal: average of 100 measurement points (10 mm).
 - From $n = 1$ (1 to 50), $n = 2$ (1 to 51), $n = 3$ (1 to 52), ..., $n = 51$ (1 to 101), $n = 52$ (2 to 102), $n = 53$ (3 to 103), $n = n$ ($n-50$ to $n+50$), ..., $n = N-51$ ($n-50$ to $n+50$), $n = N-50$ ($n=N-100$ to N), $n = N-49$ ($N-99$ to N), ..., $n = N-2$ ($N-52$ to N), $n = N-1$ ($N-51$ to N), $n = N$ ($n-50$ to N);
- Calculate moving average MA_{DA} of the drilling amplitudes for the cut-off signal: average of 100 measurement points (10 mm).
 - For $n \leq n_C$. For $n = n_C$, value of n_C ; for $n = n_C - 1$: average of ($n_C - 1$ to n_C) ... for n : average of (n to n_C), until for $n=1$: average of (1 to n_C);
 - For $n > n_C$. For $n = n_C + 1$, value of $n_C + 1$. For $n = n_C + 2$: average of ($n_C + 1$ to $n_C + 2$) ... for n : average from ($n_C + 1$ to n), until for $n = N$ average of (n_C to N);
- Determine the maximum value for the IOMA left and right: $IOMA_L$ for $n \leq n_C$. and $IOMA_R$ for $n > n_C$;
- Create a graph with drilling amplitude, MA_{DA} and IOMA for every point against the distance with position of centre. Optionally, add the (drill core) BM values (with values on secondary vertical axis) against distance (now starting from $n = 1$).

Step 4: Determination of zones and soft shell:

- The left (L) and right (R) part of the signal are divided in zones, identified as follows:
 - Zone 1: $MA_{DA} < IOMA_L * 20\%$
 - Zone 2: $MA_{DA} < IOMA_L * 40\%$
 - Zone 3: $MA_{DA} < IOMA_L * 60\%$
 - Zone 4: $MA_{DA} < IOMA_L * 80\%$
 - Zone 1: $MA_{DA} < IOMA_R * 20\%$
 - Zone 2: $MA_{DA} < IOMA_R * 40\%$
 - Zone 3: $MA_{DA} < IOMA_R * 60\%$
 - Zone 4: $MA_{DA} < IOMA_R * 80\%$
- The length of each zone is calculated:
 - Zone 1: starting from $n = 1$, find n for which $MA_{DA} > IOMA_L * 20\%$ for the first time;
 - Zone 2: starting from end of zone 1, find n for which $MA_{DA} > IOMA_L * 40\%$ for the first time;

- Zone 3: starting from end of zone 2, find n for which $MA_{DA} > IOMAL * 60\%$ for the first time;
- Zone 4: starting from end of zone 3, find n for which $MA_{DA} > IOMAL * 80\%$ for the first time;
- The same applies for the right side, starting with $n=N$ and decreasing n .
- Expand the previous graph with the all zones indicated.
- Soft shell is determined on the left as $SH_L = \text{zone } 1_{\text{left}} + \text{zone } 2_{\text{left}}$ and on the right as $SH_R = \text{zone } 1_{\text{right}} + \text{zone } 2_{\text{right}}$

E3 Python script of TU-Delft developed algorithm programmed by dr. A. Roy.

Script Softshell.py

```
import tkinter as tk
from tkinter import filedialog as fd
import os
from openpyxl import Workbook
import csv
from func import RGP, EXL, FNAME
import matplotlib.pyplot as plt
from matplotlib.backends.backend_tkagg import FigureCanvasTkAgg
from matplotlib.backends.backend_pdf import PdfPages
from fpdf import FPDF
import PyPDF2
from datetime import datetime

class Window(tk.Frame):
    def __init__(self, master = None):
        tk.Frame.__init__(self, master)
        self.master = master
        self.init_window()

    def init_window(self):
        blank_space = " "
        self.master.title(130*blank_space+"Soft Shell Calculator: Experimental
version02. Date: 17-01-2022 \u00a9TU Delft, Biobased structures and materials
group")
        self.pack(fill = 'both', expand = 1)

        self.val1 = None
        self.val2 = None
        self.val3 = None

        # self.axx = None
        # self.curve = None
        self.val4 = None

        # self.separator = ttk.Separator (self, orient = tk.VERTICAL)
        # self.separator.grid (row = 0, column = 3, sticky = "ew")

        # self.filepath1 = tk.StringVar()
        # self.filepath2 = tk.StringVar()
        self.e = tk.Entry(self, width = 30, borderwidth = 5)
        self.e.grid(row = 3, column = 1, columnspan = 1)
```

```

quitButton = tk.Button(self, text = 'Browse_rgp',
                        command = self.open_window)
quitButton.grid(row = 0, column = 0, columnspan = 1)

self.exlButton = tk.Button(self, text = 'signal_key',
                           command = self.get_file, state='disabled')
self.exlButton.grid(row = 2, column = 0, columnspan = 1)

self.browseButton = tk.Button(self, text = 'Browse_excel',
                              command = self.first_browser, state='disabled')
self.browseButton.grid(row = 1, column = 0, columnspan = 1)

self.submitButton = tk.Button(self, text = 'result',
                              command = self.submit, state='disabled')
self.submitButton.grid(row = 5, column = 0, columnspan = 1)

self.Houtmonster = tk.Button(self, text = 'Houtmonster-yes?',
                             command = self.want_Houtmonster, state='disabled')
self.Houtmonster.grid(row = 6, column = 0, columnspan = 1)

self.samplecore = tk.Button(self, text = 'Houtmonster-no?',
                             command = self.clear_button, state='disabled')
self.samplecore.grid(row = 7, column = 0, columnspan = 1)

self.PDFbutton = tk.Button(self, text="Generate PDF",
command=self.generate_pdf, state='disabled')
self.PDFbutton.grid(row = 5, column = 1, columnspan = 1)

self.loadButton = tk.Button(self, text = 'load_signalkey',
                             command = self.load_key, state='disabled')
self.loadButton.grid(row = 4, column = 0, columnspan = 1)

def open_window(self):
    file = self.show_file_browser()
    # self.filepath2.set(os.path.split(file)[1])
    self.val1 = file
    name = os.path.split(file)[1]
    if name[:-1].split('.')[0] == 'pgr':
        self.Houtmonster["state"] = "normal"
        self.samplecore["state"] = "normal"
        mylabel = tk.Label(self, text= name)
    else:
        mylabel = tk.Label(self, text= 'ERROR: Chose an .rgp file')
    mylabel.grid(row = 0, column = 1, columnspan = 1)

def show_file_browser(self):
    self.filename = fd.askopenfilename()
    return self.filename

def first_browser(self):
    file = self.show_file_browser()
    # self.filepath1.set(os.path.split(file)[1])
    # self.val2 = file
    name = os.path.split(file)[1]
    if name[:-1].split('.')[0] == 'xlsx':
        self.val2 = file
        self.exlButton["state"] = "normal"
        mylabel = tk.Label(self, text= name)
    elif name[:-1].split('.')[0] == 'vsc':
        self.exlButton["state"] = "normal"
        mylabel = tk.Label(self, text= name)
    wb = Workbook()
    ws = wb.active
    with open(file, 'r') as f:
        dialect = csv.Sniffer().sniff(f.readline(), delimiters=' ;,;\t')

```

```

        for row in csv.reader(f, dialect):
            ws.append(row)
        wb.save('name.xlsx')
        self.val2 = 'name.xlsx'
    else:
        mylabel = tk.Label(self, text= 'ERROR: Chose an excel file')
        mylabel.grid(row = 1, column = 1, columnspan = 1)

def get_file(self):
    self.loadButton["state"] = "normal"
    list = FNAME(self.val2)
    T = tk.Text(self, height=15, width=25)
    T.grid(row = 2, column = 1)
    T.insert(tk.END, list)
    self.filepath1.set(list)
    mylabel = tk.Label(self, text= list)
    #
    #
    #
    mylabel.grid(row = 1, column = 3, columnspan = 1)

def clear_button(self):
    self.val4 = 1
    self.submitButton["state"] = "normal"
    mylabel = tk.Label(self, text= 'Now press the result button')
    mylabel.grid(row = 7, column = 1, columnspan = 1)

def want_Houtmonster(self):
    self.val4 = 0
    self.browseButton["state"] = "normal"
    self.submitButton["state"] = "disabled"
    mylabel = tk.Label(self, text= 'OK')
    mylabel.grid(row = 6, column = 1, columnspan = 1)

def load_key(self):
    MM = self.e.get()
    self.val3 = MM.rstrip()
    name = self.val3
    list = FNAME(self.val2)
    str_list = list.split('\n')
    KK = 0
    for n in str_list[:-1]:
        if n == name:
            KK = 1
            break

    if KK == 1:
        self.submitButton["state"] = "normal"
        mylabel = tk.Label(self, text= f'loaded {name}')
    else:
        mylabel = tk.Label(self, text= 'ERROR: Chose correct key from the list')
    mylabel.grid(row = 4, column = 1, columnspan = 1)

def submit(self):
    self.samplecore["state"] = "normal"
    self.PDFbutton["state"] = "normal"
    list = RGP(self.val1)

    figure = plt.Figure(figsize=(6,3), dpi=100)
    figure.subplots_adjust(bottom = 0.15)
    ax = figure.add_subplot(111)
    bar = FigureCanvasTkAgg(figure, self)
    bar.get_tk_widget().grid(row=1,column=2, sticky='ew')
    ax.plot(list[0],list[1], "b", label="Drill")
    ax.plot(list[0],list[2], "brown", label="Feed")
    ax.plot(list[0],list[3], "c", label="Feed_MA")
    ax.axvline(x=list[4], color='k', linestyle='--', label="LT,RT")
    ax.axvline(x=list[5], color='k', linestyle='--')
    ax.set_xlim([list[0][0], list[0][-1]])

```

```
# ax.axvline(x=list[6], color='m', linestyle='--', label="Centre (no
threshold)")
ax.legend(loc="upper right")
# ax.set_title(f'For signal {os.path.split(self.val1)[1]}, {self.val3}')
ax.set_xlabel('Distance(mm)')
ax.set_ylabel('Amplitude(%')

figure2 = plt.Figure(figsize=(6,3), dpi=100)
figure2.subplots_adjust(bottom = 0.15)
ax2 = figure2.add_subplot(111)
line2 = FigureCanvasTkAgg(figure2, self)
line2.get_tk_widget().grid(row=2,column=2, sticky='ew')
ax2.plot(list[16],list[8], "b", label="Drill")
ax2.plot(list[16],list[9], "orange", label="Drill_MA")
ax2.plot(list[16],list[11], "y", label="IOMA")
ax2.axvline(x=list[10]+list[4], color='r', linestyle='--', label="Centre")
ax2.set_xlim([list[0][0], list[0][-1]])
ax2.legend(loc="upper right")
# ax2.set_title(f'For signal {os.path.split(self.val1)[1]}, {self.val3}')
ax2.set_xlabel('Distance(mm)')
ax2.set_ylabel('Amplitude(%')

figure3 = plt.Figure(figsize=(6,3), dpi=100)
figure3.subplots_adjust(bottom = 0.15)
ax3 = figure3.add_subplot(111)
line3 = FigureCanvasTkAgg(figure3, self)
line3.get_tk_widget().grid(row=1,column=3, sticky='ew')
ax3.plot(list[16],list[8], "b", label="Drill")
ax3.axvline(x=list[10]+list[4], color='r', linestyle='--', label="Centre")
ax3.axvline(x=list[12][1]+list[4], color='g', label="Softshell")
ax3.axvline(x=list[13][1]+list[4], color='g')
ax3.axvline(x=list[4], color='g')
ax3.axvline(x=list[16][-1], color='g')
ax3.set_xlim([list[0][0], list[0][-1]])
ax3.legend(loc="upper right")
# ax3.set_title(f'Soft shell for {os.path.split(self.val1)[1]}')
ax3.set_xlabel('Distance(mm)')
ax3.set_ylabel('Amplitude(%')

DD = 0
KK = 0
if self.val4 == 0:
    ex1 = EXL(self.val2,list[4],self.val3)
    axx = ax.twinx()
    axx.step(ex1[0],ex1[1], color='m', label="HM")
    axx.legend(loc="upper left")
    axx.set_ylabel('DS(N/mm2)')
    axx2 = ax2.twinx()
    axx2.step(ex1[0],ex1[1], color='m', label="HM")
    axx2.legend(loc="upper left")
    axx2.set_ylabel('DS(N/mm2)')
    axx3 = ax3.twinx()
    axx3.step(ex1[0],ex1[1], color='m', label="HM")
    axx3.legend(loc="upper left")
    axx3.set_ylabel('DS(N/mm2)')

figure4 = plt.Figure(figsize=(6,3), dpi=100)
figure4.subplots_adjust(bottom = 0.15)
ax4 = figure4.add_subplot(111)
line4 = FigureCanvasTkAgg(figure4, self)
line4.get_tk_widget().grid(row=2,column=3, sticky='ew')
axx4 = ax4.twinx()
ax4.step(ex1[0],ex1[5], color='k', label="Level of destruction")
```

```

        axx4.step(exl[0],exl[1], color='m', label="HM")
        ax4.axvline(x=list[10]+list[4], color='r', linestyle='--',
label="Centre")
        ax4.set_xlim([list[0][0], list[0][-1]])
        for i,j,k in zip(exl[0],exl[5],exl[5]):
        #         axx4.annotate(str(k),xy=(i,j))
        ax4.legend(loc="upper right")
        #         axx4.legend(loc='upper right', bbox_to_anchor=(0.8, 0.75))
        axx4.legend(loc="upper left")
        ax4.set_title(f'level of destruction for {self.val3}')
        ax4.set_xlabel('Distance(mm)')
        ax4.set_ylabel('Level of destruction')
        axx4.set_ylabel('DS(N/mm2)')
        axx4.text(180, 5, f'{exl[4]}', horizontalalignment='center',
verticalalignment='center')
        DD = exl[3]
        KK = exl[6]
        ax.set_title(f'For signal {os.path.split(self.val1)[1]}, {self.val3}')
        ax2.set_title(f'For signal {os.path.split(self.val1)[1]}, {self.val3}')
        ax3.set_title(f'For signal {os.path.split(self.val1)[1]}, {self.val3}')
        print(exl[7],exl[2])
    elif self.val4 == 1:
        figure4 = plt.Figure(figsize=(6,3), dpi=100)
        figure4.subplots_adjust(bottom = 0.15)
        ax4 = figure4.add_subplot(111)
        line4 = FigureCanvasTkAgg(figure4, self)
        line4.get_tk_widget().grid(row=2,column=3, sticky='ew')
        ax4.plot(list[16],list[8], "b", label="Drill")
        ax4.axvline(x=list[10]+list[4], color='r', linestyle='--',
label="Centre")
        ax4.axvline(x=list[12][0]+list[4], color='brown', label="Zone1 (20%)")
        ax4.axvline(x=list[13][0]+list[4], color='brown')
        ax4.axvline(x=list[12][1]+list[4], color='g', label="Zone2 (40%)")
        ax4.axvline(x=list[13][1]+list[4], color='g')
        ax4.axvline(x=list[12][2]+list[4], color='orange', label="Zone3 (60%)")
        ax4.axvline(x=list[13][2]+list[4], color='orange')
        ax4.axvline(x=list[12][3]+list[4], color='c', label="Zone4 (80%)")
        ax4.axvline(x=list[13][3]+list[4], color='c')
        ax4.axvline(x=list[4], color='k', linestyle='--', label="LT,RT")
        ax4.axvline(x=list[5], color='k', linestyle='--')
        ax4.set_xlim([list[0][0], list[0][-1]])
        ax4.set_title(os.path.split(self.val1)[1])
        ax4.legend(loc="upper right")
        ax4.set_xlabel('Distance(mm)')
        ax4.set_ylabel('Amplitude(%)')
        DD = 'Not applicable'
        KK = 'Not applicable'
        ax.set_title(os.path.split(self.val1)[1])
        ax2.set_title(os.path.split(self.val1)[1])
        ax3.set_title(os.path.split(self.val1)[1])

        mylabel2 = tk.Label(self, text= f'Softshell_Left_rpd(mm) = {list[12][1]},
Softshell_Right_rpd(mm) = {round(list[5]-list[4]-list[13][1],2)}, Softshell_Hout(mm)
= {KK} \n Left_threshold_rpd(mm) = {list[4]}, Right_threshold_rpd = {list[5]}\n
Measured_diameters_divers(mm) = {DD}, Calculated_diameter_rpd(mm) = {list[5]-
list[4]}')
        mylabel2.grid(row = 6, column = 2, columnspan = 1)

        mylabel6 = tk.Label(self, text= '* Disclaimer: This is an experimental
version,\n the interpretation of results is the responsibility of the user.')
        mylabel6.grid(row = 6, column = 3, columnspan = 1)

        pp = PdfPages('foo.pdf')
        pp.savefig(figure)
        pp.savefig(figure2)
        pp.savefig(figure3)
        pp.savefig(figure4)

```



```

pp.close()

pdf = FPDF()
pdf.add_page()
pdf.set_xy(0, 0)
pdf.set_font('Times', '', 14.0)
epw = pdf.w - 2*pdf.l_margin
col_width = epw/2
th = pdf.font_size
data = [['Softshell_Left_rpd(mm)', f'{list[12][1]}'],
['Softshell_Right_rpd(mm)', f'{round(list[5]-list[4]-
list[13][1],2)}'], ['Softshell_Hout(mm)', f'{KK}'], ['Left_threshold_rpd(mm)', f'{list[4]
}'], ['Right_threshold_rpd(mm)', f'{list[5]}'], ['Measured_diameters_divers(mm)', f'{DD
}'], ['Calculated_diameter_rpd(mm)', f'{round(list[5]-list[4],2)}']]
pdf.set_font('Times', 'B', 18.0)
pdf.cell(epw, 10, f'Softshell calculator v02: ©TU Delft Biobased
structures and materials.', align='C')
pdf.ln(2*th)
pdf.cell(epw, 10, f'Date: {datetime.now():%d-%m-%Y}', align='C')
pdf.ln(2*th)
pdf.set_font('Times', '', 16.0)
if self.val4 == 0:
    pdf.cell(epw, 10, f'{os.path.split(self.val1)[1]}, {self.val3}',
align='C')
elif self.val4 == 1:
    pdf.cell(epw, 10, f'{os.path.split(self.val1)[1]}', align='C')
# pdf.cell(epw, 10, 'Summary of the results', align='C')
pdf.set_font('Times', '', 14.0)
pdf.ln(4*th)
for row in data:
    for datum in row:
        pdf.cell(col_width, 2*th, datum, border=1, align='C')
pdf.ln(2*th)
pdf.ln(th)
# pdf.multi_cell(0, 5.0, txt='* Disclaimer: This is an experimental version,
the interpretation of results is the responsibility \n of the user.', align='L')
pdf.cell(-30)
pdf.image('TU.png', x = 112, y = 200, w = 0, h = 0, type = '', link = '')
pdf.set_y(270)
pdf.cell(0, 5, 'Biobased structures and materials group', align='R')
pdf.output('test.pdf', 'F')

def generate_pdf(self):
    mergeFile = PyPDF2.PdfFileMerger()
    mergeFile.append(PyPDF2.PdfFileReader('test.pdf', 'rb'))
    mergeFile.append(PyPDF2.PdfFileReader('foo.pdf', 'rb'))
# mergeFile.write('input.pdf')
if self.val4 == 0:
    y = self.val3
    y = y.replace('/', '-')
    y = y.replace('\\', '-')
    mergeFile.write(f'{os.path.split(self.val1)[1]}, {y}.pdf')
elif self.val4 == 1:
    mergeFile.write(f'{os.path.split(self.val1)[1]}.pdf')
os.remove('foo.pdf')
os.remove('test.pdf')

form = tk.Tk()
form.geometry("250x250")
#form.resizable(0, 0)
app = Window(form)
form.mainloop()
#print(app.val)

```

Script func.py

```
#import matplotlib.pyplot as plt
import numpy as np
import openpyxl
import math
#from itertools import accumulate
def RGP(filename):
    file = open(filename, 'r')
    lines = file.readlines()

    arr1 = lines[320].split()
    s1 = arr1[1]
    newstr1 = ''.join((ch if ch in '0123456789.-e' else ' ') for ch in s1)
    list1 = [float(i) for i in newstr1.split()]

    arr2 = lines[321].split()
    s2 = arr2[1]
    newstr2 = ''.join((ch if ch in '0123456789.-e' else ' ') for ch in s2)
    list2 = [float(i) for i in newstr2.split()]

    list0 = list(np.arange(0,len(list1)/10,0.1))

    lista = np.empty(len(list2), dtype=object)
    for N in range(len(list2)):
        i = N - 50
        j = N + 50
        k = 100
        if i < 0:
            i = 0
            k = j
        elif j > len(list2):
            j = len(list2)
            k = j-i
        lista[N] = sum(list2[i:j])/k
    LT = 0
    val1 = 0
    val2 = 0
    RT = 0
    for N in range(len(list1)):
        if list1[N] >= 0.5:
            LT = N/10
            break

    for i in reversed(range(len(lista))):
        if lista[i] >= 5:
            val1 = i/10
            break

    for i in reversed(range(len(lista))):
        if lista[i-1] - lista[i] >= 0.03:
            val2 = i/10
            break

    if val1>=val2:
        RT = val1
    else:
        RT = val2

    BM = 0.1*len(lista)/2

    listA = list0[int(10*LT):int(10*RT)+1]
    lista1 = list1[int(10*LT):int(10*RT)+1]
    lista2 = np.empty(len(lista1), dtype=object)
    lista0 = list(np.arange(0,len(lista1)/10,0.1))
    for N in range(len(lista1)):
        i = N - 50
```

```
j = N + 50
k = 100
if i < 0:
    i = 0
    k = j
elif j > len(lista1):
    j = len(lista1)
    k = j-i
lista2[N] = sum(lista1[i:j])/k
CM = (RT-LT)/2
Nc = int((10*RT-10*LT)//2)+1
lista1h1 = []
lista1h2 = []
temp = []
for i in reversed(lista1[:Nc]):
    temp.append(i)
    lista1h1.append(sum(temp)/len(temp))
temp = []
for i in lista1[Nc:]:
    temp.append(i)
    lista1h2.append(sum(temp)/len(temp))

lista1h = lista1h1[::-1] + lista1h2

#
# SSL = 0
# count = 0
# for f, b in zip(lista2, lista1h):
#     if f>0.4*b:
#         SSL = count/10
#         break
#     count = count + 1
#

SSL = 0
count = 0
for f in lista2:
    if f>0.4*max(lista1h1):
        SSL = count/10
        break
    count = count + 1

SSR = 0
count = len(lista1h) -1
for f in lista2[::-1]:
    if f>0.4*max(lista1h2):
        SSR = count/10
        break
    count = count - 1

SSL1 = 0
count = 0
for f in lista2:
    if f>0.2*max(lista1h1):
        SSL1 = count/10
        break
    count = count + 1

SSR1 = 0
count = len(lista1h) -1
for f in lista2[::-1]:
    if f>0.2*max(lista1h2):
        SSR1 = count/10
        break
    count = count - 1

SSL2 = 0
count = 0
for f in lista2:
```

```

        if f>0.6*max(lista1h1):
            SSL2 = count/10
            break
        count = count +1

    SSR2 = 0
    count = len(lista1h) -1
    for f in lista2[::-1]:
        if f>0.6*max(lista1h2):
            SSR2 = count/10
            break
        count = count - 1

    SSL3 = 0
    count = 0
    for f in lista2:
        if f>0.8*max(lista1h1):
            SSL3 = count/10
            break
        count = count +1

    SSR3 = 0
    count = len(lista1h) -1
    for f in lista2[::-1]:
        if f>0.8*max(lista1h2):
            SSR3 = count/10
            break
        count = count - 1

    SL = [SSL1,SSL,SSL2,SSL3]
    SR = [SSR1,SSR,SSR2,SSR3]
    return list0, list1, list2, lista, LT, RT, BM, lista0, lista1, lista2, CM,
    lista1h, SL, SR, max(lista1h1), max(lista1h2), listA

def FNAME(input_file):
    # input_file = r"37489-069_Brug_138.xlsx"
    wb = openpyxl.load_workbook(input_file)
    gh = wb.sheetnames
    # sheet = wb['Sheet2']
    sheet = wb[gh[0]]
    column_A = sheet['A']
    list = ''
    for cell in column_A:
        list = f'{list + str(cell.value)}\n'

    return list

def EXL(input_file,LT,text):
    # input_file = r"37489-069_Brug_138.xlsx"
    wb = openpyxl.load_workbook(input_file)
    gh = wb.sheetnames
    # sheet = wb['Sheet2']
    sheet = wb[gh[0]]
    points_x = [LT]
    points_y = [0]
    points_k = []
    points_u = []
    points_a = []
    points_g = [0]
    dataDict = {}

    for key, *values in sheet.iter_rows():
        dataDict[key.value] = [v.value for v in values]

    hy = dataDict.get(text)
    # for i in range(sheet.max_column-9, sheet.max_column-1):

```

```
#         y = hy[i]
#         if y is None:
#             break
#         else:
#             points_y.append(y)

for i in range(38,46):
    y = hy[i]
    if y in (None,''):
        break
    if type(y) == str:
        y = y.replace(',','.')
        y = float(y)
    points_k.append(y)

for i in range(46,54):
    y = hy[i]
    if y in (None,''):
        break
    if type(y) == str:
        y = y.replace(',','.')
        y = float(y)
    points_u.append(y)

[float(i) for i in points_u[0:4]]
ky = ['Totale verwoesting','Ernstige aantasting','Matige aantasting','Weinig
aantasting','Gezond hout']
dy = np.arange(len(ky))
for i in range(len(ky)):
    ls = [str(dy[i]),ky[i]]
    k = "-".join(ls)
    points_a.append(k)
points_a.append('Classification BGS007-2020')
points_a.reverse()

for i in range(22,30):
    y = hy[i]
    if y in (None,''):
        break
    for j in range(len(ky)):
        if y==ky[j]:
            points_g.append(dy[j])
            break

for i in range(len(points_u)):
    a = (points_k[i] - points_u[i])/points_u[i]
    b = 38.543*math.exp(-0.6965*a)
    points_y.append(b)

for i in range(14,22):
    y = hy[i]
    if y in (None,''):
        break
    if type(y) == str:
        y = y.replace(',','.')
        y = float(y)
    points_x.append(y)

new_x = np.cumsum(points_x)
up_x = [n-LT for n in new_x]

pcount = 0
for f in points_y:
    if f>8:
        break
```

```

        pcount = pcount +1

    A = ("\n".join(points_a))
    bb = str(hy[2])
    return new_x, points_y, up_x, bb.replace(',', ' '), A, points_g, up_x[pcount-1],
    pcount

# plt.plot(list1, list2)
# plt.show()

```

E4 Recommendations for execution of micro-drilling and signal analysis

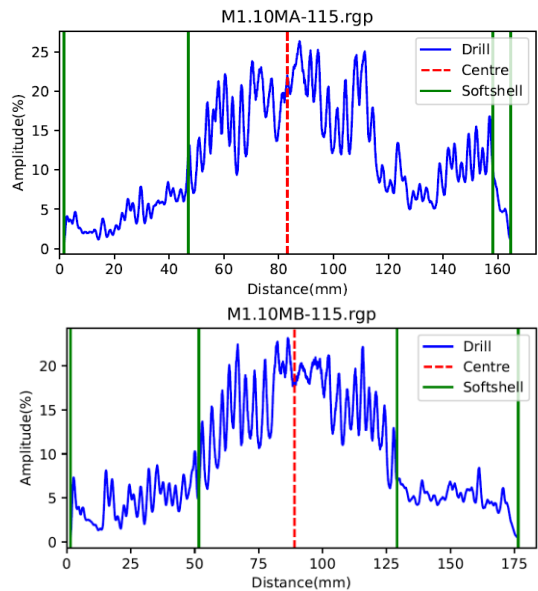
It could happen that the micro-drilling signal is characterized by the presence of peaks that can correspond to spots in the pile with higher density, penetrated by the drilling needle, such as knots and compression wood, or, less frequently, nails or stones that could be found in the outer layer of the historical piles after the extraction. In addition to peaks, also drops can be found, for example when a crack (void) is present in the pile. These phenomena can be found in historical timber piles especially from 1727, where the amplitude of the signal could be already low due to extended degradation, and where peaks and drops could have a relevant influence on the measurement of the soft shell. Another reason could be attributed to the fact that the cross section of a pile can be unevenly degraded, resulting in different degraded lengths on the right and left part of the micro-drilling signal.

An example is shown in Figure E.1, where a pile segment from 1727 (BRU0030-PL1-P1.10) was analysed. The signal M1.10MA-115 exhibits a soft shell left of 45.2 mm, while the soft shell right is only 6.6 mm. However, when observing M1.10MB-115 signal, a soft shell of roughly 50 mm is present on both left and right side. In Figure E.1, the higher density zone in the right side of the M1.10MA-115 signal could be characterized by the presence of compression wood, a knot or a possibly non-decayed area. However, if studied together with measurement M1.10MB-115, the use of both signals allows to have a clearer picture of the decay distribution around the cross section. These data are presented in Table E.1, where almost 30% difference in the estimation of the soft shell and the remaining sound cross section was calculated, using only measurement A (M1.10MA-115) and using both A+B (M1.10MA-115 and M1.10MB-115).

Another example is shown in Figure E.2, where another pile segment from 1727 (BRU0041-PL2-P1.37) was analysed. The micro-drilling measurement M1.37MA-516 exhibits a soft shell left of 3.7 mm and soft shell right of 36 mm. On the other hand, M1.37MB-516 exhibits almost no soft shell on both sides. The use of only measurement A (M1.37MA-516) shows roughly a 20% difference in the estimation of the soft shell and the remaining sound cross section (Table E.2), compared to using both A+B (M1.37MA-516 and M1.37MB-516). This case also applies to the sole investigation of measurement M1.37MB-516, where no soft shell was measured; causing an incorrect analysis of the soft shell.

Therefore, it is recommended to take both measurement into account and analysing both left and right side of the signal, since the soft shell distribution might differ around the cross section.

Among all 201 drilling A+B measurements, 31 of them (15% of the cases) were labelled as incorrect estimation of the soft shell, if only one measurement would have been considered. For the other 170 cases, the left and side measurements (A+B) of the soft shell were roughly comparable, with differences in the calculation of the remaining sound cross section below 5%. This applies especially for piles from 1886 and 1922. Table E. 3 presents the difference in terms of remaining sound cross sectional area using A vs A+B measurements or B vs A+B measurements for all the signals investigated in this research.



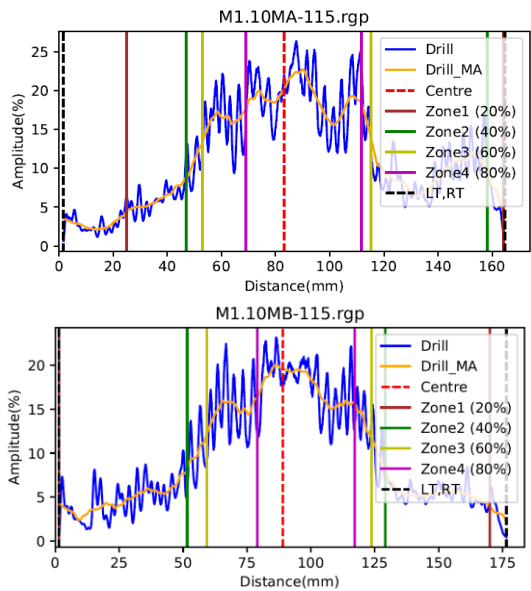


Figure E.1: soft shell calculation for micro-drilling signal A and B of pile BRU0030-PL1-P1.10M (from 1727)

Table E.1: Calculation of the remaining sound cross section for pile BRU0030-PL1-P1.10M based on the soft shell calculated with the soft shell calculator of micro-drilling measurement A and A+B

Micro drilling signals	Soft shell left (mm)	Soft shell right (mm)	Average length of the soft shell (mm)	Soft shell area A_{ss} (%)	Remaining sound c-s area A_{sound} (%)
Only A	45.2	6.6	25.9	50	50
A	45.2	6.6	37.3	64	36
B	50.1	47.3			

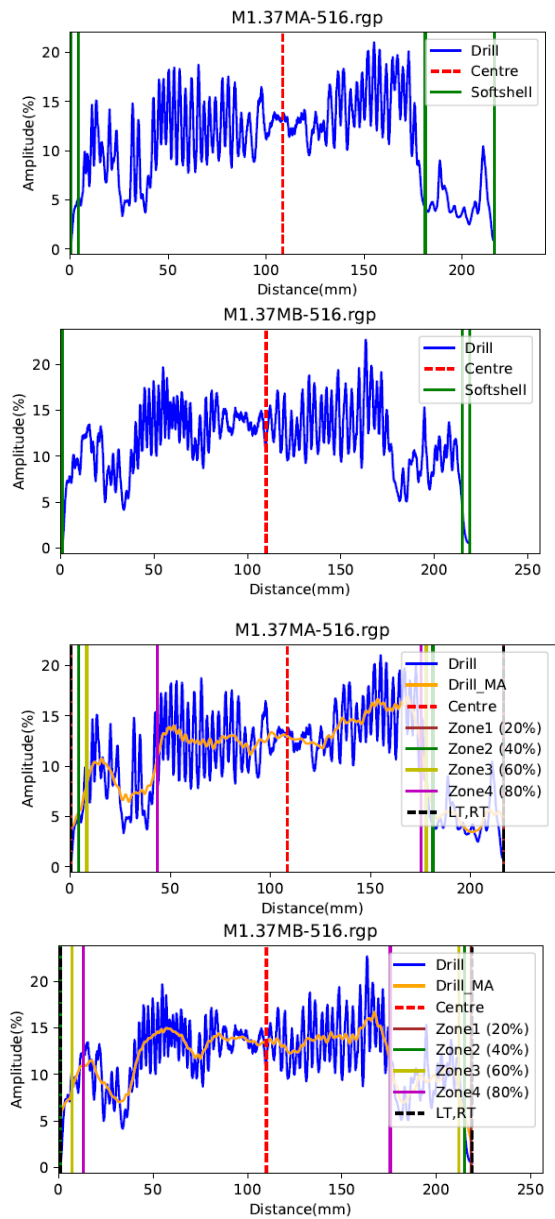


Figure E.2: soft shell calculation for micro-drilling signal A and B of pile BRU0041-PL2-P1.37 (from 1727)

Table E.2: Calculation of the remaining sound cross section for pile BRU0041-PL2-P1.37M based on the soft shell calculated with the soft shell calculator of micro-drilling measurement A and A+B

Micro drilling signals	Soft shell left (mm)	Soft shell right (mm)	Average length of the soft shell (mm)	Soft shell area A_{ss} (%)	Remaining sound c-s area A_{sound} (%)

Appendix E

Only A	3.7	36.0	19.9	33	67
A	3.7	36.0	10.6	18	82
B	0.0	2.9			

Table E. 3: Difference in terms of remaining sound cross section (%) by using only A or B measurements and using both A+B measurements calculated with the soft shell calculator

No. micro-drilling measurements	Case	Difference in % of A_{sound}	SD
170	A vs A+B	2.5	2.1
	B vs A+B	2.7	2.3
31	A vs A+B	20.7	8.4
	B vs A+B	19.1	9.0

List of Publications

Peer-reviewed published articles.

- [1] Pagella, G., Ravenshorst, G.J.P., Gard, W.F., van de Kuilen, J.W.G., 2025. Characterization of the mechanical properties of saturated spruce (*Picea abies*) and pine (*Pinus sylvestris*) foundation piles. *Journal of Building Engineering*. Forthcoming 2025.
- [2] Pagella, G., Urso, T., Mirra, M., Naldini, S., van de Kuilen, J.W., 2025. Traditional wooden foundation piles in Amsterdam and Venice: techniques for the assessment of their state of conservation. *Wood Material Science & Engineering*, 1–16. <https://doi.org/10.1080/17480272.2025.2466104>
- [3] Pagella, G., Mirra, M., Ravenshorst, G., Gard, W., van de Kuilen, J.W., 2024. Characterization of the remaining material and mechanical properties of historic wooden foundation piles in Amsterdam. *Construction and Building Materials*, 450, Article 138616. <https://doi.org/10.1016/j.conbuildmat.2024.138616>
- [4] Pagella, G., Struik, M., Mirra, M., van de Kuilen, J.W. 2024. Small-scale testing of water-saturated wooden discs for determining the strength properties of timber foundation piles. *Wood Material Science and Engineering*. <https://doi.org/10.1080/17480272.2024.2426070>
- [5] Pagella, G., Ravenshorst, G., Mirra, M., Gard, W., van de Kuilen, J.W., 2024. Innovative application of micro-drilling for the assessment of decay and remaining mechanical properties of historic wooden foundation piles in Amsterdam, *Developments in the Built Environment*, Volume 19, 2024, 100514, ISSN 2666-1659. <https://doi.org/10.1016/j.dibe.2024.100514>
- [6] Felicita, M., Pagella, G., Ravenshorst, G.J.P., Mirra, M., van de Kuilen J.W.G., 2024. Assessment of in-situ stress distribution and mechanical properties of wooden foundation piles instrumented with distributed fiber optic sensors (DFOS). *Case Studies in Construction Materials*. Vol. 20. <https://doi.org/10.1016/j.cscm.2024.e03139>
- [7] Mirra, M., Pagella, G., Lee, M., Gard, W., Ravenshorst, G., van de Kuilen, J.W.G., 2024. Characterisation of bacterial decay effects on wooden foundation piles across various historical periods. *Construction and Building Materials*. 421: 135670. <https://doi.org/10.1016/j.conbuildmat.2024.135670>

Peer-reviewed conference articles

- [1] Pagella, G., van de Kuilen, J.-W., Ravenshorst, G., 2025. Experimental prediction of the remaining strength of timber foundations in Amsterdam with micro-drilling. IABSE Congress Ghent 2025 – Forthcoming 2025.
- [2] Pagella, G., Mirra, M., Ravenshorst, G., van de Kuilen, J.-W., 2025. Strength grading of saturated round timber for structural applications. World Conference on Timber Engineering 2025 – WCTE, Brisbane (AUS). Forthcoming 2025.

- [3] Pagella, G., Ravenshorst, G.J.P., Mirra, M., van de Kuilen, J.W.G., 2024. Strength grading of saturated softwood foundation piles. In proceedings of INTER (International Network on Timber Engineering Research) - meeting 57, Padova, Italy. Timber Scientific Publishing. KIT Holzbau und Baukonstruktion, Karlsruhe, Germany.
- [4] Ravenshorst, G.J.P., Pagella, G., Mirra, M., van de Kuilen, J.W.G., Gard, W. F., 2024. Strength characterisation of existing wooden foundation piles under bridges and quay walls in Amsterdam by mechanical testing and assessment through micro-drilling. Paper presented at the 2nd annual Conference on Foundation Decarbonization and Re-use, Amsterdam, May 28 2024.
- [5] Pagella, G., Ravenshorst, G.J.P., Wolfgang, G., van de Kuilen, J.W.G., 2022. Characterization and assessment of the mechanical properties of spruce foundation piles retrieved from bridges in Amsterdam. Paper presented at International Conference on Timber Bridges ICTB2021plus, Biel, Switzerland, May 11.
- [6] Pagella, G., Mirra, M., Ravenshorst, G.J.P., van de Kuilen, J.W.G., 2022. Influence of knots and density distribution on compressive strength of wooden foundation piles. In *Current Perspectives and New Directions in Mechanics, Modelling and Design of Structural Systems*, ed. A. Zingoni, 1689-1695. Leiden, The Netherlands: CRC Press/Balkema.
- [7] Mirra, M., Pagella, G., Gard, W.F., Ravenshorst, G.J.P., van de Kuilen, J.W.G., 2023. Influence of moisture content on the assessment of decay levels by micro-drilling measurements in wooden foundation piles. Paper presented at World Conference on Timber Engineering, Oslo, Norway, June 21.
- [8] Van de Kuilen, J.W.G., Beketova-Hummel, O., Pagella, G., Ravenshorst, G.J.P., Gard, W., 2021. An integral approach for the assessment of timber pile foundations. Paper presented at World Conference on Timber Engineering (WCTE 2021), Santiago, Chile, August 9.

Survey articles, book chapters, books.

- [1] Pagella, G., Gezelschap Practische Studie (The society Practical Study) 2024. Article Extract Edition 25.5.

Curriculum vitae

Giorgio Pagella is a Civil (Structural) Engineer. After earning his MSc in Civil Engineering from the University of Padova, Italy, in 2019, he gained industry experience before joining TU Delft in 2020 as a full-time doctoral researcher in the Biobased Structures and Materials team.

His PhD research focused on the mechanical and material characterization of new and aged round wood. Since completing his PhD in October 2024, he has been working as a postdoctoral researcher at the Delft University of Technology. During his PhD, Giorgio conducted extensive mechanical characterization and analytical analyses of new and existing round wood, assessing the behaviour and remaining service life of heritage timber foundations. He worked on the assessment of historical Dutch buildings with TU Delft's Architecture Department.



Giorgio also performed large- and small-scale laboratory testing on over 600 timber specimens, analysing their material properties, durability, and performance. Additionally, he supervised BSc and MSc students, guiding them in their research and projects.

Giorgio's research aims to enhance the understanding of timber foundations to support timely maintenance interventions for historical buildings and infrastructures. He also investigates the application of timber foundation piles in modern structural design, contributing to the development of sustainable building techniques.

Since 2022, Giorgio has been a member of the European COST Action for the design of timber buildings. He has collaborated with European researchers and industry professionals, particularly on the assessment of timber durability, damage, and strength. Furthermore, Giorgio has participated in over 10 international conferences, sharing his research findings and promoting knowledge exchange within the field.

27/07/1993	Born in Padova, Italy.
2007-2012	High school diploma. Liceo C. Cattaneo, Monselice, Italy.
2013-2017	Bachelor of Science (B.Sc.) in Civil Engineering, University of Padova, Italy.
2017-2019	Master of Science (M.Sc.) in Civil Structural Engineering, University of Padova, Italy.
2019-2020	Civil Structural Designer, Net Engineering S.p.A., Padova, Italy
2020-2020	Researcher at Delft University of Technology, The Netherlands.
2020-2024	PhD Candidate at Delft University of Technology, The Netherlands.
2024-Present	Postdoc at Delft University of Technology, The Netherlands.

Acknowledgments

The pursuit of a PhD is surely a profound mental challenge, offering a great chance to develop a critical mindset to the myriad of obstacles you encounter, whether personal or professional. When I graduated from university, I never imagined myself being a PhD student, in a foreign country, far from the comforting view of the hills that once framed my home. Yet, like many good stories, mine began with an unexpected journey.

The choice of this path has been exciting from the start, most of the time spent questioning myself. But this is also part of the research, isn't it? Stepping into the unknown and exploring different paths along the way. The support of my family, partner, friends, and colleagues has been essential, helping me shape my life and grow into a better person and professional. For this, I am deeply grateful to everyone who has stood by me throughout this experience.

To my parents, Manuela and Andrea. I am grateful for your love and support, for raising me with the freedom to choose my own path, while teaching me solid values and principles to live by. Having you two by my side is sometimes taken for granted, but the sacrifices, dedication to my growth, and unwavering support you have shown throughout my whole life are priceless. To my sister Sofia, I am thankful for having you in my life. Although we live far apart, I am proud we have built solid foundations to care for each other. To Anna, my partner. I do not know if I would be the person that I am now without you. You inspire me to grow every day, teaching me to care for what truly matters and to stand by it. You have shown me how to communicate openly, be honest, and stay open-minded—despite my stubborn Venetian temper. We have built a lot together, I am surprised when I look back to where we started, and I am incredibly grateful for that. A special thanks goes to my grandparents, Maria e Bruno, for their constant support, undeniable fun, and love. I bet they would be proud of me today. Thanks to my grandma Gianna, for thinking everyday about us all, caring, and supporting my future. And to grandpa Orlando, for the priceless love he shows every time I visit. When things get difficult, they remind me of their tremendous strength to carry on in times when there was nothing but a piece of polenta, and now, we have it all. I thank André and Claudia for welcoming me into their family and always being supportive and caring, making me feel at home. I also want to express my gratitude to Peter, Coby, and Sander for their hospitality, openness, and the wonderful evenings spent together. A heartfelt thanks to the rest of my family—Marco, Chiara, Daniele, Raffaella, Francesco, Ornella, Paolo, Maddalena, Nico, Umberto, Marlene, Alessandro, Lietzen, Alberto, Caterina, Elisabetta, Angela, Celeste, Cristiano, Luca, and Mattia—for the moments we have shared together.

To the people who accompanied me through this journey, I extend my gratitude to Roberto, who has always been a guiding figure for me. I have always appreciated your support and suggestions during important decisions. Michele, I am grateful for your friendship, starting with your guidance on my MSc thesis and continuing throughout my PhD, as we shared work, joys, frustrations, successes, and a bit of Italian drama. To my oldest friends. Alessandro, our experiences may have pulled us apart, but for some reason, we have always managed to stay close, sharing our stories and music, remaining true to ourselves. Thanks to Andrea (Nagy) and Valerio, whose friendship feels real every time we meet, leaving me recharged with positive energy. Spending nights together online, the four of us, made the COVID times feel much shorter and definitely more enjoyable. To the Gameboys, with Ale, Pic, and Mario, for the unforgettable times playing music together—terrible music, perhaps, but absolutely perfect for us. I thank Diego for his genuine friendship, as we stay in touch almost every day, sharing quality moments—and probably way too many spritz evenings—in Padova. Filippo, a special thanks to you. We began this journey together, always supporting and caring for each other, sharing the “ups and downs” of a Sicilian and Venetian life in the Netherlands. With Luca Marino’s influence, we reached new heights, culminating in our unforgettable conclave evenings. Thanks to Timo, for the moments shared together as roommates during my initial staying in Delft, hospitality, and the nice evenings spent together. I am grateful to all my other friends who have been there for me when I returned home, sharing nice moments, conversations, and celebrations: Davide, Edo, Andrea B., Lorenz, Gianni, Laura, Anna, Sara, Federico, Erica, and Elia.

This journey would not have been possible without my team at TU Delft. Jan Willem, thank you for the opportunity you gave me, for your supervision, and for the bond we have built over the past year. To Geert, thanks for your patience, guidance, and kindness. I have learned a lot from you, without needing many words. Ruben, a special thanks to you. Without your amazing work and dedication, I would never have been able to complete the extensive experimental campaign I had planned. Your humility and kindness have been a great lesson to me. I thank also Michael, for having worked alongside me for many months with great enthusiasm and dedication. Thanks Wolfgang, for your wise words and advices, and to Peter, who allowed me to work “freely” in the lab and shared the fun of many bike rides. Thanks to John and Louis for the best conversations ever in the lab and for always being supportive whenever anything was needed. My gratitude also to the committee members—Henk Jonkers, Ken Gavin, Geeralt van den Ham, Roberto Scotta, and Milan Veljkovic—for their time and valuable feedback. To my colleagues, Abhijith, Alessandro, Angeliki, Anindya, Cees, Egidio, Enxhi, Francesco, Francesco D.M., Florentia, Georgios, Gerhard, Hagar, Ice, Katerina, Maria, Marko, Olena, Paul, Rita, Sergio, Trayana, Valentin, Xiuli, Yasmine, and everyone who made this journey special, contributing to create a wonderful and supportive work environment.

